FEDERAL UNIVERSITY OF CEARÁ
CENTER OF TECHNOLOGY
DEPARTMENT OF HYDRAULICS AND ENVIRONMENTAL ENGINEERING
GRADUATE PROGRAM IN CIVIL ENGINEERING: WATER RESOURCES
DOCTORAL DEGREE IN CIVIL ENGINEERING: WATER RESOURCES

MARIA APARECIDA MELO ROCHA ESTACIO

WATER QUALITY DYNAMICS IN A MULTI-PURPOSE RESERVOIR IN THE BRAZILIAN SEMIARID: RESPONSES TO HYDRO-CLIMATIC VARIABILITY AND EXTERNAL AND INTERNAL NUTRIENT LOADINGS

FORTALEZA
2024

MARIA APARECIDA MELO ROCHA ESTACIO

WATER QUALITY DYNAMICS IN A MULTI-PURPOSE RESERVOIR IN THE BRAZILIAN SEMIARID: RESPONSES TO HYDRO-CLIMATIC VARIABILITY AND EXTERNAL AND INTERNAL NUTRIENT LOADINGS

Thesis submitted to the Graduate Program in Civil Engineering: Water Resources of the Center of Technology of the Federal University of Ceará, as a partial requirement for obtaining the title of Doctor in Civil Engineering. Concentration Area: Water Resources.

Advisor: Prof. Dr. Iran Eduardo Lima Neto.
Co-advisor: Dr. Mário Ubirajara Gonçalves Barros.

FORTALEZA

2024

Dados Internacionais de Catalogação na Publicação
Universidade Federal do Ceará
Sistema de Bibliotecas
Gerada automaticamente pelo módulo Catalog, mediante os dados fornecidos pelo(a) autor(a)

E1w Estacio, Maria Aparecida Melo Rocha.
Water Quality Dynamics in a Multi-Purpose Reservoir in the Brazilian Semiarid: Responses to Hydro-Climatic Variability and External and Internal Nutrient Loadings / Maria Aparecida Melo Rocha Estacio. – 2024.
206 f. : il. color.

Tese (doutorado) – Universidade Federal do Ceará, Centro de Tecnologia, Programa de Pós-Graduação em Engenharia Civil: Recursos Hídricos, Fortaleza, 2024.
Orientação: Prof. Dr. Iran Eduardo Lima Neto.
Coorientação: Prof. Dr. Mário Ubirajara Gonçalves Barros.

1. Eutrophication. 2. Phosphorus dynamics. 3. Water resources management. I. Título.
CDD 627

MARIA APARECIDA MELO ROCHA ESTACIO

WATER QUALITY DYNAMICS IN A MULTI-PURPOSE RESERVOIR IN THE BRAZILIAN SEMIARID: RESPONSES TO HYDRO-CLIMATIC VARIABILITY AND EXTERNAL AND INTERNAL NUTRIENT LOADINGS

Thesis submitted to the Graduate Program in Civil Engineering: Water Resources of the Center of Technology of the Federal University of Ceará, as a partial requirement for obtaining the title of Doctor in Civil Engineering. Concentration Area: Water Resources.

Approved on: 05/04/2024.

EXAMINATION BOARD

Prof. Dr. Iran Eduardo Lima Neto (Advisor)
Federal University of Ceará (UFC)

Dr. Mário Ubirajara Gonçalves Barros (Co-advisor)
Water Resources Management Company of Ceará (COGERH)

Prof. Dr. José Carlos Alves Barroso Júnior
Federal University of Ceará (UFC)

Prof. Dra. Samiria Maria Oliveira da Silva
Federal University of Ceará (UFC)

Prof. Dra. Vanessa Becker
Federal University of Rio Grande do Norte (UFRN)

Prof. Dr. Tobias Bernward Bleninger
Federal University of Paraná (UFPR)

ACKNOWLEDGEMENTS

This thesis was only possible due to the collaboration and support of many people and institutions.

This study was financed in part by the Coordination for the Improvement of Higher Education Personnel – Brazil (CAPES) – Finance Code 88887.483562/2020-00. I thank CAPES for this scholarship that made possible for me to give my total dedication to this research project, I feel privileged to have had this opportunity. I also want to thank the Foundation for Scientific and Technological Support of Ceará – (FUNCAP) – Research Grant 02625308/2021. I thank FUNCAP for the financial support to this project through the Chief Scientist Project. I also would like to thank Prof. Dr. Francisco de Assis de Souza Filho, our Chief Scientist Project coordinator, for all his work and insightful contributions to this thesis.

I thank the Water Resources Management Company of the State of Ceará – (COGERH) – for also supporting this research with the extensive environmental monitoring that provided the consistent database that I worked in this thesis. I would like to thank Débora Maria Rios Bezerra, Walt Disney Paulino, Inah Maria de Abreu, Tércio Dantas Tavares e Roberto Bruno Moreira Rebouças for being such important enthusiasts of this project. Without your collaboration, this research would not have been possible. I also would like to thank Francimeyre Freire Avelino, Renata Vinhas Cruz, Hermilson Barros de Freitas, Francisco Almeida Chaves, José Rodrigo Brito, Débora Mendes, Nayane Santos, and several others that worked so hard in the field sampling campaigns and in the laboratory analysis, your work was essential for this thesis. I also would like to thank Mário Ubirajara Gonçalves Barros, who I had the honor to work with several times before. Your enthusiasm, experience, and contributions for this thesis were essential for it to work. I thank you immensely for it.

I would like to thank the Post-Graduation Program in Civil Engineering at the Federal University of Ceará, and all its professors and staff. It was an honor to be in the classroom learning from so many important researchers in our field. This program changed my life and made me appreciate working with water resources and water quality. I also wanted to thank the members of the examination board Prof. Dr. José Carlos Alves Barroso Júnior, Prof. Dra. Samiria Maria Oliveira da Silva, Prof. Dra. Vanessa Becker, and Prof. Dr. Tobias Bernward Bleninger for accepting to examine this thesis.

I would like to thank my parents, Cícera and Flávio, who have always encouraged me to pursue my dreams through education. Without their support and strength, I would not be

here. I also thank my brother, Marcus Vinicius, for always being such a supportive presence in my life, who constantly encourages me.

I thank my husband and partner in both life and academic journeys. Thank you so much for your constant support, kindness, encouragement, and for always be willing to listen to me.

I thank Taís for her friendship and support. I am incredibly lucky to have been your friend since we started in UFC together. I thank my friends Valéria and Deborah, who are always so understanding and supportive. I will always be grateful for having you in my life. I also thank Mateus, Felipe, Thayana, and Sofia, whose friendship is a constant gift that UFC gave to me.

Lastly, I would like to thank my advisor, Prof. Dr. Iran Eduardo Lima Neto for mentoring me through this doctorate. Your guidance, kindness, support, and wise words were important to me through this entire journey. I am incredibly grateful for your dedication. Your support inspired me to try to become a better student, research, and person. It has been an honor collaborating with you.

ABSTRACT

The Castanhão reservoir holds great importance for the Brazilian semiarid region due to its diverse uses: irrigation, aquaculture, and human water supply. Situated in a semiarid zone, its volume undergoes significant variations over time, especially during dry periods. Between 2012 and 2018, a prolonged drought led to a substantial decrease in the reservoir's volume, reaching as low as 2% of its capacity. Consequently, the water quality deteriorated, transforming the reservoir into a eutrophic state, complicating its management. As phosphorus plays a crucial role in eutrophication, this study aims to evaluate the spatial and temporal variability of water quality parameters. It also seeks to develop and compare different models for estimating nutrient concentration in the water inflow into the reservoir based on easily obtainable data. Additionally, it seeks to develop a mass balance model simulating the total phosphorus (TP) dynamics in the reservoir, considering its various sources such as inflow, aquaculture, and internal phosphorus (P) release from sediment-water interactions. The goal is to use this model to simulate different scenarios and assess the impact of those P sources. Monthly assessments conducted in this study confirm complete nutrient mixing in the reservoir, with temporal variations outweighing spatial ones, supporting the applicability of the proposed complete-mixing model. The study also emphasizes the prevalence of chemical stratification in dissolved oxygen levels over thermal stratification, with dissolved oxygen (DO) decreasing downstream, particularly during the rainy season. Diel assessments reveal a diel cycle of thermal stratification, primarily during the dry season, driven by higher wind speeds. This is corroborated by a significant negative correlation between wind speed and the relative water column stability index. In contrast, during the rainy season, the reservoir experiences continuous thermal stratification due to inflowing water being warmer than the reservoir’s water temperature. Notably, a twofold increase in P throughout the day during the rainy season underscores the influence of phytoplankton community dynamics on diel nutrient variation. Additionally, chemical stratification of DO occurs during both dry and rainy seasons, indicating that even during the dry season, when there is no significant inflow, internal nutrient loading can significantly impact the reservoir's water quality. An analysis of the influence of inflow on water quality variables was performed and several predictive TP concentration models were developed and compared. While Ridge and Lasso regressions demonstrated superior performance, the observation that the test performance surpassed that of the training data

suggests overfitting. This discrepancy led to the decision to adopt the non-linear model for application in the TP complete mixing model. In addition, a regression tree model showed that the flow rate is the explanatory variable that better explained the TP variation, whereas DO and temperature were the ones that better explained the total nitrogen concentration variation. The analysis of the bed sediment of Castanhão reservoir showed that the majority of P fraction is the inorganic. In addition, the sampling point closest to the dam is the one with more potential for internal P loading. The proposed model of P dynamics in the reservoir achieved good calibration performance (NSE = 0.62; PBIAS = -0.03%). Scenario simulations indicate that an 70% reduction in external load, a 30% reduction in internal load, and a 30% reduction in aquaculture load have the potential to bring the TP concentration within the class two limit by the end of the simulation period. This designation ensures that the water is suitable for human consumption after conventional treatment according to Brazilian legislation. These reductions could be achieved through improvements in sanitation, erosion control, upstream agricultural practices, aeration, sediment management, and enhancement of fish feed conversion efficiency.

Keywords: eutrophication; phosphorus dynamics; water resources management.

RESUMO

O reservatório de Castanhão tem grande importância para a região semiárida brasileira devido aos seus diversos usos: irrigação, aquicultura e abastecimento de água para consumo humano. Situado em uma zona semiárida, seu volume sofre variações significativas ao longo do tempo, especialmente durante períodos de seca. Entre 2012 e 2018, uma seca prolongada levou a uma diminuição substancial no volume do reservatório, atingindo até 2% de sua capacidade. Consequentemente, a qualidade da água deteriorou-se, e o reservatório atingiu o estado eutrófico, complicando sua gestão. Como o fósforo desempenha um papel crucial na eutrofização, este estudo tem como objetivo avaliar a variabilidade espacial e temporal dos parâmetros de qualidade da água. Ele também busca desenvolver e comparar diferentes modelos para estimar a concentração de nutrientes na água afluente ao reservatório com base em dados que possam ser facilmente medidos. Além disso, busca desenvolver um modelo de balanço de massa simulando a dinâmica de fósforo total (PT) no reservatório, considerando suas diversas fontes, como entrada de água, aquicultura e liberação interna de fósforo (P) devido às interações água-sedimento. O objetivo é usar esse modelo para simular diferentes cenários e avaliar o impacto dessas fontes de P. Avaliações mensais realizadas neste estudo confirmam a mistura completa de nutrientes no reservatório, com variações temporais superiores às espaciais, apoiando a aplicabilidade do modelo de mistura completa proposto. O estudo também enfatiza a prevalência da estratificação química nos níveis de oxigênio dissolvido (OD) sobre a estratificação térmica, com o OD diminuindo a jusante, especialmente durante a estação chuvosa. Avaliações diárias revelam um ciclo diário de estratificação térmica, principalmente durante a estação seca, impulsionado por velocidades do vento mais altas. Isso é corroborado por uma correlação negativa significativa entre a velocidade do vento e o índice de estabilidade relativa da coluna d'água. Por outro lado, durante a estação chuvosa, o reservatório experimenta uma estratificação térmica contínua devido à temperatura da água que entra no reservatório ser mais quente do que a temperatura da água do reservatório. Notavelmente, um aumento de duas vezes no P ao longo do dia durante a estação chuvosa evidencia a influência da dinâmica da comunidade fitoplanctônica na variação diária de nutrientes. Além disso, a estratificação química do OD ocorre durante as estações seca e chuvosa, indicando que mesmo durante a estação seca, quando não há entrada significativa, a carga interna de nutrientes pode impactar significativamente a qualidade da água do reservatório. Uma análise da influência do aporte de

água em seus parâmetros de qualidade foi realizada e vários modelos preditivos de concentração de PT foram desenvolvidos e comparados. Embora as regressões Ridge e Lasso tenham demonstrado desempenho superior, a observação de que o desempenho no teste superou o do treinamento sugere overfitting. Essa discrepância levou à decisão de adotar um modelo não linear para aplicação no modelo de mistura completa de TP. Além disso, um modelo de árvore de regressão mostrou que a vazão é a variável explicativa que melhor explica a variação do PT, enquanto OD e temperatura foram as que melhor explicaram a variação da concentração de nitrogênio total. A análise do sedimento do reservatório Castanhão mostrou que a maior parte da fração de P que o compõe é inorgânica. Além disso, o ponto de amostragem mais próximo da barragem é o que possui mais potencial para recarga interna de P. O modelo proposto de dinâmica de P no reservatório obteve bom desempenho de calibração (NSE = 0,62; PBIAS = -0,03%). As simulações de cenários indicam que uma redução de 70% na carga externa, de 30% na carga interna e de 30% na carga da piscicultura têm o potencial de levar a concentração de PT próxima ao limite da classe dois ao final do período de simulação. Essa designação garante que a água seja adequada para consumo humano após tratamento convencional de acordo com a legislação brasileira. Essas reduções podem ser alcançadas por meio de melhorias no saneamento, controle de erosão e de práticas agrícolas a montante, aeração, manejo de sedimentos e aumento da eficiência de conversão de ração para peixes.

Palavras-chave: eutrofização; dinâmica do fósforo; gestão de recursos hídricos.

LIST OF FIGURES

LIST OF TABLES

CONTENTS

1 INTRODUCTION

Reservoirs are constructed with diverse objectives, such as facilitating hydroelectric power generation, supplying water for irrigation, supporting industrial processes, meeting human consumption needs, enabling fish farming activities, controlling floods, and, specifically in semiarid regions, mitigating the impact of droughts (Keitel, Zak and Hupfer, 2016). However, the construction of reservoirs can alter the natural hydrological balance by modifying the watercourse flow, sediment transport, and nutrient balance (Huang, Fang and Reible, 2015; Ren *et al*., 2019). Reservoirs slow down the inflow, retaining nutrients, sediments, and toxins, thereby reducing the nutrient load downstream (Chen *et al*., 2019; Han *et al*., 2018).

The enrichment of nutrients in water bodies can lead to eutrophication and harmful algae blooms, compromising water quality and impacting human health (Barbosa *et al*., 2023; Huang *et al*., 2018; Kwak, Jeon and Duck Hur, 2018). This issue is global, with artificial lakes experiencing eutrophication more rapidly than natural ones, making it nowadays a recurrent concern (Mamun e An, 2017).

Phosphorus (P) plays a significant role in eutrophication (Harke *et al*., 2016; Huang *et al*., 2016), as it shows a strong affinity for sediment particles due to their high specific surface area and active surface points, facilitating phosphorus adsorption. External sources of P can originate from point or non-point pollution. Non-point pollution, stemming from agricultural and livestock activities and changes in the landscape that increase soil erosion, presents a considerable challenge for control due to its diffuse nature and its contribution to P transport to reservoirs (Rocha Junior, Araújo and Becker, 2024; Rocha and Lima Neto, 2021). For instance, over half of the P load entering a reservoir can accumulate significantly (Huang, Fang and Reible, 2015). In addition to external loading, P in the water column of a reservoir can arise from internal sources. Bed sediment in reservoirs can act as both a source and a sink of this nutrient, primarily due to the reductive dissolution of ferric (Fe (III)) oxyhydroxides in the sediment and subsequent release of adsorbed phosphorus in anoxic environments (Dael *et al*., 2024; Søndergaard *et al*., 2003). This highlights the importance of studying phosphorus-sediment interactions, as their impacts can persist even after reducing external loading (Liu *et al*., 2017; Tang *et al*., 2019). Therefore, accurately estimating total phosphorus (TP) concentrations and understanding its relationship with environmental factors is essential to improve nutrient management strategies to mitigate eutrophication (Li *et al*., 2017). For instance, some strategies are hypolimnetic aeration, improvements on agricultural management,

and improvements on the efficiency of fish farming feeding conversion rates (Mehdizadeh *et al.*, 2023; Sandström *et al.*, 2024; Vogel *et al.*, 2019).

Reservoirs located in semiarid regions are susceptible to prolonged drought periods, irregular precipitation, high evaporation rates, and high nutrient loads which intensifies their eutrophication process (Cavalcante *et al*., 2018; Delmiro Rocha e Lima Neto, 2022; Rabelo *et al*., 2022). Therefore, to enhance the understanding of P dynamics in water quality and to propose effective mitigation strategies, more detailed studies focusing on the pertinent factors involved in physicochemical processes are essential. Mathematical modeling emerges as a valuable tool for predicting phosphorus transport. While certain studies utilize simplified models to depict P dynamics (Barbosa e Cirilo, 2015; Bezerra, Becker e Mattos, 2014; Lima Neto *et al*., 2022; Lira, Medeiros e Neto, 2020; Vidal e Capelo Neto, 2014), there remains a gap in studies that comprehensively evaluate the water quality dynamics in a semiarid reservoir. Those studies usually do not consider the diel, monthly, seasonal, and interannual variations of water quality parameters altogether in order to use them to assess the influence of the different sources of P in its dynamics in the reservoir.

Furthermore, this research aims to simulate various scenarios to assess the effects of measures aimed at improving the water quality of the Castanhão reservoir and to facilitate the integration of water quality considerations into the overall water resources management and allocation process. Additionally, this thesis is part of a FUNCAP project – the Chief Scientist Program, which entailed numerous presentations, seminars, and meetings with key stakeholders in water resources management, not only at the state level but also nationally. These organizations and institutions include the Water Resources Management Company (COGERH), the Secretary of Water Resources of Ceará (SRH), the National Water and Basic Sanitation Agency (ANA), the Ministry of Fisheries and Aquaculture (MPA), the Brazilian Agricultural Research Corporation (EMBRAPA), the Ceará Foundation for Meteorology and Water Resources (FUNCEME), the Water and Sewage Company of the State of Ceará (CAGECE), and the Federal University of Ceará (UFC). The activities are detailed in Appendix D.

1.1 General objective

This study aims to enhance our comprehension of the intricate processes governing water quality dynamics in a semiarid reservoir. It seeks to analyze how the reservoir reacts to hydroclimatic fluctuations and both external and internal factors impacting its water quality. Additionally, the study aims to construct a model that accurately simulates the phosphorus

dynamics within the reservoir, accounting for various sources including internal loading, fish farming, and inflow of total phosphorus. This model will help determine the reservoir's phosphorus carrying capacity and forecast the potential effects of different operational and remediation strategies on water quality. Ultimately, these findings will serve as a valuable asset for the decision-making process concerning water management in this reservoir.

1.1.1 Specific objectives

1) Analyze the spatial and temporal variations of water quality parameters, such as nutrients, cyanobacteria, dissolved oxygen, and temperature, as well as their interactions within the reservoir under investigation.
2) Evaluate the potential daily patterns of water quality parameters within the same reservoir.
3) Assess the spatial and temporal patterns of water quality in the river sections upstream of the reservoir under study and develop models to estimate the concentration of total phosphorus and total nitrogen entering it.
4) Examine spatio-temporal variations of phosphorus and its different factions within the sediment layer of the aforementioned reservoir.
5) Calibrate the mass balance model estimating the concentration of TP in the reservoir and utilize it to calculate the reservoir’s P carrying capacity. Use the model to simulate different scenarios of operation and remediation techniques aimed at improving water quality in this specific reservoir.

1.2 Thesis structure

The structure of this work consists of the aggregation of five scientific papers concerning the water quality dynamics of a multi-purpose reservoir.

Figure 1 - Thesis Structure Flowchart outlining chapter titles, main objectives, and the corresponding scientific paper status.

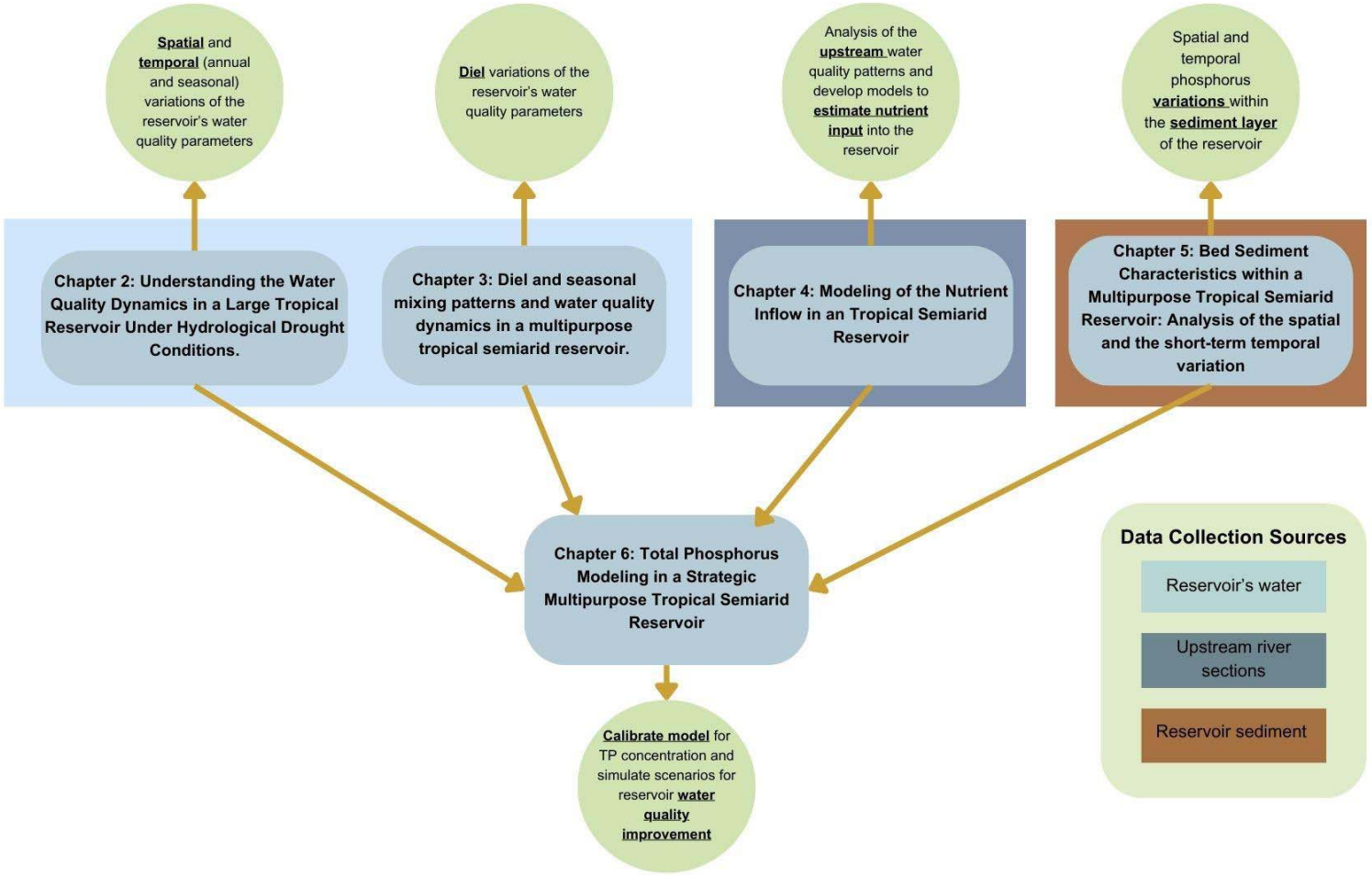

2 UNDERSTANDING THE WATER QUALITY DYNAMICS IN A LARGE TROPICAL RESERVOIR UNDER HYDROLOGICAL DROUGHT CONDITIONS

2.1 Introduction

There are several factors that contribute to water quality deterioration. Pollutant discharges in water bodies can render the water unsuitable for direct use in human consumption or other industrial applications (de Lacerda *et al*., 2018; Barçante *et al*., 2020; Panagopoulos, 2022; Rocha and Lima Neto, 2021, 2022). Droughts are another factor that have been widely recognized for their direct impacts on water quality deterioration (Li *et al*., 2018; Leite and Becker, 2019). This deterioration, marked by eutrophication and harmful algae blooms (de Oliveira *et al*., 2020; Zhang *et al*., 2021), not only escalates water treatment costs (Carmichael *et al*., 2016; Pontes Filho *et al*., 2020) but also triggers critical consequences such as fish kills due to hypoxia, especially during the rainy season (Carneiro *et al*., 2023).

Understanding water quality dynamics can be complex, as it is the result of interactions between numerous physical and environmental factors (Park *et al*., 2021). Furthermore, the impacts of drought on water quality exhibit significant variation depending on the specific characteristics of each water body and its surrounding catchments (Li *et al*., 2017). Therefore, effective reservoir management necessitates a comprehensive understanding of regional differences, as well as temporal and spatial patterns of nutrients and other physical, chemical, and biological parameters (Hudson and Vandergucht, 2015; Huo *et al*., 2019).

Several studies have explored the dynamics of water quality in semiarid and Tropical region reservoirs. However, these studies have predominantly focused on studying one water quality parameter within various reservoirs (Carneiro *et al*., 2023; ; Zhong *et al*., 2022; Wiegand *et al*., 2021; Germán *et al*., 2021), or have been conducted outside drought periods, often lacking more than a year's worth of data (Molisani *et al*., 2013, 2015; Santos *et al*., 2016). Whereas in the present study we incorporated a five-year profiling monitoring of several important water quality parameters in six different sampling points in a large and deep reservoir during and after a drought period. This extensive monitoring allows to comprehend the spatio-temporal variation and the many interactions within the water quality dynamics of a reservoir that were not observed in previous studies.

In addition, while the findings of previous studies provide important contributions, they do not provide an in-depth perspective of the water quality dynamics of the reservoir to

support management programs in Tropical semiarid reservoirs. These programs have to approach solutions for water allocation decisions that minimize conflicts and for the many fish kills that occur in the reservoir. In order to find the solutions, a high availability of multiparameter water quality data is required, which is usually the main difficulty encountered by previous studies and that the present study seeks to overcome it through its in-depth monitoring.

Thus, this study aims to address this knowledge gap by utilizing a newly established, comprehensive water quality monitoring system to unravel the intricacies of water quality dynamics in a semiarid reservoir. We investigate the spatial and temporal patterns and interactions among key water quality parameters essential for environmental management, including nutrients, algae, cyanobacteria, dissolved oxygen, and temperature.

Our focal point is the Castanhão reservoir, a vital water body situated in the Brazilian semiarid region, serving purposes ranging from irrigation and fish farming to water supply (Raulino *et al*., 2021). Notably, this reservoir supplies water to the metropolitan region of the State of Ceará (about five million inhabitants) through water transfer. The severe and prolonged drought that has afflicted the region since 2012 (Sousa Estácio *et al*., 2022) has led to a substantial reduction in the reservoir's volume, pushing it into a state of eutrophication/hyper eutrophication (Ceará, 2022a). Consequently, in-depth field monitoring efforts commenced in 2016, incorporating various sampling points and profiling analyses, rendering the reservoir exceptionally suited for the extensive investigation proposed in this study.

Our dataset spans from 2016 to early 2022, during which the reservoir's volume consistently remained below 20% of its capacity, representing a prolonged hydrological drought period. This study not only enhances our comprehension of the spatio-temporal dynamics of water quality within a Tropical reservoir during hydrological drought conditions but also provides a valuable reference for state-based water agencies seeking scientifically grounded decisions in water management. These decisions aim to alleviate water conflicts related to allocation and utilization processes, and the findings are anticipated to benefit reservoir management in similar semiarid regions worldwide.

2.2 Materials and methods

2.2.1 Study Area

This study was conducted in Castanhão. A reservoir built in 2002 in the Brazilian semiarid (Figure 2). It has a storage capacity of 6.7 billion of m³, a dam crest elevation of 111 m, and a maximum height of 71 m (Ceará, 2022a). The catchment area of Castanhão reservoir is 45,309 km², which is characterized by mild slopes varying normally from 0 to 15° (Ceará, 2022a). The main uses of Castanhão's water are for human consumption, agriculture, and fish farming. This reservoir is part of a water transfer system that supplies water to the capital of the State Ceará and its metropolitan region, with 4.1 million inhabitants (Sousa Estácio *et al*., 2022).

Figure 2 – Map of the study area: the location of Brazil within South America and the state of Ceará within Brazil, with indication of the Brazilian semiarid region, Castanhão reservoir, and its drainage network (left panels). Representation of Castanhão reservoir and its sampling points (right panel).

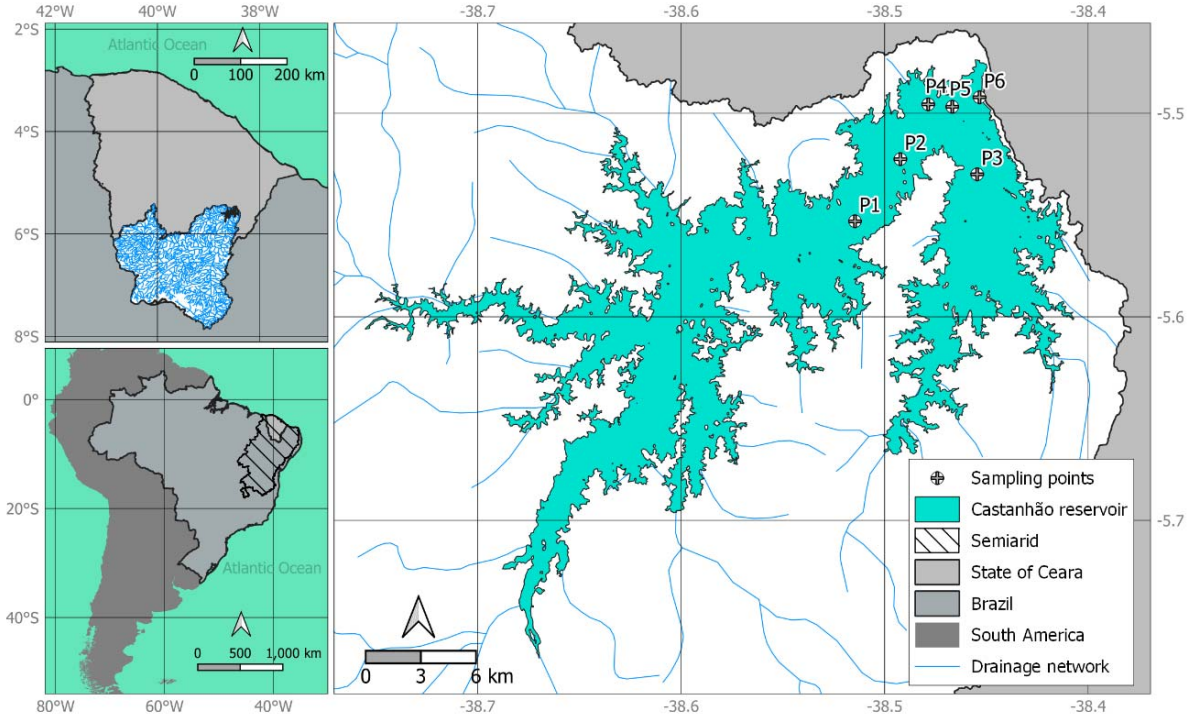

Source: The author.

The predominant soil types are argisols, luvisols, neosols, chernosols, latosols, and planosols, in which shrubby caatinga vegetation develops (Ceará, 2022b). In addition, the reservoir is in a region of shallow soils located in the crystalline geological formation (Ceará, 2022b). This type of soil, associated with the semiarid climate, results in intermittent rivers and usually negligible baseflow. The annual rainfall in the reservoir's catchment is 836 mm/year

(Rocha and Lima Neto, 2021, 2022). The rainfall is usually concentrated from January to May, resulting in a strong seasonal variation.

During the dry months the reservoir's inflow is practically null. Then, because of the high evaporation rates, the volume severely decreases. From 2012 to 2019 this region was affected by a severe meteorological drought event, which resulted in a Castanhão's volume decrease from 75% of its volume to around 2% (Sousa Estácio *et al*., 2022).

Those changes associated with pollution and internal phosphorus recharge triggered the eutrophication of the reservoir (Rocha and Lima Neto, 2021), which caused cyanobacteria blooms that make water treatment more expensive (Zhai *et al*., 2022), and oxygen depletion, which caused fish kill in the fish farming areas (Molisani *et al*., 2015). In addition, due to its multiple uses, and its location in a semiarid region, the water allocation of Castanhão is a potential source of conflicts. For instance, depending on the amount of fish farming allowed in the reservoir there are different impacts on the water quality of this reservoir, which can negatively interfere with the other uses.

2.2.2 Data and Analyses

2.2.2.1 Data acquisition

Since Castanhão is one of the most important reservoirs of the State of Ceará, a more detailed water quality monitoring was initiated in 2016. Instead of surface analysis in one sampling point, other sampling points and more water quality parameters with a profiling analysis were added to the monitoring campaigns. The main purpose of this monitoring was to consider not only the water quantity, but also the water quality in the water allocation. In order to closely monitor the water quality, the acquisition of more consistent water quality data was essential.

The sampling campaigns were divided in two: profiling and water quality (Figure S 1). Profiling was performed using a YSI EXO 2 probe that measures dissolved oxygen (DO), temperature, total dissolved solids (TDS), salinity, and pH. These physicochemical parameters were measured in all the six sampling points from surface (0.3 m depth) every 0.5 m until reaching 8 m depth, then the measurements were made each 1 m until reaching the depth 0.5 m above sediment layer. In order for the data to be suitable for comparative analysis, the samplings were always conducted at approximately the same time, with a maximum difference of 30 to 40 minutes.

Water samples were taken in points P3, P4, and P6, in five different calculated depths (Table S 2) within the water column. Then the samples were taken to a laboratory to quantify the following parameters: Total phosphorus (TP), total nitrogen (TN), chlorophyll a (Chl-a), pheophytin, orthophosphate, nitrate, nitrite, ammoniacal nitrogen, true color, biochemical oxygen demand, and cyanobacteria cell density. All those analyses were performed according to Apha (2017).

The profiling parameters were measured monthly from January 2016 to February 2022. The water quality parameters analyzed in the laboratory were from samples taken in each trimester from May 2016 to September 2020 and monthly from October 2020 to January 2022.

2.2.2.2 Data processing

The data was processed using R Core Team (2022). In order to assess spatial variation of the parameters, and the data distribution, boxplot and correlation analysis between the sampling points were used. Then, since droughts are known to highly influence the water quality of a reservoir (Wiegand *et al*., 2021), inter-annual and intra-annual variations for each parameter were assessed. This allowed to assess both the impact of a long-range negative trend of water level, and wet and dry rainfall seasons on the water quality of Castanhão.

The strength and persistence of thermal and chemical stratification (for DO) were also analyzed, since those factors highly influence the water quality dynamics of a reservoir (Nong *et al*., 2023). The strength of chemical stratification for DO (SCS) was calculated according to the equation below (Noori *et al*., 2021; Yu *et al*., 2010):

$$SCS = \frac{DO_S - DO_B}{0.5 \times (DO_S + DO_B)} \quad (1)$$

Where DO_s and DO_B are DO concentrations in the surface (0.3 m depth) and at the bottom (0.5 m above sediment layer) of the reservoir, respectively. A null SCS indicates that the DO is not stratified.

Thermal stratification was evaluated using two different indexes. First, the thermocline strength index (TSI) was calculated using the following equation (Yu *et al*., 2010):

$$TSI = \Delta T / \Delta h \ (°C/m) \quad (2)$$

Where ΔT is the temperature difference between the surface (0.3 m depth) and the bottom (0.5 m above sediment layer) of the reservoir, respectively. Δh is the depth of the water column in meters. Thermocline is recognized to exist when TSI >1 (°C/m) and the higher the value of TSI, stronger is the thermal stratification (Yu *et al*., 2010).

Then, the relative water column stability (RWCS) coefficient was also calculated to evaluate thermal stratification in Castanhão (Carneiro *et al*., 2023; Cui *et al*., 2021b).

$$RWCS = (\rho_B - \rho_s)/(\rho_4 - \rho_5) \quad (3)$$

Where ρ_B and ρ_s represent the water density (g/L) at the bottom and surface of the water column, respectively. ρ_4 and ρ_5 represents the water densities at 4 and 5 °C, respectively.

Water densities were calculated using Equation 4, considering normal atmospheric pressure and disregarding salinity of the water (Carneiro *et al*., 2023).

$$\rho = a_0 + a_1 T + a_2 T^2 + a_3 T^3 + a_4 T^4 + a_5 T^5 \quad (4)$$

In which the coefficients are: a_0 = 999.842594, a_1 = 6.793953× 10−2, a_2 = − 9.095290× 10−3, a_3 = 1.001685× 10−4, a_4 = − 1.120083× 10−6 and a_5 = 6.536332 × 10−9. An RWCS ≥50 was considered as a reference to confirm thermal stratification in the water column.

2.3 Results and Discussion

2.3.1 Reservoir Hydrology

Figure 3 shows the variations of volume, inflow, outflow, and evaporation in Castanhão reservoir during the analyzed period in the present study. It is important to highlight that from 2016 to 2017 the reservoir volume drastically decreased (Figure 3A) due to the drought period. Between 2016 and 2022, the average monthly inflow during rainy season was 66.62 Mm^3, with a maximum value of around 500 Mm^3/month. Even with the increase in volume observed in March 2020 (Figure 3B), the reservoir volume is still much lower than the one observed in the pre-drought period. Drought periods can have high negative impacts on the water quality of a reservoir, e.g., higher salinity, less DO concentration leading to hypoxia of the hypolimnion, increase in Chl-a concentrations, and eutrophication (de Lacerda *et al*., 2018).

Figure 3 – A) Daily volume of the Castanhão reservoir, the shaded area corresponds to the period during which monitoring for the present study was conducted. Mm^{-3} stands for million cubic meters. B) Detail of the average monthly volume of Castanhão reservoir from January 2016 to January 2022. C) Monthly inflow of Castanhão reservoir. D) Monthly evaporated volume of Castanhão reservoir. E) Monthly controlled reservoir release.

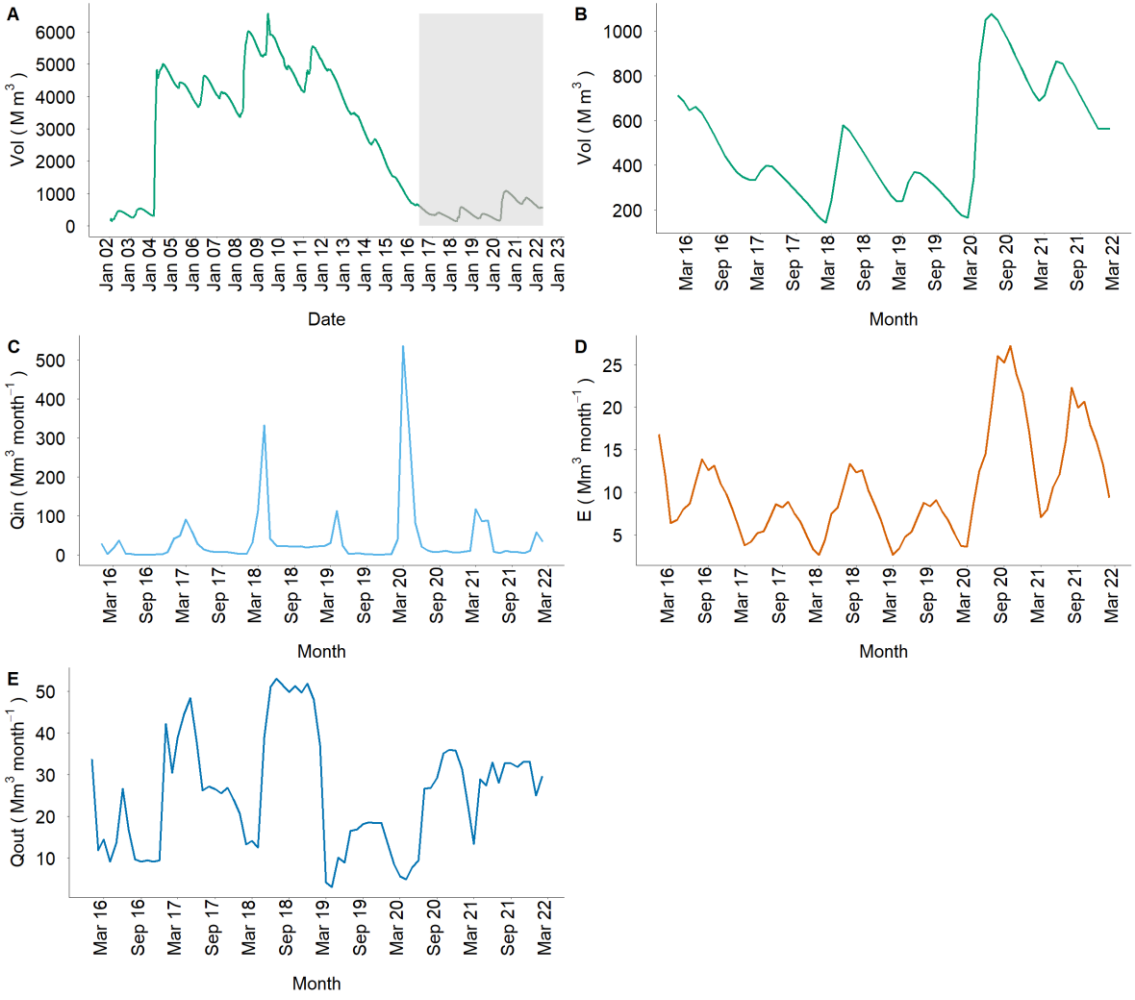

Source: The author.

2.3.2 Spatial variation of TP and TN

Pearson's correlation analysis was performed to assess the spatial variation of water quality parameters within the sampling points (Figure S 6). Points P3, P4, and P6 were selected among the six sampling points to optimize the use of laboratory resources and expedite the monitoring process. These three sampling points have considerably different characteristics, where P3 is on the right branch of the reservoir, P4 is on the left branch and it is the point where fish farming is more concentrated, and P6 is the closest point to the dam.

Since Castanhão is a large and deep reservoir, it would be expected that the water quality variables would present significant spatial variation. However, TP and TN concentration correlation between the three sampling points was significantly high ($p < 0.001$) (Figure S 6A and Figure S 6B, respectively). All the correlation coefficients for TP can be considered perfectly positive ($r > 0.8$), and all the coefficients for TN can be considered strongly positive (Yu *et al*., 2020). This makes evident that those parameters follow similar variation patterns through time in the surface (0.3 m) within the sampling points. A pattern also confirmed by the time series of TP and TN (Figure S25 and Figure S26, respectively), which show that the variation of these parameters is similar through each month.

Figure 4 – Boxplots comparing the values of nutrient concentrations among the sampling points. A) Concentration values for total phosphorus (depth sampling ranging from 0.3 to 25 m), B) for total nitrogen (depth sampling ranging from 0.3 to 25 m). Boxplots comparing nutrient concentration within different depths of P6 at the water column C) Concentration values for total phosphorus, D) for total nitrogen.

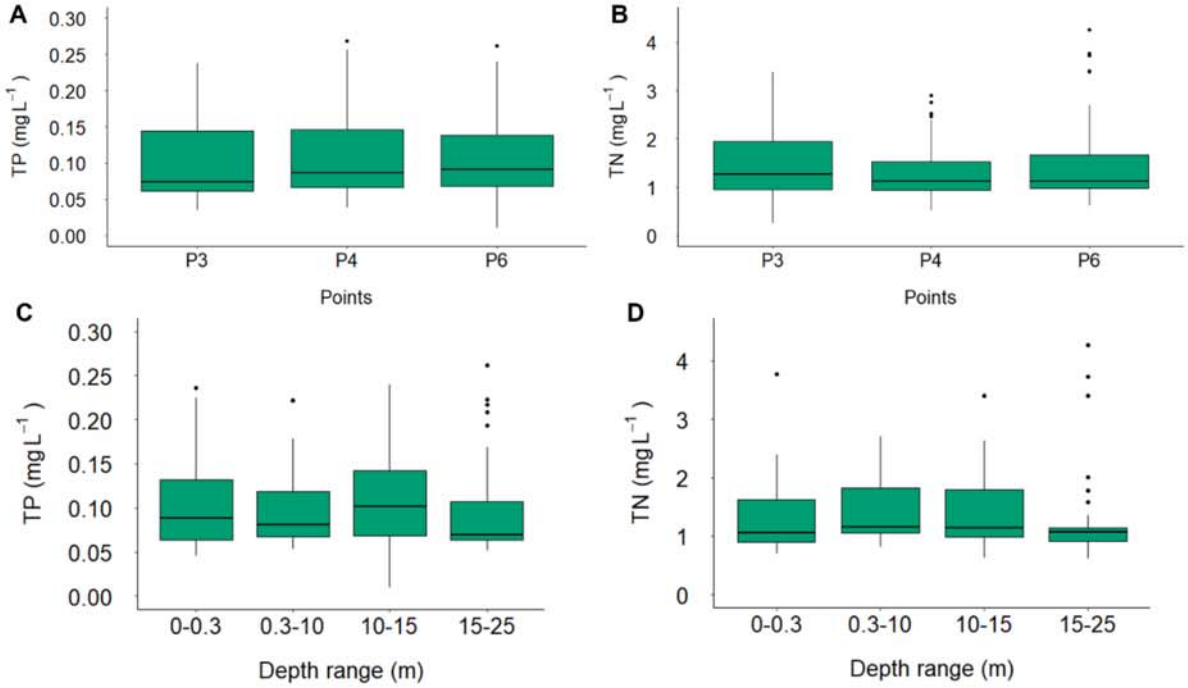

Source: The author.

Figure 4A and Figure 4B shows that the median values of TP and TN concentration for each sampling point are similar, corroborating that there is no significant variation in the horizontal distribution of TP and TN. Similar homogeneous horizontal TP distribution was found in a tropical shallow reservoir located in Ethiopia, where there was a lack of thermal stratification, and consequently a frequent mixing of water column (Tibebe *et al*., 2019).

However, Castanhão could present significant variation in the vertical nutrient distribution (de Oliveira *et al*.,2021). Figure 4C and Figure 4D show that there is no pattern of TP (median 0.07 – 0.1 mg/L) and TN (median 1 – 1.3 mg/L) concentrations within the water column of P6, which is the deepest sampling point. Those results associated with the strong correlation of TP and TN between points (Figure S 6A and Figure S 6B) indicate that the nutrient spatial distribution for Castanhão reservoir can be approximated to a complete mixing. Even though the median values within the vertical profile of TP and TN are similar, it is notable that in the deepest section of the water column there are more outliers than the other depth sections (Figure 4C and Figure 4D). This could be associated with the release of nitrogen and

phosphorus from the sediment layer due to variations on the redox conditions, thermal stratification, pH and the hydrodynamics of the reservoir (Kwak *et al*., 2018). These effects are more pronounced in areas where the water column is deeper and in reservoirs with caged aquaculture activity (Zhang *et al*., 2022) such as Castanhão reservoir.

Nutrient distribution in reservoirs may vary widely from one reservoir to another. For instance, de Oliveira *et al*. (2021) conducted a study in a deep reservoir located in a semiarid climate, while Pearce *et al*. (2017) examined a shallow reservoir in a temperate climate. Both studies reported a spatially uniform distribution of nutrient concentration within their respective studied reservoir. However, it is worth noting that there was an exception to this uniform distribution: the point closest to the dam in both cases. They were probably influenced by the mixture associated with the water intake of the reservoir (de Oliveira *et al*., 2021) and due to higher TP concentration in the sediment of the point closest to the dam (Pearce *et al*., 2017). The distribution of nutrients in reservoirs can be influenced by anthropogenic activities, leading to variations in both TP and TN concentrations within the reservoir (López-Doval *et al*., 2017). Additionally, it has been observed that TP concentrations may vary while TN concentrations remain relatively stable in response to these anthropogenic impacts (Varol, 2020).

Other important factors that can influence the nutrient distribution are thermal, and chemical stratification (Sun *et al*., 2022; Yang *et al*., 2021). So, to understand the complete mixing of nutrients in Castanhão reservoir and its water quality dynamics, it is essential to evaluate physicochemical parameters such as DO, Temperature, and TDS (Section 2.3.3).

In addition, to be more certain of the homogeneous spatial distribution of TP and TN concentration in Castanhão, sampling points located more upstream should be analyzed. For instance, Molisani *et al*. (2015) analyzed nutrient variation in Castanhão reservoir for one year and the TP concentration did not vary much within the sampling points located at the middle of the reservoir, at the cage area, and at the dam (which are close to the sampling points in the present study). However, the authors also analyzed a sampling point that it is not present in our study: the inlet sampling point. This is a sampling point close to the reservoir entrance, which presented significantly higher TP concentration in the study conducted by Molisani *et al*. (2015). The authors suggested that higher values of TP in the inlet point indicated that upstream nutrient sources had a greater impact on water quality conditions in the reservoir than the fish farming area. However, their study was conducted when the reservoir was at 60% capacity,

whereas during the present study, the reservoir's level was much lower (below 20%). Therefore, the potential impact of fish farming on nutrient input can be greater.

2.3.3 Spatial variation of temperature, DO, and TDS

Figure S22 compares the physicochemical water quality parameters of the sampling points. P1, P2, P4, and P5 are in the left branch of the reservoir; P3 is in the right branch of the reservoir; P6 is the closest point to the dam retaining wall. The temperature values of P1, P2, P3, and P4 have similar median values (around 28.5°C) but P5 and P6 presented slightly lower median values (around 28 and 27.5°C respectively) (Figure S22B).

The spatial distribution of TDS appears to be among three groups: P1 and P3; P2 and P4; and P5 and P6 (Figure S22C). The highest values were observed in P5 and P6; and the lowest data dispersion is at P1 and P3. In the present study, conductivity, salinity, and TDS are perfectly positively correlated, therefore the highest values of TDS in P5 and P6 indicate that salinity was also higher in those points. P5 and P6 are also the sampling points with the lowest DO concentrations, which is expected since higher salinity values leads to the water holding less oxygen (Chapra, 2008; Ahmed and Lin, 2021). In addition, higher concentrations of TDS can promote the formation and deposition of Calcium bound phosphorus to the sediment, which is a fraction of phosphorus that can later be released to the water column under low pH conditions (Wen *et al*., 2020).

The observed spatial variation of TDS, and temperature can be determining factors for the spatial distribution of phytoplankton, considering that no significant spatial variation of nutrients was observed on a monthly time scale (Xue *et al*., 2018; Chen *et al*., 2023). This observation can be further used as a tool for predicting cyanobacteria blooms, which is a recurrent challenge in reservoir management.

The TSI values for Castanhão reservoir are all < 1°C/m (Figure S4) which according to Yu *et al*. (2010) means that there is not a significative presence of thermocline. Another index used to estimate the occurrence of thermal stratification is the RWCS, when its value is above 50 it is possible to characterize thermal stratification in the water column (Cui *et al*., 2021a). Figure S 5 shows that there are periods in the Castanhão reservoir where RWCS is higher than 50, with P2 being the sampling point where thermal stratification is the strongest. This analysis confirms that Castanhão does not exhibit as strong or frequent thermal stratification as other reservoirs (Carneiro *et al*., 2023; Noori *et al*., 2021; Yu *et al*., 2010), but the peaks of thermal stratification strength usually occur during the wet season (Figure S 5). This weak and not

frequent thermal stratification can be the main reason of the complete mixing of nutrients in Castanhão reservoir observed in the monthly time scale.

Since the present study was conducted mainly during a drought period, the thermal stratification may be stronger when the reservoir reaches higher capacity, which can cause the absence of complete mixing of nutrients. However, even with its low water volume during drought period, the mean hydraulic residence time (HRT) of Castanhão is around 30 months (Figure S 2), which can be considered a long HRT. For instance, this value is already higher than the one-month limit mentioned by Elçi *et al*. (2007), who states that reservoirs with high water volumes flowing through them (HRT<1 month) would tend not to present thermal stratification. This can indicate that nutrient distribution in Castanhão has a particular behavior not observed in other studies.

The dynamics of DO can be more complex in reservoirs than in lakes due to the different factors that can affect its dynamics, e.g., gradients in flow velocity, thermal stratification, nutrient concentration, organic matter decomposition, and phytoplankton growth (Hudson and Vandergucht, 2015; Yu *et al*., 2010). DO is clearly decreasing from upstream to downstream, where the median values go from around 6.3 mg/L in P1 to around 3 mg/L in P6 (Figure S22A). The point where DO concentration varies the least is P1, which is the sampling point with the higher median value of DO during the studied period, and with the lowest values of SCS (Figure S 3).

DO concentration decreasing from upstream to downstream can be due to the weak thermal stratification at Castanhão reservoir (Figure S 4 and Figure S 5) when compared to the chemical stratification of DO (SCS Figure S 3). When thermal stratification is not strong, there is a much thicker layer of water moving in the downwind direction, which results of sediments reaching further within the reservoir (Elçi *et al*., 2007). Therefore, the sediments can be deposited within greater distances and probably can accumulate more in the most downstream sampling point (P6 – the closest to the dam) of Castanhão reservoir. This sedimentation will later result in organic particle decomposition which can lead to oxygen metaliminetic or hypolimnetic depletion (Gelder *et al*., 2003; Hudson and Vandergucht, 2015). Another important parameter that influences DO dynamics in a reservoir is the phytoplankton activity since photosynthesis can increase DO concentration (Li *et al*., 2015; Conceição *et al*., 2021), therefore this interaction should also be taken into consideration when analyzing the water quality dynamics in a reservoir.

2.3.4 Spatial variation of Chl-a and Cyanobacteria cell density

Similar to TP and TN, Chl-a concentration presented a uniform spatial distribution, with significantly high ($p<0.001$) and strongly positive correlation between the concentrations within the sampling points (Figure S 6C).

This was not as strongly observed for the cyanobacteria cell density (Figure S 6D), where the correlation coefficients were moderately positive ($0.2<r<0.5$). The significance of correlation between P4 and P6 was not significant ($p>0.05$). In contrast, the correlation between the points P3 and P4, and P3 with P6 can be considered significant ($p<0.01$ and $p<0.05$, respectively).

Even though Chl-a correlation between points was strongly positive (Figure S 6C), Figure 5A shows that P3 has slightly higher Chl-a concentration than P6, whereas P3 and P4 present similar median Chl-a concentration (Figure 5A).

Cyanobacteria cell density appeared to follow the same spatial variation pattern as Chl-a (Figure 5B), with higher median values in P3 and P4 and lower median value in P6. However, the spatial differences between the median values of cyanobacteria are higher than the ones for Chl-a. This is corroborated by the lower correlation values for cyanobacteria cell density between the sampling points P3, P4 and P6 (Figure S 6D).

Figure 5 – Boxplots comparing the values of concentrations among the sampling points. A) for chlorophyll a concentration (depth sampling of 0.3 m), and B) for cyanobacteria cell density (depth sampling of 0.3 m).

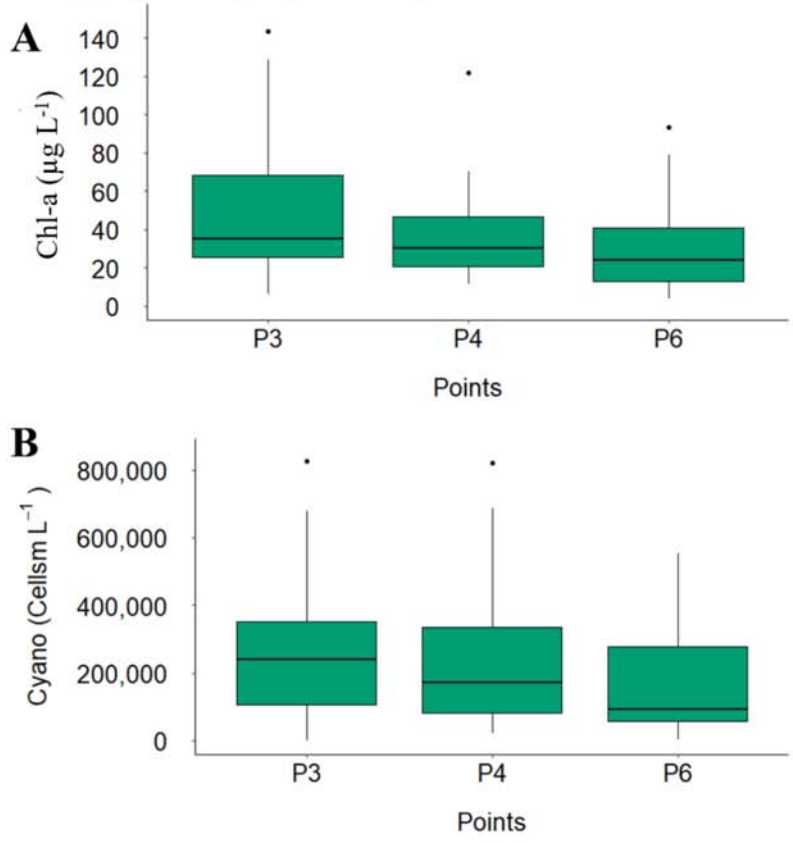

Source: The author.

The fact that the spatial distribution differences of cyanobacteria are higher the ones observed for Chl-a, and that there is no significant correlation between those two parameters (Figure S19, Figure S20, and Figure S21), indicates that Chl-a is not following cyanobacteria cell density variation, which is not the case in other studies, where Chl-a is found as one of the most important variables for cyanobacterial blooms prediction (Park *et al*., 2021; Su *et al*., 2018; Lunetta *et al*., 2015).

This may be because Chl-a serves as a proxy for estimating overall algae biomass, encompassing both eukaryotic algae and cyanobacteria (Li *et al*., 2022). Therefore, it is expected that those organisms would respond differently to an environmental stressor. For instance, cyanobacteria are highly susceptible to competition with algae when there is a limitation of nutrient supply, where cyanobacteria dominate at low N:P ratios (Grover *et al*., 2022). In order to confirm this non-significant association between those organisms, water samples should be collected from different water depths, since there could be uncertainties

associated with assuming that phytoplankton distribution is uniform and with sampling Chl-a only from the surface (Li *et al*., 2022).

Regarding the influence of phytoplankton on the DO concentrations, P4 was the only point that presented a significant correlation between cyanobacteria cell density and DO concentration ($r = 0.58$, $p<0.01$). P4 is also a sampling point with higher DO concentration and cyanobacteria cell density than P6 (Figure S22A and Figure 5B), which is an indicator that photosynthetic activity in P4 is leading to an increase on the cyanobacteria biomass and contributing to an increase in DO concentration (Conceição *et al*., 2021; Li *et al*., 2015).

The spatial variation of phytoplankton cell density and DO concentration indicates that the water intake could be benefited by a selective withdrawal. For instance, this technique could enable epilimnetic water releases, where there is more DO available when comparing with the hypolimnion layer (Duka *et al*., 2021). In addition, the release of warmer waters can contribute to decrease the thermal stability during the rainy season (Wang *et al*., 2024), which is when the peaks of thermal stratification usually occur (Figure S 5).

2.3.5 Temporal variations of water quality parameters

2.3.5.1 Total phosphorus, total nitrogen, and phytoplankton

TP median values clearly increased from 2017 to 2019, then it decreased from 2020 to the beginning of 2022. This decrease was probably due to a dilution effect since the reservoir volume presented a significant intake in 2020 (Figure 3B). The years that presented the highest data dispersion were 2017 and 2020, with values going from around 0.075 mg/L to 0.2 mg/L (Figure S23A). The year 2017 was the one where the hydrological drought was intense and the reservoir volume was significantly decreasing, therefore the nutrient variation was more susceptible to the internal phosphorus loading. As for the year 2020, the reservoir volume substantially increased and the non-point pollution sources were possibly the main factors responsible for the high variation in TP concentration (Lu *et al*., 2021).

As for the intra-annual changes of TP concentration, Figure 6A shows that the month with the highest concentration values was May, which is at the end of the rainy season. This shows that the water inflow of the reservoir is one of the main contributors for the increase of TP in the reservoir. In addition, the data dispersion for this month is lower when compared to the months of January, April and July, which were the months with the highest data dispersion. Indicating that the TP concentration at the end of the rainy season was consistently high. Finally, the months with the lowest TP concentration were March, September, November and December.

Among these, September, November, and December are months within the dry season, when the TP load from reservoir inflow is practically null.

Figure 6 – Boxplots comparing water quality changes within the months, with sampling depths ranging from 0.3 to 24.6 m. A) total phosphorus, B) total nitrogen, C) chlorophyll a and D) cyanobacteria cell density. The horizontal line in each boxplot represents the median value.

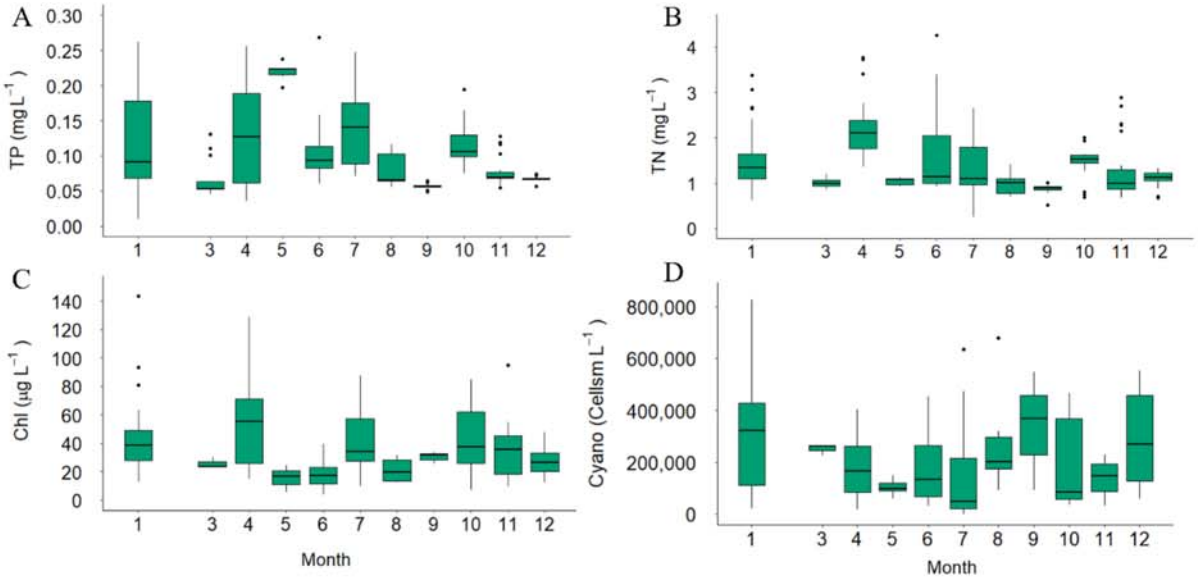

Source: The author.

Between 2016 and 2019 TN median concentration values remained similar until it decreased in 2020, the median going from around 1.6 mg/L to around 0.8 mg/L in 2020, slightly increasing to 1 mg/L in 2021 and 1.2 mg/L in the beginning of 2022 (Figure S23B). This decrease in 2020 was possibly due to the significant increase in the reservoir volume, which caused a dilution effect to dominate the effects on TN concentrations.

Concerning the intra-annual variation of TN, the month with the highest median value was April (around 2.1 mg/L) (Figure 6B). It is possible to observe an increase from March to April (rainy season) and then a decrease pattern from April to July (from around 2.1 to 1 mg/L). Confirming that, like TP, the TN load from the reservoir inflow is an important contributor to the increase in TN concentrations in the reservoir. However, the variation in TP concentration is more pronounced than the one observed in TN concentration (Figure 6).

Chl-a concentration presented a clear increase pattern in the same years that TP also increased (from 2018 to 2019), with median values going from 50 to 80 µg/L (Figure S23C). Then, in 2020 it decreased to a median of 20 µg/L and then increasing to 40 µg/L in 2022. The variation of Chl-a following the one observed for TP concentration is expected since the

increase on nutrient concentration causes an increase on phytoplankton productivity (Guimarães and Neto, 2023; de Oliveira *et al*., 2020).

The month where the median Chl-a concentration was the highest was April (around 60 µg/L) (Figure 6C), which is also the month where TP and TN concentrations start to increase. During the dry period (July to December) the variation pattern of Chl-a (Figure 6C) seems to be similar to the one observed for TP (Figure 6A): increase from June to July, decrease from July to August, and a clear decrease from October and December. However, during the rainy period, those parameters did not present similar variations. For instance, TP increased significantly from April to May, and Chl-a concentration decreased. This may be caused by Chl-a dilution from high inflow and because the increase in sediment loads can limit primary production rates (Dalu *et al*., 2015).

Cyanobacteria cell density increased from 2020 to 2022 (Figure S23D). In addition, the intra-annual variation did not present any clear patterns between rainy and dry season (Figure 6D). This may have happened because cyanobacteria are organisms that can regulate buoyancy in the water column throughout the day in order to find the best environment conditions (Barçante *et al*., 2020). Since the data analyzed in the present study was taken only at the surface (0.3 m depth) it may not have captured in depth information on the behavior of cyanobacteria.

2.3.5.2 Dissolved oxygen, temperature, and total dissolved solids

The median values of DO throughout the years remained around 5 mg/L with higher data dispersion during the years 2017 and 2022 (Figure S24A) but a clear pattern of DO concentration variation was observed between rainy and dry season (Figure 7A). During the rainy season (January to June) the median DO concentration decreases, and the data dispersion increases. In contrast, during the dry season (July to December) median DO concentration increases from June to August and remain similar from August to December. In addition, the data dispersion during dry season considerably decreases when compared to the rainy season.

Figure 7 – Boxplots comparing profiling monitoring variables changes within the months, with sampling depths ranging from 0.3 m under the water surface to 0.5 m above sediment layer. A) presents dissolved oxygen concentrations, B) temperatures, C) Total dissolved solids. The horizontal line in each boxplot represents the median value.

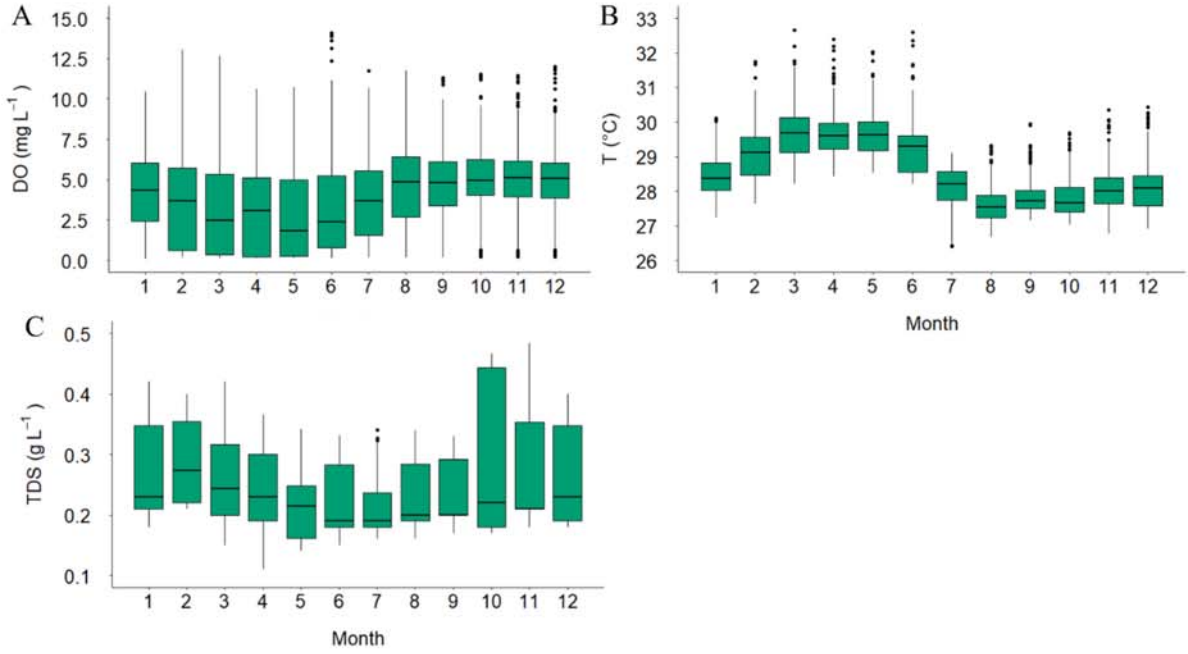

Source: The author.

The high impact of the rainy period on worsening the water quality that was observed in the present study is not observed in all regions. For instance, in the reservoir studied by Li *et al*. (2015), located in a temperate monsoon climate, the heavy rainfall events disturb stratification and causes an increase of DO at the bottom of the reservoir. In contrast, the reservoir studied by Dalu and Wasserman (2018), located in a tropical region, presented better water quality, including higher DO concentration, during dry seasons and the opposite during wet season. This is caused by the heavy rainfall which leads to high nutrient input and the increase water temperature, both effects observed in the present study (Figure 7A and Figure 7B), which contribute to the formation of an anoxic zone at the bottom of the reservoir (Li *et al*., 2015).

At the beginning of the rainy period (January) the temperature starts to increase, the median values remained similar from March to May (Figure 7B). Then, it starts to decrease from June to August and the median remained similar until December, the end of the dry season. In addition, the median values increased from 2016 to 2022 (around 27.5 to 29 °C) (Figure S24B). The increase in the water temperature starts in 2020, which is also the year where the reservoir volume significantly increased (Figure 3A). The temperature increase in 2020 and during the rainy period may be due to a different temperature in the water inflow (Chung *et al*.,

2008; Li *et al*., 2020), which could be confirmed by studying the inflow upstream the reservoir. The fact that water temperature decreases from upstream to downstream of Castanhao reservoir (Figure S22B) also corroborates the hypothesis that the water temperature from the inflow of the reservoir is higher than the water temperature of the reservoir.

In general, TDS concentration decreased from the years 2016 to 2020 (Figure S22C). However, there was a slight increase from 2020 to 2022, but not returning to the same levels as 2016. Between the months of February and June, the median values of TDS also decreased, but remained similar during the other months of the year (Figure 7C). This decrease during rainy season could be due to a dilution effect, and the high TDS concentration values in 2016 and 2017 could be due to the decrease in the reservoir volume, which associated with evaporation contributed to a concentration of dissolved material (Jones and van Vliet, 2018; Li *et al*., 2017).

2.3.6 Pearson's Correlation analyses

Pearson's correlation analysis was performed to verify if there is a pattern on the correlation between the physicochemical parameters (DO, pH, salinity, and temperature) at the top and at the bottom of the reservoir (Figure S7 to Figure S18).

The main pattern observed was that DO concentration was strongly or perfectly positive correlated to the pH at the top and at the bottom of the reservoir ($p<0.001$). Even though pH does not have a direct effect on DO (Banerjee *et al*., 2019), changes in pH can be an important mechanism for nutrient precipitation or release from sediments, which affect the DO concentration (Zhang *et al*., 2014), therefore this positive correlation would be expected.

The correlation between DO and temperature had three main groups. In P1 and P2, DO was moderately positive ($r = 0.29$ and $r= 0.45$; $p<0.05$ and $p<0.001$, respectively) correlated to the temperature only at the surface of the reservoir (Figure S7 and Figure S9). However, at the bottom of the reservoir, DO in P5 and P6 presented a moderately negative correlation with temperature ($r = -0.46$; $p<0.001$, Figure S16 and Figure S18). This may be due to higher photosynthetic activity in P1 and P2 than in P5 and P6, which leads to higher surface DO concentrations. In addition, the higher upstream temperatures can contribute to increase phytoplankton biomass and DO concentration (He *et al*., 2019; Li *et al*., 2021; Pećić *et al*., 2023). As for P5 and P6, the ones with the lowest DO concentration (Figure S22A) and more persistent chemical stratification of DO (Figure *S 3*), the negative correlation between DO and temperature indicates that in those sampling points, temperature can be one of the factors that

is contributing to the low DO concentrations; since higher temperature decreases oxygen solubility in the water (Nong *et al*., 2023; Wei *et al*., 2022). In contrast, P3 and P4 did not show any significant correlation between DO and temperature both at the bottom and at the top of the reservoir.

Regarding the correlation between Chl-a and nutrients, in P3 (Figure S19), Chl-a was strongly positive correlated with both TP (0.56, $p<0.01$) and TN (0.72, $p<0.001$). In P4 (Figure S20), which is the closest point to the fish farming, Chl-a was moderately positive correlated with TP (0.46, $p<0.05$) and strongly positive correlated to TN (0.60, $p<0.01$). However, in P6 (Figure S21), which is closest to the dam retaining wall, Chl-a was not significantly correlated to TP, but it was moderately positive correlated to TN (0.43, $p<0.05$). Depending on the species composition of the phytoplankton in each sampling point, they respond differently to the same N:P ratio in the water (Huo *et al*., 2019; Summers and Ryder, 2023), which could explain why the Chl-a correlation with nutrients varies within the sampling points.

In contrast with other studies (Søndergaard *et al*., 2011), cyanobacteria cell density did not present significant correlation with TP, TN and Chl-a. This could be because cyanobacteria samples were taken at a depth of 0.3 m, it is possible that there is a significant presence of cyanobacteria deeper into the water column (Rosińska *et al*., 2017). Another reason is that for Castanhão, the change in the nutrients and Chl-a concentration may not have an immediate effect on cyanobacteria cell density. For instance, Gu *et al*. (2020) found that phosphorus loads affected only the maximum cyanobacteria biomass, but not the growth cycle. They concluded that the growth cycle of cyanobacteria was not related to phosphorus concentration.

2.4 Conclusions

The spatio-temporal variation of several water quality parameters and their interactions were assessed in Castanhão reservoir, situated in the Brazilian semiarid region. The results indicate that TP and TN concentrations did not exhibit significant variation among the sampling points. This uniform distribution of nutrients can be attributed to the weak thermal stratification observed in the Castanhão reservoir, where the chemical stratification of dissolved oxygen prevails over thermal stratification. These findings suggest the feasibility of applying a complete-mixing model for evaluating nutrient dynamics in reservoirs within semiarid regions in future studies.

The spatio-temporal variation of several water quality parameters and their interactions were assessed in Castanhão reservoir, situated in the Brazilian semiarid region. The results indicate that TP and TN concentrations did not exhibit significant variation among the sampling points. This finding suggests the feasibility of applying a complete-mixing model in a monthly time-step for evaluating nutrient dynamics in reservoirs within semiarid regions in future studies. The observed uniform distribution of nutrients can be attributed to the weak thermal stratification observed in the Castanhão reservoir, where the chemical stratification of dissolved oxygen prevails over thermal stratification It is noteworthy, however, that although thermal stratification is not a frequent occurrence, it typically manifests during the rainy season. This season is characterized by higher water temperatures compared to the dry season, suggesting the possibility of warmer water entering the reservoir during this period. To confirm this hypothesis, a detailed analysis of the inflow water temperature is essential. During the rainy season, a noticeable degradation in water quality occurred, marked by peak concentrations of TP and TN. This underscores the significance of temporal variation of nutrients which surpassed spatial variation. Additionally, dissolved oxygen concentrations displayed significant spatial and temporal patterns. DO concentration decreased from upstream to downstream, with notable decline during the rainy season, resulting in hypoxia levels. Given that this condition is favorable to fish mortality events, the rainy season emerges as a critical window for reservoir managers to implement preventive measures.

Chlorophyll a exhibited a uniform distribution across the sampling points and displayed positive correlations with both TP and TN. However, cyanobacteria cell density did not exhibit significant correlations with nutrients and chlorophyll a, contrary to previous studies.

The absence of significant spatial variation in nutrient distribution suggests that the assumption of complete nutrient mixing can be applied to develop models of phosphorus dynamics in order to predict phosphorus concentrations in the reservoir based on the different sources of this nutrient. This can be an important tool for water managers to simulate scenarios and decide on a water allocation plan that minimizes the negative impacts on the water quality of reservoirs within similar regions. However, it is essential to consider the spatial variation of dissolved oxygen when assessing the internal loading of phosphorus. It is worth noting that the analysis of cyanobacteria in this study was limited to the reservoir's surface. Future studies examining the variation of cyanobacteria cell densities and other parameters throughout the water column throughout the day could be valuable for managing and predicting harmful

cyanobacteria blooms, as these organisms are known to adjust their depth to optimize photosynthesis.

Furthermore, this study focused on physico-chemical and biological data within the reservoir itself. Given the significant deterioration in water quality during the rainy season, future studies could include an assessment of water quality from upstream tributaries to gain a more comprehensive understanding of the system.

3 DIEL AND SEASONAL MIXING PATTERNS AND WATER QUALITY DYNAMICS IN A MULTIPURPOSE TROPICAL SEMIARID RESERVOIR

3.1 Introduction

Tropical semiarid regions experience significant temporal and spatial climatic variability, leading to an increased occurrence of extreme drought periods (Pontes Filho *et al*., 2020; Wiegand *et al*., 2021). To address water scarcity consequences, reservoirs have been constructed worldwide (Rabelo *et al*., 2022). However, prolonged drought periods, coupled with irregular precipitation and high evaporation rates, render these reservoirs in semiarid regions vulnerable to water quality deterioration and eutrophication (Rocha and Lima Neto, 2022; Guimarães and Lima Neto, 2023). Eutrophication causes many negative effects on water quality including oxygen depletion, high phytoplankton biomass, and complications in drinking water-treatment (Dalu and Wasserman, 2018). Furthermore, in a region where water is a scarce resource, reservoirs serve diverse purposes (Santos *et al*., 2016), which can cause conflicts among various stakeholders. A prominent example is the Castanhão reservoir, an important large, deep, tropical semiarid reservoir situated in the Brazilian semiarid region, primarily dedicated to human consumption, irrigation, and fish farming (de Lacerda *et al*., 2018; Rocha and Lima Neto, 2021). Fish farming activity is associated with substantial nutrient emissions with the potential to impact sediment composition and to increase the eutrophication potential (Santos *et al*., 2016; Henry-Silva *et al*., 2019). This activity associated with drought events and the significant decrease in reservoir water level caused the water quality to deteriorate and increased the occurrence of fish mortality events.

A fundamental step to unravel the water quality dynamics of a reservoir is to comprehend its thermal and chemical stratification regime. Recent research by Melo Rocha *et al*. (2024) has revealed that chemical stratification of dissolved oxygen (DO) in a semiarid reservoir surpasses thermal stratification, resulting in the homogeneous distribution of nutrients throughout the reservoir. However, this observation was based on monthly parameter analyses, whereas tropical reservoirs are particularly susceptible to presenting diel thermal stratification cycles (Augusto-Silva *et al*., 2019). Therefore, the nutrient distribution may not be homogeneous if there is a diel cycle of thermal stratification. For instance, the existence of diel cycles thermal stratification can generate hypoxia events and, consequently, influence the internal loading of phosphorus by increasing the release of P from bed sediment to the water column (Cavalcante *et al*., 2021). Therefore, a diel analysis can be a tool for water managers to

act in order to prevent hypoxia events. However, there are several important aspects that can influence the thermal stratification cycles, such as water depth, temperature, inflow, and wind speed (Flores *et al*., 2024). Furthermore, a diel assessment of water quality is crucial for also comprehending the distribution of nutrients and phytoplankton within the reservoir, particularly cyanobacteria, which actively migrate within the water column in search of optimal nutrient and light conditions (O'Neil *et al*., 2012).

While several studies have explored water quality dynamics in reservoirs (Shilei *et al*., 2020; Noori *et al*., 2021; Shi *et al*., 2022;), few have undertaken diel evaluation of water quality variables, but not on tropical semiarid reservoirs. Some existing research has focused on diel analysis of water quality in tropical or subtropical lakes, but they focused on the thermal stratification variables, not including key aspects of the water quality such as nutrients and phytoplankton community variables (MacIntyre *et al*., 2002; Macintyre *et al*., 2014; Augusto-Silva *et al*., 2019; Liu *et al*., 2019). Even though the study by Herrera and Nadaoka (2021) assessed diel variations in physical, chemical, and biological variables, it was performed in a shallow lake (maximum depth of 2.5 meters), primarily dedicated to aquaculture, which differs markedly from many multipurpose reservoirs in the semiarid region. Furthermore, a few studies were conducted in tropical semiarid reservoirs to better understand their hydrodynamics and water quality dynamics using 2D modelling (Rocha *et al*., 2022; Lima Neto, 2023). However, water quality data was usually scarce since there was no extensive field monitoring data on a diel scale such as the one performed in the present study.

Therefore, our primary objective is to use data from diel monitoring campaigns in a tropical semiarid reservoir in order to investigate if there are diel cycles of thermal and chemical stratification of DO and how they potentially influence water quality dynamics in a daily scale. We conducted two monitoring campaigns during the rainy season and two during the dry season to incorporate seasonal variations. Specifically, we aimed to answer the following questions: Is there a diel cycle of thermal stratification and DO in this reservoir? Is there a spatial variation in the nutrients and phytoplankton distribution within the reservoir on throughout the day? Do the diel patterns change seasonally?

3.2 Materials and methods

3.2.1 Study Area

This study was conducted in the Castanhão reservoir, located in the Brazilian semiarid region (Figure 8). The reservoir, commissioned in 2002. It has a storage capacity of

6.7 billion cubic meters, a dam crest elevation of 111 m, and a catchment area of 45,309 km² (Ceará, 2022a). Its main water uses include human consumption, fish farming and agriculture.

Figure 8 - Map of the study area, the Castanhão reservoir located in the Brazilian semiarid region. The sampling point P6 is the one closest to the dam retaining wall, and P7 is the high-density fish farming area.

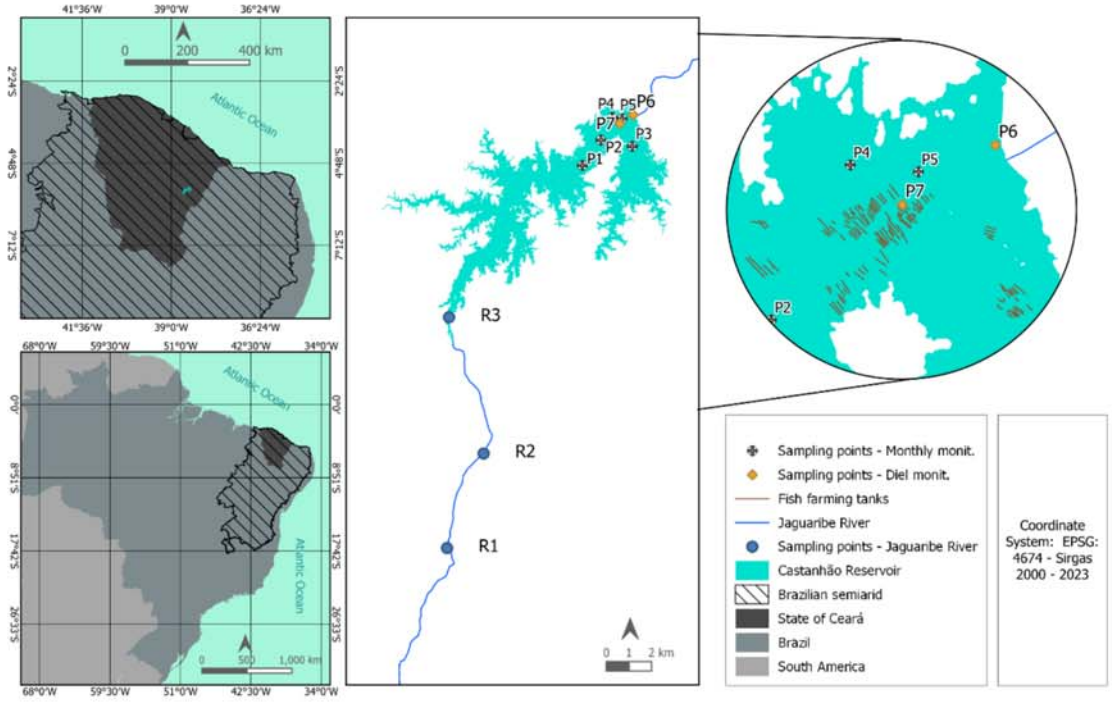

Source: The author.

Castanhão is situated in a region characterized by shallow soils in the crystalline geological formation (Ceará, 2022b). The main land uses are agriculture with irrigated crop production, subsistence agriculture, and animal husbandry (Ceará, 2022b). The climate in the semiarid region presents predominantly irregularities in rainfall, both in time and space. It presents an annual mean rainfall usually ranging from 400 to 1,000 mm and with an annual mean temperature of 27.85°C. The rainfall occurs mainly from January to March (Santos *et al.*, 2016). Potential evaporation in this region can reach about 2,100 mm. The rainfall regime and the high evaporation contribute to generating intermittent rivers and to high water level variations in the reservoirs (Molisani *et al.*, 2013).

The annual average of rainfall in Castanhão's catchment is 836 mm/year. During the dry season, the inflow to the reservoir is nearly null. Between 2016 and 2022, the average monthly inflow during rainy season was 66.62 million m³ and the maximum value of around

500 million m^3/month, while the outflow ranged from 10 to 50 million m^3/month (Melo Rocha *et al*., 2024).

The region encountered severe drought conditions from 2012 and 2018, leading to a substantial decline in the reservoir's volume from 75% to approximately 2% (Ceará, 2022a). Consequently, the drought had a significant impact on the water quality, where its trophic state alternates between eutrophic and hypereutrophic conditions.

3.2.2 Water quality sampling campaigns

We performed four diel campaigns with a 24-hour period analysis in four different dates: two during the dry season (October 19th, 2021 and November 8th, 2022) and two during the rainy season (March 30th 2022 and May 31st 2023).

At each diel campaign, there were two types of data collection. First, water samples were collected at three different depths in order to analyze several water quality variables: the phytoplankton cell counts (subdivided in cyanobacteria and phytoplankton cell count in general excluding cyanobacteria) (Apha, 2017; Margalef, 1983; Utermohl, 1958; Lund *et al*., 1958); total phosphorus (TP) (4500-P-J and 4500-P-E, Apha,2017), total nitrogen (TN) (4500 P-J and 4500-NO3--E, Apha, 2017), nitrate (4500-NO3-, Apha, 2017), nitrite (4500-NO2-, Apha, 2017) and Chl-a (10200 H, Apha, 2017); ammoniacal nitrogen (350.2, USEPA, 1974). Then, the water profiling was performed using a YSI EXO 2 probe to measure dissolved oxygen (DO), temperature, and pH. These variables were measured from surface (0.3 m depth) every 0.5 m until reaching 8 m depth, then the measurements were carried out each 1 m until it reached 0.5 m above the sediment layer.

The campaigns collected water quality data at two different locations: P6, the point closest to the dam, and P7, the point located in the largest fish farming area (Figure 8). Except in the May 2023 campaign, where only the profiling data collected with the probe was available.

In order to compare the water temperature in the inflow of the reservoir, temperature measurements were performed once a month in both the reservoir and the main tributary of this reservoir. In the tributary, temperature readings were obtained at three distinct sampling points labeled as R1, R2, and R3. Meanwhile, within the reservoir, water temperature measurements were recorded at six different sampling points designated as P1, P2, P3, P4, P5, and P6 (Figure 8). Also, int these sampling points, monthly water sampling was conducted in order to quantify chlorophyll-a concentration (Chl-a).

3.2.3 Data analysis

The strength of thermal and chemical stratification (for DO) throughout the day was analyzed. This analysis was essential to facilitate comparisons between the rainy and dry seasons, as well as between our selected sampling points, P6 and P7. Relative Water Column Stability (RWCS) coefficient was calculated to evaluate thermal stratification within the water column (Carneiro *et al*., 2023). RWCS ≥50 was considered as a reference to characterize the thermal stratification in the water column (Cui *et al*., 2021). The RWCS coefficient (Equation 5) was calculated as follows:

$$RWCS = (\rho_B - \rho_s)/(\rho_4 - \rho_5) \quad (5)$$

Where ρ_B and ρ_s represent the water density (g/L) at the bottom and surface of the water column, respectively. Additionally, ρ_4 and ρ_5 denote the water densities at 4 and 5 °C, respectively.

To compute these water densities, Equation 6 was employed, which assumes normal atmospheric pressure and disregards water salinity (Carneiro *et al*., 2023).

$$\rho = a_0 + a_1T + a_2T^2 + a_3T^3 + a_4T^4 + a_5T^5 \quad (6)$$

In which the coefficients are: a_0 = 999.842594, a_1 = 6.793953× 10−2, a_2 = − 9.095290× 10−3, a_3 = 1.001685× 10−4, a_4 = − 1.120083× 10−6 and a_5 = 6.536332 × 10−9. An RWCS ≥50 was considered as a reference to confirm thermal stratification in the water column.

In the present study, the Strength of Chemical Stratification for Dissolved Oxygen (SCS) was employed to assess the strength of chemical stratification related to DO concentrations within the water column. A null SCS indicates the absence of chemical stratification for DO (Noori *et al*., 2021).

The SCS is computed using the formula:

$$SCS = \frac{DO_S - DO_B}{0.5 \times (DO_S + DO_B)} \quad (7)$$

In this equation, DO_S represents the DO at the surface (at a depth of 0.3 meters), while DO_B corresponds to the DO concentration at the bottom (0.5 meters above the sediment layer) of the reservoir. An SCS value of zero indicated a mixing condition (Noori *et al*., 2021).

These indices allow to quantify and understand the thermal and chemical stratification patterns in the present study, providing valuable insights into the reservoir.

The data processing was carried out using R (R Core Team, 2022). To assess temporal variations in the studied variables throughout the diel analysis, boxplots were employed. Additionally, profiles of temperature, DO, and pH were constructed to detect diel patterns. To determine the statistical significance of variations between median values, a three-step analysis was performed. First, the Shapiro-Wilk normality test was applied to assess the normal distribution of the data. Subsequently, the Kruskal-Wallis test was employed to evaluate overall differences among groups. Finally, post hoc pairwise comparisons were conducted using the Dunn test, with the Bonferroni adjustment for multiple comparisons. A significance level of 0.05 was utilized throughout the statistical analysis.

To determine the statistical significance of variations between median values of the samples, a series of analysis were performed. First, the Shapiro-Wilk normality test was applied to assess the normal distribution of the data. Subsequently, the non-parametric test Kruskal-Wallis was applied to evaluate overall differences among groups. Finally, post hoc pairwise comparisons were conducted using the Dunn test, with the Bonferroni adjustment for multiple comparisons. A significant level of 0.05 was utilized throughout the statistical analysis. In addition, the relationship between the variables was analyzed using Pearson's correlation coefficient. A significance level of 0.05 was chosen to determine statistical significance.

3.3 Results and discussion

3.3.1 Analysis of the temperature distribution

The variation of the water column temperature is depicted in Figure 9, a heatmap for over a 24-hour period. This enables the evaluation of whether a daily cycle of thermal stratification exists or not. At P6 during the rainy season (March 2022), as shown in Figure 9B, a consistent thermal stratification persists throughout the day, with no discernible homogenization of the water column. In contrast, Figure 9C demonstrates a diel cycle of thermal stratification during the dry season (November 2022). Stratification peaks in the afternoon, coinciding with increased water temperature. Subsequently, as water temperature declines, its distribution within the water column becomes more uniform, reaching maximum homogeneity around 4 AM. A pattern also observed Figure 9A October 2021 (dry season). However, Figure 9D shows that at the end of the rainy season (May 2023), the stratification-destratification pattern is more similar to the one

observed during the dry season (Figure 9A and C). Rocha *et al*. (2022) similarly observed greater stratification stability in the 2D model simulation during the rainy season in a semiarid reservoir. This finding contradicted their initial expectations, as they had anticipated complete mixing due to the influence of inflow velocities on reservoir stability. Regarding P7, the same patterns of thermal stratification observed in P6 occurred (Figure S 34), indicating that the area where the fish farming activity is more concentrated does not have a direct impact on the thermal stratification regime within the water column.

Figure 9 - Temperature profiles at the sampling point P6 in A) October 2021, dry season, B) March 2022, rainy season, C) November 2022, dry season, and B) May 2023, rainy season.

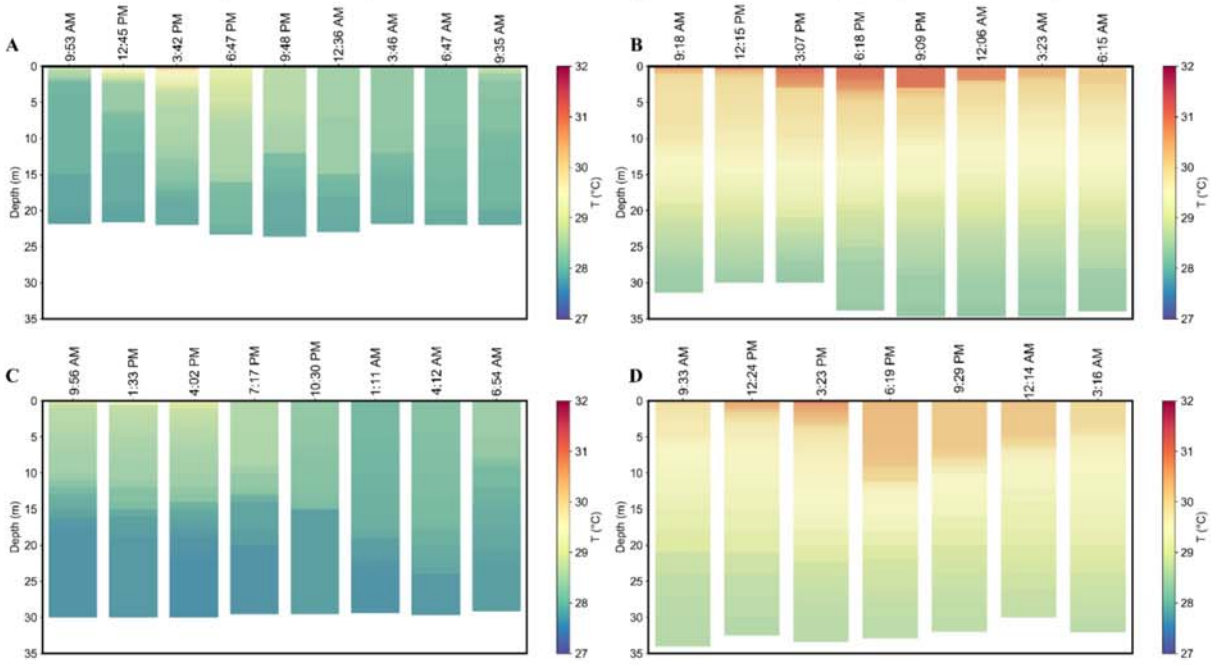

Source: The author.

To confirm the observed patterns with the previous heatmap (Figure 9) and to conduct a more objective analysis of the variation in thermal stratification throughout the day, the RWCS index was calculated (Figure S 35). Considering that an RWCS value above 50 indicates the occurrence of thermal stratification, it was confirmed that in the analysis conducted in March 2022 (rainy season), the water column exhibited thermal stratification throughout the entire 24-hour period, as the RWCS remained above 50. The maximum RWCS value recorded on this date was 100 at P7, which is lower than the value observed by Cui *et al*. (2021) during a period of stratification (approximately 200). However, this discrepancy can be attributed to the difference in reservoir depth between Cui *et al*. (2021) and the present study, with maximum depths of 60 m and 30 m, respectively.

In contrast, the analyses of October 2021 and November 2022 (dry season) showed a cycle of stratification and destratification throughout the day, as observed in Figure S 35. The RWCS calculated for the analysis of May 2023 (rainy season) indicated that on this date, a cycle of stratification and destratification occurred, although less intense than observed in October 2021 and November 2022.

Those results further support the hypothesis of stronger thermal stratification during the rainy season. However, the apparent stratification cycle observed in the end of the rainy season of 2023 (May) is a daily pattern similar to the one observed during the dry season analysis, with RWCS values surpassing 50 only during the early to midafternoon hours. This difference suggests a potential link between the occurrence of thermal stratification and reservoir inflow. Indeed, preceding the diel analysis in March 2022, there was a notable increase in reservoir volume, whereas the analysis conducted in May 2023 coincided with a decrease in reservoir volume (Figure S 36).

Further analysis of the inflow water temperature showed that during the rainy season of 2022 the inflow water temperature was higher than the temperature in the reservoir (Figure S 37A). Therefore, possibly due to the significant inflow during the rainy season, it created a density gradient that contributed to thermal stratification (Fenocchi *et al*., 2017; Duka *et al*., 2021;). In addition, monthly RWCS calculations in several sampling points of the reservoir showed that, during the rainy season, a majority of the reservoir sampling points exhibits values either above or close to 50 (Figure S 37B), which serves as a robust indicator of significant stratification.

Another important factor that possibly contributed to the more intense thermal stratification observed in March 2022 is the significant difference ($p<0.05$) between the water temperature when comparing the rainy and dry seasons. During the rainy season, temperatures are consistently higher than during the dry season, which is a pattern also observed in other Brazilian semiarid reservoirs as reported by Carneiro *et al*. (2023) and as reported by Melo Rocha *et al*. (2024) for the same reservoir but at a monthly timescale. The increase in water temperatures is a well-known contributor to intensified thermal stratification (Wei *et al*., 2022; Miao *et al*., 2023).

Wind speed variation throughout the day in March and November 2022 was analyzed (Figure S 38), since this is another factor that influences thermal stratification and contributes to the occurrence of a diel cycle (Azadi *et al*., 2021; Yang *et al*., 2021). In March

2022, at the beginning of the rainy season, wind speeds remained relatively low, with maximum values below 3 m/s. However, the median wind speed throughout the day in November 2022 is significantly higher ($p<0.05$) than the median observed throughout the day in March 2022, with a maximum speed of 9 m/s in November 2022. Furthermore, a Pearson's correlation analysis performed with data from 2022 revealed a significant ($p<0.05$) and strong negative correlation ($r=-0.67$) between wind speed and RWCS. This implies that stronger wind speed contributes to less thermal stability of the water column. Therefore, during the dry season, thermal stratification in the studied reservoir is significantly influenced by wind intensity, even though it is a deep reservoir, as shallow reservoirs are typically more susceptible to wind-induced turbulence (Augusto-Silva *et al*., 2019; Luo *et al*., 2022).

In tropical reservoir studies, the prevailing observation has been a dominance of diel thermal stratification cycles over seasonal variations (Araújo *et al*., 2017; Herrera and Nadaoka, 2021). However, our present study reveals a far more intricate dynamic. Contrary to recent investigations of tropical reservoirs, we have identified distinct patterns of thermal stratification: a stable stratification during the rainy season and a diurnal stratification cycle during the dry season.

Notably, Curtarelli *et al*. (2014) examined a large tropical reservoir that exhibited complete mixing during the austral summer, which is their rainy season. Only on days without mesoscale convective systems activity diurnal stratification occurred. Which is what usually occurs because high inflow volumes are capable to cause vertical disturbance and significantly reduce water column stability (Li *et al*., 2015). This contradicts the findings of the present study, where in March (rainy season) there is a thermal stratification event throughout the entire day.

Additionally, even though Cavalcante *et al*. (2007) observed a minor diel temperature cycle in a large, deep tropical reservoir similar to the one in the present study, but this cycle was during the rainy season, also further contrasting our findings. Furthermore, even though Hu *et al*. (2015) explored a large, shallow subtropical reservoir, which usually presents a diel cycle of thermal stratification, it lacked any discernible thermal stratification pattern. These disparities underscore the necessity of considering multiple parameters to comprehensively understand the hydrodynamic processes within reservoirs.

3.3.2 Analysis of dissolved oxygen distribution

3.3.2.1 Temporal variation

The intensity of dissolved oxygen diel variations followed a similar seasonal pattern as the one observed in temperature variation at both P6 (Figure 10) and P7 (Figure S 39): a diel cycle of DO stratification and destratification in the dry seasons and a stable stratification during the rainy season.

Figure 10 - Dissolved oxygen profiles at the sampling point F in A) October 2021, dry season, B) March 2022, rainy season, C) November 2022, dry season, and B) May 2023, rainy season.

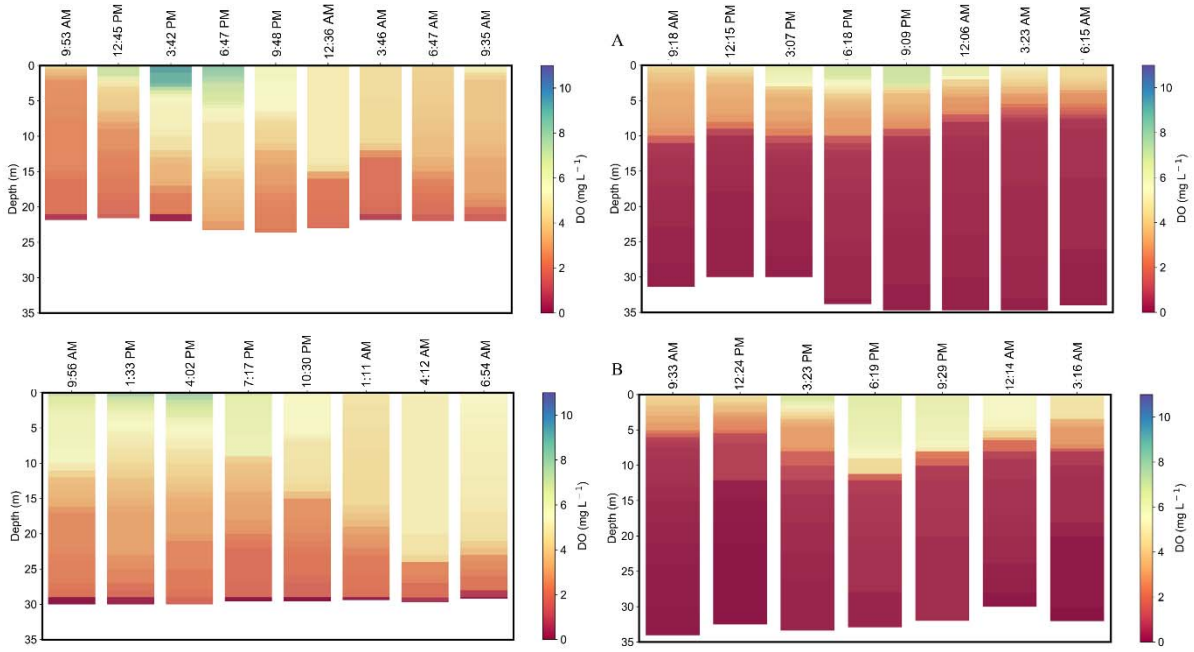

Source: The author.

The SCS was calculated to provide a more objective comparison of DO stratification variations within the day and within the seasons. The SCS values confirmed that the chemical stratification was strong and occurred during both rainy and dry seasons, where most of the values remain above one the entire day (Figure S 40) marking the occurrence of a DO stratification.

However, the heatmap of DO within the water column (Figure 10) highlights that, during the rainy period (both in March 2022 and May 2023), DO throughout the water column exhibits notably lower values compared to those observed in October 2021 and November 2022 in both P6 and P7 (Figure 10 and Figure S 39). During the rainy season, both sampling points exhibited DO concentrations approaching zero in over half of the water column (Figure 10A).

There are several factors that influence the DO variation in the studied reservoir. First, rain events can contribute to the reduced availability of DO due to the transport of sediments and nutrients into the reservoir with rainfall (Arora *et al*., 2017; Flores *et al*., 2024). Also, the stronger thermal stratification when there is inflow to the reservoir, as previously

discussed, contributes to limit the exchange within the water column and, consequently, it limits the vertical transfer of oxygen in the water column (Miao *et al*., 2023). Finally, the location of the reservoir in a tropical semiarid area, makes it more susceptible to the occurrence of eutrophication and, therefore, oxygen depletion (Cunha and Cunha, 2023).

The water volume of the studied reservoir significantly varies both within the seasons and within the years e.g., due to the occurrence of drought periods. Even though it is large and deep, this reservoir presented significant water quality deterioration due to a drought period that occurred in the region between 2012 and 2018 (Pontes Filho *et al*., 2020; Sousa Estacio *et al*., 2022), where the reservoir water quality went from oligotrophic to eutrophic/hypereutrophic (Ceará, 2023).

Therefore, the pronounced seasonal disparity in DO levels is further intensified by the eutrophication within the examined reservoir. This eutrophication primarily stems from multiple factors, including the reduction in water volume, the influx of external nutrients and organic matter, as well as the nutrient discharge associated with fish farming activities (Henry-Silva *et al*., 2019). Additionally, internal nutrient release from sediments under anoxic conditions contributes significantly to this phenomenon (Rocha and Lima Neto, 2022).

3.3.2.1 Spatial variation

The detail of how the DO concentration varies throughout the day in both P6 and P7 is shown in Figure 11. In October 2021, the diel variation of DO concentration at P7 is smaller than at P6 where at P7 the only significant difference between the median values throughout the day is between 11 AM and 8 PM ($p<0.05$) (Figure 11B). Whereas at P6, the median values of DO at the same date significantly vary throughout most of the day (Figure 11A). In March 2022 there was no significant difference throughout the day within both sampling points (Figure 11C and D), with P6 presenting median values lower than 1 mg/L throughout the entire day. In November 2022, the only significant difference throughout the day was in P6 between 1 AM and 7 PM (Figure 11E). In May 2023, the DO concentrations in P6 significantly varied ($p<0.05$) throughout the day while in P7 there was no significant difference ($p>0.05$) (Figure 11G and H).

Figure 11 - Boxplots presenting the dissolved oxygen variations throughout the day at each measurement time in an analysis at P6 during the A) Dry season of 2021 in P6, B) Dry season of 2021 in P7, C) Rainy season of 2022 in P6, D) Rainy season of 2022 in P7, E) Dry season of 2022 in P6, F) Dry season of 2022 in P7, G) Rainy season of 2023 in P6, and H) Rainy season of 2023 in P7. The horizontal line at each boxplot represents the median values within the water column.

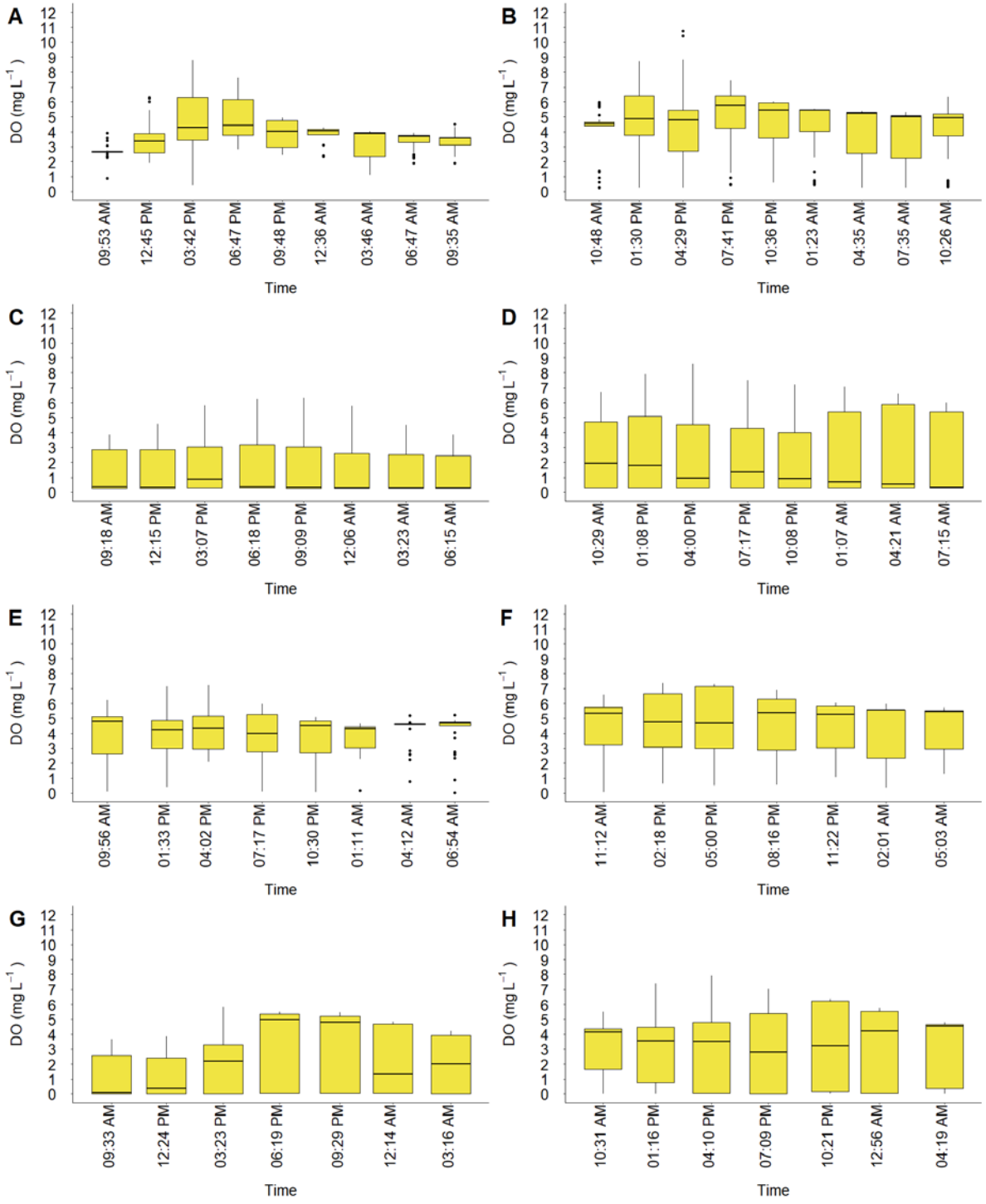

Source: The author.

The fact that the median value of DO vary more significantly throughout the day at P6 than at P7 is possibly linked to the photosynthetic activity within the reservoir. Observing Figure 11, it is evident that, overall, there is greater dispersion of DO data measured at P7 compared to P6. This increased dispersion highlights a greater contrast between surface and bottom DO concentrations, suggesting that P7 is more influenced by phytoplankton photosynthetic activity. Consequently, it can be concluded that DO concentrations at P6 vary more significantly throughout the day than those at P7, as the variation in DO at P6 throughout the day is more pronounced than its variation throughout the water column. Conversely, the opposite occurred at P7.

This observation is corroborated by the significant strong positive correlation between cyanobacteria abundance and DO ($r=0.52$, $p<0.05$) as well as between Chl-a and DO ($r=0.52$, $p<0.05$). Confirming that in the studied reservoir, the phytoplankton community significantly influences DO dynamics, with photosynthesis contributing to oxygen production (Justus *et al*., 2019; Portinho *et al*., 2021; Cooray *et al*., 2022). Furthermore, Pearson's correlation revealed a strong negative correlation between DO and depth ($r=-0.77$, $p<0.05$), confirming the impact of photosynthesis in the epilimnion and the hindrance of DO circulation to the hypolimnion due to thermal stratification (Zhang *et al*., 2015; Li *et al*., 2020).

3.3.3 Nutrient distribution

3.3.3.1 Temporal variation

Total phosphorus diel variation presented different seasonal patterns. During both dry season dates (October 2021 and November 2022) there were no significant differences throughout the day observed between the median TP values at each measurement point (Figure S 43). However, there was a notable increase in TP concentrations throughout the day during the rainy season (March 2022) in both sampling points. Figure 12 provides a detailed comparison of TP variations throughout the day between P6 and P7 in March 2022. In both monitoring points, TP concentrations were consistently higher during nighttime compared to the morning and afternoon, presenting a two-fold median increase. It is worth noting that P6 exhibited more pronounced variations in TP concentrations within the water column compared to P7 as it presents more data dispersion.

Figure 12 - TP concentration variation throughout the day in March 2022, during the rainy season. The horizontal line at each boxplot represents the median values within the water column.

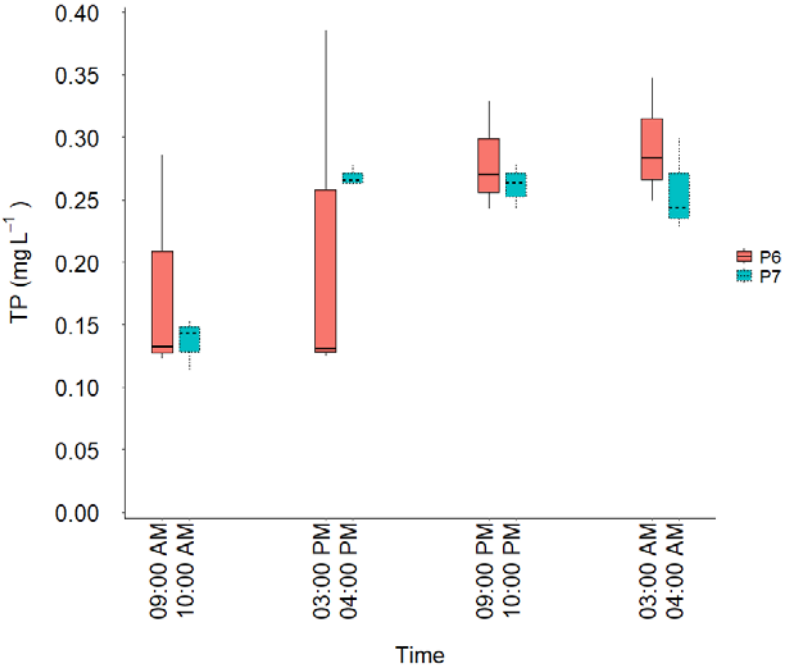

Source: The author.

The increase in TP concentration throughout the day may be attributed to two distinct processes. Firstly, it is well-established that, in stratified bodies, such as observed in March 2022, photosynthesis significantly influences reservoir dynamics. In the presence of light, photosynthesis generates oxygen at the expense of nutrients in the epilimnion (Cooray *et al*., 2022). In contrast, the hypolimnion is characterized by organic matter decomposition, leading to oxygen depletion and nutrient accumulation (Cooray *et al*., 2022). Consequently, in the absence of light, photosynthesis ceases, resulting in the decrease of nutrient consumption by phytoplankton. A similar pattern was also observed in an experiment conducted by Wang *et al*. (2019), wherein hours of light were associated with lower concentrations of soluble reactive phosphorus, while algae decomposing was linked to an increase in this component during late hours of the day.

Another critical factor is the oxygen depletion in the hypolimnion, which favors the release of phosphorus from sediments, further contributing to its increase (Lima Neto *et al*., 2022; Moura *et al*., 2020; Rocha and Lima Neto, 2022). With the reduction of nutrient consumption through photosynthesis, TP increase and accumulation during nighttime would be expected. Additionally, during the rainy season, there is a significant influx of TP into the

reservoir, further contributing to its increase. This understanding helps explain the observed diel increase in TP concentration during the rainy season, specifically from afternoon to night.

When comparing the seasonal variation of TP concentrations, Figure 13 shows that during the rainy season, TP median concentration increased approximately threefold in comparison to the analyses conducted during the dry season. This observation reinforces the importance of conducting additional studies on the reservoir inflow. The reservoir's location, surrounded by potential TP sources—both point and non-point (Souza *et al.*, 2017) — emphasizes the necessity for in-depth research in this area.

Figure 13 - Difference in TP concentration between the measurements at each month. The horizontal line at each boxplot represents the median values within the water column.

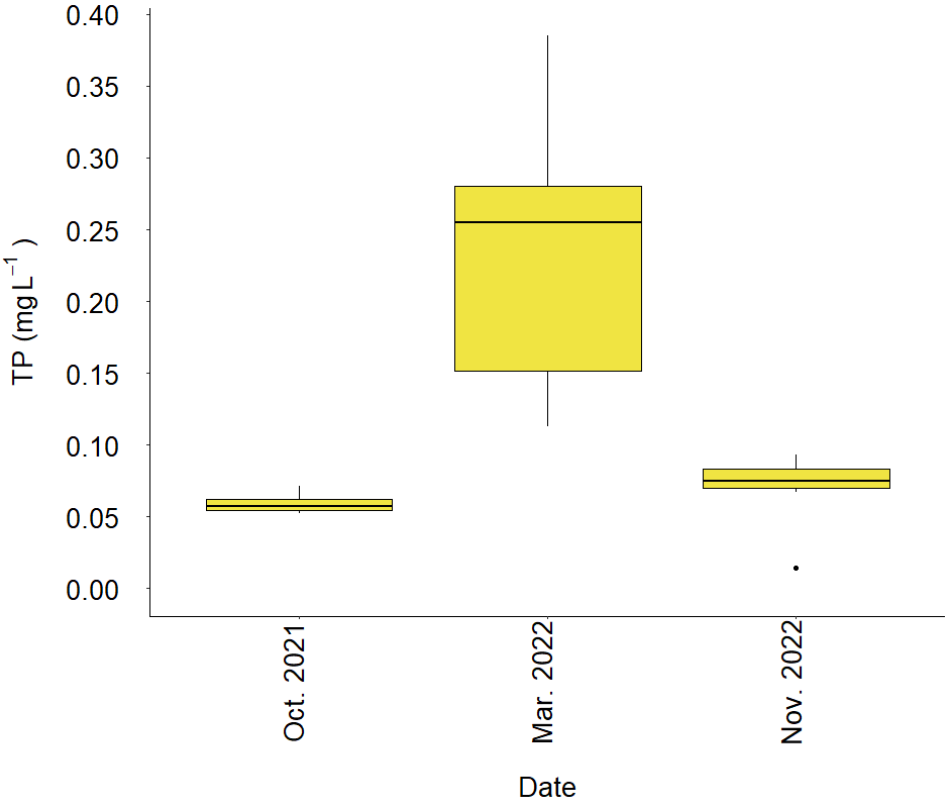

Source: The author.

Finally, there was no clear seasonal or diel variation pattern on TN, nitrate, nitrite, and Ammoniacal nitrogen concentrations. This could indicate that in the reservoir's catchment there is a dominance of point and non-point pollution of phosphorus instead of nitrogen. However, since the nitrogen dynamics in a reservoir is complex and depends on several factors, a long-term and detailed studies on the nutrient input to the reservoir should be performed in

order to evaluate this hypothesis (Shen *et al*., 2013; Rocha and Lima Neto, 2023; Yu *et al*., 2023).

3.3.3.2 Variation with depth

Total phosphorus usually increases with depth in a reservoir, due to its consumption by photosynthetic organisms at the surface and the possible release of phosphorus from the sediment to the water column. However, TP concentration presented this trend during the entire day only in March 2022 at P6. Furthermore, TP concentrations remained practically homogeneous within the water column at P7 (Figure S 51B). The results of correlation confirmed that there was no significant trend of variation of TP within the water column.

In contrast, orthophosphate exhibited a decrease trend with depth at all three diel analyses (Figure S 52). This was confirmed by the significant moderate positive correlation between orthophosphate and depth ($r = 0.44$, $p<0.05$). This contradiction between TP and orthophosphate patterns is probably because the dynamics of phosphorus within the water quality is being highly regulated by the phytoplankton community. Since Orthophosphate is an inorganic fraction of phosphorus that is directly available to the phytoplankton community (Krempin *et al*., 1981; Sharmin *et al*., 2020; Wen *et al*., 2020). Thus, it would be expected that the variation of Orthophosphate with depth would be significant, since the majority of the organisms that consume this nutrient tend to remain at the surface.

As for TN, there was no clear variation trend with depth throughout the day but in October 2021, P7 presented more variation of TN concentrations within the water column throughout the day than P6 (Figure S 53A). Which was the opposite of what occurred in March 2022, where throughout the entire day TN concentrations increased with depth at P6 but remained practically unchanged at P7 (Figure S 53B). In November 2022, TN concentrations varied with depth in the morning, before 5 PM, and remained practically homogeneous at night (Figure S 53C). Even though the pattern of TN variation with depth changed according to the diel analysis measurement, correlation analysis indicates that the general pattern for TN was that it increased with depth ($r=0.25$, $p<0.05$), which was moderately positive. This pattern is expected since the main processes that occur are the consumption of nutrients by phytoplankton at the surface and an internal recharge at the bottom of the water column (Barbosa *et al*., 2019; Grover *et al*., 2022; Sun *et al*., 2022).

3.3.3.3 Biomass variation

Usually, Chl-a and TP are positively correlated (Burkholder *et al*., 2022; Chen *et al*., 2022), since the more nutrients available, it is expected that the phytoplankton would respond positively. However, in the present study we found a significant moderate negative correlation between Chl-a and TP ($r = -0.37$; $p<0.05$). This is possibly because the drivers of Chl-a can vary according with the temporal resolution (Nunes Carvalho *et al*., 2022; Zhang *et al*., 2018). Since the present study evaluated the diel variation of nutrients, the consumption of nutrients by the phytoplankton community was possibly the process that predominated in the data.

In addition, the period with more detailed values of Chl-a concentration within the water column available was the rainy period, in March 2022. So, the accumulation of TP throughout the day during the rainy season (Section 3.3.1) could have predominated over the dry season dynamics, which may have contributed to the significant negative correlation between Chl-a and TP. This highlights that depending on the time scale the water quality of a reservoir is studied, there are different processes that predominate the interaction of nutrient dynamics with the phytoplankton community.

Chl-a concentration median was significantly higher in October 2021 than in March and November 2022 (Figure S 46). In October 2021, the median concentration was around 26 µg/L while the median concentration was around 13 and 11 in March and in November 2022, respectively. When comparing the Chl-a concentration difference between the sampling points, Figure 14A shows that the median concentration at P7 is significantly higher than at P6 ($p<0.05$). In addition, Figure 14B depicts the variation of Chl-a throughout the day at both sampling points. This demonstrates how the concentration of Chl-a at P7 is higher than at P6 throughout the entire day, which indicates the impact of the high-density fish farming area on increasing the phytoplankton abundance.

Figure 14C shows a time series of the variation of Chl-a concentrations within several sampling points within the reservoir. There is no clear upstream to downstream pattern on the Chl-a variation, which supports the hypothesis that the higher Chl-a concentrations at P7 may be due to an impact of the fish farming activity. Furthermore, Figure 14C also shows that the sampling point with the highest Chl-a concentration within the reservoir in the majority of the time-series is P3. This is possibly because this sampling point is in the right branch of the

reservoir, which is the one that does not receive direct input from the river and, therefore, is a more lentic zone, with higher retention time (Soares *et al*., 2012).

Figure 14 – Comparison of the impact of the fish farming activity on the chlorophyll a concentration the reservoir. A) shows the difference in chlorophyll a concentration between the sampling points. Sampling point D is the one closest to the dam and F is the sampling point in the fish farming area, B) shows the Variation of chlorophyll a concentration throughout the day in March 2022 (rainy season), and C) Monthly variation of chlorophyll-a concentration within several sampling points in the reservoir. The horizontal line at each boxplot represents the median values within the water column.

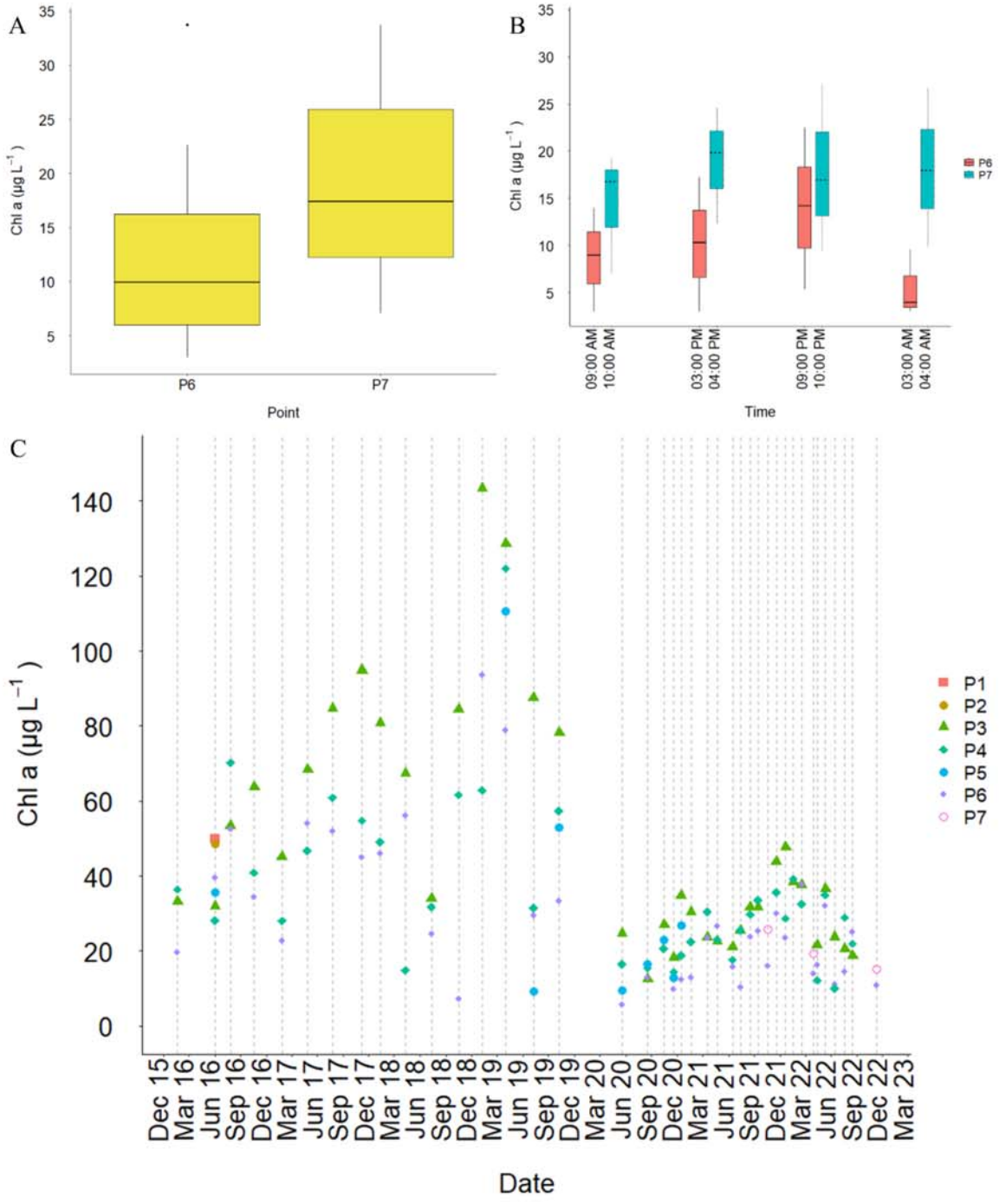

Source: The author.

Regarding the general abundance variation of cyanobacteria and other organisms in general, in October 2021, surface samples analyses show that P7 exhibited higher abundance of cyanobacteria cells than P6, with the peak abundance being over 1.2 x 106 cells/mL at P7 at 11 AM (Figure S 47). However, when analyzing the abundance of other organisms of the phytoplankton community (Figure S 48), P6 presented higher abundance values than at P7 throughout the entire day, with peak abundance at P6 being over 7,000 cells/mL.

In contrast, in March 2022 (rainy season) there was no clear tendency between the sampling points since the abundance of cyanobacteria consistently varied throughout the day (Figure S 49). This was the same case for the abundance of other organisms of the phytoplankton community (Figure S 50). This suggests that, during the rainy season, both sampling points present high occurrence of phytoplankton due to the nutrient inflow in the reservoir.

It is interesting to remark that there was a significant moderate negative correlation between other organisms from the phytoplankton community and depth ($r=-0.35$, $p<0.05$), but there was no significant correlation between cyanobacteria abundance and depth. This could be explained by the fact that cyanobacteria can regulate their depth within the water column according to the best conditions (O'Neil *et al*., 2012; Barros *et al*., 2019; Barçante *et al*., 2020;).

Furthermore, there was a strong negative correlation between pH and depth ($r=-0.68$, $p<0.05$), which could be due to phytoplankton photosynthesis process. Since this process absorbs CO2 and releases O2 which increases the pH in the epilimnion. With an increase of depth, photosynthesis process decreases and consequently pH decreases (Portinho *et al*., 2021; Wei *et al*., 2022).

The importance of the phytoplankton community on pH variation was confirmed by the strongly positive correlations between other organisms of the phytoplankton community abundance and Chl-a with pH ($r=0.52$, $p<0.05$; $r=0.67$, $p<0.05$, respectively) and a moderately positive correlation between cyanobacteria abundance with pH ($r=0.41$, $p<0.05$).

3.4 Conclusion

Our study revealed that a diel cycle of thermal stratification dominates during the dry season, which was highly correlated to stronger wind speed values in this season. In contrast, during the rainy season, a stable thermal stratification pattern is influenced by warmer water from the reservoir's inflow, highlighting the intricate relation of climatic conditions on thermal

stratification. Notably, the chemical stratification of DO occurs at both dry and rainy season, differently than thermal stratification.

The inverse correlation between TP and Chl-a and the twofold increase of TP concentration throughout the day during the rainy season revealed that in a diel time-scale analysis, there is a significant impact of nutrient consumption by photosynthesis on the diel TP balance. Another key finding was that TP concentration increased threefold during the rainy season, but there was no clear seasonal variation of TN concentration.

However, it is essential to acknowledge certain limitations of the present study. There is a need for further analysis to comprehensively assess the impacts of the rainy season in the reservoir using water quality data from the reservoir's inflow. Additionally, expanding the scope of diel analysis to other months of the year would explain whether the trends identified in this study are seasonal or monthly in nature. Lastly, this study calls for more comprehensive investigations into phytoplankton data within the water column during dry seasons, as the present study was limited to surface data during this period.

In conclusion, these findings advance our knowledge of semiarid reservoir diel dynamics, underscoring the intricate interplay of climatic, hydrodynamic, and biological factors in shaping water quality. This study provides a foundation for future research to further explore into these interactions and their implications for effective reservoir management and conservation.

4 MODELING NUTRIENT INFLOW TO AN TROPICAL SEMIARID RESERVOIR

4.1 Introduction

Eutrophication of aquatic ecosystems such as reservoirs is a recurrent water quality issue worldwide. This problem is continuously growing due to many influencing factors surrounding the river catchments, e.g., alteration of land-use patterns, farming activities, usage of pesticides, fertilization, improper operation of septic tanks etc. (Athauda *et al.*, 2023; Mamun, Ferdous and An, 2021; Oliveira, de *et al.*, 2020). Eutrophication has several negative consequences such as oxygen depletion due to the excessive amount of organic matter produced by algal blooms, possible production of toxic substances, and increase in water treatment costs (Padedda *et al.*, 2017). In addition, eutrophication can hinder the multiple uses of water in a reservoir (Barbosa *et al.*, 2019). The main drivers for eutrophication are nitrogen and phosphorus (P), with the latter being usually the limiting one in freshwater ecosystems (Sun *et al.*, 2022). Nutrients can enter reservoirs from various sources, including both point and non-point origins (Kong *et al.*, 2015). One of the most challenging sources to estimate is the non-point input, which mainly occurs when nutrients are carried into the reservoir through storm runoff (Li *et al.*, 2015). Therefore, the application of effective measures to remediate the eutrophication of reservoirs demands a quantitative and qualitative understanding of the sources and drivers of nutrient input (Xiong *et al.*, 2021).

Tropical semiarid regions frequently go through drought periods, high interannual precipitation variation which generates intermittent rivers (de Lacerda *et al.*, 2018; Lima Neto *et al.*, 2022). Consequently, the reservoirs located in this region are more vulnerable to the negative effects of nutrient input and eutrophication. Hence the difficulty that many reservoirs in this region encounter to meet national water quality standards (Rocha and Lima Neto, 2021).

Physical-based and empirical models are options commonly used to estimate nutrient input with good accuracy (Li *et al.*, 2017). Physical-based models are widely used to evaluate the nutrient input in reservoirs and lakes, since they accurately represent the many processes that drive the water quality dynamics (Fong *et al.*, 2023; Robertson, Saad and Koltun, 2022). However, these models demand a large amount of data and computational resources which can limit the calibration and validation process.

The high complexity and data demand of physical-based models created the need for the development of models that are less complex but also present good predictions. In that

context, development of research using empirical models to estimate nutrient input in lakes and reservoirs is continuously increasing. They can be used combined with mechanistic models (Kong *et al.*, 2015) or by themself (Montefiore and Nelson, 2022).

A widely used approach in empirical modeling is to use data-driven modes. Specifically, to use surrogate variables to predict the desired variable. Studies using other water quality variables as surrogates were performed with accurate and relevant results. For instance, they were applied to estimate the nutrient concentration (Castrillo and García, 2020; Schilling, Kim and Jones, 2017), to assess the risk of the presence of microcystin, a cyanotoxin, in the water of a reservoir (He *et al.*, 2021), and to evaluate the importance of climate and hydrological variables on the chlorophyll a concentration in semiarid reservoirs (Guimarães and Lima Neto, 2023; Nunes Carvalho, Lima Neto and Souza Filho, 2022).

Rocha and Lima Neto (2021) applied empirically-fitted models to several semiarid reservoirs and obtained accurate results, but it was limited to an analysis of P and the data was still scarce and would not allow for comparing different model approaches. Therefore, there is still a gap on studies that focus on analyzing the water quality patterns in river sections upstream eutrophic reservoirs and on comparing different model approaches to predict nutrient input in Tropical semiarid water bodies.

Therefore, this paper aims to evaluate the water quality trends and patterns of one of the largest rivers in the Brazilian semiarid region in the sections upstream Castanhão reservoir, which attends to human supply, irrigation, and fish farming. In addition, we aim to develop a novel methodology that uses surrogate variables that are easily measured to predict the nutrient concentration. Specifically, we aim to 1) Validate a methodology of estimating the flow rate based on a reverse water balance; 2) Evaluate the spatio-temporal variation of water quality in the river; 3) Compare different models using surrogate variables that are simple to obtain during field monitoring to predict the TP and TN concentrations in the river.

4.2 Materials and Methods

4.2.1 Study Area

The present study focused on the Jaguaribe river basin (Figure 15), located in the state of Ceará, Brazil, with 72,645 km² (Molisani *et al.*, 2013). This watershed is in a semiarid region, where there are two main seasons during the year: rainy and dry. The high interannual variability of the rainfall, associated with high evaporation rates contribute to Jaguaribe being

an intermittent river that has its main flow during the rainy season (January – July). The main activities held in the basin are irrigated crop production and animal husbandry (Ceará, 2024) (Rocha and Lima Neto, 2021).

The river sections studied in the present paper are upstream the largest multiple use reservoir in Brazil: Castanhão reservoir. With 6.7 billion cubic meters, this reservoir suffers from constant eutrophication, fish kills, and proliferation of cyanobacteria.

Figure 15 – Map of the study area: the location of Brazil within South America and the state of Ceará within Brazil, with indication of the Brazilian semiarid region, Castanhão reservoir, and its drainage network (left panels). Representation of Jaguaribe river and the sampling points in the present study (right panel).

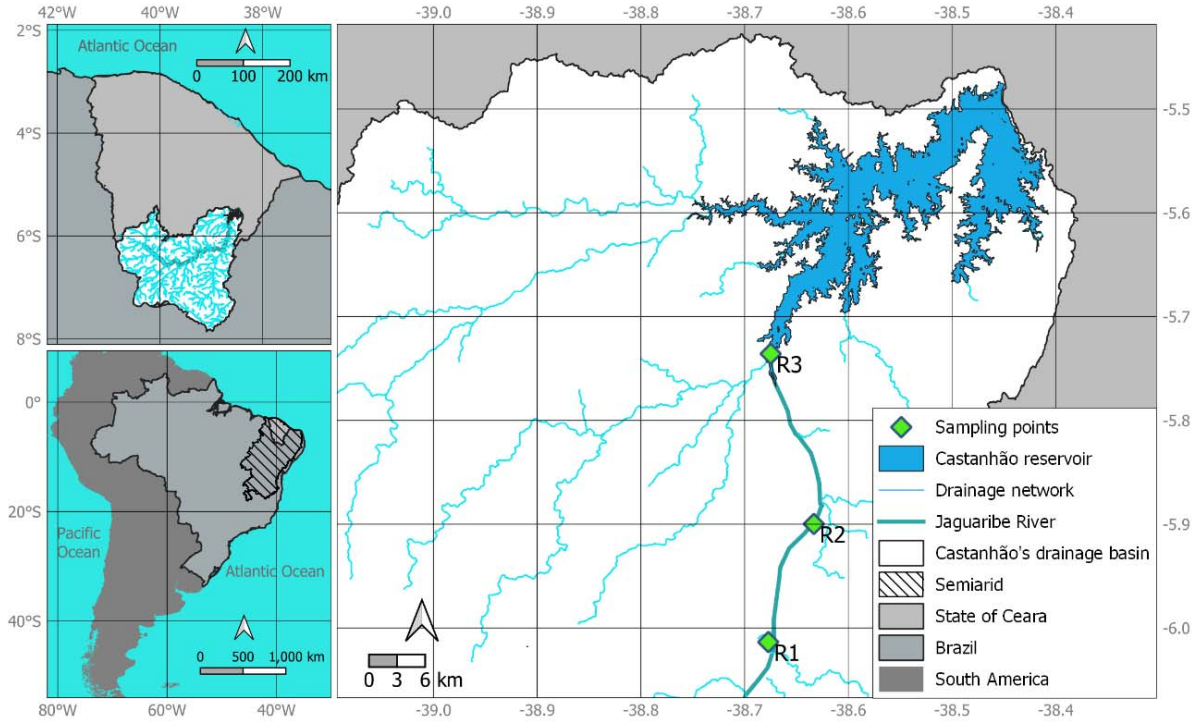

Source: The author.

4.2.2 Data acquisition and methodology

The present study utilized quarterly water quality data collected from three distinct sampling points along the Jaguaribe River (R1, R2, R3), situated upstream of Castanhão Reservoir. In general, the data collection spanned from August 2016 to June 2023. In this period, water quality was monitored using a YSI EXO 2 probe to measure DO, temperature, salinity, total dissolved solids (TDS), and pH. The parameters TP, TN, nitrite, nitrate, biochemical oxygen demand (BOD), turbidity, and true color (TC) were estimated following APHA (2017).

The ammoniacal nitrogen was estimated following USEPA, (1974) and the average flow rate in the river sections was measured using the Sontek Riversurveyor - M9.

The period used to assess spatial differences on the water quality and flow rate within the Jaguaribe River was between June 2021 and January 2023. This period was selected to accommodate the inclusion of sampling point R3 in later monitoring campaigns. In addition, the sampling campaigns were mainly conducted at nearly the same time, with a maximum difference of 30 to 40 minutes.

One of the objectives of this paper was to validate the water balance calculations to estimate the inflow in Castanhão reservoir by comparing the calculations with the flow rate measurements in the sampling points.

The average flow rate in the Jaguaribe river can be calculated using the daily water level data from Castanhão reservoir, which enables the estimation of inflows to the reservoir using a water balance calculation. The following equations (Ceará, 2021) were applied:

$$^{dV}/_{dt} = Q_{in}(t) - Q_{out}(t) \quad (8)$$

$$Q_{out,i} = E_i + WS_i + GF_i + Q_{PS} \quad (9)$$

Where $^{dV}/_{dt}$ is the time variation of the stored volume V, Q_{in} represents the reservoir inflow (m^3 day^{-1}), and Q_{out} represents the outflows that were considered for Castanhão reservoir (m^3 day^{-1}): the volume evaporated – Q_E, the flow for continuous water supply – Q_{WS}, the gate flow – Q_{GF}, and the pumping station flow – Q_{PS}.

The volume evaporated E was estimated by multiplying the monthly reference evaporation rate for the lake by the average surface area of the lake on day i. The average surface area was calculated by the level-area curve, considering the measured levels at the beginning of days i and i + 1. The reference evaporation rate (considered constant for each month of the year) was defined by the evaporation calculated at the reference meteorological station for Castanhão reservoir established by COGERH (Ceará, 2021).

Figure 16 presents a summary of the methodology that was applied in the present study. The data was processed and modeled using R Core Team (2022). In addition, the relation between the variables was analyzed using Pearson's correlation. Then, linear regression was performed using the flow rate as an explanatory variable to predict several important water quality parameters such as TP, TN, turbidity, salinity, DO, temperature, etc. Finally, other models were applied in order to predict TP and TN concentrations in the Jaguaribe river.

Figure 16 - Scheme of the methodology applied in the present study.

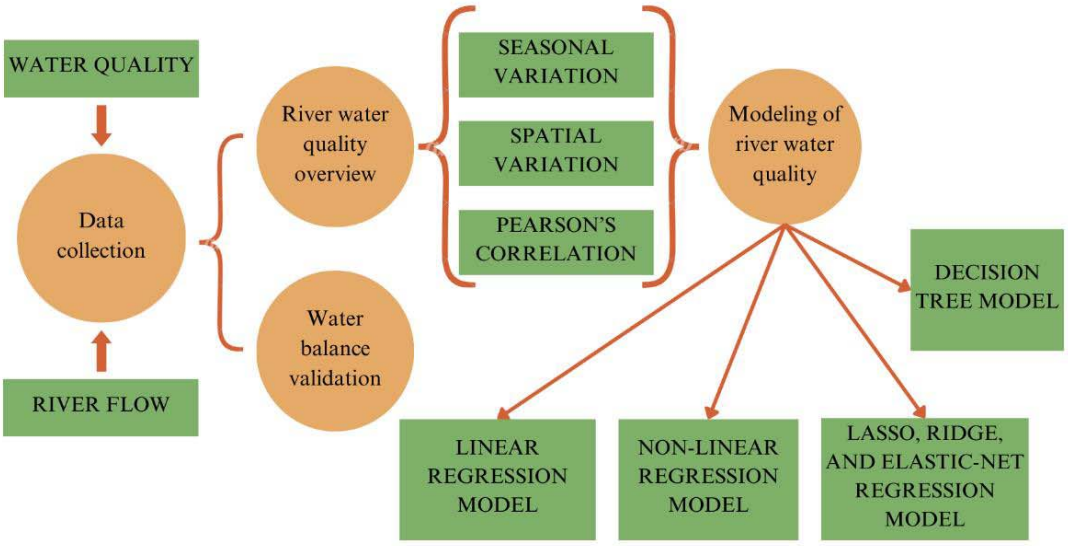

Source: The author.

4.2.3 Models

Linear regression model was applied to find which water quality variables presented linear relationship with the flow rate.

In addition, four non-parametric machine learning models were applied to predict TP and TN concentrations in the river and a transient complete-mix model was also applied to predict TP concentrations. Their performance was then compared to assess which one would be the best prediction model. Data for this comparison was randomly split into training (75%) and testing (25%) datasets using the R package "caret". The metrics that were used to compare the model performances were the Nash-Sutcliffe coefficient (NSE), the coefficient of determination (R^2), and the root mean squared error (RMSE). The RMSE and the R^2 was calculated also using the R package "caret", whereas the NSE was calculated using the R package "hydroGOF".

4.2.3.1 Linear regression model

Linear regression aims to use explanatory/independent variables to predict a dependent variable (James *et al*., 2013). As shown in the equation below:

$$Y = \beta_0 + \sum_1^m \beta_j X_j \quad (10)$$

Where X_j is a vector for the jth independent variable, β_j and β_0 are unknown parameters that represent the slope and the intercept, respectively, and m is the number of

explanatory variables. The algorithm calculates the unknown parameters by minimizing the sum of the squared residuals (SSR) i.e., the difference between measured and predicted value.

In the case of the present study, the flow rate was the explanatory variable used to predict several important water quality parameters: TP, TN, turbidity, salinity, DO, temperature, Nitrate, Nitrite, Ammoniacal Nitrogen, BOD, pH, TC, and TDS.

4.2.3.2 Regularized Regression Models

Regularization is a technique where penalties can be added to the model to reduce their variance and, therefore, prevent overfitting. This is particularly useful in shorter datasets. Ridge, Lasso, and Elastic-Net regression were the three techniques applied in the present study (James *et al*., 2013; Nunes Carvalho, Lima Neto and Souza Filho, 2022).

Lasso regression adds a penalty to the sum of the absolute coefficients (ℓ1 penalty), and it can cause a variable selection by setting coefficients to zero if λ is sufficiently large. λ determines how severe the penalty is and it assumes a positive value.

$$SSR_{Lasso} = \sum_{j=1}^{n}\left(y_{o,i} - y_{p,i}\right)^2 + \lambda \sum_{j=1}^{m} |\beta_j| \quad (11)$$

Where $y_{o,i}$ is the observed value, $y_{p,i}$ is the predicted value, n is the number of observations, β is the coefficient vector, and m is the number of explanatory variables.

The Ridge regression adds a penalty to the square of the magnitude of the coefficients (ℓ2 penalty). This penalty shrinks the coefficients, but it keeps all the variables in the model:

$$SSR_{Ridge} = \sum_{j=1}^{n}\left(y_{o,i} - y_{p,i}\right)^2 + \lambda \sum_{j=1}^{m} {\beta_j}^2 \quad (12)$$

The combination of the two penalties is the elastic-net regularization, this technique is controlled by the parameter α, which ranges from 0 (Ridge) to 1 (Lasso).

4.2.3.3 Regression Tree

The decision tree model provides a set of rules that explain the relationship between the explanatory and dependent variables. Regression tree is a type of decision tree that selects the average of the observed values within each subset that minimizes the mean squared error (James *et al*., 2013).

4.3 Results and discussion

4.3.1 Overview of water quality characteristics in the Jaguaribe River

4.3.1.1 Temporal variation

Figure 17 presents the seasonal variation of DO, Temperature, and pH in each sampling point. During the dry season, the median value of DO is higher in R1 (the most upstream sampling point) than in R2 and R3. Which is the opposite of what is observed in the rainy season, where the highest median value of DO was observed in the most downstream sampling point (R3) (Figure 17A). This difference could be due to the high sediment and nutrient runoff during rain events, which increases turbidity and, consequently, decreases the DO (Allen *et al.*, 2020). This can be confirmed by the significant negative correlation between TP and DO (R = - 0.53) observed in the analyzed data and by the fact that, during the rainy season, the sampling point where the DO was the highest, the TP concentration was one of the lowest (R3) (Figure 18).

R3 presented the lowest median value of pH and temperature during the dry season, whereas, during the rainy season, the median values within the sampling points were similar, highlighting the impact of seasonality on the spatial variation of water quality. In general, median temperature values were higher and median pH values were lower during the rainy season comparing to the dry season. Median concentration values of TN increased during the rainy season (Figure 18B) but not as substantially as the increase observed in TP concentration (Figure 18A), suggesting that TP is the predominant nutrient in the downstream reservoir during rainy season and, consequently, has more potential to impact reservoir water quality.

Pearson's correlation analysis shows that the inflow was significantly correlated with TP (r = 0.62), DO (r = -0.53), and TDS (r = -0.69), but not with TN (r=0.05). This confirms the previous hypothesis that the main nutrient input in the reservoir is due to storm runoff is TP.

Figure 17 - Seasonal variation of A) dissolved oxygen, B) temperature and C) pH within the three different sampling points upstream Castanhão reservoir in Jaguaribe River (R1, R2, R3) from June 2021 to January 2023.

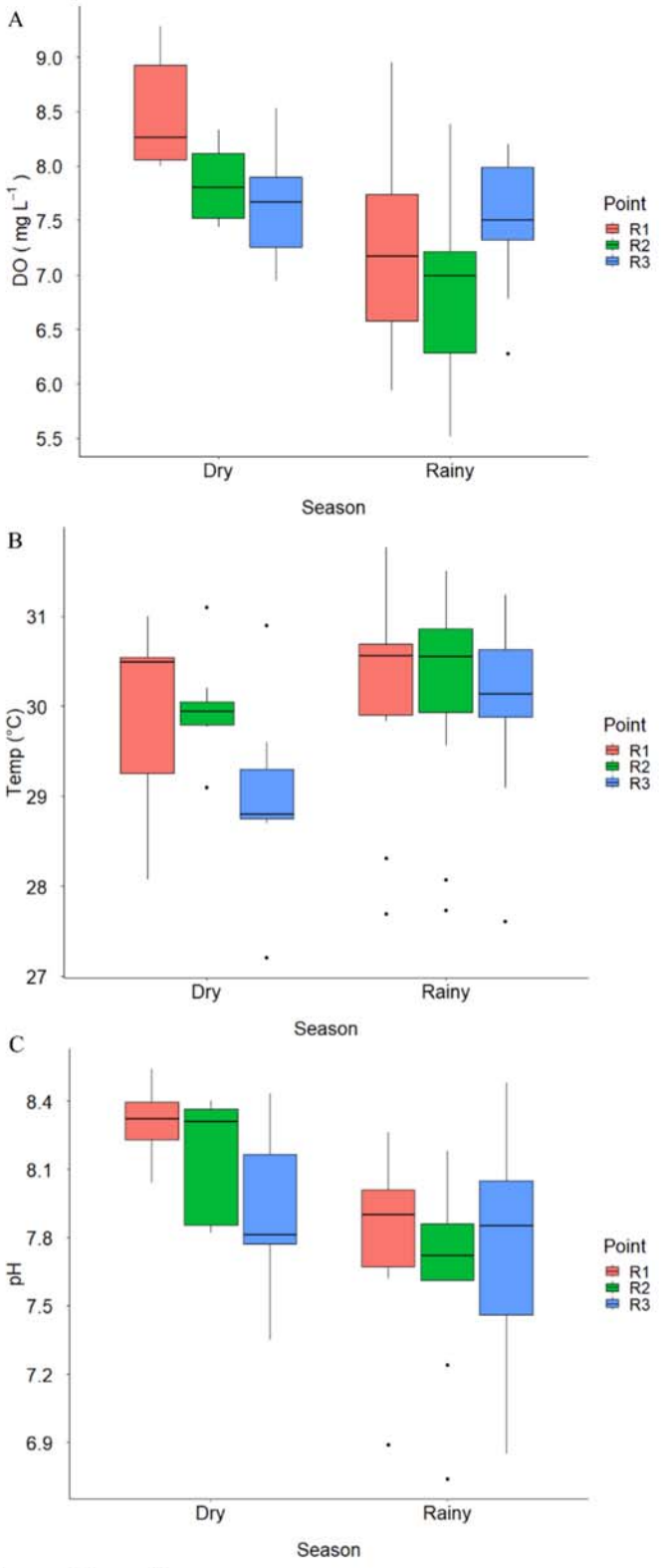

Source: The author.

Figure 18 - Seasonal variation of A) total phosphorus and B) total nitrogen concentration within the three different sampling points upstream Castanhão reservoir in Jaguaribe River (R1, R2, R3) from June 2021 to January 2023.

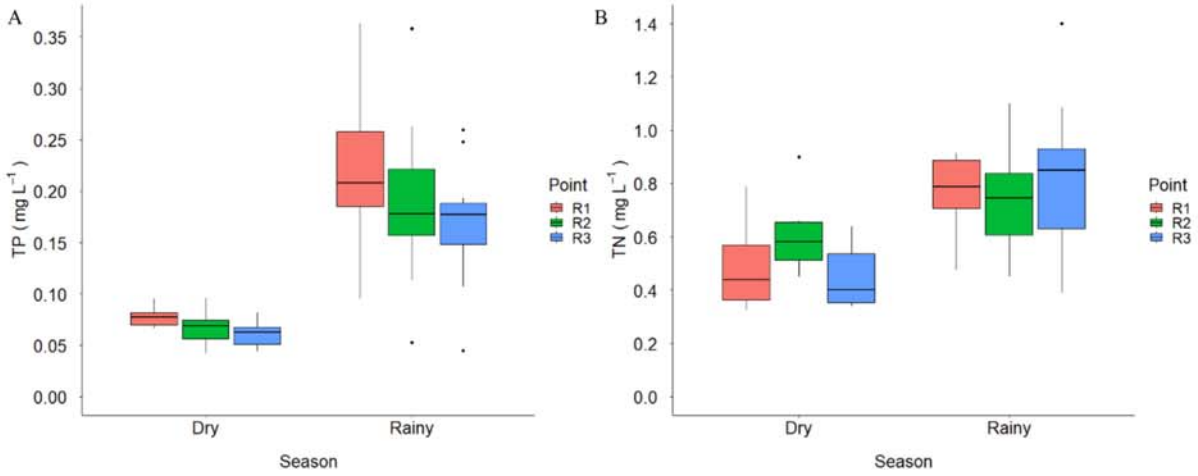

Source: The author.

4.3.1.1 Spatial variation

The sampling point R3 is the one with the lowest TP concentration between April 2022 and February 2023 (Figure 19). As for R1 and R2, they presented more variance within the analyzed period, with a maximum TP concentration of around 0.35 mgL^{-1} to a minimum of 0.05 mgL^{-1}. This suggests that the sampling points R1 and R2 are more susceptible to the point and non-point sources of pollution.

It is important to highlight that, between the rainy season of 2022 (January 2022 to June 2022), the TP concentration in the three sampling points (R1, R2, R3) in Jaguaribe river were above the class three limit established by the Brazilian legislation (Figure 19). This is the limit for the water to be considered suitable for human consumption after conventional treatment. Which reinforces the observation that the rainy season is a critical period for water quality in the river and reservoirs in this area and, therefore, special management actions should be taken.

Figure 19 – Time series comparing the spatial variability of total phosphorus concentration within the three different sampling points upstream Castanhão reservoir in Jaguaribe River (R1, R2, R3) from June 2021 to January 2023.

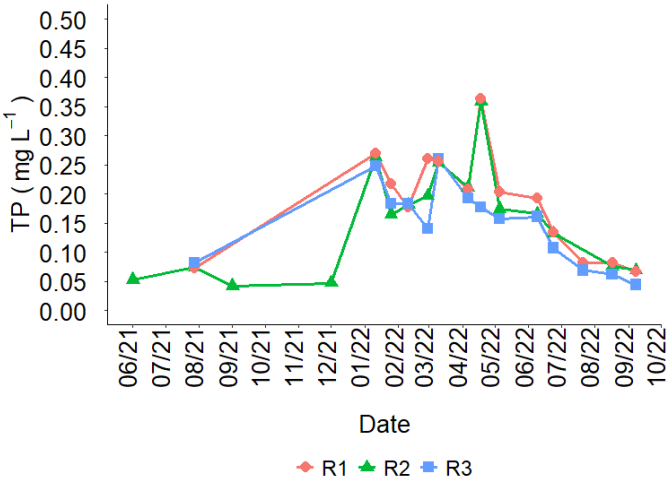

Source: The author.

Observing each measurement date in Figure 20 and Figure 21 there are three types of trends within the water quality variables. First, Ammoniacal nitrogen, TN, and Temperature presented spatial differences within the river, but there was no seasonal or upstream-downstream pattern. In contrast, Nitrite and Salinity presented a seasonal pattern, where the spatial variation on Nitrite concentration was more pronounced and the Salinity was less pronounced during the rainy season. Pearce, Chambers and Hasenmueller (2017) observed a similar opposite pattern, but with Nitrite-Nitrate species and specific conductivity during the rainy season, where the nutrients were higher, and the specific conductivity was lower during the rainy season. This opposite pattern is possibly due to a nutrient runoff and to a dilution effect of salts during the rain events.

Those spatial variations confirm how the dynamics of point and non-point sources of pollutants is complex (Sun *et al*., 2024), especially the non-point sources, which have a broader range (Zhang *et al*., 2024) and are predominant in rural areas such as the one in the present study, that has little vegetation cover and high exposed soil (Castro, 2018).

As for the DO and pH spatial variations, R3 presented the highest DO and pH values from March to September 2022 (predominantly rainy season) and then the lowest values from September 2022 to February 2023 (predominantly dry season). This tendency possibly occurred because R3 received less nutrients and sediments from upstream points and then presented less

effects of the degradation and dilution of organic matter and nutrients, which decreases the local oxygen consumption (Ma *et al.*, 2024).

Figure 20 – Time series comparing the spatial variability of A) Ammoniacal nitrogen concentration, B) Nitrate concentration, C) Nitrite concentration, and D) Total nitrogen concentration within the three different sampling points upstream Castanhão reservoir in Jaguaribe River (R1, R2, R3) from June 2021 to January 2023.

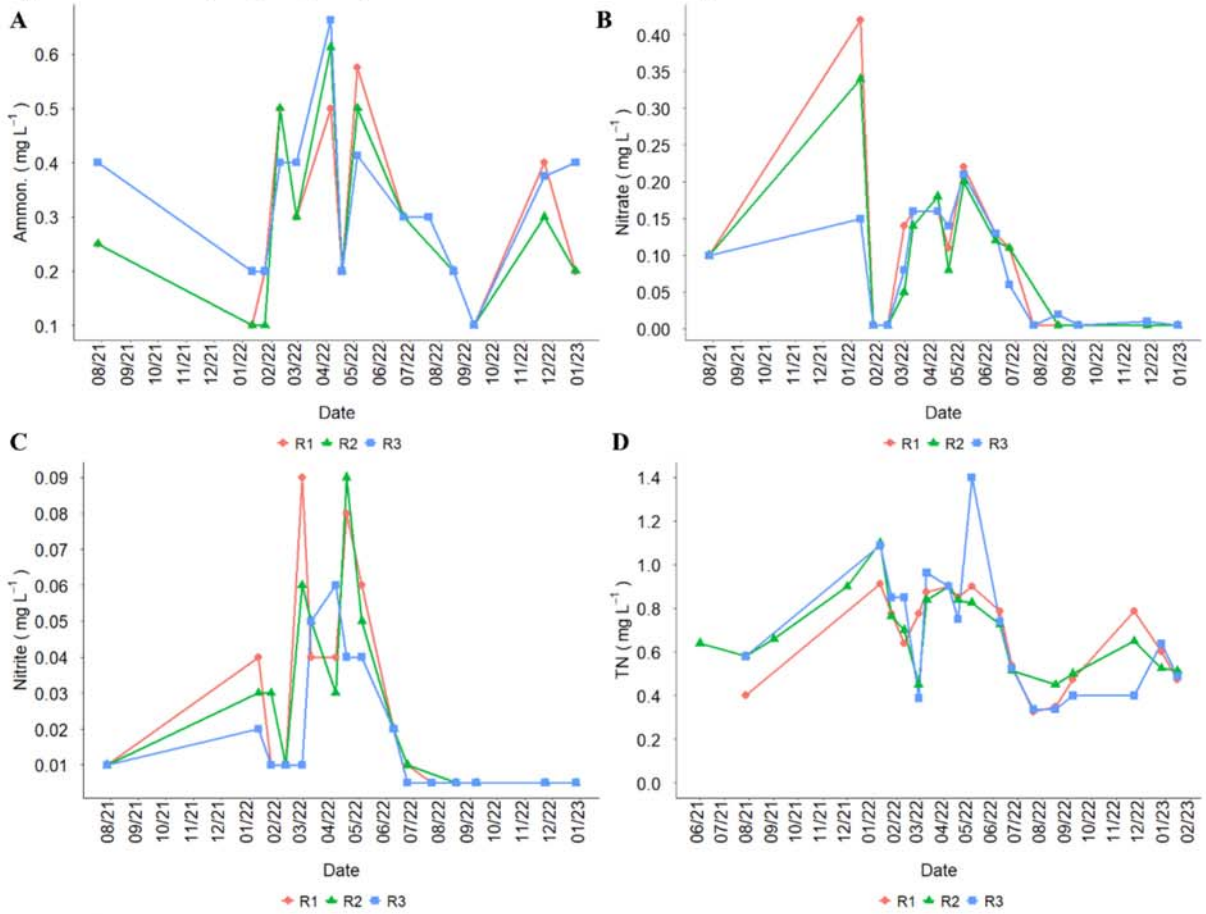

Source: The author.

Figure 21 – Time series comparing the spatial variability of A) Dissolved oxygen concentration, B) pH, C) Temperature, and D) Salinity within the three different sampling points upstream Castanhão reservoir in Jaguaribe River (R1, R2, R3) from June 2021 to January 2023.

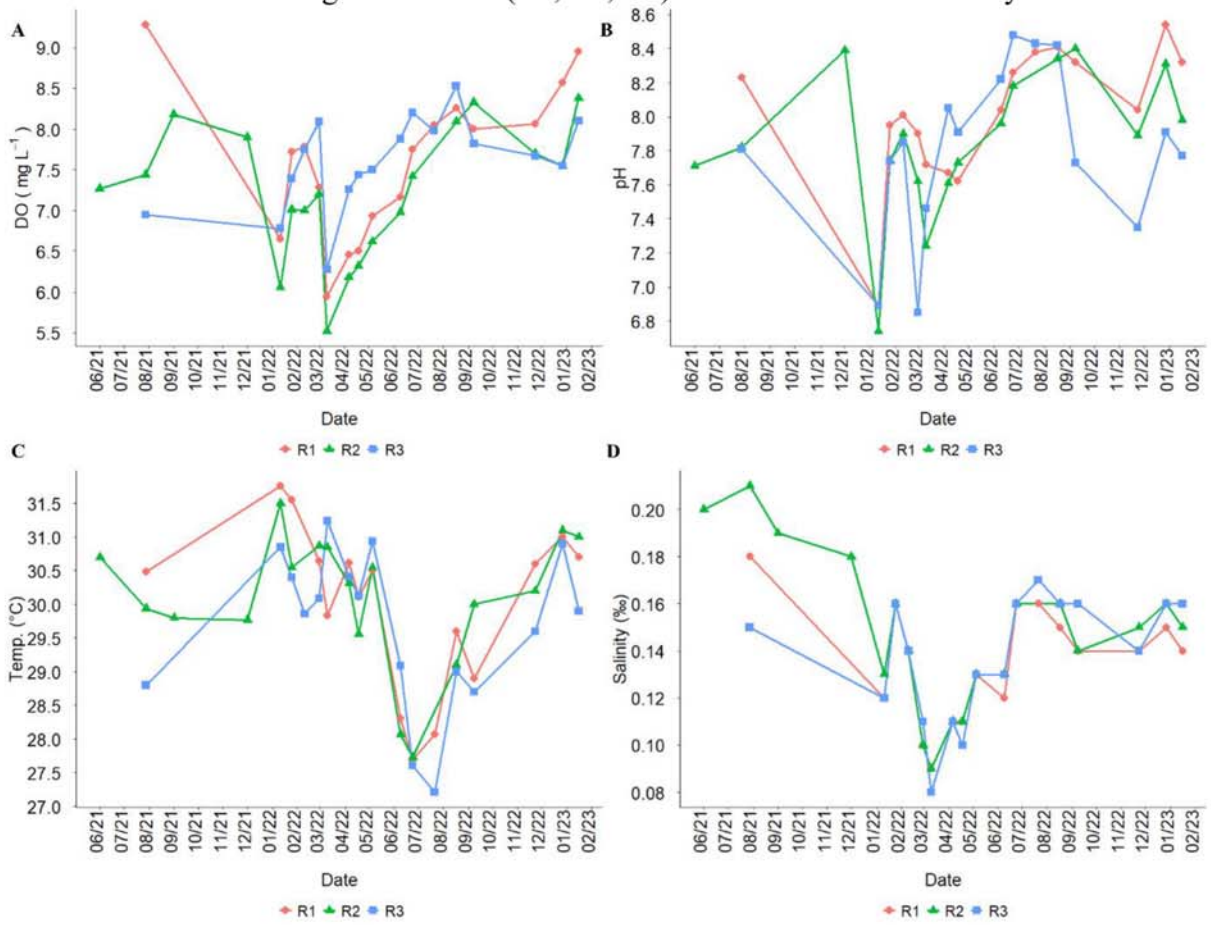

Source: The author.

4.3.2 Analyzing the water inflow into the Castanhão reservoir

Analyzing the flow rate measurements within the three different sections of Jaguaribe River, it is possible to see that the flow rate did not vary substantially within the sampling points (Figure 22), which suggests that there is no significant evidence of point source pollution, e.g., sewage discharges, within the studied area between 2021 and 2023. The biggest spatial differences between the measurements occurred during the rainy period, however this could be attributed to imprecision on the measurement, since the flow rates during this period are high and it is harder to apply the measurement method.

Figure 22 – Comparison between the inflow measurements of the three different sampling points upstream Castanhão reservoir in Jaguaribe River (R1, R2, R3) from June 2021 to January 2023.

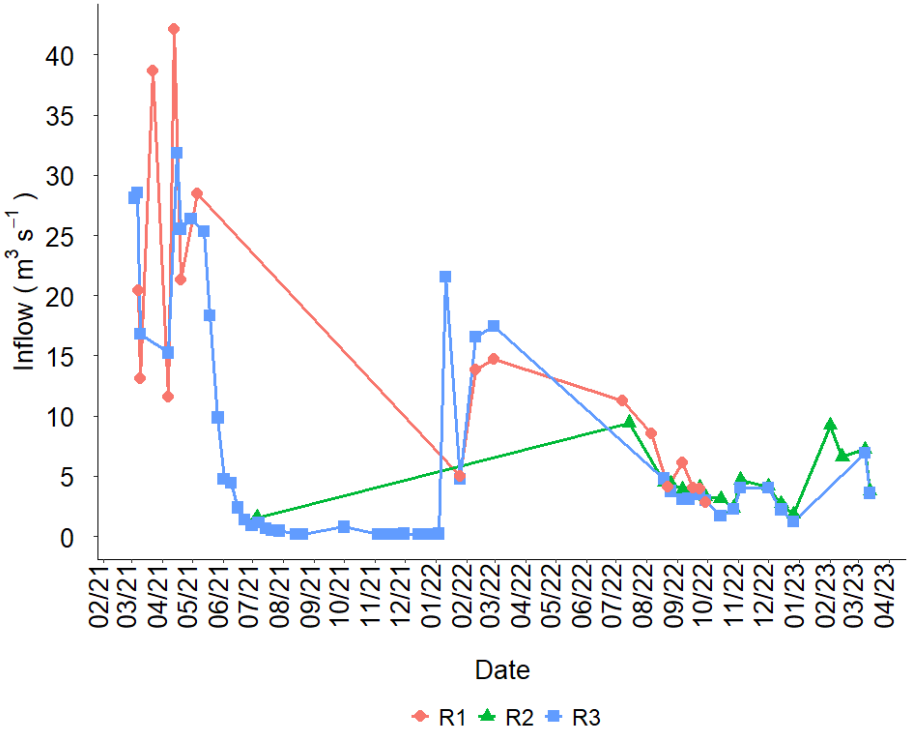

Source: The author.

The average inflow calculations of Castanhão reservoir using the water balance were then compared with the flow rate measurements in Jaguaribe river from March 2016 to March 2023. The value found for NSE was 0.93, which for flow calculations can be considered very good (Moriasi *et al*., 2015). Figure 23 and Figure 24 graphically show the goodness of fit between the measured and the calculated inflow. Therefore, the inflow calculated using the water balance is suitable to be used for estimating the nutrient loads in the river in dates where there are no *in-situ* measurements. This methodology can be useful to data scarce regions.

Figure 23 - Scatter plot of the measured inflow values by the ones calculated with the water balance. The diagonal line represents the perfect fit of calculated and measured data.

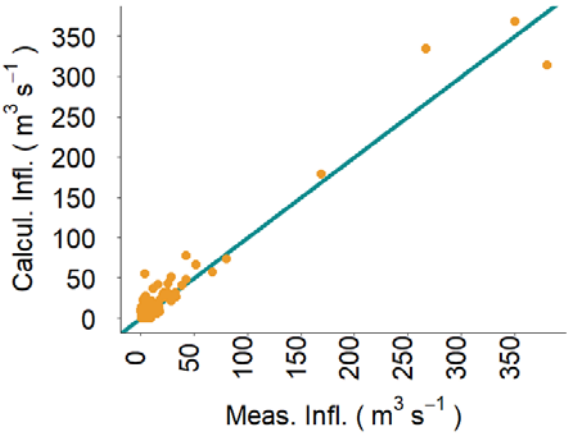

Source: The author.

Figure 24 – Time series of calculated inflow values using water balance and the inflow measurements taken in each of the within the three different sampling points upstream Castanhão reservoir in Jaguaribe River (R1, R2, R3) from March 2016 to March 2023.

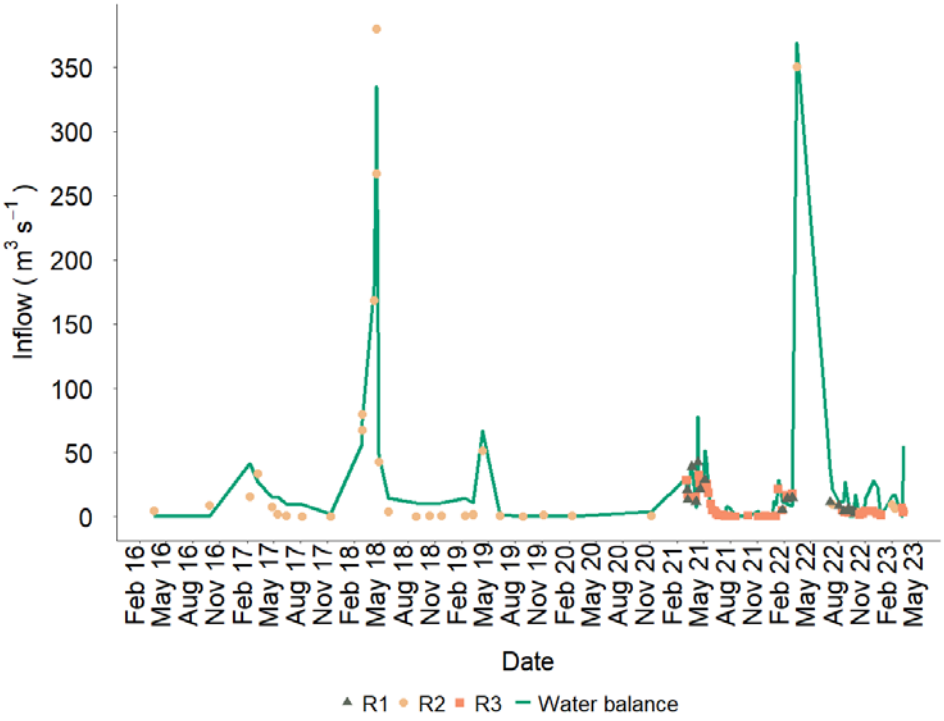

Source: The author.

4.3.3 Linear regression models

The use of inflow to predict important water quality parameters was tested first by using linear regression models. Figure 25 and Figure 26 show that the only models considered

to have a satisfactory performance [R^2 >0.4; Moriasi *et al.* (2015)] were the ones used to predict salinity (R^2=0.419), turbidity (R^2=0.431), and TC (R^2=0.467). Both TC and turbidity presented a positive linear relationship with inflow, where higher inflow values were associated with higher turbidity and TC values. This would be expected since the inflow promotes sediment and nutrients runoff which increase both suspended (sediments and organic matter) and dissolved (dissolved organic matter and minerals) substances, i.e., turbidity and TC (Zhang *et al.*, 2021; Zobkov and Zobkova, 2020).

Figure 25 – Linear regression model of inflow as the explanatory variable for predicting A) Total phosphorus, B) Total nitrogen, C) Nitrite, D) Nitrate, E) Biochemical oxygen demand, and F) Dissolved oxygen. The coefficient of determination (R^2) is displayed on the top left corner of each graph.

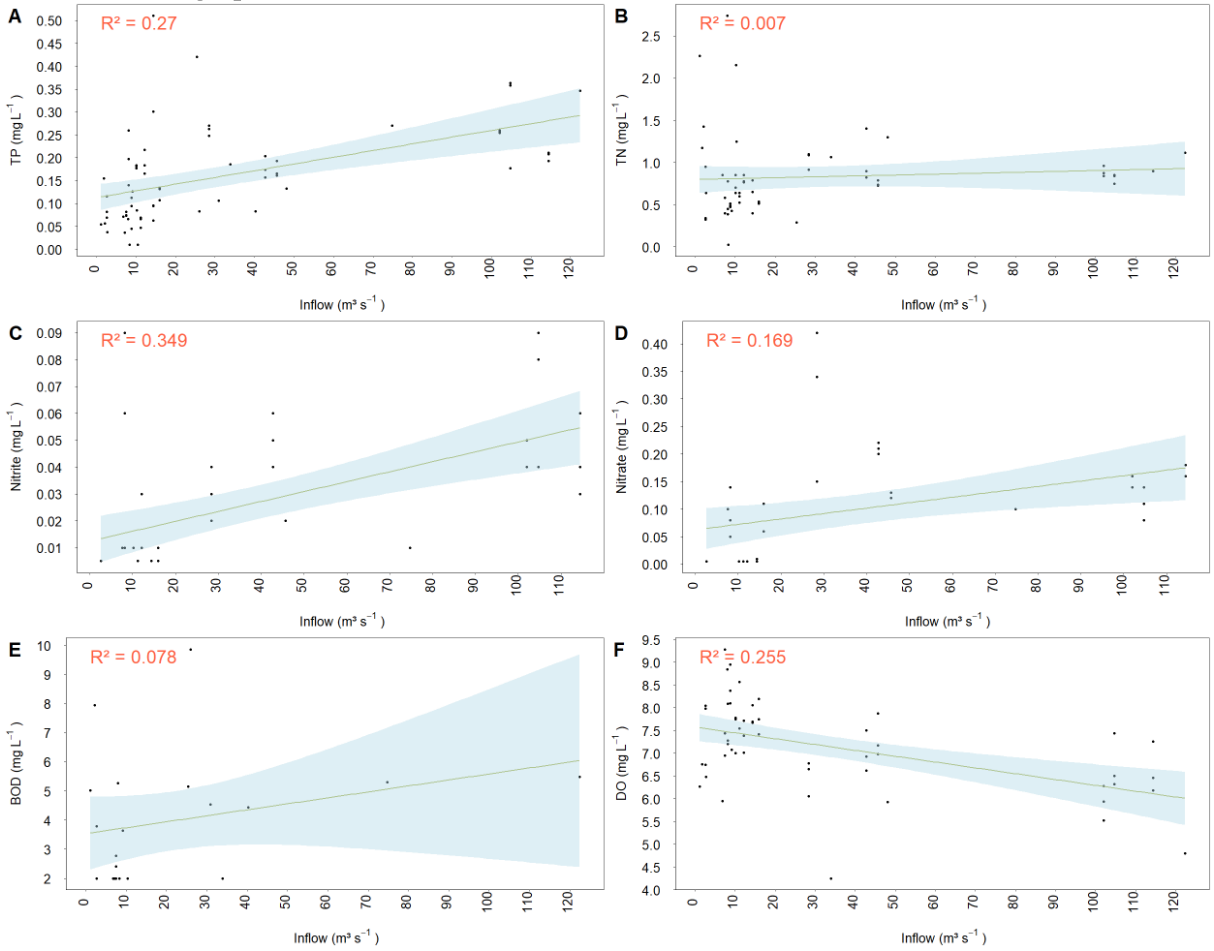

Source: The author.

Figure 26 – Linear regression model of inflow as the explanatory variable for predicting A) Ammoniacal nitrogen, B) pH, C) Salinity, D) Turbidity, E) True color, F) Temperature, and G) Total dissolved solids. The coefficient of determination (R^2) is displayed on the top left corner of each graph.

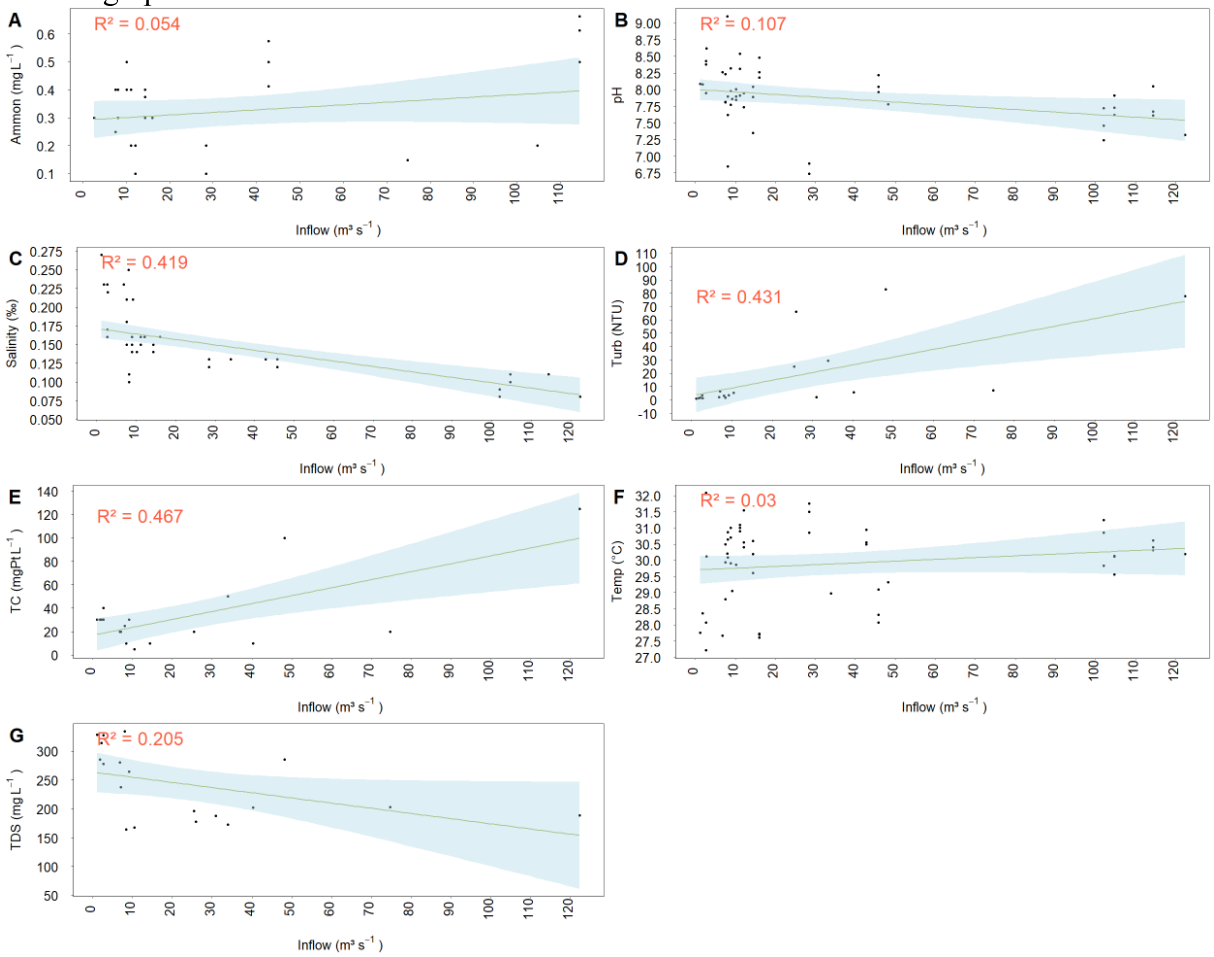

Source: The author.

4.3.4 Non-linear and regularized regression models

In order to predict the TP concentration in Jaguaribe River, different models were tested. Table 1 shows the model performance using the non-linear regression equation of inflow to predict TP concentration. The coefficients obtained for this equation were A = 25.5; B = 0.08; C = 59.64; D = 1.32.

A, B, and D values were smaller than the ones found by Rocha and Lima Neto, (2021). This difference can be due to the larger dataset used in the present study. In addition, the smaller A coefficient may indicate that the contribution of point sources in the analyzed river section in the present study are lower than those estimated by Rocha and Lima Neto (2021). Which corroborates their hypothesis that the non-point source contribution in the region of Castanhão reservoir is underestimated by the environmental inventory performed by the State's

water agency. Figure 27 presents the calculated TP load versus the measured load. Based on this figure, it is possible to see that the model deviations were usually during peak events.

Table 1 - Metrics of non-linear model

Metrics	**Value**	**Classification** (Moriasi *et al.*, 2015)
NSE	0.51	Very good
PBIAS	-0.042	Very good
RMSE	0.06	-

Source: The author.

Figure 27 - Calculated versus measured TP load in Castanhão reservoir using the non-linear model equation.

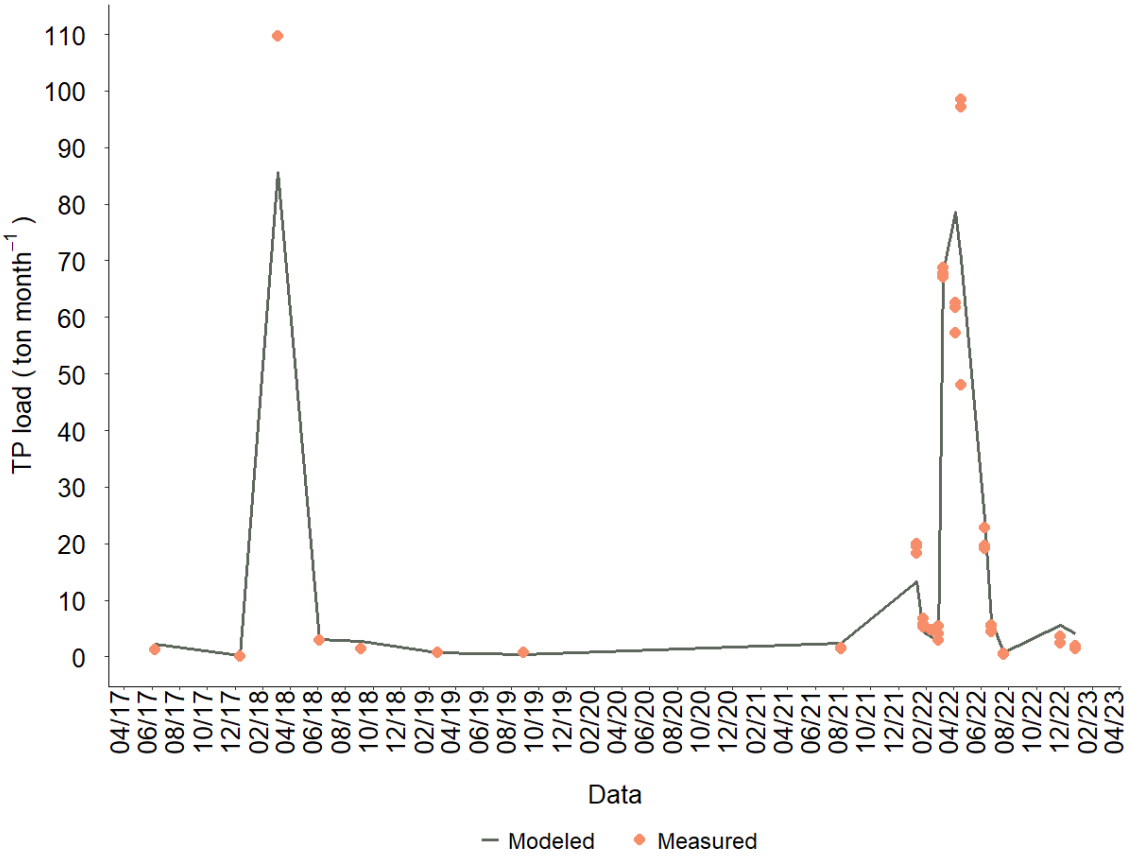

Source: The author.

The regularized linear models Lasso, Ridge, and Elastic-net regression were also tested to predict both TP and TN concentrations. Figure 28 illustrates a scatterplot depicting observed and predicted TP concentration values in the river, employing Lasso, Ridge, and Elastic-Net regression models with flow rate, DO, temperature, and pH as explanatory variables. Additionally, non-linear predicted values were derived solely using flow rate as the explanatory variable. Visually, the three models exhibited similar predicted TP concentration values,

although the model that best approximated the measured TP concentration varied depending on the date.

Figure 28 – Scatterplot comparing measured and modeled total phosphorus concentration values obtained during both the training and testing phases of Ridge, Lasso, and Elastic-Net regression, alongside the non-linear model.

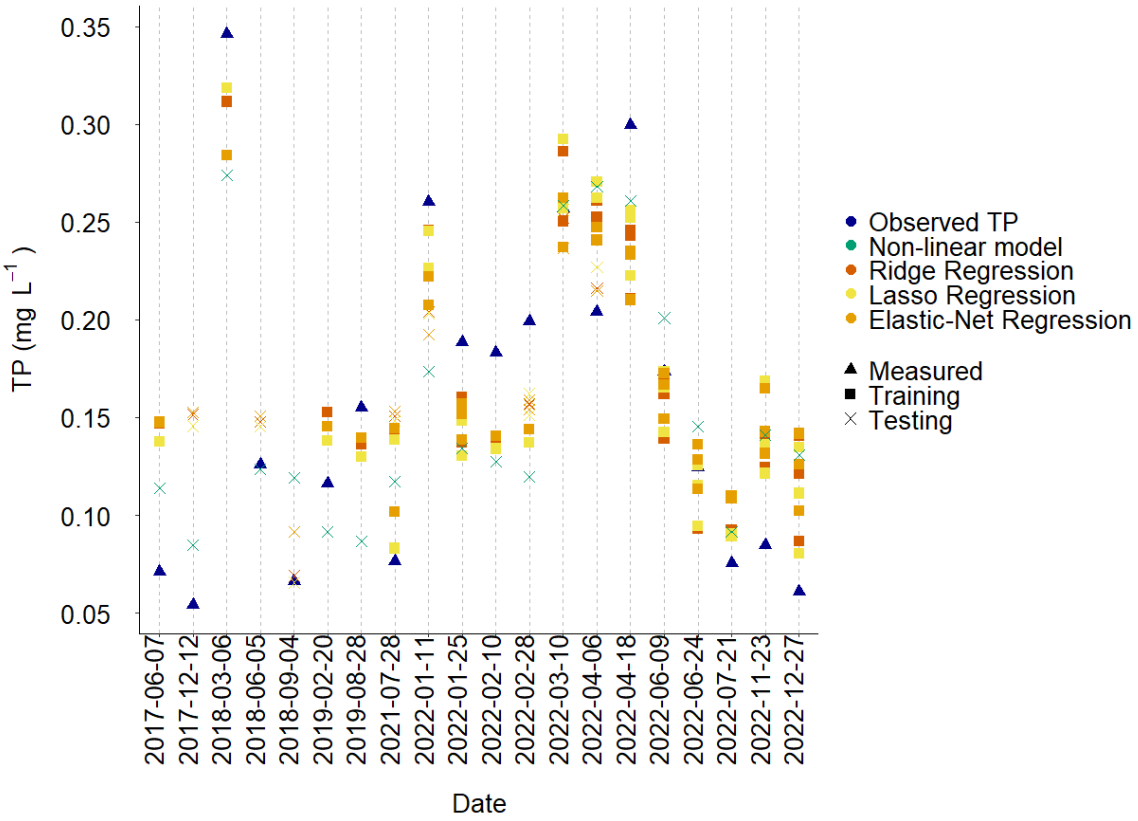

Source: The author.

Table 2 presents the metrics for a more objective performance evaluation. It shows that Lasso and Ridge regression presented a similar performance, being better than both elastic-net regression and the non-linear model. However, when observing the difference between the training and the testing metrics for all three regression models, it is possible to observe that the testing performance was better than the training performance. When this occurs, it is a sign that the model could present an overfitting behavior to the data. In order to confirm that the Lasso and Ridge regressions were not overfitting the data, it is important to increase the numbers of observations. Therefore, the model chosen to be further used in Chapter 6 was the non-linear model, since this was already tested in another study for several reservoirs within the semiarid region and seemed to represent well both the dilution and the TP runoff effects of the flowrate (Rocha and Lima Neto, 2021). Nevertheless, further validation of the non-linear model with newer data is necessary to validate predictions.

Table 2 – Training performance of the different model configurations.

Model	Dataset	R^2	RMSE (mg L^{-1})	NSE
Non-linear equation	Complete	0.51	0.06	0.51
Ridge regression	Train	0.62	0.054	0.62
	Test	0.60	0.046	0.60
Lasso regression	Train	0.63	0.054	0.63
	Test	0.60	0.046	0.60
Elastic-net regression	Train	0.58	0.057	0.58
	Test	0.53	0.050	0.53

Source: The author.

In contrast with the TP prediction, the TN prediction with temperature, pH, inflow, and DO as the explanatory variables in the Ridge, Lasso and Elastic-net regression presented a "Not Satisfactory" performance, since the coefficient of determination for the three models was smaller than 0.3. This result can be explained by the high complexity of the nitrogen cycle. For instance, nitrogen is not immediately discharged into water bodies from human activities, but its transport in the soil can present a significant time lag (Zhang *et al*., 2024). In addition, there are several processes involved in the nitrogen transportation in a basin e.g., atmospheric, advective, and diffusive fluxes (Rocha and Lima Neto, 2023).

4.3.5 Regression tree model

Using a regression tree model allows both to predict the chosen dependent variable, but also to see how the observations are distributed within different groups. Figure 29 shows the regression tree obtained using temperature, DO, pH, and flow rate to predict TP concentration in Jaguaribe River. It is important to highlight that the regression tree selected only the flow rate as the explanatory variable that significantly explained the variance of TP in this period. In addition, the groups of TP concentrations based on the flow rate of the observed data followed a positive relationship between TP and inflow, where higher flow rate values generated higher TP concentrations. This shows that the process that dominates the TP concentration in the river is the nutrient runoff during the rainy season.

The model performance predicting TP concentration from the testing dataset can be considered very good since the coefficient of determination was higher than 0.8 ($R^2 = 0.81$) and the NSE was higher than 0.65 (NSE = 0.79). In addition, the RMSE was of 0.034 mg L^{-1}, which is smaller than the RMSE values obtained with the model applied in the previous section.

Figure 29 – Regression tree to predict TP concentration using pH, temperature, DO, and flow rate as explanatory variables.

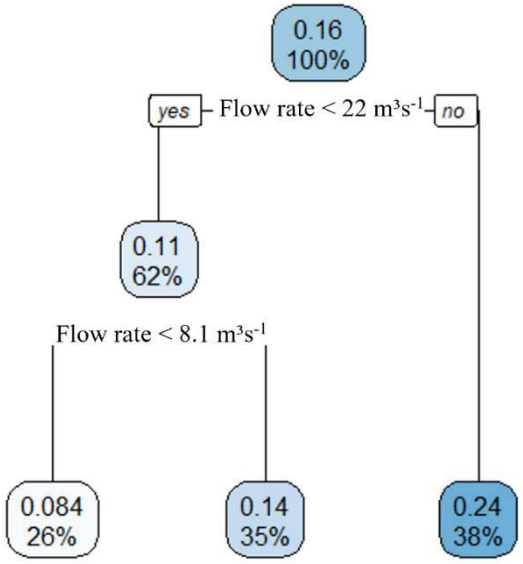

Source: The author.

Figure 30A shows the use of only flow rate as the explanatory variable to predict TN concentration in the river. In contrast with TP, TN did not present a dominant positive relation with flow rate. This regression tree showed that the lower flow rate values (smaller than 8.1 m^3s^{-1}) generated the highest TN concentration. Indicating that the TN input in the reservoir could present both storm runoff and dilution processes due to the river flow rate. However, the performance of this model was not satisfactory, with a coefficient of determination close to zero.

In contrast, Figure 30B shows the regression tree generated using DO, pH, temperature, and flow rate as the explanatory variable to predict TN. The model performance on predicting TN concentration was satisfactory, with a coefficient of determination of 0.55 and RMSE = 0.19 mg L^{-1} (Moriasi *et al.*, 2015). In this case, the variables that the model considered to explain most of the variance of TN were DO and temperature, confirming the hypothesis that the flow rate of the river is not a good predictor of TN concentration. This can indicate that the runoff of pollutants within the basin is not the primary factor to TN input in the river. However, a more detailed analysis should be performed, since, as mentioned previously, the nitrogen cycle is complex and recent studies even found evidence that there is a time leg in nitrogen transport in the soil (Zhang *et al.*, 2024). Another factor that should be further investigated is if there was any change in the quantity of nitrogen fertilizers usage within the years, which can also impact the cycle. For instance, Yu *et al.* (2023) found that in the region they studied the use of nitrogen

fertilizers decreased and the use of phosphate fertilizers increased. Changes such as this one could, for example, explain why the TP concentrations in the river are influenced by its flow rate, but with TN concentrations it does not occur the same.

In addition, Figure 30 shows that lower DO concentration is related to high TN concentrations, which is expected since the excess of nutrients in the water indicates a high presence of organic matter in the water, where its decomposition consumes DO (Cooray *et al.*, 2022). In addition, the lower TN concentrations were related to higher DO concentrations and lower temperatures.

Figure 30 – Regression tree to predict TN concentration using A) only flow rate and B) pH, temperature, DO, and flow rate as explanatory variables.

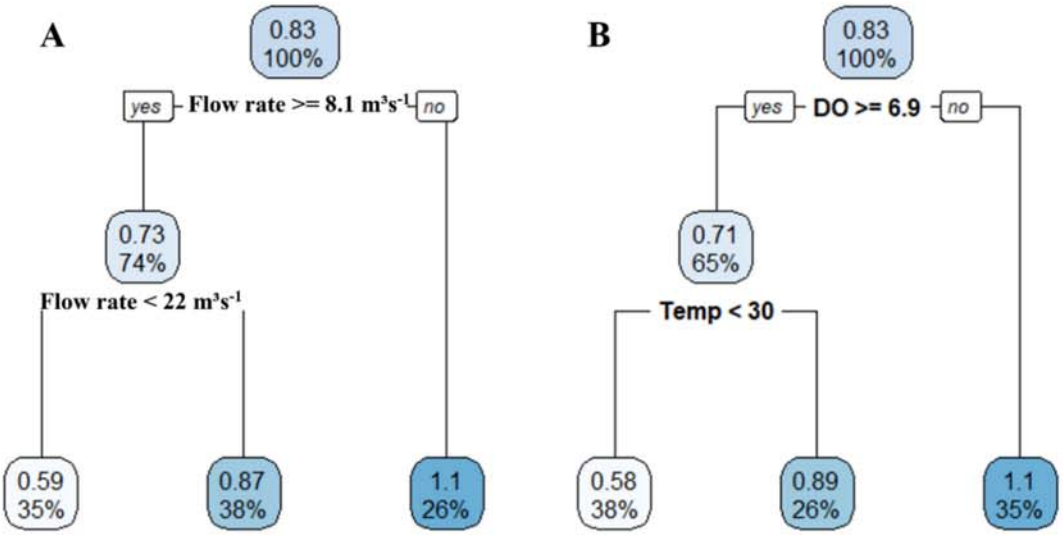

Source: The author.

4.4 Conclusion

The water quality dynamics in intermittent rivers of semiarid regions is complex, and studies often encounter the challenge of limited datasets. This study revealed that during the rainy season, the most downstream monitored sampling point presents a better water quality, with high DO concentration and lower TP concentration. In contrast, during the dry season, the most upstream sampling point is the one with higher DO concentration. Also, the increase in TN concentration in the river during the rainy season is not as substantial as the increase in TP concentration.

The calculation of the daily average flow of the river using the reverse water balance proved to be adequate and accurate, which helps overcome the difficulty of obtaining daily average flow data of the river on the same days as water quality measurements are made. Thus, it was possible to increase the database used for training and testing the models for predicting TP concentration in the river entering the reservoir, something that can be done in other reservoirs that also have scarce inflow data.

In the studied period, the river flow rate did not exhibit substantial spatial differences, suggesting that there are no significant point sources of pollution, such as sewage discharge. However, to accurately confirm this finding, field visits along the length of the river should be conducted.

During the rainy season, runoff and river flow into the reservoir serve as potential sources of sediments, nutrients, dissolved, and suspended organic matter. This hypothesis was confirmed by the significant linear relationship observed between the inflow into the reservoir and the true color and turbidity. Given the importance of these parameters in water treatment, the linear models developed in this study can be utilized to predict the true color and turbidity of the water entering the reservoir. Additionally, further linear models could be calibrated to establish the relationship between the true color and turbidity values of inflow water to the reservoir and the resulting values within the reservoir itself.

In general, the regularized linear models demonstrated excellent performance in predicting TP concentration in the river using flow rate, dissolved oxygen, pH, and water temperature as explanatory variables, with Ridge and Lasso regression standing out as the best-performing model. This underscores the potential of simple surrogate models to aid other studies in predicting TP loading into reservoirs based on inflow rate, a valuable tool given the scarcity of such data in reservoirs worldwide. Estimating TP loading into a reservoir enables the validation of further models predicting TP concentration in the reservoir, thus enhancing reservoir management practices. While the models used in this study presented promising results, conducting further studies with larger datasets and more complex models could provide a deeper understanding of both non-point and point sources of TP in the entire reservoir basin and it could enhance the confidence in the models' robustness by mitigating the risk of overfitting to the data.

Furthermore, this study revealed that river flow does not significantly explain the variance of TN concentration in the river. Therefore, further studies focusing on TN dynamics

in the basin are crucial, as this nutrient can also play a significant role in influencing water quality.

5 BED SEDIMENT CHARACTERISTICS WITHIN A MULTIPURPOSE TROPICAL SEMIARID RESERVOIR: ANALYSIS OF THE SPATIAL AND THE SHORT-TERM TEMPORAL VARIATION

5.1 Introduction

The nutrient dynamics within a reservoir network is an important contributor to the occurrence of eutrophication (Cortez *et al.*, 2022; Walsh, Corman and Munoz, 2019). The bed sediment of a reservoir can directly influence its water quality dynamics. For instance, it can store nutrients, heavy metals, and other components that have the potential to disturb the aquatic ecosystem and hinder the use of water for several purposes (McCarty, 2019; Wu *et al.*, 2021). Therefore, the knowledge of the sediment composition is essential to manage the water quality of a reservoir.

One of the most notable and studied impacts of the bed sediment composition in the water quality of a reservoir is the one due to the phosphorus (P) presence in the sediment (Cavalcante *et al.*, 2021; Huang *et al.*, 2016; Sondergaard, Jensen e Jeppesen, 2001; Tay *et al.*, 2022). Depending on the composition of the inorganic fractions of P in the sediment, it would have higher or lower potential to release P to the water column. For instance, Aluminum and Iron bound phosphorus (P_{FeAl}) is released from the sediment to the water column depending on the redox conditions (Wang *et al.*, 2017), where in anoxic environments, the P is dissolved to the water column (Fang *et al.*, 2024; Moura *et al.*, 2020). Another fraction of inorganic P that can interfere on the eutrophication process is the Calcium bound P (P_{Ca}), which is dissolved from the sediment to the water column in low pH conditions (Jin *et al.*, 2006). Several studies have shown that these fractions can maintain a reservoir in a eutrophic state even after doing procedures to decrease the amount of external P input to the lakes or reservoirs (Carleton e Lee, 2023; Ghaisas, Maiti and White, 2019; Husk *et al.*, 2024; Tang *et al.*, 2014).

Other studies focused on the bed sediment of a lake or reservoir. For instance, the assessment of the influence of different sediment characteristics on the increase of chlorophyll concentration in a shallow eutrophic cove (McCarty, 2019), the investigation of investigated the influence of different forms of P and the impact of seasonal hypoxia on internal P release (Lv, Zhang and Yin, 2024) and the study of the response of water quality characteristics to water-sediment factors e.g., water discharge and water level (Geng *et al.*, 2024).

However, many studies are from temperate climate zones and in shallow reservoirs. Therefore, a study in a large and deep reservoir located in a semiarid region could increase the

understanding of the sediment influence on the water quality. This is important because deeper reservoirs are more susceptible to present longer thermal stratification periods (Yue *et al*., 2023), which increases the anoxia occurrence in the sediment-water interface and, consequently, the release of P and in some cases N to the water column (Shi *et al*., 2021).

There are several studies of reservoir sediments performed in semiarid reservoirs, with laboratory experiments such as the one from Cavalcante *et al.* (2021), that experimentally investigated the potential release of P from the sediment of a reservoir in several controlled conditions. Moura *et al.* (2020) evaluated the potential release of sediments with different composition in anoxic and aerobic conditions. In addition, statistics and modeling techniques were used by Rocha and Lima Neto (2022) to quantify the internal loading of P.

However, those studies focused on the potential release of P from the water column, which is a particularly important analysis. Nevertheless, a general analysis of the sediment characteristics in a complex reservoir was not performed yet. For instance, the reservoir from the present study is large and deep, located in a semiarid region, subject to a high interannual variability of precipitation, water level in addition to a high evaporation rate (de Lacerda *et al.*, 2018). In addition to all those complex factors, this is a multipurpose reservoir that includes different uses that can affect the sediment characteristics: water supply, irrigation, and fish farming (FF) activity. The FF activity alone can impact on the sediment, since the P from the fish feeds can be highly adsorbed by particulate matter in the sediments (Portinho *et al*., 2021).

Therefore, we aim to provide a comprehensive analysis of the physical and chemical properties of the bed sediment of a multipurpose large and deep reservoir located in an Tropical semiarid region. Specifically, we aim to 1) Analyze if there are spatial differences in the granulometry and chemical composition of the sediment; 2) To assess if there is a seasonal effect in a short-term period in the chemical composition of the sediment; and 3) Validate the age versus P_{FeAl} concentration in the sediment relation and estimate the potential release coefficient of the bed sediment of the studied reservoir based on the P_{FeAl} versus release rate relation.

5.2 Materials and methods

5.2.1 Study Area

The present study was conducted in Castanhão (Figure 31), a reservoir built in 2002 in the Brazilian semiarid region. Its storage capacity is 6.7 billion of m^3, a dam crest elevation

of 111 m, and a maximum height of 71 m (Ceará, 2022a). The catchment area of this reservoir is of 45,309 km², which is characterized by mild slopes, usually varying. The historical annual average precipitation in the reservoir basin is 756.5 mm and the potential evaporation for the basin is around 2,100 mm (de Lacerda *et al.*, 2018). In general, the semiarid region where the reservoir is located presents a rainy season between January and June, and a dry season from July to December. This region suffers from high interannual variability of precipitation, intermittent rivers, and high variability of the reservoirs' water volume.

Similar to many reservoirs in this region, Castanhão is a multipurpose reservoir with the main predominant uses being human supply, irrigation, and FF activities. This reservoir is part of a water transfer system that supplies water to the capital of the State Ceará and its metropolitan region, with 4.1 million inhabitants.

Figure 31 – Map of the study area presenting the location of Brazil within South America and the state of Ceará within Brazil, with a highlight of the Brazilian semiarid region, Castanhão reservoir, and its drainage network (left panels). Representation of Castanhão reservoir and the regular monitoring sampling points as well as the sampling points where the sediment collection was performed (right panel).

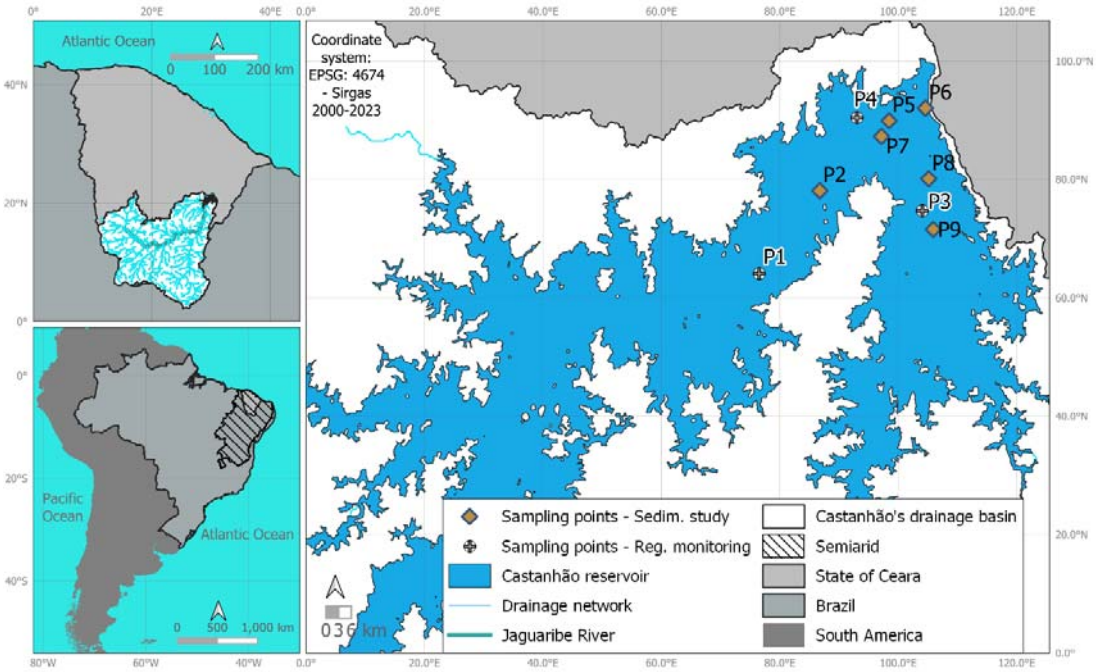

Source: The author.

5.2.2 Data collection and analysis

Reservoir sediment samples were collected in six different campaigns: 2021-11-18, 2021-12-22, 2022-02-17, 2022-06-24, 2022-12-14, and 2023-11-30. In the first date, the

samples were taken from P5 and P6 (Figure 31), then the sampling points P2, P7, P8, and P9 were added to the sediment sampling campaigns. These points were selected because they are situated in different zones of the reservoir. Specifically, P2 is positioned in the upstream area, while P5 and P7 are in close proximity to the fish farming zone. P6 is situated near the reservoir dam, and P8 and P9 are located in the right branch of the reservoir, characterized by slower flow.

The sediments were collected using a dredge. Even though the sampling points P1, P3, and P4 are not included in the sediment collection monitoring, they are included in the regular water quality monitoring for the profiling measurements of DO, pH, and Temperature, providing more insights into the hydrodynamics of the reservoir.

Then the samples were analyzed in the laboratory for quantifying the iron and the aluminum (SMWW, 2017), the total nitrogen (TN), and the organic matter content in the sediment. As well as the solid percentage (SMWW, 2017). The TN and organic matter analysis was performed by an accredited laboratory following its Standard Operating Procedure.

The sediment granulometry was also assessed for P5 and P6 in the samples collected in November 2021, and for P2, P7, P8, and P9 in December 2021. This analysis was performed according to Brazilian Standard (NBR 7181/1984).

The phosphorus fractionation analysis was performed using the same methodology as (Moura *et al.*, 2020). The fractions that were quantified were: TP, Inorganic P (P_{Inorg}), Organic P (P_{Org}). And the P_{Inorg} fractions were Iron-Aluminum bound P (P_{FeAl}), Calcium bound P (P_{Ca}), mobile P (P_{Mob}), and residual P (P_{Res}).

To ensure that the procedures for quantifying phosphorus in sediment were correct, the analysis of this parameter was conducted in two different laboratories and compared in Figure S 60, revealing no significant differences.

The data was processed using R Core Team (2022) and to determine the statistical significance of variations between median values of the samples, the Shapiro-Wilk normality test was applied to assess the normal distribution of the data. Subsequently, the Kruskal-Wallis test was applied to evaluate overall differences among the sampling points. Finally, post hoc pairwise comparisons were conducted using the Dunn test, with the Bonferroni adjustment for multiple comparisons. A significance level of 0.05 was utilized throughout the statistical analysis.

5.3 Results and discussion

5.3.1 Sediment granulometry

The physical characteristics of the reservoir's sediment was assessed for the studied sampling points. Figure 32 depicts the particle size distribution within the sediment of the sampling points. The major particle size in P9 is clay, and it has an almost similar part of fine sand and silt (40%, 30%, and 27%, respectively). Even though they both are located in the right branch of the reservoir, P9 and P8 present a different particle size distribution, where clay is the predominant particle size in P9 (40%) and fine sand is the predominant particle size in P8 (68%).

In the left branch of the reservoir, the most upstream sampling point, P2 presented a similar particle size distribution to P5, where it predominates the fine sand and the clay – 55% and 30%, respectively for P2, and 48% and 33%, respectively for P5. However, in P6 clay and silt predominate (43% and 29%, respectively), whereas in P7 predominates fine sand and silt (50% and 34% respectively). The two sampling points with the least amount of clay particles are P7 and P8. The two sampling points with the most amount of clay particles are P6 and P9.

Figure 32 – Spatial variation of particle size distribution of the sediment in the analyzed sampling points.

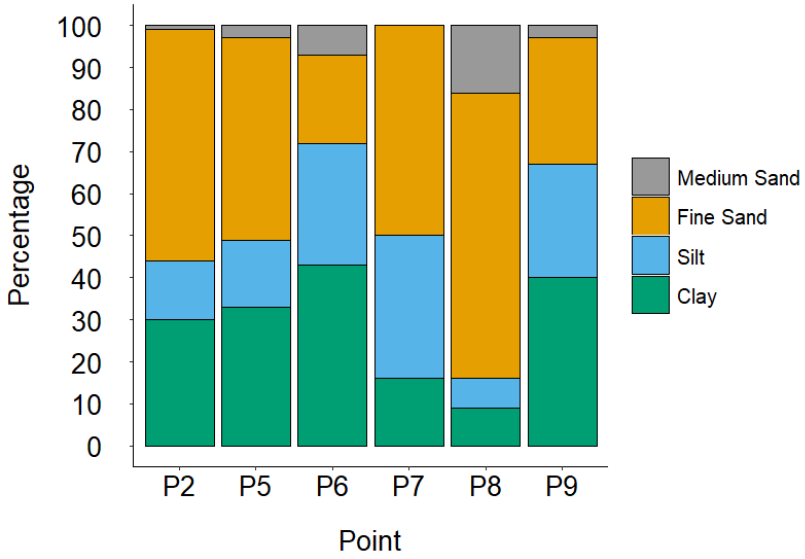

Source: The author.

5.3.2 Chemical characteristics

5.3.2.1 Spatial variation

Figure 33 depicts the general P composition in the sediment of the different sampling points analyzed in the present study. The highest median concentration of P_{inorg} was found in P6 (848.16 mg kg^{-1}, Figure 33A), which was significantly higher ($p<0.05$) than the

median found in P5 (472.29 mg kg^{-1}) and P7 (370.24 mg kg^{-1}), which were the points with the lowest P_{inorg} median concentration values. The median values found in P8, P9, and P2 were 533.55, 562.88, and 558 mg kg^{-1}, respectively.

The only significant difference ($p<0.05$) in the spatial distribution of P_{org} in the sediment was that the median concentration of P7 (33.39 mg kg^{-1}, Figure 33B) is significantly lower than the ones found in P2, P6, and P9 (315.39, 261.56, and 251.47 mg kg^{-1}, respectively). Even though the median value of P6 and P8 (261.56 and 258.24 mg kg^{-1}) are similar to the one observed in P9, the variance in P6 and P8 is notably high, which shows that there was a variation of P_{org} fraction in these sampling points during the analyzed period. The median concentration in P5 (131.45 mg kg^{-1}) was the second lowest observed among the sampling points.

Ni, Wang and Wang (2016) found that P_{Org} was significantly positively correlated to TP in the overlying water and, therefore, it was an important source of P that increases with eutrophication. However, this is possibly not the case of Castanhão reservoir since the majority of P in the sediment was inorganic, which was the opposite of Ni, Wang and Wang (2016), where the P_{Org} was the dominant form of P.

The spatial distribution of P_{total} significantly varied within all sampling points (Figure 33C). For instance, the median in P6 was significantly higher ($p<0.05$) than all the sampling points except in P2 (1033.6 and 901.76 mg kg^{-1}, respectively). The lowest P_{total} median concentration was observed in P7 (406.03 mg kg^{-1}), which was significantly lower ($p<0.05$) than P6, P9, and P2 (1033.6, 801.23, and 901.76 mg kg^{-1}, respectively). The median P_{total} value in P7 is visually equally smaller than P8 and P9 (median P_{total} in P8 is 809.97 mg kg^{-1}), however, the significance of this difference was lower, since the p-value obtained was 0.055. As it occurred with the P_{Org} fraction (Figure 33B) the median value for P_{total} observed in P5 was the second lowest (595.52 mg kg^{-1}).

Figure 33 – Inorganic and organic phosphorus content in sediment samples from various points across the reservoir.

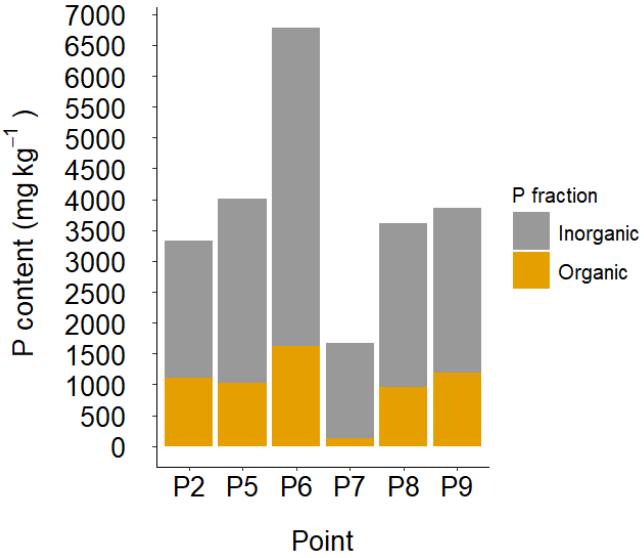

Source: The author.

Figure 34 shows the variation of inorganic fractions of phosphorus in the sediments within the sampling points The sampling points with the highest P_{FeAl} concentration were P9 and P6 (Figure 34A), with median concentrations of (190 and 173 mg kg^{-1}). The median values of these two sampling points were significantly ($p<0.05$) higher than the sampling points P5, P7, and P8. With P2 being the sampling point with the intermediate median P_{FeAl} concentration, being significantly different only from P7.

The two sampling points with the most clay content were also the sampling points with the most P_{FeAl} content in the sediment, possibly due to the strong affinity of P to lower sediment gran sizes, which have fine particle size and larger surface areas (Wen *et al*., 2020; Yin *et al*., 2023). This shows that the sediment particle size is an important physical characteristic which can influence the distribution of components in the sediments. In addition, metallic elements and organic matter usually show a high affinity to fine particles (Palma *et al*., 2014). However, this was not observed by Mu *et al*. (2020) where the TP sediment content was higher in the point where the silt and clay contents were lower. This occurred due to the presence of cage fish in this reservoir, which can increase the TP deposition.

Even though the FF activity is related to an increase in the TP and TN content in the sediment, the sampling point that is located right in the FF area (P7) was the one with the lower TP concentration. This indicates that the nutrients released from the FF activity are

transported to downstream sampling points which is consistent, since P6 (the point closest to the dam) is the one with the highest TP concentration.

P6 was the sampling point with the most P_{FeAl} content. This sampling point is the deepest and it presents the lowest DO concentration throughout the year (Figure S22). This shows that this is a critical point of P release from sediment to the water column, since the release rate of P from sediment increases in anoxic conditions (Lv, Zhang e Yin, 2024).

The sampling point with the highest median value of P_{Ca} was P6 (median =238 mg kg^{-1} – Figure 34A), which is significantly ($p<0.05$) higher than the median values of P5, P7, P8, and P9 (medians of 84, 113, 109, and 149 mg kg^{-1}). With P2 (median = 171 mg kg^{-1}) being again the intermediate sampling point, not being significantly different from any sampling point.

The P_{Ca} fraction is usually inert, but it can be released under low pH conditions (Jin *et al.*, 2006; Wu *et al.*, 2014). In the studied reservoir, there was no spatial variation trend in the P_{Ca} as observed by Fang *et al*. (2024). However, in contrast with their result, in the present study the sampling point closest to the dam presented the highest P_{Ca} content. This once again shows that this sampling point is critical for the water quality in the reservoir, which is concerning, since it is close to the reservoir intake point.

Kwak, Jeon and Duck Hur (2018) found that the stagnant condition in a certain region of the studied reservoir was the one with the most P_{Ca}, which was not the case observed in the present study. The more stagnant zones located in the right branch of the reservoir (P8 and P9) presented lower P_{Ca} content when compared to the point closest to the dam (P6).

As for the P_{mob}, P6 is the one that presents the highest median value (273.65 mg kg^{-1}), being significantly different ($p<0.05$) from the median values of P2, P7, and P9 (204.11, 143.23, 116.53 mg kg^{-1}, respectively). In addition, the median values of P_{mob} from P5 (233.76 mg kg^{-1}) and P8 (242.4 mg kg^{-1}) were significantly different from P7 and P9, which were the sampling points with the lowest P_{mob} concentration.

Figure 34 - Distribution of Inorganic Phosphorus Fractions in Sediment Samples from Different Points Across the Reservoir. 'FeAl' denotes Iron-Aluminum Bound Phosphorus, and 'Ca' indicates Calcium-Bound Phosphorus.

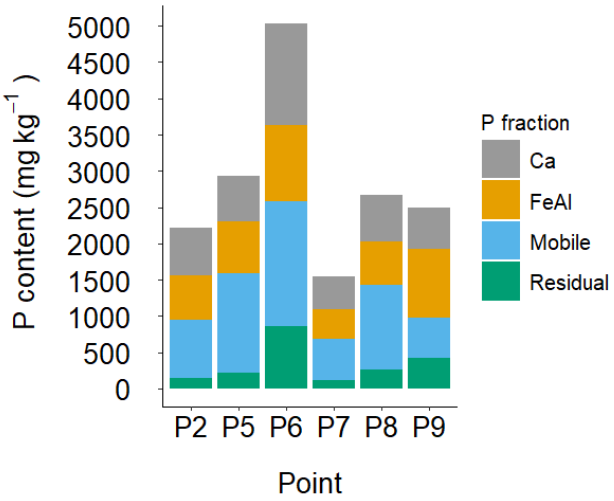

Source: The author.

As for the P_{Res} P6 also presented the highest median concentration (172.1 mg kg^{-1}, Figure 34D), being significantly higher than P2, P5, and P7 (33.84, 33.31,30.66 mg kg^{-1}). However, it presented a high variance, which made it not significantly higher than P8 and P9 (55.79 and 105.87 mg kg^{-1}, respectively).

There was no significant difference ($p>0.05$) in the Aluminum, Iron, and TN concentration between the sampling points (Figure S 54). However, the median concentrations of TN in P8 and P9 were higher than the observed in the other sampling points, however the variance in these sampling points was high. Figure S 57C makes evident that the TN concentration in P8 and P9 notably increased from December 2021 to February 2022. This can be due to the runoff caused by the rainy season.

5.3.2.2 Temporal variation

P_{Inorg}, P_{Org}, and TP content in the sediments presented notable variation throughout the studied period (Figure 35). With the median value of P_{Inorg} varying from 720 to 500 mg kg^{-1}, P_{Org} varying from 370 to 150 mg kg^{-1}, and the TP varying from 1050 mg kg^{-1} to around 600 mg kg^{-1}. For all three fractions of P, the highest median was observed in November 2021, but only the P_{Org} presented a decrease trend from November 2021 to June 2022 (Figure 35B). Whereas P_{Inorg} presented an increase trend from June 2022 to September 2023 (Figure 35C). In addition, the P_{Inorg} presents more occurrences of outliers than the P_{Org} fraction, which can be related to the sedimentation of P_{Inorg} due to aerobic conditions. It is important to highlight that

the variance of the boxplot referring to November 2021 is lower than the other ones because in this period only P5 and P6 were analyzed.

Figure 36 shows the detailed variation of phosphorus fractions by sampling point at each date. It is possible to see how the P-Org variation throughout the time was not uniform within the sampling points (Figure 36B), which was not the case for P_{Inorg}. In general, this fraction varied uniformly within the sampling points, for instance, from June 2022 to September 2023 all the points, presented an increase on the P_{Inorg}, except P8, which decreased from June to December 2022.

Figure 35 – Phosphorus fractions in the reservoir sediment grouped by each measurement date. A) represents the inorganic phosphorus, B) the organic phosphorus, and C) total phosphorus. The horizontal line in each boxplot represents the median concentration for each date.

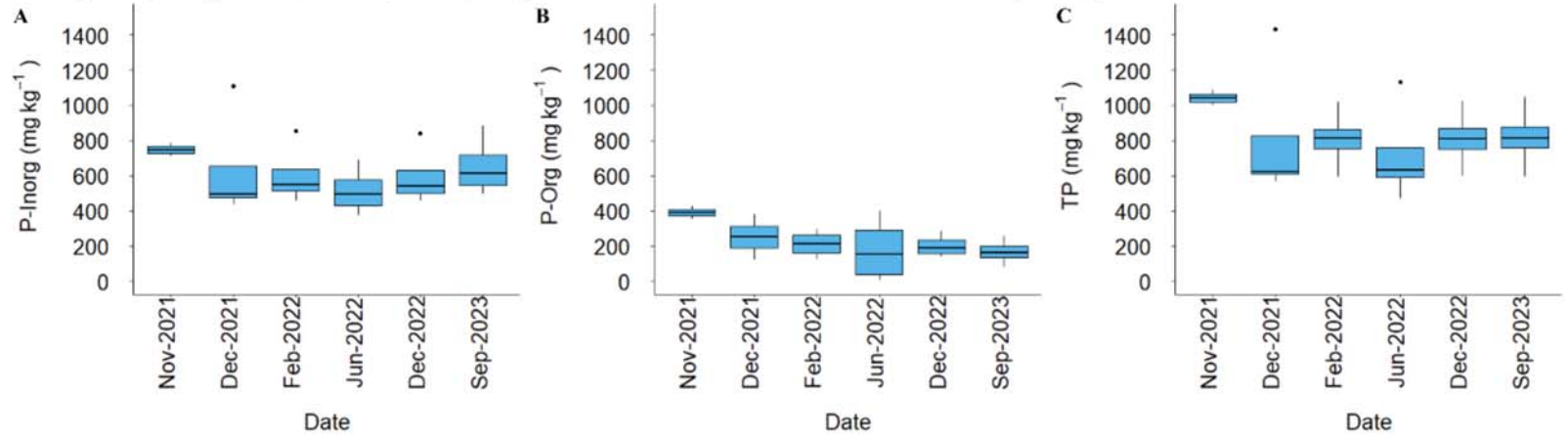

Source: The author.

Figure 36 – Time series of the concentration of phosphorus fractions in the reservoir sediment. A) shows the inorganic phosphorus, B) the organic phosphorus, and C) the total phosphorus.

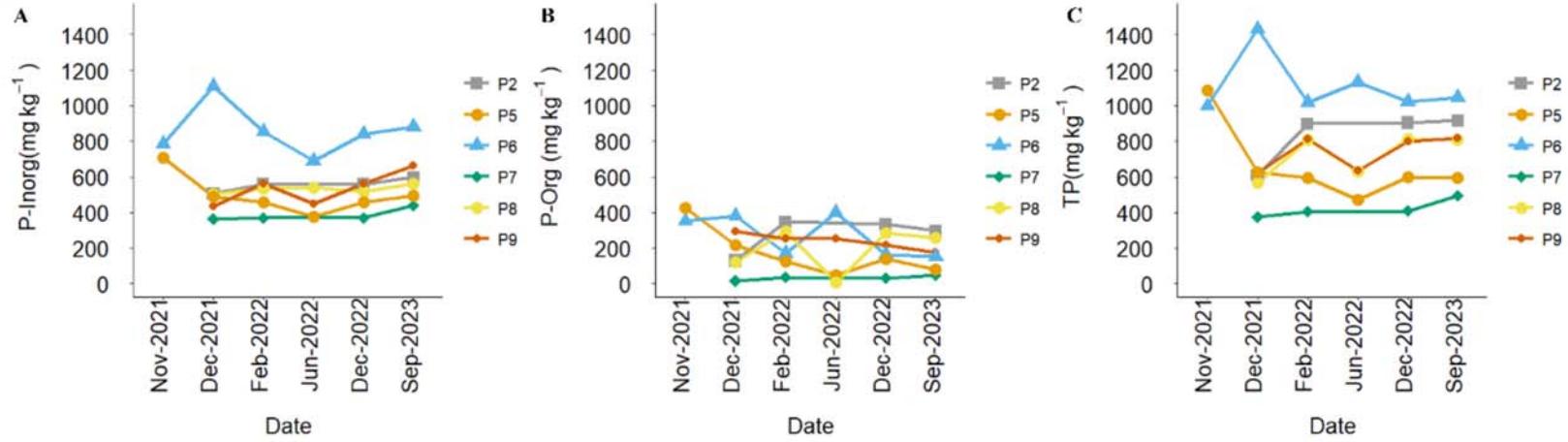

Source: The author.

The P_{Ca} (Figure 37B) median concentration increases from around 75 mg kg^{-1} in December 2021 to 160 mg kg^{-1} in June 2022, indicating a P_{Ca} input during the rainy season. However, P_{FeAl} varies more within the sampling points than the P_{Ca} (Figure 34). In addition, Fang *et al*. (2024) found that the increase of aerobic conditions due to the growth of submerged plants during the summer made the P_{FeAl} the predominant fraction of P and that in the winter the P_{Ca} predominated. This can indicate that the increase in P_{Ca} observed during the rainy season in the present study could occur due to the anoxic conditions being more intense in this season (Figure 7), but a long-term analysis should be performed in order to confirm significant variation trends in the sediment content. In addition, the median value of P_{FeAl} increased from 138 mg kg^{-1} in November 2021 to around 150 mg kg^{-1} in September 2023. This is a lower increase when compared to the variation observed in P_{Ca}, however, it indicates that the P_{FeAl} slowly increases with age (Figure 37A) as observed in Moura *et al.* (2020).

Figure 37 – Phosphorus fractions in the reservoir sediment grouped by each measurement date. A) represents the Iron Aluminum bound Phosphorus, B) the Calcium bound phosphorus, C) Mobile phosphorus, and D) the residual phosphorus. The horizontal line in each boxplot represents the median concentration for each date.

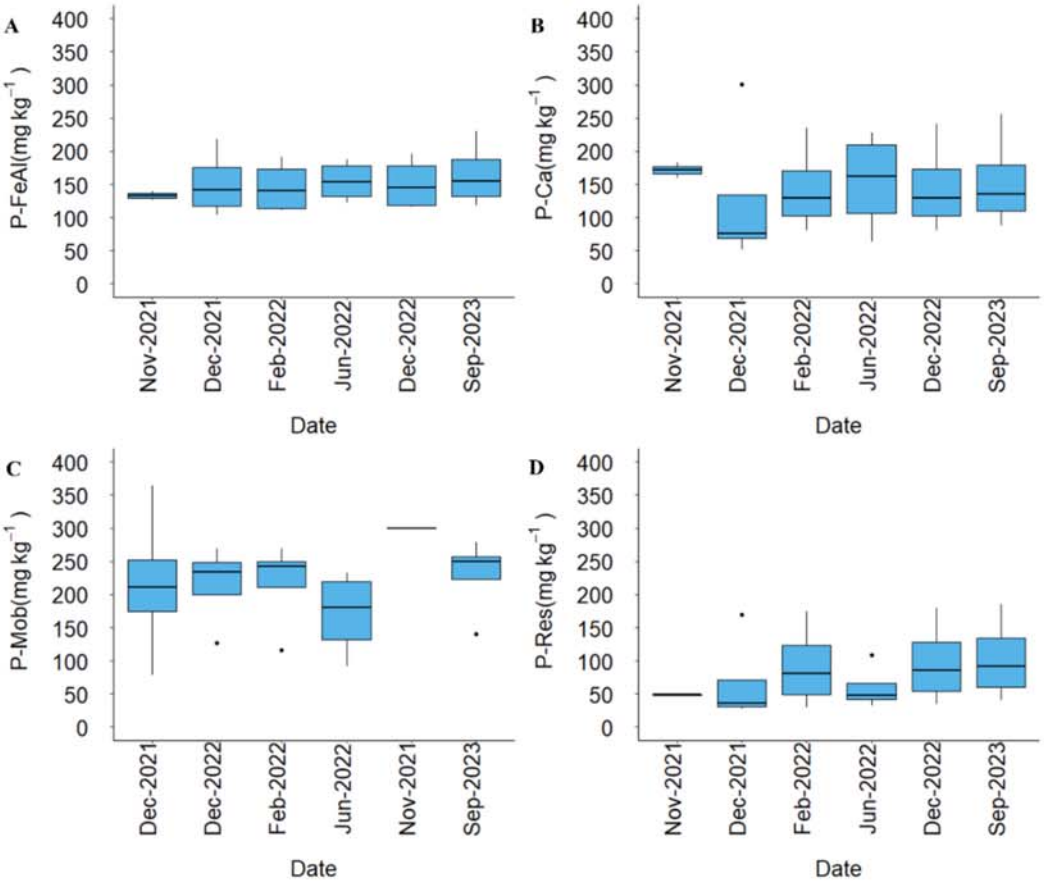

Source: The author.

As the P_{FeAl} fraction, Aluminum and Iron content in the sediment presented an increase trend throughout the analyzed period (Figure 38A and B), however, their increase was higher than the one observed for the P_{FeAl} fraction. The median Aluminum went from 6,800 to 10,000 mg kg^{-1} and the median Iron content went from 20,000 to 32,000 mg kg^{-1}. To know the concentration of these and other geochemically immobile elements can be used as a tracer to define the sources of the sediments (Fonseca, Araújo and Pinho, 2021), which can be important, for instance, to decide which measures are going to be effective on mitigating the eutrophication of reservoirs.

Figure 38 – Concentration of A) Aluminum, B) Iron, and C) Total nitrogen in the reservoir's sediment grouped by measurement date. The horizontal line in each boxplot represents the median concentration for each date.

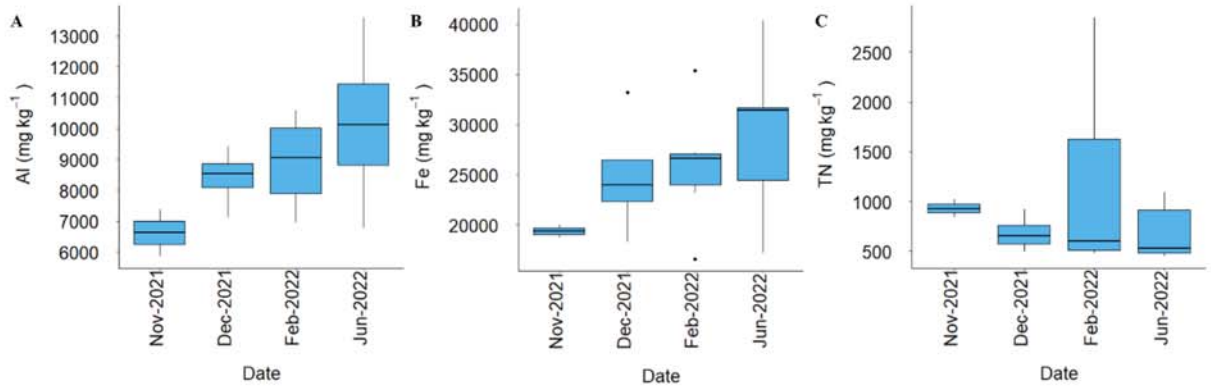

Source: The author.

5.3.3 Potential phosphorus release

Moura *et al*. (2020) found a promising relationship between P_{FeAl} concentration in the reservoir sediment with its age. Therefore, Figure 39 presents this relation between age and P_{FeAl} content in the sediment with the value obtained for Castanhão reservoir highlighted in red. Considering that the average P_{FeAl} content within the reservoir in 2023 was 160 mg kg^{-1} (Figure 39), the P_{FeAl} content adjusts well with the relation age and P_{FeAl}. Even though the point in Castanhão is not as close from the fitted line as the points from Cavalcante *et al*. (2018) and Cavalcante *et al*. (2021), it varied in a similar proportion as the sampling point for one of the reservoirs from Moura *et al*. (2020). However, the age is not the only relevant factor to consider when estimating the P_{FeAl} content, it can also depend on the sedimentation and the conditions of the local soil (Cavalcante *et al*., 2021).

Figure 39 – Validation of the Iron-Aluminum bound phosphorus versus reservoir age relation with the inclusion of Castanhão. The Castanhão value represents the P_{FeAl} concentration within the reservoir in its age of 21 years, considering the year when the analysis was performed (2023) with a standard deviation of 38.83 mg kg^{-1}.

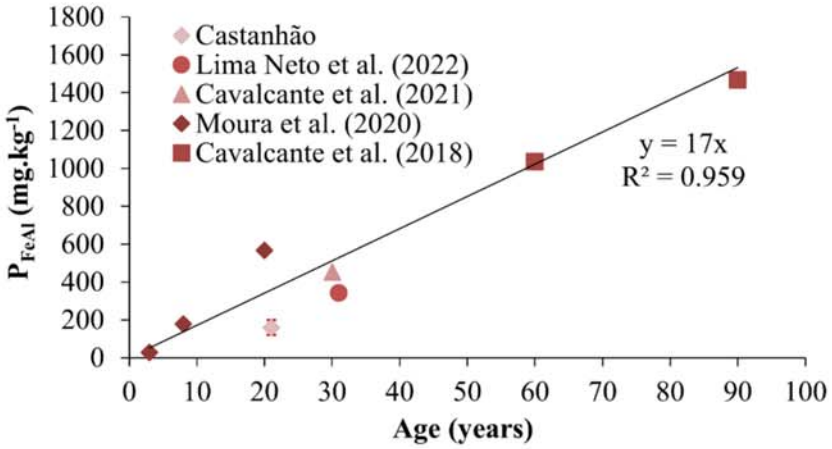

Source: The author.

Using the relation between P_{FeAl} content and P release rate k_r, the value of for Castanhão reservoir would be of 3.1 mg $m^{-2}day^{-1}$. The release rate experimentally found by Moura *et al*. (2020) was of 11 mg $m^{-2}day^{-1}$ for a P_{FeAl} dominated sediment and 4 mg $m^{-2}day^{-1}$ for the P_{Ca} dominated sediment, they presented a P_{FeAl} content of 567 and 177 mg kg^{-1}. Whereas Cavalcante *et al*. (2021) found in a sediment where the aluminum-bound P was the major P form, the minimum P release was in an aerobic state, pH 6 and temperature 28°C, and maximum P release in anoxic state pH 10 and temperature 31°C with the release rate values of 0.22 mg $m^{-2}day^{-1}$, and 2.1 mg $m^{-2}day^{-1}$, respectively. Both the Aluminum and Iron-bound P are inorganic fractions that are more susceptible to dissolve into the water column under alkaline conditions. This shows how the P release rate from sediments varies according to not only the P_{FeAl} content in the sediment, but also due to environmental conditions such as redox potential, pH and temperature, which should be further included in a model to estimate the release rate of P from sediments.

5.4 Conclusions

The monitoring of the sediment composition in Castanhão reservoir allowed a better understanding of its potential for internal loading of P within its different regions.

The majority of the P content in Castanhão's sediment was from the inorganic fraction, with the sampling point closest to the dam being the one where this fraction accumulates the most.

The two sampling points with the highest P_{FeAl} sediment content (P6 and P9) were also the ones where the predominant particle size was clay. This fraction of P was predominant in the sampling point closest to the dam, which is the deepest point and where the DO concentrations are lower. Showing that this is a favorable place for internal P loading. Since the water intake is close to this sampling point, the viability application of measures to control internal loading such as hypoliminium aeration should be further studied. This could improve the quality of the abstracted water for its treatment.

Contradicting what was expected, the sampling point inside the fish farming activity (P7) was not the one with the most P content in the sediment. Which indicates that the P originating from this activity is transportated to downstream sampling points, for instance P6. An analysis of the direction of the flow in the reservoir should be performed in order to assess how the P transport occurs in this reservoir, including the transport to the right branch of the reservoir, which is where the second highest P_{FeAl} median concentration was found.

The main notable temporal variation occured in the P_{Ca} fraction. It increased for around two-fold after the rainy season of 2022. However, this should be confirmed by a long-term analysis, where it would be possible to assess any significant trends on sediment composition.

Even though Castanhão reservoir was well represented by the age versus P_{FeAl} content relation, the age seems not to be the only relevant factor for P_{FeAl} content in the sediment. Therefore, an assessment of the P_{FeAl} content, sedimentation rates and local soil conditions within different reservoirs should be performed on further studies in order to investigate which are the important factors on sediment composition.

Finally, the value for release rate based on the P_{FeAl} content was reasonable when compared to the ones from other reservoirs. A relevant study experimentally calculating the release rate from sediments from the different sampling points under controlled conditions could further improve the P_{FeAl} versus release rate relation and provide an understanding of what factors influence the most on P release.

Even though the present study did not present a long-term evaluation of sediment characteristics variation, it provided with important information to confirm past studies and to elaborate further studies in order to improve the knowledge on internal P loading.

6 TOTAL PHOSPHORUS MODELING IN A STRATEGIC MULTIPURPOSE TROPICAL SEMIARID RESERVOIR

6.1 Introduction

Phosphorus is the limiting nutrient and is considered the key factor on the eutrophication of lakes and reservoirs (Liang, Soranno and Wagner, 2020; Robson, 2014). The quantification and reduction of P is a water management challenge much explored in several studies (Morales-Marín, Wheater and Lindenschmidt, 2017; Su *et al*., 2022). The main P loading into reservoirs comes from external sources, which can be point or non-point (Fong *et al*., 2023). Usually, the non-point sources are the hardest to quantify since they are broader and present more complex mechanisms (Wang *et al*., 2023). However, studies from the past years have found that even when external pollution of P is controlled by management measures, the reservoir or lake water quality would not improve due to internal P input from sediment (Wen *et al*., 2020). This occurs because sediment can be both a source and a sink of P (Liu *et al*., 2017). Several studies found that P can be released from sediment to the water column in anoxic conditions, high temperature, and high pH when the iron-bound P is the major fraction of inorganic P in the sediment (Cavalcante *et al*., 2021; Kwak, Jeon and Duck Hur, 2018), a fraction that increases the older the reservoir gets (Moura *et al*., 2020). Which shows the importance of considering both internal and external loading of P when modeling the P dynamics in reservoirs.

The reservoirs in Tropical semiarid regions are more susceptible to eutrophication mainly due to the high occurrence of drought periods, high evaporation rates and both intra and inter-annual precipitation variability (Rocha *et al*., 2022; Santos *et al*., 2017). The reservoirs in this region are built to support multiple uses e.g., human supply and fish farming activities. This combination of facts adds more complexity to the water quality management of reservoirs in this region.

Several studies were conducted with the aim of quantifying or predicting external P loading into reservoirs (Fong *et al*., 2023; Montefiore and Nelson, 2022; Rocha and Lima Neto, 2021; Sun *et al*., 2024), others focused on studying the internal loading potential of reservoirs (Adhikari *et al*., 2015; Cavalcante *et al*., 2021; Moura *et al*., 2020; Olsson *et al*., 2022; Rocha and Lima Neto, 2022). The external P loading is the base of Vollenweider's model (Chapra, 2008), whereas (Chapra and Canale, 1991) introduced the two-layer P model with the P exchange in the water-sediment interaction. Lira, Medeiros and Neto (2020) developed a two-

compartment model of P dynamics in a reservoir, considering both the external and internal loading of P. Whereas Lima Neto *et al*. (2022) focused on estimating external and internal P loading and then developed the P dynamics model.

However, there is still a gap regarding studies that develop a conceptual predictive model that incorporates the P dynamics due to different P sources in reservoirs with significant water level variation and that are more susceptible to thermal stratification and, consequently, to anoxic conditions due to its great depth. Furthermore, there is also a need for studies that evaluate scenarios of P loading reduction and that estimates the P carrying capacity of the reservoir.

Therefore, the present study aims to develop a model that incorporates the water level variation and the variation of redox conditions using field data to assess P dynamics in a large and deep reservoir where the major P sources are external, internal, and from the fish farming activity. Specifically we aim to 1) Use the inflow and TP concentration relation from Chapter 4 to estimate the external P load; 2) Estimate the TP load from the fish farming activity; 3) Develop a method to calculate the area of the deposition zone; 4) Calibrate the P dynamics model; 5) Simulate which reductions of TP loading should be done so as the reservoir fits the class 2 (Brazil, 2005) water quality limit established by Brazilian legislation; and 6) Calculate the carrying capacity of the reservoir in order for it to remain in the class 2 limit (Brazil, 2005).

6.2 Materials and Methods

6.2.1 Study Area

The present study was conducted in the Castanhão reservoir and the upstream sections of the Jaguaribe River, situated within the municipality of Jaguaribara-CE. The reservoir was constructed in 2002 (Figure 40) and it has a storage volume of 6.7 billion m^3, a maximum height of 71 m, and a drainage area of 45309 km^2 (Ceará, 2022a). Among its multiple uses, this reservoir is of great importance for the water supply of Fortaleza and its metropolitan region through the Jaguaribe-Metropolitan water transfer system (Sousa Estácio *et al*. 2022).

Figure 40 – Map of the study area the Castanhão reservoir with representation of the six water quality sampling points in the reservoir and the three sampling points in the Jaguaribe river, where the inflow rate into the reservoir and water quality analysis was done.

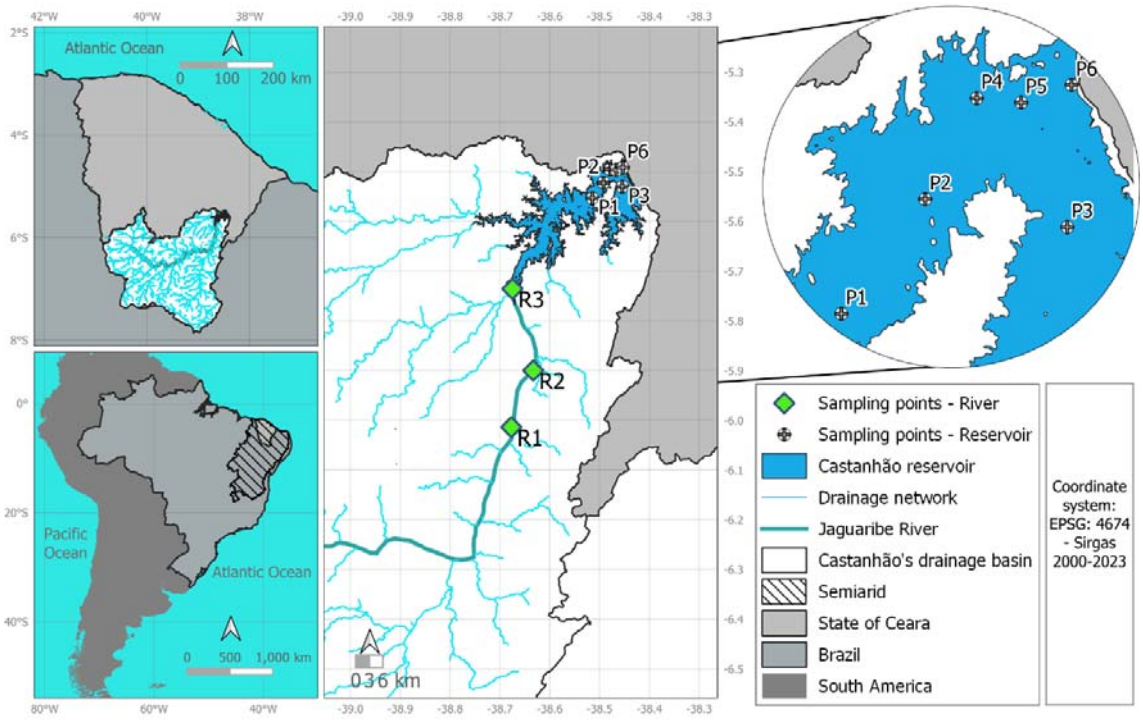

Source: The author.

The annual precipitation in the drainage basin is 836 mm/year (Rocha and Lima Neto, 2021) with a seasonal variation in which rainfall is concentrated in the months from January to May. During the dry season - in the second semester - the inflow into the reservoir is practically null. Located in a semiarid region, during the period from 2012 to 2018, the reservoir area experienced an intense drought in which the reservoir volume decreased from 75% of its total volume to 2% (Sousa Estácio *et al*. 2022). This reduction in volume had a significant impact on the water quality of the reservoir, which began to oscillate between eutrophic and hypereutrophic states (Ceará, 2022b).

6.2.2 Data and analysis

6.2.2.1 Data Acquisition

Field data collection was conducted, and the sampling campaigns were divided into two stages. The profiling stage involved the use of the YSI EXO 2 multiparameter probe to measure dissolved oxygen (DO) at six collection points (Figure 40) from the surface (0.3 meters depth) to 0.5 meters above the bottom sediment layer at intervals of 0.5 meters down to a depth of 8

meters, where measurements were then taken every 1 meter. The second stage of the collection campaign involved sampling for analysis of other water quality parameters in the laboratory. In this stage, samples were collected from points 3, 4, and 6, at five different depths along the water column. The samples were analyzed to quantify total phosphorus (TP) according to the methods outlined in Apha (2017).

Profiling data was measured monthly from January 2016 to December 2022, while samples for laboratory analysis were collected quarterly from May 2016 to September 2020 and monthly from October 2020 to December 2022. It is worth noting that points 3, 4, and 6 were chosen from among the six points to facilitate logistics, ensuring expediency in laboratory sample analysis and because they are representative of the reservoir. P3 is located in the left branch of the reservoir and near the fish farming area, P4 is in the right branch of the reservoir, and P6 is close to the dam. Inflow discharges to the reservoir, as well as TP concentration, were measured at three sections in the Jaguaribe river to the reservoir: R1, R2, and R3 (Figure 40). The flow rate was measured using the SonTek Riversurveyor M9 flow meter.

6.2.2.2 Inflow calculation

Castanhão reservoir has daily water level data, which enables the estimation of inflows to the reservoir using a water balance calculation. This calculation was performed using the following equations:

$$^{dV}/_{dt} = Q_{in}(t) - Q_{out}(t) \quad (13)$$

$$Q_{out,i} = E_i + WS_i + GF_i + Q_{PS} \quad (14)$$

Where $^{dV}/_{dt}$ is the time variation of the stored volume V, Q_{in} represents the inflow ($m^3\ day^{-1}$), and Q_{out} represents the outflows that were considered for this reservoir ($m^3\ day^{-1}$): the volume evaporated – Q_E, the flow for continuous water supply – Q_{WS}, the gate flow – Q_{GF}, and the pumping station flow – Q_{PS}.

The volume evaporated E was estimated by multiplying the monthly reference evaporation rate for the lake by the average surface area of the lake on day i. The latter was calculated by the level-area curve, considering the measured levels at the beginning of days i and $i + 1$. The reference evaporation rate (considered constant for each month of the year) was defined by the evaporation calculated at the reference meteorological station for Castanhão reservoir established by COGERH (Ceará, 2021).

6.2.2.3 TP modeling

In the present study, we adapted the complete-mixing model of Vollenweider to describe the phosphorus budget in the water considering the internal TP loading from sediment, the fish farming TP loading, and the high water-level variations in the reservoir considering a monthly time-step:

$$d(V.TP_{out})/_{d_t} = Q_{in}.TP_{in} + FF - Q_{out}.TP_{out} - k_s.V.TP_{out} + k_r A_{sed} \quad (15)$$

where: TP_{in} is the total phosphorus concentration in the inflow water (mg m^{-3}); TP_{out} is the total phosphorus concentration in the water column assuming a complete-mix (mg m^{-3}); Q_{in} is the inflow rate calculated with the water balance (m^3 $month^{-1}$); FF is the total phosphorus load that comes from the fish farming tanks (mg $month^{-1}$); Q_{out} is the outflow rate from the reservoir (m^3 $month^{-1}$); k_s is the first-order settling rate of total phosphorus in the water column ($month^{-1}$); k_r is the zero-order release rate of total phosphorus from the sediment to the water column (mg $m^{-2}month^{-1}$); and A_{sed} is the surface area where the total phosphorus is released to the water under anoxic conditions (m^2).

Equation 12 represents the variation of phosphorus accumulation through time [$d(V.TP_{out})/dt$] that depends on the external loading of P [$Q_{in}.TP_{in}$], internal loading of P from the sediment [$k_r.A_{sed}$], the loading of P from fish farming activities [FF], the P decay due to settling [$k_s.V.TP_{out}$], and the output of P load [$Q_{out}.TP_{out}$].

The reservoir water balance was solved to obtain monthly data for the entire calibration period (2020-2022), TP_{in} concentrations were estimated based on the non-linear inflow-TP model obtained in Chapter 4, *Section 4.3.4*.

This equation was numerically solved on Eulerian form to obtain the TP concentration at the time i+1 as follows:

$$TP_{out(i+1)} = \frac{V_i.TP_{out,i} + (W_i - Q_{out,i}TP_{out,i} - k_s.V_i TP_{out,i} + k_r A_{sed,i}).\Delta t}{V_{i+1}} \quad (16)$$

where: W is the sum of the inflow TP load and the TP load from the fish farming activities.

DO profiling in a sampling point in the reservoir was used to estimate the A_{sed} term. In the present study, the volume percentage of the reservoir that was in an anoxic state (DO<1.5 mgL^{-1}) (Moura *et al.*, 2020) at each month of the calibration of the model was calculated. As seen in Chapter 2, there is a clear seasonality on the DO distribution within the water column,

with the rainy period being the one where the anoxic DO concentration practically reaches the surface, and the dry period being the one with better DO conditions. Therefore, mean anoxic volume percentage of the reservoir was calculated for the dry and rainy season, based on the monthly profiling data of P6, which is the sampling point with the lowest DO concentration values. With the profiling data, the oxycline level was assessed and then converted to the reservoir volume using the level-area curve, this was considered the anoxic volume. Then this value was divided by the reservoir total volume in that day to obtain the percentage of anoxic volume. This was calculated for all the days where the profiling analysis was performed and then an average for rainy and dry period was calculated. The percentages found were 14% and 53% for the dry and rainy period, respectively. Finally, the anoxic percentages were applied to the volume and then the A_{sed} term was calculated for each month of the calibration period.

To estimate the TP load originating from fish farming activities, we utilized data obtained through a questionnaire administered by COGERH, along with satellite imagery and drone-captured images. These sources were employed to assess fish production among all cage farm owners within the reservoir.

In order to validate the accuracy of the collected data, we cross-referenced it with fish production records provided by the Brazilian Aquaculture Association. Notably, the data from the association consistently exceeded the estimates derived from satellite imagery and drone-captured images. This discrepancy can be attributed to inherent imprecisions in the images, such as the inability to distinguish between active and non-active cages.

As a result, the dataset from the Brazilian Aquaculture Association was chosen as the primary and more reliable source for the present study.

Subsequently, Equation 19 was employed to estimate the TP load released into the reservoir (Ono and Kubitza, 2003).

$$TP_{releas.} = FCR \times PC \times NDR \times Prod \quad (17)$$

Where $TP_{releas.}$ is the TP released into the water column in kilograms; FCR is the feed conversion rate, considered as 1.5; PC is the phosphorus content, considered as 0.008; NDR is the non-digestibility rate, considered as 1.5; and $Prod$ is the annual production (Sato *et al.*, 2016; Ono and Kubitza, 2003).

Figure 41 depicts the estimated TP (total phosphorus) load attributed to fish farming activity in Castanhão Reservoir from 2013 to 2023. A noticeable decreasing trend in the TP load is evident, primarily attributable to reduced fish production. This decline is largely attributed to

the prolonged drought period that commenced in 2012, leading to a substantial decrease in the reservoir's water level.

Figure 41 – Estimated TP load per year in Castanhão reservoir between the years 2013 and 2023.

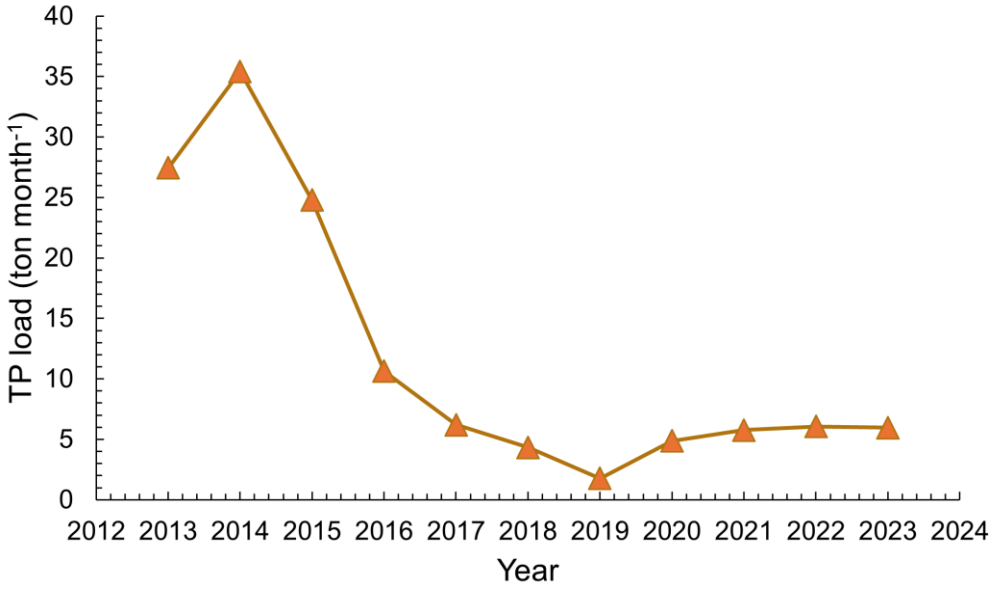

Source: The author.

The model was then calibrated using the Solver tool in Microsoft Excel by maximizing the NSE coefficient altering both k_s and k_r terms.

6.2.2.4 Model performance metrics

NSE coefficient (Nash and Sutcliffe, 1970) was used to optimize the calibration and evaluate the model performance:

$$NSE = 1 - [Sum(Y_{meas,i} - Y_{mod,i})^2 / Sum(Y_{meas,i} - Y_{mean})^2 \quad (18)$$

where: $Y_{meas,i}$ is the variable value measured at each time step, $Y_{mod,i}$ is the variable modeled value, and Y_{mean} is the mean of the measured variables. NSE varies from -1 to 1, and the closer the value is to 1, the better the model performance.

The root mean squared error (RMSE), and the percent bias (PBIAS) were also calculated to evaluate the model accuracy and performance of the model.

$$RMSE = \sqrt{\frac{1}{n} . \sum_{i=1}^{n} \left(Y_{mod,i} - Y_{meas,i}\right)^2} \quad (19)$$

$$PBIAS = \frac{\sum_{i=1}^{n} Y_{meas,i} - Y_{mod,i}}{\sum_{i=1}^{n} Y_{meas,i}} \times 100 \quad (20)$$

The PBIAS indicates how well the model simulates the average magnitudes for the output response of interest.

6.2.2.5 Scenario simulation

After the calibration, a scenario simulation was conducted to assess the impacts of various intervention measures aimed at reducing TP concentration in the reservoir to values lower than 0.05 mgL^{-1}. This value is the threshold in the Brazilian legislation so the water can be considered suitable to water supply after conventional treatment (BRASIL, 2005). The three scenarios tested were: an 80% reduction of the TP external load, a 20% reduction of TP load from fish farming activities, and a 20% reduction of internal TP load. In addition, this scenario simulation also allows to answer the question: what is the limit of the TP load that enter the reservoir for it to be considered class 3 according to the Brazilian legislation?

6.3 Results and discussion

6.3.1 Total phosphorus model performance

The model calibration for the years 2020 to 2022 obtained an NSE value of 0.62 which according to Moriasi *et al*. (2015) can be considered good. The PBIAS value was -0.03, which can also be considered good. Since the PBIAS is lower than one, this means that the model is slightly underestimating the measured values. As for the RMSE, it was of $2.4x10^{-2}$ mgL^{-1}. The standard deviation (SD) of measured TP concentration was $4x10^{-2}$ mgL^{-1}, therefore the model calibration accuracy according to Moriasi *et al.* (2015) can be considered satisfactory, since the ratio between RMSE and SD is 0.6.

Figure 42 presents the comparison of modeled and measured TP concentrations for the calibration period. It is possible to observe that the model presents more difficulty on predicting the peak TP concentrations. This possibly occurs because during the rainy season there is an intense TP load inflow from the upstream.

Figure 42 – Modeled and measured total phosphorus concentration in Castanhão reservoir between January 2020 and December 2022. The horizontal line represents the threshold (TP < 0.03 mgL^{-1}) in the Brazilian legislation for the water to be considered suitable for human supply after conventional treatment. The error bars contain the mean standard deviation observed on each total phosphorus measurement date (SD = 0.02).

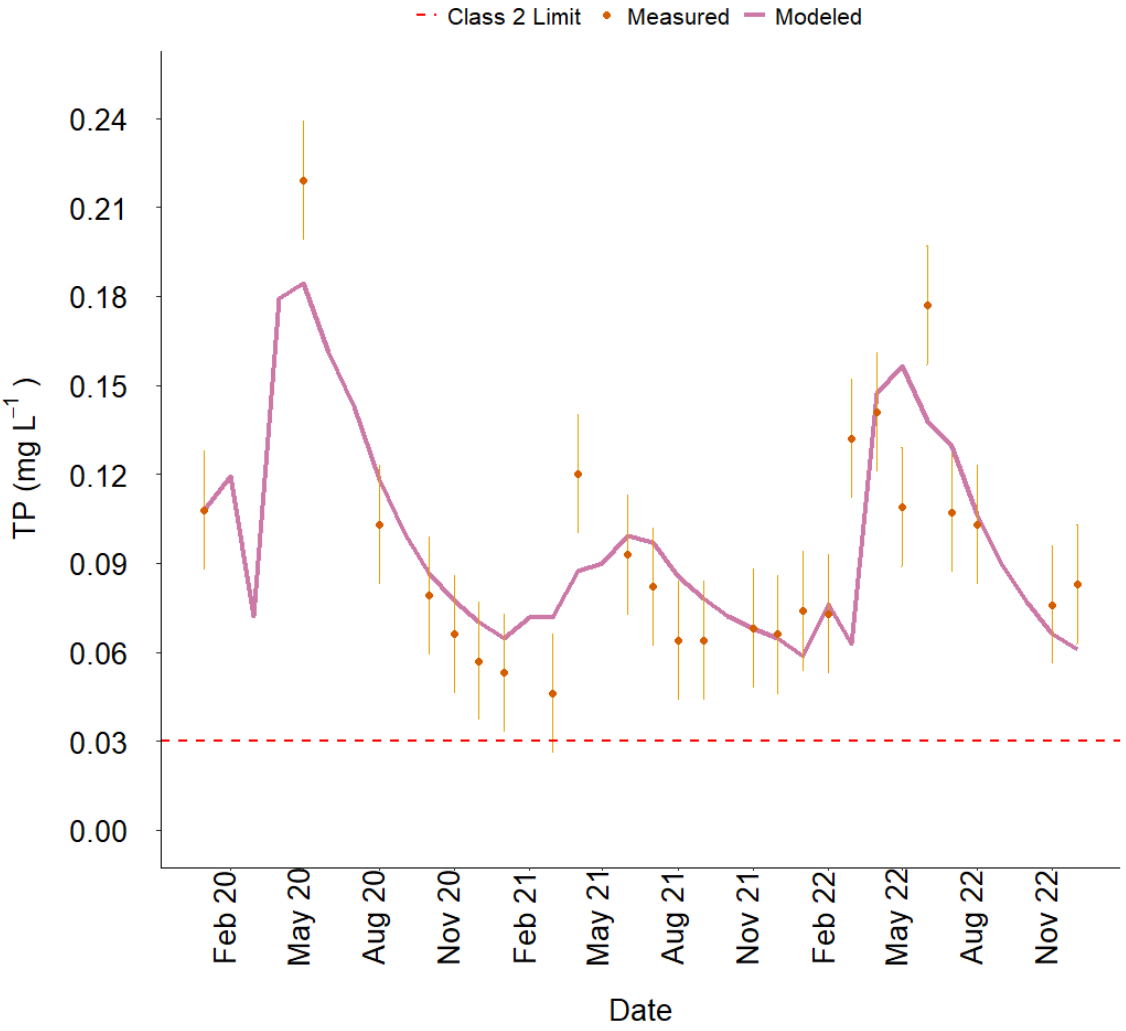

Source: The author.

Regarding the k_s and k_r coefficients obtained during calibration, they were 0.26 $month^{-1}$ and 267 mg $m^{-2}month^{-1}$, respectively. The value of k_s determined in the calibration of the model in the present study aligns with the k_s values of other reservoirs within the Brazilian semiarid region, ranging from 0.185 to 1.7 $month^{-1}$ (Lima Neto *et al.*, 2022; Toné and Lima Neto, 2019). Toné and Lima Neto (2019) used the TP decay equation adapted for the semiarid region, revealing that phosphorus decay in semiarid reservoirs occurs four times faster than in temperate lakes (Figure 43).

Figure 43 – Comparison between the k_s coefficient values obtained with the calibration in the present study for Castanhão reservoir and other k_s coefficients from reservoirs in the semiarid region. HRT is the hydraulic residence time.

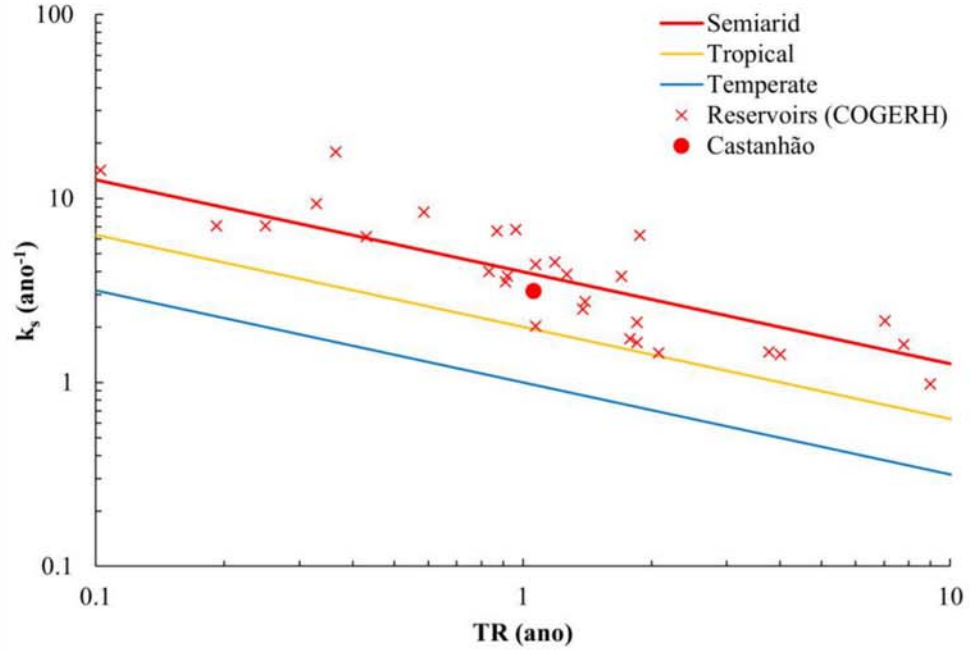

Source: The author.

Moura *et al.* (2020) demonstrated that k_r values vary depending on sediment composition. For instance, a reservoir with the highest P_{FeAl} exhibited an experimental k_r = 330 mg $m^{-2}month^{-1}$, while a reservoir with an intermediate concentration of P_{FeAl} showed k_r=120 mg $m^{-2}month^{-1}$, and a reservoir with very little P_{FeAl} exhibited k_r = 0 mg $m^{-2}month^{-1}$.

The k_r value obtained in this study was higher than that reported by Lima Neto *et al.* (2022) for an older reservoir in the same region (k_r=165 mg $m^{-2}month^{-1}$). This observation contrasts with the relationship established between reservoir age and the potential for P release from the sediment bed (section 5.2), where older reservoirs were expected to exhibit a higher potential for P release from sediment.

This difference may be attributed to variations in the activities conducted in the reservoir, which can influence sediment deposition. For example, Castanhão is characterized by extensive fish farming activities and was constructed by flooding a city, potentially leading to an increased P content in the sediment. For instance, the TP content in the sediment of Castanhão is much higher than the one found in the reservoir studied by Lima Neto *et al.* (2022),

they found a maximum TP content of 350 mg kg^{-1}, whereas in Castanhão, the median values of TP through time were around 800 mg kg^{-1} (Figure 35).

Despite these variations, the k_r value obtained in the calibration is close to the one estimated according to the age-P_{FeAl} relation. Based on Figure 39, in 2023, with 21 years old, the P_{FeAl} content in Castanhão reservoir was supposed to be 357 mg kg^{-1}. Using this value in the P_{FeAl}-k_r relation found in Moura *et al*. (2020), the k_r for this reservoir was supposed to be 210 mg m^{-2} $month^{-1}$, which is a value close to the one found in the calibration process performed in this study (267 mg m^{-2} $month^{-1}$).

In addition, it is important to highlight that the release rate of P from sediments also varies according to not only the P_{FeAl} content, but also according to environmental conditions such as redox potential, pH, and temperature.

Figure 44 presents the seasonal differences of TP input according to its source. During the rainy season (Figure 44A), the amount of TP that was released from sediment is higher than during the dry season (Figure 44B), which was expected since the rainy season is the one with the most occurrence of anoxia (see Chapter 2). It is worth noting that during the dry period the main sources of TP to the water column are the internal TP load from sediment (5.63 tons) and the TP load from fish farming activity (5.56 tons). In addition to the direct impacts of TP input from the fish farming activity, it can also have indirect effects on the dynamics of TP. For instance, reducing the TP input from the fish farming activity can indirectly contribute to the decrease of the deposition zone area as the reduction in aquaculture can decrease deposition and further decomposition of organic matter (Santos *et al*., 2016), which may lead to a reduction in the anoxic area of the reservoir (Hudson and Vandergucht, 2015). This underscores the importance of closely monitoring all the sources of TP.

Figure 44 – TP (tons) and its different input sources during the A) rainy and B) dry season.

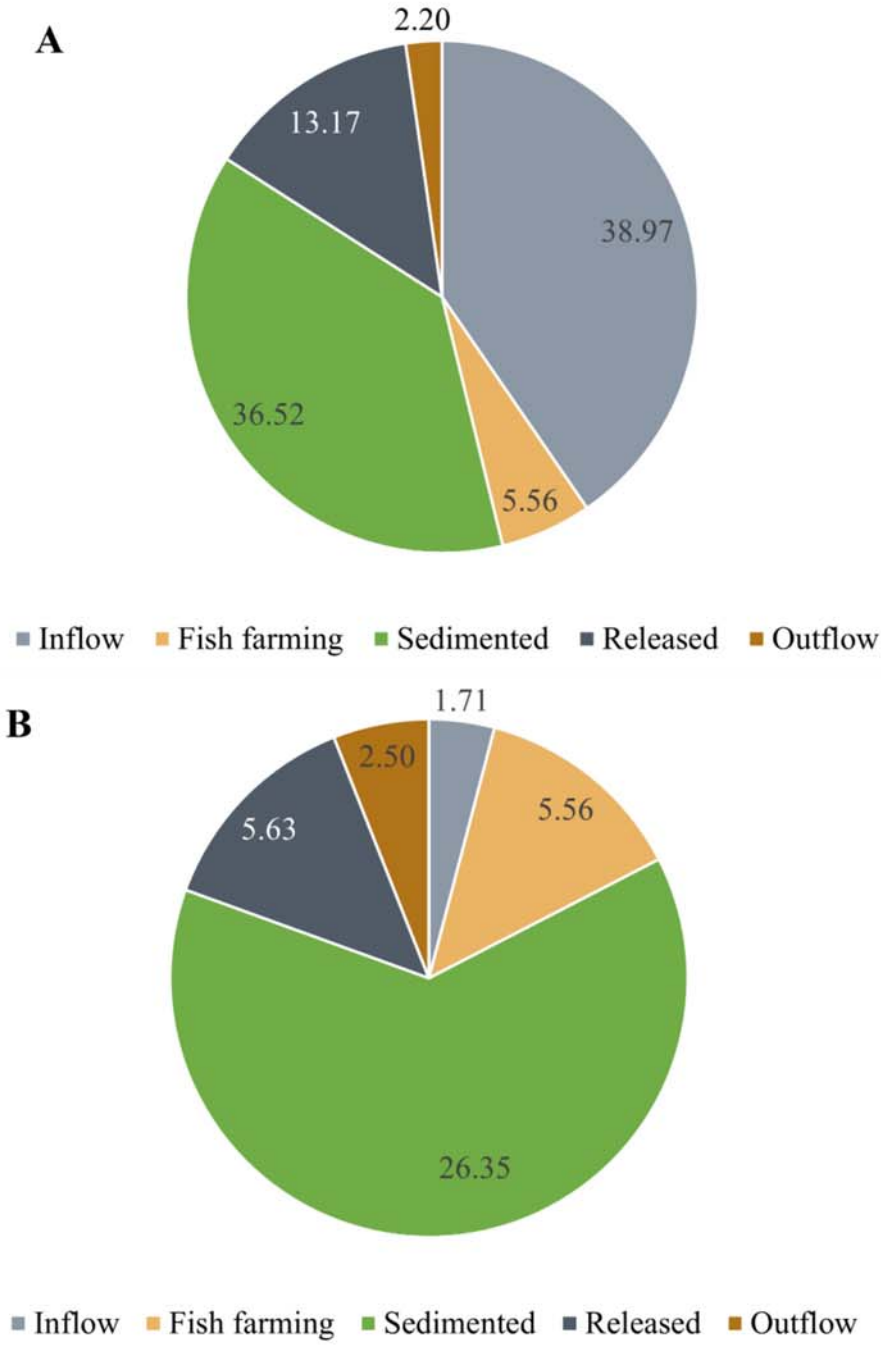

Source: The author.

6.3.2 Scenario simulation

6.3.2.1 Specific reductions of phosphorus loading from different sources

Figure 45 presents the results from the scenario simulated with the objective of reducing the TP concentrations to a level close to the class 2 limit. Seven scenarios of reduction

were applied. Firstly, the fish farming load was set to zero (Scenario 1), followed by zeroing the TP load from internal loading (Scenario 2) and zeroing the external TP (Scenario 3). Additionally, simulations were conducted to reduce the TP load from all three main TP load sources by 30%, 50%, and 80% (Scenarios 4, 5, and 7, respectively). The latter (Scenario 7) resulted in TP concentrations in the reservoir below the class 2 limit for almost the entire simulated period. Finally, Scenario 6 presents the combined reductions in all three main TP sources in the reservoir, with a 70% reduction in the external load, along with a 30% reduction in the internal load and a 30% reduction in the fish farming load. The implementation of Scenario 6 extends the scope of actions that can be taken to reduce the TP concentration in the studied reservoir by targeting all three main sources. With this scenario, it is possible to reach the Class 2 compliance limit by the end of the simulation period.

Figure 45 – Comparison of TP concentration values obtained from calibration against those from scenario simulations involving TP input load reduction. It delineates each scenario: Scenario 1, with a null Fish farming load; Scenario 2, featuring a null Internal load; Scenario 3, where the external load is null; Scenario 4, applying a 30% reduction across all three main TP loads (external, internal, and fish farming); Scenario 5, with a 50% reduction; Scenario 6, entailing a 70% reduction in the external load alongside 30% reductions in both the internal and fish farming loads. Finally, Scenario 7 represents an 80% reduction across all three main TP load sources. Class 2 limit is the water that is suitable for human supply after conventional treatment, irrigation, and aquaculture (Brazil, 2005).

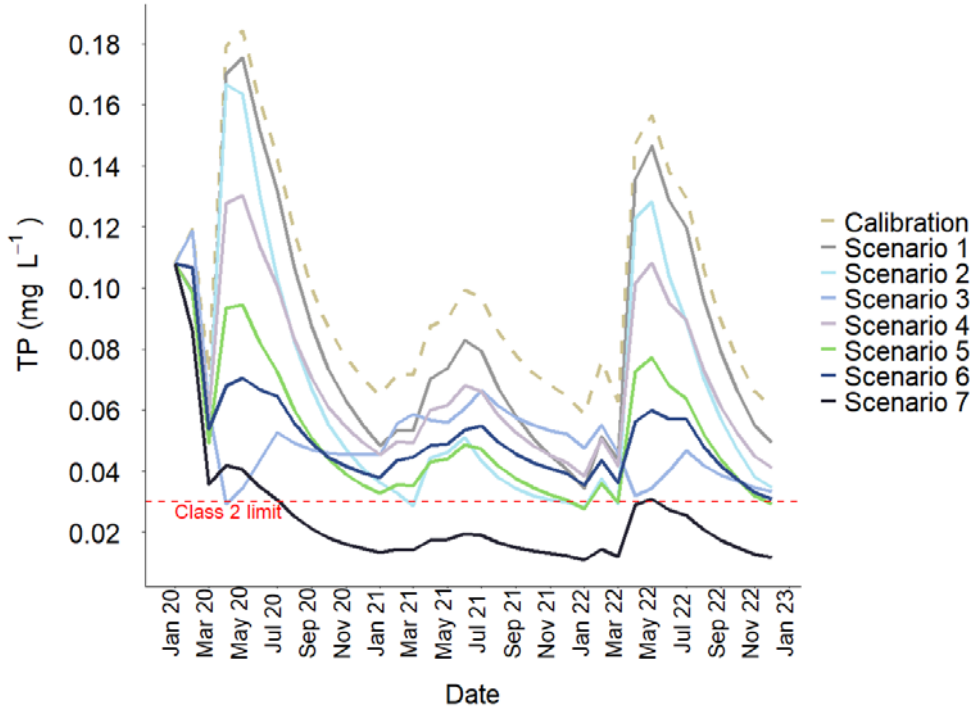

Source: The author.

In order to achieve such level of reduction of TP loading there are many alternatives. To reduce the external loading the improvement on rural sewage and agricultural drainage, improving the management of fertilizer use, and protection of high erosive riverbanks (Nazari-Sharabian and Taheriyoun, 2022; Sandström *et al*., 2024).

In addition, the creation of wetlands buffer zones, which act as natural filters of nonpoint source pollutants, can lower nutrient input to the reservoir. Cultivation and systematically harvest of macrophytes in the reservoir are also a promising nature-based technique that can potentially sequester nutrients and other pollutants from water and, consequently, can reduce the TP load (Fletcher *et al*., 2022).

Hypolimnetic aeration is another possible measure to control long-term eutrophication by reducing internal phosphorus loading in the reservoir. Using this method, the oxygen demand deeper within the water column is provided by oxygen from the atmosphere without destroying the reservoir's natural thermal stratification and improving the outflow water quality (Lima Neto, Cardoso and Woods, 2016; Lima Neto and Parente, 2016; Mehdizadeh *et al*., 2023). However, this technique can modify the sediment composition. For instance, (Chen *et al.*, 2021) after the aeration of the sediment-water interface of a pond, the content of mobile phosphorus increased by three-fold, which. Therefore, the application of this technique should be associated with others. Another promising technique to reduce the internal loading is to use modified clay and aquatic plants, which was proven a good remediation method to control internal loading of nutrients (Huo *et al.*, 2024).

When concerning the reduction of TP load from fish farming, a solution could be improving feed conversion rates, which increases the efficiency of the feeding process and reduces the amount of TP that goes to the water column (Cobo *et al*., 2019; Vogel *et al*., 2019).

Certainly, there are many factors that should be considered when applying measures to reduce TP concentration in a reservoir and further studies should be performed in order to assess the suitability and efficiency of different methods in the region where it should be applied.

6.3.2.2 Carrying capacity of the reservoir.

Several tests were conducted using the calibrated model to estimate which would be the total carrying capacity of the reservoir in order for it to fit the class 2 limit in the Brazilian legislation (Brazil, 2005). This limit is that the concentration of TP in the water has to be lower than 0.03 mgL^{-1} for it to be considered suitable for human supply after conventional treatment,

for primary contact recreation, such as swimming, and the irrigation of vegetables, fruit plants, parks, gardens, sports fields, and leisure areas with which the public may come into direct contact; and aquaculture and fishing activity. Those uses coincide with the main uses of this reservoir and, therefore, this should be the class in which the reservoir best fits.

Figure 46 depicts the impact on the modeled TP concentration in the reservoir for the calibrated period if the carrying capacity of the reservoir was to receive about 8.3 tons month^{-1} (100 tons year^{-1}) of TP loading. This figure show that this carrying capacity is the one that would be suitable for maintaining the reservoir around the class 2 limit (Brazil, 2005). The P load calculated in the calibration for the three main sources of P to the reservoir (fish farming, internal loading, and external loading) was of 423.55 tons year^{-1}, whereas the P load from the scenario simulated in the previous section (6.3.2.1) was of 198.87 tons year^{-1}.

Figure 46 – Simulation of TP concentration in the reservoir if the TP load was of 100 tons year^{-1}. Class 2 limit is the water that is suitable for human supply after conventional treatment, irrigation, and aquaculture (Brazil, 2005).

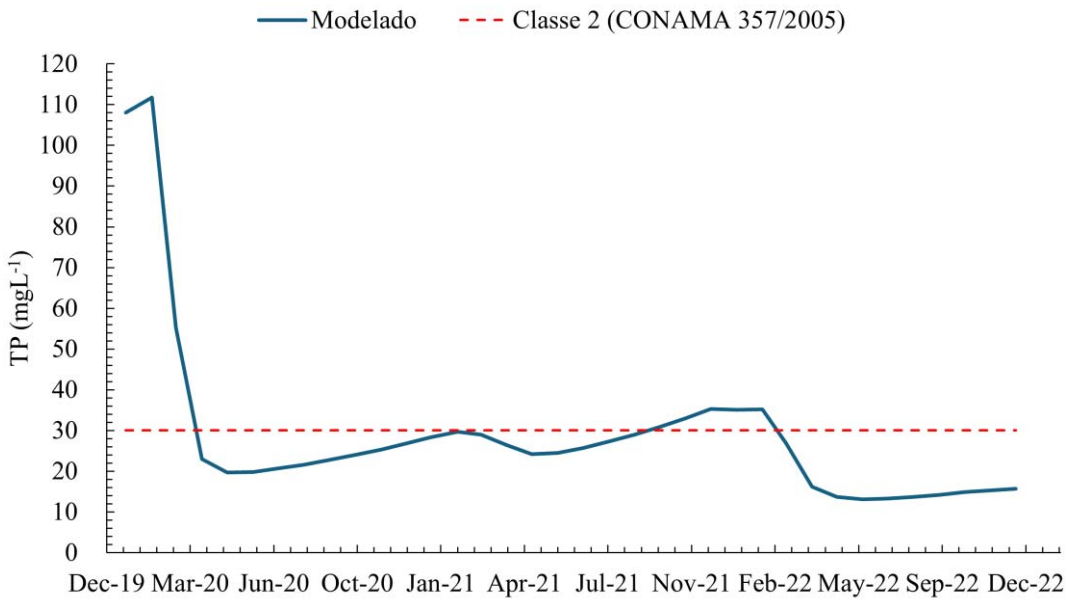

6.4 Conclusions

The model calibrated in the present study is a tool that can be an asset for improving the water management in reservoirs after its validation. It was elaborated with novel techniques to estimate the area of the P deposition zone based on an extensive water quality monitoring

campaign, incorporating water level variation and the different sources of P (external, internal, and from fish farming).

It also shows potential to be adapted to other multipurpose reservoirs. It showed a good calibration performance based on several performance metrics and the values obtained for the P sedimentation and release rate are consistent when comparing to the ones obtained in other reservoirs and when considering the characteristics of the reservoir.

This model also showed that during the rainy period, the main source of P is the one from external input, whereas during the rainy season is the one from internal loading and fish farming activities. This shows how the potential impact of the fish farming activities particularly increases during dry seasons and drought periods.

The scenario simulation and the P carrying capacity calculation show the sensibility of the model to the different sources of TP and how they should be reduced in order for the reservoir to fit the appropriate water quality class based on its main uses. This is another useful tool for water managers to plan the intervention measures to improve the water quality of a reservoir and to aid the process of distributing permissions for fish farming and the process of water allocation. Future studies could encompass the creation of prospective and participatory scenarios, employing methodologies like Michel Godet's prospective scenario planning. This will allow for the integration of water quality considerations into water resource management planning.

Even though this model needs to be further validated, its calibration showed its consistency and its potential for the use of this tool to improve the water quality management in the studied reservoir and possibly other reservoirs under similar conditions.

7 GENERAL CONCLUSIONS

The present thesis conducted a detailed study at various temporal scales and considering different factors influencing reservoir quality. In Chapter 2, monthly variations were examined, revealing that temporal fluctuations in nutrient concentrations surpassed spatial variations, supporting the hypothesis of a complete mix approach. Chapter 3 shifted focus to diel temporal scales, highlighting thermal stratification patterns correlated with seasonal changes and wind speeds, with total phosphorus levels exhibiting an increase throughout the day in the rainy season. Chapter 4 expanded the study upstream the reservoir, identifying the most downstream sampling point in the river upstream the reservoir as exhibiting superior water quality, particularly during the dry season, and emphasized total phosphorus as a significant factor in reservoir eutrophication. In Chapter 5, sediment analysis revealed inorganic fractions as predominant, with notable concentrations of iron-aluminum-bound phosphorus (P_{FeAl}), particularly near the dam, necessitating further investigation for mitigation strategies. Finally, Chapter 6 synthesized previous findings to calibrate a mass balance model, projecting scenarios for reservoir water quality, suggesting significant reductions in external, internal, and fish farming loads could bring total phosphorus content within acceptable limits, while highlighting the urgent need for a drastic reduction in current phosphorus loads to ensure compliance with water quality standards.

This thesis undertook a comprehensive examination of water quality dynamics in a large, deep, semiarid reservoir, covering various aspects. The obtained results will be crucial for advancing planning and readiness for drought events. Previously, much emphasis was placed on managing water quantity, but the continuous degradation of water quality has become a pressing concern, resulting in adverse impacts on various water uses. Consequently, integrating quality management into water resource management has become imperative.

Through the findings of this thesis, not only was a deeper understanding of water quality dynamics in a semiarid reservoir attained, but also a tool was developed to aid in integrating water quality management into resource management practices. As a result, it will be possible in the future to formulate a water quality management policy and even restructure the process of allocating water usage rights, considering both available quantity and the impact of such allocations on reservoir quality.

Overall, this thesis provides valuable results, insightful discussions, and tools that contributed to the understanding of the water quality dynamics of an important reservoir and

that can be helpful to other similar studies in other reservoirs. In addition, the research used data from an in-depth water quality monitoring that was seen in very few semiarid reservoirs. This data allowed the development of a tool that can be used by the State's water management company in order to aid the decision making of the managers regarding water allocation in the reservoir.

REFERENCES

ADHIKARI, P. L.; WHITE, J. R.; MAITI, K.; NGUYEN, N. Phosphorus speciation and sedimentary phosphorus release from the Gulf of Mexico sediments: Implication for hypoxia. **Estuarine, Coastal and Shelf Science**, v. 164, p. 77–85, 2015.

AHMED, M. H.; LIN, L. S. Dissolved oxygen concentration predictions for running waters with different land use land cover using a quantile regression forest machine learning technique. **Journal of Hydrology**, v. 597, n. March, 2021.

ALLEN, G. R.; SCHWARTZ, F. W.; COLE, D. R.; LANNO, R. P.; PRABHU, A.; ELEISH, A. Algal blooms in a freshwater reservoir – A network community detection analysis of potential forcing parameters. **Ecological Informatics**, v. 60, n. September, 2020.

APHA (2017). Standard Methods for the Examination of Water and Wastewater (23rd ed.). Washington DC: American Public Health Association.

ARAÚJO, C. A. S.; SAMPAIO, F. G.; ALCÂNTARA, E.; CURTARELLI, M. P.; OGASHAWARA, I.; STECH, J. L. Effects of atmospheric cold fronts on stratification and water quality of a tropical reservoir: Implications for aquaculture. **Aquaculture Environment Interactions**, v. 9, n. Mpa 2013, p. 385–403, 2017.

ARORA, M.; CASAS-MULET, R.; COSTELLOE, J. F.; PETERSON, T. J.; MCCLUSKEY, A. H.; STEWARDSON, M. J. **Impacts of Hydrological Alterations on Water Quality**. [s.l.] Elsevier Inc., 2017.

ATHAUDA, A. M. N.; ABINAIYAN, I.; LIYANAGE, G. Y.; BANDARA, K. R. V.; MANAGE, P. M. Spatio-Temporal Variation of Water Quality in the Yan Oya River Basin, Sri Lanka. **Water, Air, & Soil Pollution**, v. 234, n. 3, 2023.

AUGUSTO-SILVA, P. B.; MACINTYRE, S.; MORAES RUDORFF, C. DE; CORTÉS, A.; MELACK, J. M. Stratification and mixing in large floodplain lakes along the lower Amazon River. **Journal of Great Lakes Research**, v. 45, n. 1, p. 61–72, 2019.

AZADI, F.; ASHOFTEH, P. S.; CHU, X. Evaluation of the effects of climate change on thermal stratification of reservoirs. **Sustainable Cities and Society**, v. 66, n. November 2019, 2021.

BANERJEE, A.; CHAKRABARTY, M.; RAKSHIT, N.; BHOWMICK, A. R.; RAY, S. Environmental factors as indicators of dissolved oxygen concentration and zooplankton abundance: Deep learning versus traditional regression approach. **Ecological Indicators**, v. 100, n. March 2018, p. 99–117, 2019.

BARBOSA, C. C.; CALIJURI, M. DO C.; ANJINHO, P. DA S.; SANTOS, A. C. A. DOS. An integrated modeling approach to predict trophic state changes in a large Brazilian reservoir. **Ecological Modelling**, v. 476, n. June 2022, 2023.

BARBOSA, I. B. R.; CIRILO, J. A. Contribuição média de fósforo em reservatório de abastecimento de água - Parte 1. **Engenharia Sanitaria e Ambiental**, v. 20, n. 1, p. 39–46, mar. 2015.

BARBOSA, J. DO S. B.; BELLOTTO, V. R.; SILVA, D. B. DA; LIMA, T. B. Nitrogen and phosphorus budget for a deep tropical reservoir of the Brazilian Savannah. **Water (Switzerland)**, v. 11, n. 6, 2019.

BARÇANTE, B.; NASCIMENTO, N. O.; SILVA, T. F. G.; REIS, L. A.; GIANI, A. Cyanobacteria dynamics and phytoplankton species richness as a measure of waterbody recovery: Response to phosphorus removal treatment in a tropical eutrophic reservoir. **Ecological Indicators**, v. 117, n. May, 2020.

BARROS, M. U. G.; WILSON, A. E.; LEITÃO, J. I. R.; PEREIRA, S. P.; BULEY, R. P.; FERNANDEZ-FIGUEROA, E. G.; CAPELO-NETO, J. Environmental factors associated with toxic cyanobacterial blooms across 20 drinking water reservoirs in a semi-arid region of Brazil. **Harmful Algae**, v. 86, n. May, p. 128–137, 2019.

BEZERRA, A.; BECKER, V.; MATTOS, A. Balanço de Massa de Fósforo Total e o Estado Trófico em Reservatórios do Semiárido Brasileiro. **Revista Brasileira de Recursos Hídricos**, v. 19, n. 2, p. 67–76, 2014.

Brazil. Conselho Nacional do Meio Ambiente (CONAMA). Resolução CONAMA N° 357, de 17 de março de 2005.

BURKHOLDER, J. A. M.; KINDER, C. A.; DICKEY, D. A.; REED, R. E.; ARELLANO, C.; JAMES, J. L.; MACKENZIE, L. M.; ALLEN, E. H.; LINDOR, N. L.; MATHIS, J. G.; THOMAS, Z. T. Classic indicators and diel dissolved oxygen versus trend analysis in assessing eutrophication of potable-water reservoirs. **Ecological Applications**, v. 32, n. 4, p. 1–30, 2022.

CARLETON, J. N.; LEE, S. S. Modeling lake recovery lag times following influent phosphorus loading reduction. **Environmental Modelling and Software**, v. 162, n. February, 2023.

CARMICHAEL, W.; BOYER, G. L.; CARMICHAEL, W. W.; BOYER, G. L. Health impacts from cyanobacteria harmful algae blooms : Implications for the North American Great Lakes Health impacts from cyanobacteria harmful algae blooms : Implications for the North American Great Lakes. **Harmful Algae**, v. 54, n. April, p. 194–212, 2016.

CARNEIRO, B. L. D. S.; JESUS D ROCHA, M. DE; BARROS, M. U. G.; PAULINO, W. D.; LIMA NETO, I. E. Predicting anoxia in the wet and dry periods of tropical semiarid reservoirs. **Journal of Environmental Management**, v. 326, n. November 2022, 2023.

CASTRILLO, M.; GARCÍA, Á. L. Estimation of high frequency nutrient concentrations from water quality surrogates using machine learning methods. **Water Research**, v. 172, 2020.

CASTRO, José Artur Borges de. **Análise temporal do uso e ocupação do solo da bacia do Médio Jaguaribe – CE.** 2018. Trabalho de Conclusão de Curso (Graduação em Engenharia Florestal) - Universidade Federal Rural de Pernambuco, Departamento de Ciência Florestal, Recife.

CAVALCANTE, H.; ARAÚJO, F.; BECKER, V.; LUCENA BARBOSA, J. E. DE. Internal phoshorus loading potential of a semiarid reservoir: An experimental study. **Acta Limnologica Brasiliensia**, v. 33, p. 1–13, 2021.

CAVALCANTE, H.; ARAÚJO, F.; NOYMA, N. P.; BECKER, V. **Phosphorus fractionation in sediments of tropical semiarid reservoirsScience of the Total Environment**, 2018.

CAVALCANTE, P. R. S.; SOCORRO RODRIGUES, M. DO; BARROSO, M. F. S.;

BARBIERI, R.; SERRA, C. L. M.; OLIVEIRA, R. C. A. Diel variation of limnological parameters in a reservoir in northeastern Brazil (Boa Esperança, Maranhão/Piauí): Rainy period. **Lakes and Reservoirs: Research and Management**, v. 12, n. 1, p. 35–42, 2007.

CEARÁ, 2024. Companhia de Gestão dos Recursos Hídricos: Inventários ambientais. Disponível em: https://cdn.funceme.br/hidro-ce/data/arquivos/invetarios/CASTANH%C3%83O.pdf. Acesso em: 02 fev. 2024.

CEARÁ, 2022a. Companhia de Gestão dos Recursos Hídricos: Monitoramento Quantitativo e Qualitativo dos Recursos Hídricos. Available online: http://www.hidro.ce.gov.br (accessed on 05 July. 2022.

CEARÁ, 2022b. Companhia de Gestão dos Recursos Hídricos: Inventários ambientais. Available online: http://www.hidro.ce.gov.br/hidro-ce-zen d/mi/midia/show/150 (accessed on 05 July. 2022).

CEARÁ, 2021. Relatório de Cálculo das Afluências aos Reservatórios Estratégicos do Ceará: Definição das Vazões Oficiais. Available online: https://portal.cogerh.com.br/wp-content/uploads/2022/12/relatorio-de-calculo-das-afluencias-aos-reservatorios-estrategicos-do-ceara-definicao-das-vazoes-oficiais.pdf (accessed on 08 August 2023).

CHAPRA, S. C.. **Surface Water-Quality Modeling**. Waveland Press, Long Grove, IL 835 p, 2008.

CHAPRA, S. C.; CANALE, R. P. Long-term phenomenological model of phosphorus and oxygen for stratified lakes. **Water Research**, v. 25, n. 6, p. 707–715, jun. 1991.

CHEN, C.; WANG, Y.; PANG, X.; LONG, L.; XU, M.; XIAO, Y.; LIU, Y.; YANG, G.; DENG, S.; HE, J.; TANG, H. Dynamics of sediment phosphorus affected by mobile aeration: Pilot-scale simulation study in a hypereutrophic pond. **Journal of Environmental Management**, v. 297, n. June, 2021.

CHEN, K.; DUAN, L.; LIU, Q.; ZHANG, Y.; ZHANG, X.; LIU, F.; ZHANG, H. Spatiotemporal Changes in Water Quality Parameters and the Eutrophication in Lake Erhai of Southwest China. **Water (Switzerland)**, v. 14, n. 21, 2022.

CHEN, S., LIU, H., ZHANG, H., LI, K., WANG, N., SUN, W., LIU, X., NIU, L., MA, B., YANG, F., LI, H., ZHAO, D., XING, Y. Temporal patterns of algae in different urban lakes and their correlations with environmental variables in Xi'an, China. **J. Environ. Sci**. (China) 133, 138–151, 2023. https://doi.org/10.1016/j.jes.2022.07.036

CHEN, X.; XU, B.; ZHENG, Y.; ZHANG, C. Nexus of water, energy and ecosystems in the upper Mekong River: A system analysis of phosphorus transport through cascade reservoirs**. Science of the Total Environment**, 2019.

CHUNG, S.-W.; LEE, H.; JUNG, Y. The effect of hydrodynamic flow regimes on the algal bloom in a monomictic reservoir. **Water Science and Technology**, v. 58, n. 6, p. 1291–1298, 1 out. 2008.

COBO, Á.; LLORENTE, I.; LUNA, L.; LUNA, M. A decision support system for fish farming using particle swarm optimization. **Computers and Electronics in Agriculture**, v. 161, n. October 2017, p. 121–130, 2019.

CONCEIÇÃO, L. P.; JESUS AFFE, H. M. DE; SILVA, D. M. L. DA; CASTRO NUNES, J. M. DE. Spatio-temporal variation of the phytoplankton community in a tropical estuarine gradient, under the influence of river damming. **Regional Studies in Marine Science**, v. 43, 2021.

COORAY, A. T.; SIRIWARDANA, C.; KOLIYABANDARA, P. A.; LIYANAGE, S. Hydrochemistry of an ancient traditional irrigation reservoir in Padaviya, Sri Lanka. **Journal of the Indian Chemical Society**, v. 99, n. 11, 2022.

CORTEZ, F.; MONICELLI, F.; CAVALCANTE, H.; BECKER, V. Effects of prolonged drought on water quality after drying of a semiarid tropical reservoir, Brazil. **Limnologica**, v. 93, n. February, 2022.

CUI, G.; LI, X. D.; LI, S.; DING, S.; LI, Q.; YANG, M.; LV, H.; WANG, Y. Varying water column stability controls the denitrification process in a subtropical reservoir, Southwest China. **Journal of Environmental Sciences (China)**, v. 111, p. 208–219, 2021.

CUI, G.; WANG, B.; XIAO, J.; QIU, X. L.; LIU, C. Q.; LI, X. D. Water column stability driving the succession of phytoplankton functional groups in karst hydroelectric reservoirs. **Journal of Hydrology**, v. 592, n. October 2020, 2021.

CUNHA, G.K.G., CUNHA, K.P.V. da. Effects of land use changes on the potential for soil to contribute phosphorus loads in watersheds. **Environmental Development**, 45, 100825, 2023. https://doi.org/10.1016/j.envdev.2023.100825

CURTARELLI, M. P.; OGASHAWARA, I.; ARAÚJO, C. A. S.; ALCÂNTARA, E. H.; LORENZZETTI, J. A.; STECH, J. L. Influence of summertime mesoscale convective systems on the heat balance and surface mixed layer dynamics of a large Amazonian hydroelectric reservoir. **Journal of Geophysical Research: Oceans**, v. 119, n. 12, p. 8472–8494, dez. 2014.

DAEL, T. VAN; VERMEIREN, C.; SMOLDERS, E. Internal loading of phosphorus in streams described by a Sediment-Water Exchange Model for Phosphorus (SWEMP): From lab to field scale**. Science of the Total Environment**, v. 912, n. July 2023, 2024.

DALU, T.; DUBE, T.; FRONEMAN, P. W.; SACHIKONYE, M. T. B.; CLEGG, B. W.; NHIWATIWA, T. An assessment of chlorophyll-a concentration spatio-temporal variation using Landsat satellite data, in a small tropical reservoir. **Geocarto International**, v. 30, n. 10, p. 1130–1143, 2015.

DALU, T.; WASSERMAN, R. J. Cyanobacteria dynamics in a small tropical reservoir: Understanding spatio-temporal variability and influence of environmental variables. **Science of the Total Environment**, v. 643, p. 835–841, 2018.

DELMIRO ROCHA, M. DE J.; LIMA NETO, I. E. Phosphorus mass balance and input load estimation from the wet and dry periods in tropical semiarid reservoirs. **Environmental Science and Pollution Research**, v. 29, n. 7, p. 10027–10046, 12 fev. 2022.

DUKA, M. A.; SHINTANI, T.; YOKOYAMA, K. Thermal stratification responses of a monomictic reservoir under different seasons and operation schemes. **Science of the Total Environment**, v. 767, 2021.

ELÇI, Ş.; WORK, P. A.; HAYTER, E. J. Influence of Stratification and Shoreline Erosion on

Reservoir Sedimentation Patterns. **Journal of Hydraulic Engineering**, v. 133, n. 3, p. 255–266, 2007.

FANG, Q.; TANG, Y.; ZHU, J.; LIAO, H.; DU, X.; BAI, G.; YANG, H.; WU, Z.; ZHANG, Y. Nutrient status of overlying water and sediment of West Lake, Hangzhou, China. **HydroResearch**, v. 7, p. 55–70, 2024.

FENOCCHI, A.; ROGORA, M.; SIBILLA, S.; DRESTI, C. Relevance of inflows on the thermodynamic structure and on the modeling of a deep subalpine lake (Lake Maggiore, Northern Italy/Southern Switzerland). **Limnologica**, v. 63, p. 42–56, 2017.

FLETCHER, J.; WILLBY, N.; OLIVER, D. M.; QUILLIAM, R. S. Resource recovery and freshwater ecosystem restoration — Prospecting for phytoremediation potential in wild macrophyte stands. **Resources, Environment and Sustainability**, v. 7, n. September 2021, 2022.

FLORES, E.; MERMA-MORA, L.; COLAS, F.; CARDICH, J.; SONIA, S.; LORENZO, A.; AGUIRRE-VELARDE, A.; CORREA, D.; GUTI, D. Bottom-water hypoxia in the Paracas Bay (Peru , 13 . 8 ◦ S) associated with seasonal and synoptic time scale variability of winds and water stratification. **Journal of Marine**, v. 241, n. July 2023, 2024.

FONG, P.; MCCRIMMON, C.; VALIPOUR, R.; SHRESTHA, R. R.; LIU, Y.; RAO, Y. R. Modelling streamflow and phosphorus fluxes in the Lake of the Woods watershed. **Journal of Great Lakes Research**, v. 49, n. 1, p. 65–81, 2023.

FONSECA, R.; ARAÚJO, J. F.; PINHO, C. G. Importance of the spatial distribution of rare earth elements in the bottom sediments of reservoirs as a potential proxy for tracing sediments sources. A case study in the dominican republic. **Geosciences (Switzerland)**, v. 11, n. 12, 2021.

GELDER, B., LOFTIS, J., KOSKI, M. EUTROPHICATION OF RESERVOIRS ON THE COLORADO FRONT RANGE by Brett Johnson & Laurel Saito Completion Report No . 194 Eutrophication of Reservoirs on the Colorado Front Range. **Water**, 2003

GENG, M. *et al.* Assessing the impact of water-sediment factors on water quality to guide river-connected lake water environment improvement. **Science of the Total Environment**, v. 912, n. September 2023, 2024.

GERMÁN, A., SHIMONI, M., BELTRAMONE, G., RODRÍGUEZ, M.I., MUCHIUT, J., BONANSEA, M., SCAVUZZO, C.M., FERRAL, A. Space-time monitoring of water quality in an eutrophic reservoir using SENTINEL-2 data - A case study of San Roque, Argentina. **Remote Sens. Appl. Soc. Environ**. 24, 2021. https://doi.org/10.1016/j.rsase.2021.100614

GHAISAS, N. A.; MAITI, K.; WHITE, J. R. Coupled iron and phosphorus release from seasonally hypoxic Louisiana shelf sediment**. Estuarine, Coastal and Shelf Science**, 2019.

GROVER, J. P.; SCOTT, J. T.; ROELKE, D. L.; BROOKS, B. W. Competitive superiority of N-fixing cyanobacteria when fixed N is scarce: Reconsiderations based on a model with heterocyst differentiation. **Ecological Modelling**, v. 466, n. February, 2022.

GU, P.; LI, Q.; ZHANG, H.; LUO, XIN; ZHANG, W.; ZHENG, Z.; LUO, XINGZHANG. Effects of cyanobacteria on phosphorus cycling and other aquatic organisms in simulated eutrophic ecosystems. **Water (Switzerland)**, v. 12, n. 8, 2020.

GUIMARÃES, B. M. D. M.; NETO, I. E. L. Chlorophyll-a prediction in tropical reservoirs as a function of hydroclimatic variability and water quality. **Environmental Science and Pollution Research**, v. 30, n. 39, p. 91028–91045, 2023.

HAN, C.; ZHENG, B.; QIN, Y.; MA, Y.; YANG, C.; LIU, Z.; CAO, W.; CHI, M. Impact of upstream river inputs and reservoir operation on phosphorus fractions in water-particulate phases in the Three Gorges Reservoir. **Science of the Total Environment**, 2018.

HARKE, M. J.; STEFFEN, M. M.; GOBLER, C. J.; OTTEN, T. G.; WILHELM, S. W.; WOOD, S. A.; PAERL, H. W. A review of the global ecology, genomics, and biogeography of the toxic cyanobacterium, Microcystis spp. **Harmful Algae**, v. 54, p. 4–20, 2016.

HE, W.; LUO, J.; XING, L.; YU, X.; ZHANG, J.; CHEN, S. Effects of temperature-control curtain on algae biomass and dissolved oxygen in a large stratified reservoir: Sanbanxi Reservoir case study. **Journal of Environmental Management**, v. 248, n. January, 2019.

HE, X.; WANG, H.; ZHUANG, W.; LIANG, D.; AO, Y. Risk prediction of microcystins based on water quality surrogates: A case study in a eutrophicated urban river network. **Environmental Pollution**, v. 275, 2021.

HENRY-SILVA, G. G.; MELO-JUNIOR, H. D. N.; ATTAYDE, J. L. Extreme drought events and the sustainability of fish farming in net cages in reservoirs of the semi-arid northeastern region in Brazil. **Acta Limnologica Brasiliensia**, v. 31, 2019.

HERRERA, E. C.; NADAOKA, K. Temporal dynamics and drivers of lake ecosystem metabolism using high resolution observations in a shallow, tropical, eutrophic lake (Laguna Lake, Philippines). **Journal of Great Lakes Research**, v. 47, n. 4, p. 997–1020, 2021.

HU, Z.; XIAO, Q.; YANG, J.; XIAO, W.; WANG, W.; LIU, S.; LEE, X. Temporal dynamics and drivers of ecosystem metabolism in a large subtropical Shallow Lake (Lake Taihu). **International Journal of Environmental Research and Public Health**, v. 12, n. 4, p. 3691–3706, 2015.

HUANG, J.; ZHANG, Y.; HUANG, Q.; GAO, J. When and where to reduce nutrient for controlling harmful algal blooms in large eutrophic lake Chaohu, China? **Ecological Indicators**, v. 89, n. August 2017, p. 808–817, 2018.

HUANG, L.; FANG, H.; HE, G.; JIANG, H.; WANG, C. Effects of internal loading on phosphorus distribution in the Taihu Lake driven by wind waves and lake currents. **Environmental Pollution**, v. 219, p. 760–773, 2016.

HUANG, L.; FANG, H.; REIBLE, D. Mathematical model for interactions and transport of phosphorus and sediment in the Three Gorges Reservoir. **Water Research**, v. 85, p. 393–403, 2015.

HUDSON, J.; VANDERGUCHT, D. Spatial and temporal patterns in physical properties and dissolved oxygen in Lake Diefenbaker , a large reservoir on the Canadian Prairies. **Journal of Great Lakes Research**, 2015.

HUO, L.; YANG, P.; YIN, H.; ZHANG, E. Enhanced nutrient control efficiency in sediments using modified clay inactivation coupled with aquatic vegetation in the confluence area of a eutrophic lake. **Science of the Total Environment**, v. 907, n. October 2023, 2024.

HUO, S.; HE, Z.; MA, C.; ZHANG, H.; XI, B.; ZHANG, J.; LI, X.; WU, F.; LIU, H. Spatio-

temporal impacts of meteorological and geographic factors on the availability of nitrogen and phosphorus to algae in Chinese lakes. **Journal of Hydrology**, v. 572, n. 8, p. 380–387, 2019.

HUSK, B.; JULIAN, P.; SIMON, D.; TROMAS, N.; PHAN, D.; PAINTER, K.; BAULCH, H.; SAUVÉ, S. Improving water quality in a hypereutrophic lake and tributary through agricultural nutrient mitigation: A Multi-year monitoring analysis. **Journal of Environmental Management**, v. 354, n. February, 2024.

JIN, X.; WANG, S.; PANG, Y.; CHANG WU, F. Phosphorus fractions and the effect of pH on the phosphorus release of the sediments from different trophic areas in Taihu Lake, China. **Environmental Pollution**, v. 139, n. 2, p. 288–295, 2006.

JONES, E.; VLIET, M. T. H. VAN. Drought impacts on river salinity in the southern US: Implications for water scarcity. **Science of the Total Environment**, v. 644, p. 844–853, 2018.

JUSTUS, B. G.; DRIVER, L. J.; GREEN, J. J.; WENTZ, N. J. Relations of dissolved-oxygen variability, selected field constituents, and metabolism estimates to land use and nutrients in high-gradient Boston Mountain streams, Arkansas. **Environmental Monitoring and Assessment**, v. 191, n. 10, 2019.

KEITEL, J.; ZAK, D.; HUPFER, M. Water level fluctuations in a tropical reservoir : the impact of sediment drying , aquatic macrophyte dieback , and oxygen availability on phosphorus mobilization. p. 6883–6894, 2016.

KONG, X.; DONG, L.; HE, W.; WANG, Q.; MOOIJ, W. M.; XU, F. Estimation of the long-term nutrient budget and thresholds of regime shift for a large shallow lake in China. **Ecological Indicators**, v. 52, p. 231–244, 2015.

KREMPIN, D. W.; MCGRATH, S. M.; SOOHOO, J. B.; SULLIVAN, C. W. Orthophosphate uptake by phytoplankton and bacterioplankton from the Los Angeles Harbor and Southern California coastal waters. **Marine Biology**, v. 64, n. 1, p. 23–33, 1981.

KWAK, D. H.; JEON, Y. T.; DUCK HUR, Y. Phosphorus fractionation and release characteristics of sediment in the Saemangeum Reservoir for seasonal change. **International Journal of Sediment Research**, v. 33, n. 3, p. 250–261, 2018.

LACERDA, L. D. DE; SANTOS, J. A.; MARINS, R. V.; SILVA, F. A. T. F. DA. Limnology of the largest multi-use artificial reservoir in NE Brazil: The Castanhão Reservoir, Ceará State. **Anais da Academia Brasileira de Ciencias**, v. 90, n. 2, p. 2073–2096, 2018.

LEITE, J. C. N; BECKER, V.. Impacts of drying and reflooding on water quality of a tropical semi-arid reservoir during an extended drought event. **Acta Limnologica Brasiliensia**, vol. 31, e15, 2019. https://doi.org/10.1590/S2179-975X6918.

LIANG, Z.; SORANNO, P. A.; WAGNER, T. The role of phosphorus and nitrogen on chlorophyll a: Evidence from hundreds of lakes. **Water Research**, v. 185, p. 116236, 2020.

LI, N.; HUANG, T.; LI, Y.; SI, F.; ZHANG, H.; WEN, G. Inducing an extended naturally complete mixing period in a strati fi ed reservoir via arti fi cial destrati fi cation. **Science of the Total Environment**, v. 745, 2020.

LI, N.; WANG, J.; YIN, W.; JIA, H.; XU, J.; HAO, R.; ZHONG, Z.; SHI, Z. Linking water environmental factors and the local watershed landscape to the chlorophyll a concentration in reservoir bays. **Science of the Total Environment**, v. 758, 2021.

LI, S.; BUSH, R. T.; MAO, R.; XIONG, L.; YE, C. Extreme drought causes distinct water acidification and eutrophication in the Lower Lakes (Lakes Alexandrina and Albert), Australia. **Journal of Hydrology**, v. 544, p. 133–146, 2017.

LI, T.; LI, S.; LIANG, C.; BUSH, R. T.; XIONG, L.; JIANG, Y. A comparative assessment of Australia's Lower Lakes water quality under extreme drought and post-drought conditions using multivariate statistical techniques. **Journal of Cleaner Production**, v. 190, p. 1–11, 2018.

LI, X.; HUANG, T.; MA, W.; SUN, X.; ZHANG, H. Effects of rainfall patterns on water quality in a stratified reservoir subject to eutrophication: Implications for management. **Science of the Total Environment**, v. 521–522, p. 27–36, 2015.

LI, Y.; SHI, K.; ZHANG, YUNLIN; ZHU, G.; QIN, B.; ZHANG, YIBO; LIU, M.; ZHU, M.; DONG, B.; GUO, Y. Remote sensing of column-integrated chlorophyll a in a large deep-water reservoir. **Journal of Hydrology**, v. 610, n. March, 2022.

LI, Y.; SUN, J.; LIN, B.; LIU, Z. Thermal-hydrodynamic circulations and water fluxes in a tributary bay of the Three Gorges Reservoir. **Journal of Hydrology**, v. 585, n. November 2019, 2020.

LI, Y.; ZHANG, YUNLIN; SHI, K.; ZHU, G.; ZHOU, Y.; ZHANG, YIBO; GUO, Y. Monitoring spatiotemporal variations in nutrients in a large drinking water reservoir and their relationships with hydrological and meteorological conditions based on Landsat 8 imagery. **Science of the Total Environment**, v. 599–600, p. 1705–1717, 2017.

LIMA NETO, I. E.; CARDOSO, S. S. S.; WOODS, A. W. On mixing a density interface by a bubble plume. **Journal of Fluid Mechanics**, v. 802, p. R3, 10 set. 2016.

LIMA NETO, I. E.; MEDEIROS, P. H. A.; COSTA, A. C.; WIEGAND, M. C.; BARROS, A. R. M.; BARROS, M. U. G. Assessment of phosphorus loading dynamics in a tropical reservoir with high seasonal water level changes. **Science of the Total Environment**, v. 815, 2022.

LIMA NETO, I. E.; PARENTE, P. A. B. Influence of mass transfer on bubble plume hydrodynamics. **Anais da Academia Brasileira de Ciências**, v. 88, n. 1, p. 411–422, 2 fev. 2016.

LIRA, C. C. S.; MEDEIROS, P. H. A.; NETO, I. E. L. Modelling the impact of sediment management on the trophic state of a tropical reservoir with high water storage variations. **Anais da Academia Brasileira de Ciencias**, v. 92, n. 1, p. 1–18, 2020.

LIU, MIAO; ZHANG, YUNLIN; SHI, K.; ZHU, G.; WU, Z.; LIU, MINGLIANG; ZHANG, YIBO. Thermal stratification dynamics in a large and deep subtropical reservoir revealed by high-frequency buoy data. **Science of the Total Environment**, v. 651, p. 614–624, 2019.

LIU, Q.; DING, S.; CHEN, X.; SUN, Q.; CHEN, M.; ZHANG, C. Effects of temperature on phosphorus mobilization in sediments in microcosm experiment and in the field. **Applied Geochemistry**, p. 1–9, 2017.

LÓPEZ-DOVAL, J. C.; MONTAGNER, C. C.; ALBURQUERQUE, A. F. DE; MOSCHINI-CARLOS, V.; UMBUZEIRO, G.; POMPÊO, M. Nutrients, emerging pollutants and pesticides in a tropical urban reservoir: Spatial distributions and risk assessment. **Science of**

the Total Environment, v. 575, p. 1307–1324, 2017.

LU, J.; LIU, T.; ZHANG, X.; GAO, R.; LIU, Y. A dynamic flux model for analyses of phosphorus exchange between overlying water and sedimentary deposits of a reservoir in the cold area of north China. v. 161, n. December 2019, 2021.

LUND, J.W., KIPLING, C., LECREN, E.D. The inverted microscope method of estimating algal number and the statistical basis of estimations by counting. **Hydrobiologia**, 11 (2), 143e170, 1958.

LUNETTA, R. S.; SCHAEFFER, B. A.; STUMPF, R. P.; KEITH, D.; JACOBS, S. A.; MURPHY, M. S. Evaluation of cyanobacteria cell count detection derived from MERIS imagery across the eastern USA. **Remote**, v. 157, p. 24–34, 2015.

LUO, A.; CHEN, H.; GAO, X.; CARVALHO, L.; XUE, Y.; JIN, L.; YANG, J. Short-term rainfall limits cyanobacterial bloom formation in a shallow eutrophic subtropical urban reservoir in warm season. **Science of the Total Environment**, v. 827, 2022.

LV, Y.; ZHANG, M.; YIN, H. Phosphorus release from the sediment of a drinking water reservoir under the influence of seasonal hypoxia. **Science of the Total Environment**, v. 917, n. February, p. 1–10, 2024.

MA, R.; CHEN, Z.; WANG, B.; XU, C.; JIA, Z.; LI, L.; HU, J. Journal of Hydrology : Regional Studies Spatiotemporal variations and controlling mechanism of low dissolved oxygen in a highly urbanized complex river system. v. 52, n. August 2023, 2024.

MACINTYRE, S.; ROMERO, J. R.; KLING, G. W. Spatial-temporal variability in surface layer deepening and lateral advection in an embayment of Lake Victoria, East Africa. **Limnology and Oceanography**, v. 47, n. 3, p. 656–671, 2002.

MACINTYRE, S.; ROMERO, J. R.; SILSBE, G. M.; EMERY, B. M. Stratification and horizontal exchange in lake victoria, East africa. **Limnology and Oceanography**, v. 59, n. 6, p. 1805–1838, 2014.

MAMUN, M.; FERDOUS, J.; AN, K. G. Empirical estimation of nutrient, organic matter and algal chlorophyll in a drinking water reservoir using landsat 5 tm data. **Remote Sensing**, v. 13, n. 12, 2021.

MAMUN, M.; AN, K. G. Major nutrients and chlorophyll dynamics in Korean agricultural reservoirs along with an analysis of trophic state index deviation. **Journal of Asia-Pacific Biodiversity**, 2017.

MCCARTY, J. A. Algal Demand Drives Sediment Phosphorus Release in a Shallow Eutrophic Cove. **Transactions of the ASABE**, v. 62, n. 5, p. 1315–1324, 2019.

MEHDIZADEH, G.; NIKOO, M. R.; TALEBBEYDOKHTI, N.; VANDA, S.; NEMATOLLAHI, B. Hypolimnetic aeration optimization based on reservoir thermal stratification simulation. **Journal of Hydrology**, v. 625, n. March, 2023.

MELO ROCHA, M.A., BARROS, M.U.G., COSTA, A.C., de ASSIS DE SOUZA FILHO, F., LIMA NETO, I.E. Understanding the Water Quality Dynamics in a Large Tropical Reservoir Under Hydrological Drought Conditions. **Water Air and Soil Pollution**, 235, 1–17, 2024. https://doi.org/10.1007/s11270-024-06890-3

MIAO, H.; ZHENG, W.; CHEN, X.; YU, G.; LI, X.; CHU, Y.; XU, P.; KUBUR BOKHARI, A.; WANG, F. Development of subsurface chlorophyll maximum layer and its contribution to the primary productivity of water column in a large subtropical reservoir. **Environmental Research**, v. 231, p. 116118, ago. 2023.

MOLISANI, M.; BECKER, H.; BARROSO, H.; HIJO, C.; MONTE, T.; VASCONCELLOS, G.; LACERDA, L. The influence of castanhão reservoir on nutrient and suspended matter transport during rainy season in the ephemeral Jaguaribe river (CE, Brazil). **Brazilian Journal of Biology**, v. 73, n. 1, p. 115–123, 2013.

MOLISANI, M. M.; MONTE, T. M. DO; VASCONCELLOS, G. H.; SOUZA BARROSO, H. DE; MOREIRA, M. O. P.; BECKER, H.; REZENDE, C. E. DE; FRANCO, M. A. L.; FARIAS, E. G. G. DE; CAMARGO, P. B. DE. Relative effects of nutrient emission from intensive cage aquaculture on the semiarid reservoir water quality. **Environmental Monitoring and Assessment**, v. 187, n. 11, 2015.

MONTEFIORE, L. R.; NELSON, N. G. Can a simple water quality model effectively estimate runoff-driven nutrient loads to estuarine systems? A national-scale comparison of STEPLgrid and SPARROW. **Environmental Modelling and Software**, v. 150, n. December 2021, 2022.

MORALES-MARÍN, L. A.; WHEATER, H. S.; LINDENSCHMIDT, K. E. Assessment of nutrient loadings of a large multipurpose prairie reservoir. **Journal of Hydrology**, 2017.

MORIASI, D. N.; GITAU, M. W.; PAI, N.; DAGGUPATI, P. Hydrologic and water quality models: Performance measures and evaluation criteria. **Transactions of the ASABE**, v. 58, n. 6, p. 1763–1785, 2015.

MOURA, D. S.; LIMA NETO, I. E.; CLEMENTE, A.; OLIVEIRA, S.; PESTANA, C. J.; APARECIDA DE MELO, M.; CAPELO-NETO, J. Modeling phosphorus exchange between bottom sediment and water in tropical semiarid reservoirs. **Chemosphere**, v. 246, 2020.

MU, Z.; WANG, Y.; WU, J.; CHENG, Y.; LU, J.; CHEN, C.; ZHAO, F.; LI, Y.; HU, M.; BAO, Y. The influence of cascade reservoir construction on sediment biogenic substance cycle in Lancang River from the perspective of phosphorus fractions. **Ecological Engineering**, v. 158, n. June, 2020.

NAZARI-SHARABIAN, M.; TAHERIYOUN, M. Climate change impact on water quality in the integrated Mahabad Dam watershed-reservoir system. **Journal of Hydro-Environment Research**, v. 40, n. February 2021, p. 28–37, 2022.

NETO, I. E. L. Modeling water quality in a tropical reservoir using CE-QUAL-W2: handling data scarcity, urban pollution and hydroclimatic seasonality. **Revista Brasileira de Recursos Hidricos**, v. 28, p. 1–11, 2023.

NI, Z.; WANG, S.; WANG, Y. Characteristics of bioavailable organic phosphorus in sediment and its contribution to lake eutrophication in China. **Environmental Pollution**, v. 219, p. 537–544, 2016.

NONG, X.; LAI, C.; CHEN, L.; SHAO, D.; ZHANG, C.; LIANG, J. Prediction modelling framework comparative analysis of dissolved oxygen concentration variations using support vector regression coupled with multiple feature engineering and optimization methods: A case study in China. **Ecological Indicators**, v. 146, n. December 2022, 2023.

NOORI, R.; ANSARI, E.; BHATTARAI, R.; TANG, Q.; ARADPOUR, S.; MAGHREBI, M.; TORABI HAGHIGHI, A.; BENGTSSON, L.; KLØVE, B. Complex dynamics of water quality mixing in a warm mono-mictic reservoir. **Science of the Total Environment**, v. 777, 2021.

NUNES CARVALHO, T. M.; LIMA NETO, I. E.; SOUZA FILHO, F. DE A. Uncovering the influence of hydrological and climate variables in chlorophyll-A concentration in tropical reservoirs with machine learning. **Environmental Science and Pollution Research**, n. Sperling 2005, 2022.

O'NEIL, J. M.; DAVIS, T. W.; BURFORD, M. A.; GOBLER, C. J. The rise of harmful cyanobacteria blooms: The potential roles of eutrophication and climate change. **Harmful Algae**, v. 14, p. 313–334, 2012.

OLIVEIRA, K. L. DE; RAMOS, R. L.; OLIVEIRA, S. C.; CHRISTOFARO, C. Spatial variability of surface water quality in a large Brazilian semiarid reservoir and its main tributaries. **Environmental Monitoring and Assessment**, v. 193, n. 7, 2021.

OLIVEIRA, T. F. DE; SOUSA BRANDÃO, I. L. DE; MANNAERTS, C. M.; HAUSER-DAVIS, R. A.; FERREIRA DE OLIVEIRA, A. A.; FONSECA SARAIVA, A. C.; OLIVEIRA, M. A. DE; ISHIHARA, J. H. Using hydrodynamic and water quality variables to assess eutrophication in a tropical hydroelectric reservoir. **Journal of Environmental Management**, v. 256, n. July 2019, 2020.

OLSSON, F.; MACKAY, E. B.; BARKER, P.; DAVIES, S.; HALL, R.; SPEARS, B.; EXLEY, G.; THACKERAY, S. J.; JONES, I. D. Can reductions in water residence time be used to disrupt seasonal stratification and control internal loading in a eutrophic monomictic lake? **Journal of Environmental Management**, v. 304, n. December 2021, 2022.

PADEDDA, B. M.; SECHI, N.; LAI, G. G.; MARIANI, M. A.; PULINA, S.; SARRIA, M.; SATTA, C. T.; VIRDIS, T.; BUSCARINU, P.; LUGLIÈ, A. Consequences of eutrophication in the management of water resources in Mediterranean reservoirs: A case study of Lake Cedrino (Sardinia, Italy). **Global Ecology and Conservation**, v. 12, p. 21–35, 2017.

PALMA, P.; LEDO, L.; SOARES, S.; BARBOSA, I. R.; ALVARENGA, P. Spatial and temporal variability of the water and sediments quality in the alqueva reservoir (Guadiana Basin; Southern Portugal). **Science of the Total Environment**, v. 470–471, n. 2014, p. 780–790, 2014.

PANAGOPOULOS, A. Process simulation and analysis of high‐pressure reverse osmosis (HPRO) in the treatment and utilization of desalination brine (saline wastewater). **International Journal of Energy Research**, 46(15), 23083-23094, 2022.

PARK, Y.; KYU, H.; SHIN, J.; CHON, K.; KIM, S.; HWA, K.; HWI, J.; BAEK, S. A machine learning approach for early warning of cyanobacterial bloom outbreaks in a freshwater reservoir. v. 288, n. February, 2021.

PEARCE, A. R.; CHAMBERS, L. G.; HASENMUELLER, E. A. Characterizing nutrient distributions and fluxes in a eutrophic reservoir, Midwestern United States. **Science of the Total Environment**, v. 581–582, p. 589–600, 2017.

PEĆIĆ, M.; GRAŠIĆ, S.; GAJIĆ, D.; POPOVIĆ, S.; SUBAKOV SIMIĆ, G.; PREDOJEVIĆ, D. Periphyton efficiency in phosphorus accumulation affected by phytoplankton dynamics in

reservoir for water supply. **Ecological Engineering**, v. 191, n. March, 2023.

PONTES FILHO, J. D.; SOUZA FILHO, F. A. DE; MARTINS, E. S. P. R.; STUDART, T. M. C. Copula-Based Multivariate Frequency Analysis of the 2012-2018 Drought in Northeast Brazil. **Water (Switzerland)**, 2020.

PORTINHO, J. L.; GOMES, A. C. C.; KOGA-VICENTE, A.; MILANI, F. C. C.; PENTEAN, R. B.; MANZATTO, C. V.; SPINELLI-ARAUJO, L.; VICENTE, L. E. The pathways influence of agricultural expansion on water quality of fish farming in Ilha Solteira reservoir, São Paulo, Brazil. **Aquaculture**, v. 536, n. January 2020, 2021.

R Core Team. R: A Language and Environment for Statistical Computing. R Foundation for Statistical Computing, 2022. https://www.R-project.org

RABELO, U. P.; COSTA, A. C.; DIETRICH, J.; FALLAH-MEHDIPOUR, E.; OEL, P. VAN; LIMA NETO, I. E. Impact of Dense Networks of Reservoirs on Streamflows at Dryland Catchments. **Sustainability (Switzerland)**, v. 14, n. 21, 2022.

RAULINO, J.B.S., SILVEIRA, C.S., LIMA NETO, I.E. Assessment of climate change impacts on hydrology and water quality of large semi-arid reservoirs in Brazil. **Hydrol Sci J**, 66 (8), 1321–1336, 2021. https://doi.org/10.1080/02626667.2021.1933491

REN, K.; HUANG, S.; HUANG, Q.; WANG, H.; LENG, G.; CHENG, L.; FANG, W.; LI, P. A nature-based reservoir optimization model for resolving the conflict in human water demand and riverine ecosystem protection. **Journal of Cleaner Production**, v. 231, p. 406–418, 2019.

ROBERTSON, D. M.; SAAD, D. A.; KOLTUN, G. F. An extrapolation method for estimating loads from unmonitored areas using watershed model load ratios. **Journal of Great Lakes Research**, v. 48, n. 6, p. 1550–1562, 2022.

ROBSON, B. J. State of the art in modelling of phosphorus in aquatic systems: Review, criticisms and commentary. **Environmental Modelling and Software**, v. 61, p. 339–359, 2014.

ROCHA JUNIOR, C.; ARAÚJO, F.; BECKER, V. Influence of land use on spatial distribution of mobile phosphorus forms in the sediment of a tropical semi-arid reservoir. **Science of the Total Environment**, v. 914, n. August 2023, 2024.

ROCHA, M. J. D.; LIMA NETO, I. E. Nitrogen mass balance and uptake velocity for eutrophic reservoirs in the Brazilian semiarid region. **Environmental Science and Pollution Research**, v. 30, n. 42, p. 95621–95633, 2023.

ROCHA, M. DE J. D.; LIMA NETO, I. E. Modeling flow-related phosphorus inputs to tropical semiarid reservoirs. **Journal of Environmental Management**, v. 295, n. February, p. 113123, 2021.

ROCHA, M. DE J. D.; LIMA NETO, I. E. Internal phosphorus loading and its driving factors in the dry period of Brazilian semiarid reservoirs. **Journal of Environmental Management**, v. 312, n. March, 2022.

ROCHA, S. M. G.; SILVA, J. V. B. DA; LEMOS, W. E. D.; SOUZA FILHO, F. DE A. DE; LIMA NETO, I. E. Two-Dimensional Modelling of the Mixing Patterns in a Tropical

Semiarid Reservoir. **Sustainability (Switzerland)**, v. 14, n. 23, 2022.

ROSIŃSKA, J.; KOZAK, A.; DONDAJEWSKA, R.; GOŁDYN, R. Cyanobacteria blooms before and during the restoration process of a shallow urban lake. **Journal of Environmental Management**, v. 198, p. 340–347, 2017.

SANDSTRÖM, S.; LANNERGÅRD, E. E.; FUTTER, M. N.; DJODJIC, F. Water quality in a large complex catchment: Significant effects of land use and soil type but limited ability to detect trends. **Journal of Environmental Management**, v. 349, n. October 2023, 2024.

SANTOS, J. A.; MARINS, R. V.; AGUIAR, J. E.; CHALAR, G.; SILVA, F. A. T. F.; LACERDA, L. D. Hydrochemistry and trophic state change in a large reservoir in the Brazilian northeast region under intense drought conditions. **Journal of Limnology**, v. 76, n. 1, p. 41–51, 2017.

SANTOS, J. A. DOS; OLIVEIRA, K. F. DE; SILVA ARAÚJO, I. C. DA; AVELINO, I. I. F.; SOUSA CAJUÍ, K. N. DE; LACERDA, L. D. DE; MARINS, R. V. Phosphorus partitioning in sediments from a tropical reservoir during a strong period of drought. **Environmental Science and Pollution Research**, v. 23, n. 23, p. 24237–24247, 2016.

SCHILLING, K. E.; KIM, S. W.; JONES, C. S. Use of water quality surrogates to estimate total phosphorus concentrations in Iowa rivers. **Journal of Hydrology: Regional Studies**, v. 12, n. April, p. 111–121, 2017.

SHARMIN, A.; HAI, M. A.; HOSSAIN, M. M.; RAHMAN, M. M.; BILLAH, M. B.; ISLAM, S.; JAKARIYA, M.; SMITH, G. C. Reducing excess phosphorus in agricultural runoff with low-cost, locally available materials to prevent toxic eutrophication in hoar areas of Bangladesh. **Groundwater for Sustainable Development**, v. 10, n. September 2019, 2020.

SHEN, Z., CHEN, L., Ding, X., HONG, Q., LIU, R. Long-term variation (1960-2003) and causal factors of non-point-source nitrogen and phosphorus in the upper reach of the Yangtze River. **Journal of Hazardous Materials**, 252–253, 45–56, 2013. https://doi.org/10.1016/j.jhazmat.2013.02.039

SHI, J.; WANG, L.; YANG, Y.; HUANG, T. A case study of thermal and chemical stratification in a drinking water reservoir. **Science of the Total Environment**, v. 848, n. 13, 2022.

SHI, J.; WANG, L.; YANG, Y.; HUANG, T. Effects of seasonal thermal stratification on ammonia nitrogen transformation in a source water reservoir. **Processes**, v. 9, n. 12, p. 1–12, 2021.

SHILEI, Z.; YUE, S.; TINGLIN, H.; YA, C.; XIAO, Y.; ZIZHEN, Z.; YANG, L.; ZAIXING, L.; JIANSHENG, C.; XIAO, L. Reservoir water stratification and mixing affects microbial community structure and functional community composition in a stratified drinking reservoir. **Journal of Environmental Management**, v. 267, n. August 2019, 2020.

SOARES, M. C. S.; MARINHO, M. M.; AZEVEDO, S. M. O. F.; BRANCO, C. W. C.; HUSZAR, V. L. M. Eutrophication and retention time affecting spatial heterogeneity in a tropical reservoir. **Limnologica**, v. 42, n. 3, p. 197–203, 2012.

SØNDERGAARD, M.; LARSEN, S. E.; JØRGENSEN, T. B.; JEPPESEN, E. Using

chlorophyll a and cyanobacteria in the ecological classification of lakes. **Ecological Indicators**, v. 11, n. 5, p. 1403–1412, 2011.

SØNDERGAARD, M.; JENSEN, J. P.; JEPPESEN, E. Role of sediment and internal loading of phosphorus in shallow lakes. **Hydrobiologia**, v. 506–509, p. 135–145, 2003.

SONDERGAARD, M.; JENSEN, P. J.; JEPPESEN, E. Retention and internal loading of phosphorus in shallow, eutrophic lakes. **TheScientificWorldJournal**, v. 1, p. 427–442, 2001.

SOUSA ESTÁCIO, Á. B.; MELO ROCHA, M. A.; CAETANO DE OLIVEIRA, M.; OLIVEIRA DA SILVA, S. M.; SOUZA FILHO, F. DE A. DE; MARINHO DE CARVALHO STUDART, T. Priority of Water Allocation during Drought Periods: The Case of Jaguaribe Metropolitan Inter-Basin Water Transfer in Semiarid Brazil. **Sustainability**, v. 14, n. 11, p. 6876, 4 jun. 2022.

SOUZA, E. G. DE; STUDART, T. M. DE C.; PINHEIRO, M. I. T.; CAMPOS, J. N. B. Segurança hídrica do reservatório Castanhão-CE: Aplicação da matriz de sistematização institucional. **Engenharia Sanitaria e Ambiental**, v. 22, n. 5, p. 877–887, 2017.

SU, H.; ZOU, R.; ZHANG, X.; LIANG, Z.; YE, R.; LIU, Y. Exploring the type and strength of nonlinearity in water quality responses to nutrient loading reduction in shallow eutrophic water bodies: Insights from a large number of numerical simulations. **Journal of Environmental Management**, v. 313, n. December 2021, 2022.

SU, X.; STEINMAN, A. D.; XUE, Q.; ZHAO, Y.; XIE, L. Evaluating the contamination of microcystins in Lake Taihu , China : The application of equivalent total MC-LR concentration. **Ecological Indicators**, v. 89, n. February, p. 445–454, 2018.

SUMMERS, E. J.; RYDER, J. L. A critical review of operational strategies for the management of harmful algal blooms (HABs) in inland reservoirs. v. 330, n. December 2022, 2023.

SUN, C.; WANG, S.; WANG, H.; HU, X.; YANG, F.; TANG, M.; ZHANG, M.; ZHONG, J. Internal nitrogen and phosphorus loading in a seasonally stratified reservoir: Implications for eutrophication management of deep-water ecosystems. **Journal of Environmental Management**, v. 319, n. June, 2022.

SUN, H.; TIAN, Y.; LI, L.; ZHUANG, Y.; ZHOU, X.; ZHANG, H.; ZHAN, W.; ZUO, W.; LUAN, C.; HUANG, K. Unraveling spatial patterns and source attribution of nutrient transport: Towards optimal best management practices in complex river basin. **Science of the Total Environment**, v. 906, n. October 2023, 2024.

TANG, Q.; PENG, L.; YANG, Y.; LIN, Q.; QIAN, S. S.; HAN, B. P. Total phosphorus-precipitation and Chlorophyll a-phosphorus relationships of lakes and reservoirs mediated by soil iron at regional scale. **Water Research**, v. 154, p. 136–143, 2019.

TANG, X.; WU, M.; DAI, X.; CHAI, P. Phosphorus storage dynamics and adsorption characteristics for sediment from a drinking water source reservoir and its relation with sediment compositions. **Ecological Engineering**, 2014.

TAY, C. J.; MOHD, M. H.; TEH, S. Y.; KOH, H. L. Internal phosphorus recycling promotes rich and complex dynamics in an algae-phosphorus model: Implications for eutrophication management. **Journal of Theoretical Biology**, v. 532, 2022.

TIBEBE, D.; KASSA, Y.; MELAKU, A.; LAKEW, S.; TANA, L. Investigation of spatio-temporal variations of selected water quality parameters and trophic status of Lake Tana for sustainable management ,. v. 148, n. May, p. 374–384, 2019.

TONÉ, A.; LIMA NETO, I. Modelagem simplificada do fósforo total em lagos e reservatórios brasileiros. **Revista DAE**, v. 221, n. 68, p. 142–156, 2019.

USEPA, Environmental Protection Agency (EUA). Direct Nesslerization. Washington, D.C., 1974.

UTERMÖHL, H. Zur vervollkommnung der quantitativen phytoplank- ton methodik. **Limnology** 9, 1–38, 1958. http://dx.doi.org/10.1080/05384680.1958. 11904091.

VAROL, M. Spatio-temporal changes in surface water quality and sediment phosphorus content of a large reservoir in Turkey. **Environmental Pollution**, v. 259, 2020.

VIDAL, T. F.; CAPELO NETO, J. Dinâmica de nitrogênio e fósforo em reservatório na região semiárida utilizando balanço de massa. **Revista Brasileira de Engenharia Agrícola e Ambiental**, v. 18, n. 4, p. 402–407, abr. 2014.

VOGEL, E.; DECIAN, M.; SILVA, M. C. DA; MAUAD, J. C.; CASTRO SILVA, T. S. DE; RUVIARO, C. F. Production of exotic fish and Brazilian hybrids in similar conditions: Are there considerable differences of environmental performance? **Aquaculture**, v. 513, n. November 2018, 2019.

WALSH, J. R.; CORMAN, J. R.; MUNOZ, S. E. Coupled long-term limnological data and sedimentary records reveal new control on water quality in a eutrophic lake. **Limnology and Oceanography**, v. 64, p. S34–S48, 2019.

WANG, H., DENG, Y., YANG, Y., LU, J., TUO, Y., YAN, Z., CHEN, M. Optimization of selective withdrawal strategy in a warm monomictic reservoir based on thermal stratification. **Ecological Indicators**. 158, 111294, 2024. https://doi.org/10.1016/j.ecolind.2023.111294

WANG, J.; ZHENG, B.; KANG, X.; YU, H.; LI, D.; JIANG, X. Diel variation of water inorganic nitrogen and phosphorus during algal blooms. **Polish Journal of Environmental Studies**, v. 28, n. 2, p. 867–875, 2019.

WANG, S.; WANG, A.; YANG, D.; GU, Y.; TANG, L.; SUN, X. Understanding the spatiotemporal variability in nonpoint source nutrient loads and its effect on water quality in the upper Xin'an river basin, Eastern China. **Journal of Hydrology**, v. 621, n. April, 2023.

WANG, Z.; LU, S.; WU, D.; CHEN, F. Control of internal phosphorus loading in eutrophic lakes using lanthanum-modified zeolite. **Chemical Engineering Journal**, v. 327, p. 505–513, 2017.

WEI, M.; HUANG, S.; ZHANG, T.; LI, M.; LI, L.; AKRAM, W.; GAO, R.; GE, Z.; SUN, Y. DOM stratification and characteristics versus thermal stratification – A case study in the Panjiakou Reservoir, China. **Journal of Hydrology: Regional Studies**, v. 42, n. June, 2022.

WEN, S.; WANG, H.; WU, T.; YANG, J.; JIANG, X.; ZHONG, J. Vertical profiles of phosphorus fractions in the sediment in a chain of reservoirs in North China: Implications for pollution source, bioavailability, and eutrophication. **Science of the Total Environment**, v. 704, 2020.

WIEGAND, M. C.; NASCIMENTO, A. T. P. DO; COSTA, A. C.; LIMA NETO, I. E. Trophic state changes of semi-arid reservoirs as a function of the hydro-climatic variability. **Journal of Arid Environments**, v. 184, n. September 2020, 2021.

WU, YUNHAI; WEN, Y.; ZHOU, J.; WU, YUNYING. Phosphorus release from lake sediments: Effects of pH, temperature and dissolved oxygen. **KSCE Journal of Civil Engineering**, v. 18, n. 1, p. 323–329, 2014.

WU, Z.; MA, T.; LAI, X.; LI, K. Concentration, distribution, and assessment of dissolved heavy metals in rivers of Lake Chaohu Basin, China. **Journal of Environmental Management**, v. 300, n. September, 2021.

XIONG, L.; XI, B.; WU, Y.; LIU, S.; ZHANG, L.; HUANG, X.; MACREADIE, P. I. Nutrient input estimation and reduction strategies related to land use and landscape pattern (LULP) in a near-eutrophic coastal bay with a small watershed in the South China sea. **Ocean and Coastal Management**, v. 206, n. February, 2021.

XUE, Q., REDISKE, R.R., GONG, Z., SU, X., XU, H., CAI, Y., ZHAO, Y., XIE, L. Spatio-temporal variation of microcystins and its relationship to biotic and abiotic factors in Hongze Lake, China. **J. Great Lakes Res.** 44, 253–262, 2018. https://doi.org/10.1016/j.jglr.2017.12.004

YANG, Y.; CHEN, M.; DENG, Y.; SCHLADOW, S. G.; LI, J.; TUO, Y. C. Impact of climate change on thermal and mixing regimes in a deep dimictic reservoir on the Qinghai-Tibetan Plateau, China. **Journal of Hydrology**, v. 603, n. October, 2021.

YIN, Y.; ZHANG, W.; CAO, X.; CHEN, X.; TANG, J.; ZHOU, Y.; LI, Q. Evaluation of sediment phosphorus dynamics in cascade reservoir systems: A case study of Weiyuan River, China. **Journal of Environmental Management**, v. 346, n. May, 2023.

YU, C.; LI, Z.; XU, Z.; YANG, Z. Lake recovery from eutrophication: Quantitative response of trophic states to anthropogenic influences. **Ecological Engineering**, v. 143, n. November 2019, 2020.

YU, H.; TSUNO, H.; HIDAKA, T.; JIAO, C. Chemical and thermal stratification in lakes. **Limnology**, v. 11, n. 3, p. 251–257, 2010.

YU, S.; DU, X.; LEI, Q.; WANG, X.; WU, S.; LIU, H. Long-term variations of water quality and nutrient load inputs in a large shallow lake of Yellow River Basin: Implications for lake water quality improvements. **Science of the Total Environment**, v. 900, n. May, 2023.

YUE, Y.; YANG, Z.; CAI, L.; BAI, C.; HUANG, Y.; MA, J.; YANG, M. Effects of stratification and mixing on spatiotemporal dynamics and functional potential of microbial community in a subtropical large-deep reservoir driven by nutrients and ecological niche. **Ecological Indicators**, v. 156, n. July, 2023.

ZHAI, Q.; SONG, L.; JI, X.; YU, Y.; YE, J.; XU, W.; HOU, M. Research progress of advanced oxidation technology for the removal of Microcystis aeruginosa: a review. **Environmental Science and Pollution Research**, v. 29, n. 27, p. 40449–40461, 2022.

ZHANG, H.; LIU, K.; HUANG, T.; LI, N.; SI, F.; FENG, J.; HUANG, X.; MIAO, Y. Effect of thermal stratification on denitrifying bacterial community in a deep drinking water reservoir. **Journal of Hydrology**, v. 596, n. February, 2021.

ZHANG, L.; WANG, S.; WU, Z. Coupling effect of pH and dissolved oxygen in water column on nitrogen release at water-sediment interface of Erhai Lake, China. **Estuarine, Coastal and Shelf Science**, v. 149, p. 178–186, 2014.

ZHANG, M., WEN, S., WU, T., WANG, S., LI, X., GONG, W., WANG, H., LIU, C., ZHONG, J. Patterns of internal nitrogen and phosphorus loadings in a cascade reservoir with a large water level gradient: Effects of reservoir operation and water depth. **Journal of Environmental Management**. 320, 115884, 2022. https://doi.org/10.1016/j.jenvman.2022.115884

ZHANG, M.; SHI, X.; YANG, Z.; YU, Y.; SHI, L.; QIN, B. Long-term dynamics and drivers of phytoplankton biomass in eutrophic Lake Taihu. **Science of the Total Environment**, v. 645, p. 876–886, 2018.

ZHANG, X.; QI, Y.; LI, H.; WANG, X.; YIN, Q. Assessing the response of non-point source nitrogen pollution to land use change based on SWAT model. **Ecological Indicators**, v. 158, n. September 2023, 2024.

ZHANG, Y.; WU, Z.; LIU, M.; HE, J.; SHI, K.; ZHOU, Y.; WANG, M.; LIU, X. Dissolved oxygen stratification and response to thermal structure and long-term climate change in a large and deep subtropical reservoir (Lake Qiandaohu, China). **Water Research**, v. 75, p. 249–258, 2015.

ZHANG, Y.; YAO, X.; WU, Q.; HUANG, Y.; ZHOU, Z.; YANG, J.; LIU, X. Turbidity prediction of lake-type raw water using random forest model based on meteorological data: A case study of Tai lake, China. **Journal of Environmental Management**, v. 290, n. April, 2021.

ZHONG, Y., SU, Y., ZHANG, D., SHE, C., CHEN, N., CHEN, J., YANG, H., BALAJI-PRASATH, B. The spatiotemporal variations in microalgae communities in vertical waters of a subtropical reservoir. J. Environ. Manage. 317, 2022. https://doi.org/10.1016/j.jenvman.2022.115379

ZOBKOV, M. B.; ZOBKOVA, M. V. New spectroscopic method for true color determination in natural water with high agreement with visual methods. **Water Research**, v. 177, 2020.

APPENDIX A – SUPPLEMENTARY RESULTS FROM CHAPTER 2

DESCRIPTIVE STATISTICS

Table S 1– Descriptive statistics of the quality variables (at 0.3 m depth).

Variable	Unity	Points	Coefficient of variation	Variance	Mean	Standard deviation	Number of observations	Median
Total phosphorus	mgL^{-1}	Point #3	0.522	0.003	0.112	0.059	32	0.092
		Point #4	0.492	0.003	0.116	0.057	32	0.105
		Point #6	0.492	0.003	0.113	0.056	31	0.093
Total nitrogen	mgL^{-1}	Point #3	0.441	0.472	1.558	0.687	32	1.3125
		Point #4	0.375	0.269	1.381	0.518	32	1.419
		Point #6	0.482	0.460	1.407	0.678	31	1.15
Cyanobacteria	$cellsmL^{-1}$	Point #3	0.739	3.89E+10	2.67E+05	1.97E+05	32	2.54E+05
		Point #4	0.863	4.51E+10	2.46E+05	2.12E+05	31	1.75E+05
		Point #6	0.871	2.29E+10	1.74E+05	1.51E+05	33	9.40E+04
Chlorophyll a	μgL^{-1}	Point #3	0.628	1067.818	52.043	32.677	31	38.49
		Point #4	0.592	497.751	37.706	22.310	31	31.47
		Point #6	0.664	435.443	31.416	20.867	30	24.915

Source: The author.

Table S2- Descriptive statistics of the variables measured using a multiparameter probe.

Variable	Unity	Points	Coefficient of variation	Variance	Mean	Standard deviation	Number of observations	Median
		P1	0.331	11074.67	318.317	105.236	1005	292
		P2	0.316	12734.87	357.218	112.849	1783	325
		P3	0.329	14078.11	361.111	118.651	1209	320

Conductivity	µS/cm	P4	0.336	13294.87	343.034	115.303	1171	299
		P5	0.312	13222.37	368.214	114.989	1829	330
		P6	0.310	13415.61	372.809	115.826	2284	333.5
DO	mgL^{-1}	P1	0.405	5.048	5.542	2.247	1005	5.6
		P2	0.657	7.882	4.275	2.807	1783	4.83
		P3	0.572	6.787	4.552	2.606	1209	4.81
		P4	0.653	7.649	4.233	2.766	1171	4.29
		P5	0.669	6.314	3.758	2.513	1829	4.21
		P6	0.693	3.788	2.810	1.946	2284	3.04
pH	-	P1	0.064	0.249	7.828	0.499	1005	7.78
		P2	0.067	0.268	7.757	0.517	1783	7.7
		P3	0.070	0.307	7.885	0.554	1209	7.83
		P4	0.059	0.207	7.665	0.456	1171	7.62
		P5	0.051	0.152	7.626	0.390	1829	7.57
		P6	0.040	0.089	7.440	0.298	2284	7.435

Salin	‰	P1	0.340	0.003	0.151	0.051	1005	0.14
		P2	0.327	0.003	0.169	0.055	1783	0.15
		P3	0.338	0.003	0.171	0.058	1209	0.15
		P4	0.347	0.003	0.163	0.056	1171	0.14
		P5	0.321	0.003	0.175	0.056	1829	0.16
		P6	0.319	0.003	0.177	0.056	2284	0.16
TDS	gL^{-1}	P1	0.331	0.005	0.207	0.068	1005	0.19
		P2	0.316	0.005	0.232	0.073	1783	0.21
		P3	0.329	0.006	0.235	0.077	1209	0.21
		P4	0.335	0.005	0.223	0.075	1171	0.2
		P5	0.312	0.005	0.240	0.075	1829	0.22
		P6	0.311	0.005	0.242	0.075	2284	0.22
		P1	0.032	0.880	28.973	0.938	1005	28.78
		P2	0.032	0.833	28.670	0.913	1783	28.49
		P3	0.033	0.862	28.521	0.929	1209	28.36

Temperature	°C	P4	0.031	0.794	28.700	0.891	1171	28.52
		P5	0.031	0.803	28.414	0.896	1829	28.19
		P6	0.031	0.788	28.168	0.888	2284	27.961

WATER SAMPLING AND GENERAL CHARACTERISTICS OF THE RESERVOIR

Figure S 1 – Water quality monitoring performed. A) shows the monitoring team at the boat used to collect the samples in the reservoir and B) shows part of the fish farming area in the reservoir.

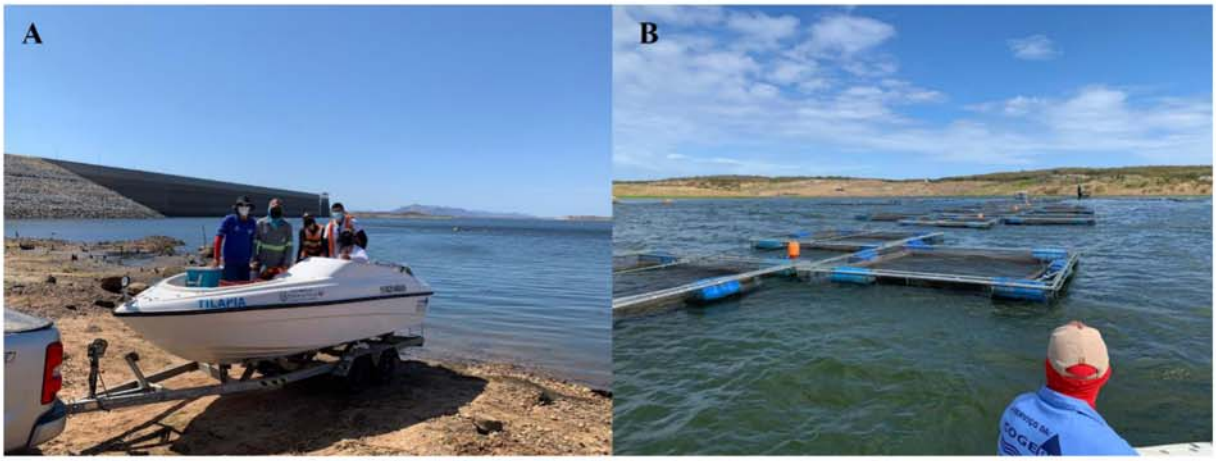

Source: The author.

Table S 2 – Formula to calculate the 5 depths in which water samples would be collected in order to be analyze water quality parameters in the laboratory. Where MD states for the maximum depth of the water column (m); T is transparency; AZ is the depth where the DO started to be < 1 mg/L.

Depth	Formula
1	0.3 m
2	$(T\ x3)/2$
3	$\big(MD + (T\ x\ 3)\big)/2$
4	$(MD + AZ)/2$
5	$MD - 0.5$

Source: The author.

Figure S 2 – Hydraulic residence time of Castanhão reservoir calculated using two different methods.

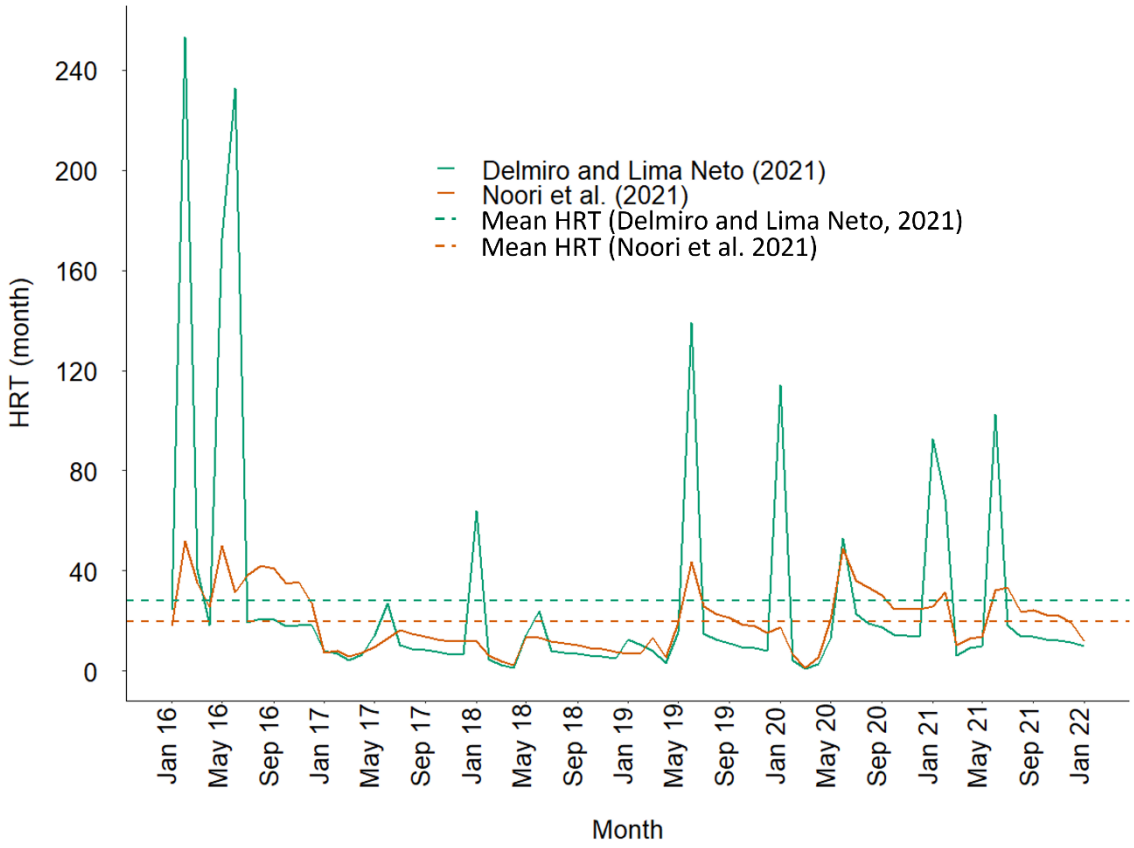

Source: The author.

THERMAL AND CHEMICAL STRATIFICATION-DO

Figure S 3 – Time series of the strength of chemical stratification for dissolved oxygen (SCS). A SCS of value zero indicates no stratification. A) Is sampling point P1, B) P2, C) P3, D) P4, E) P5, F) P6.

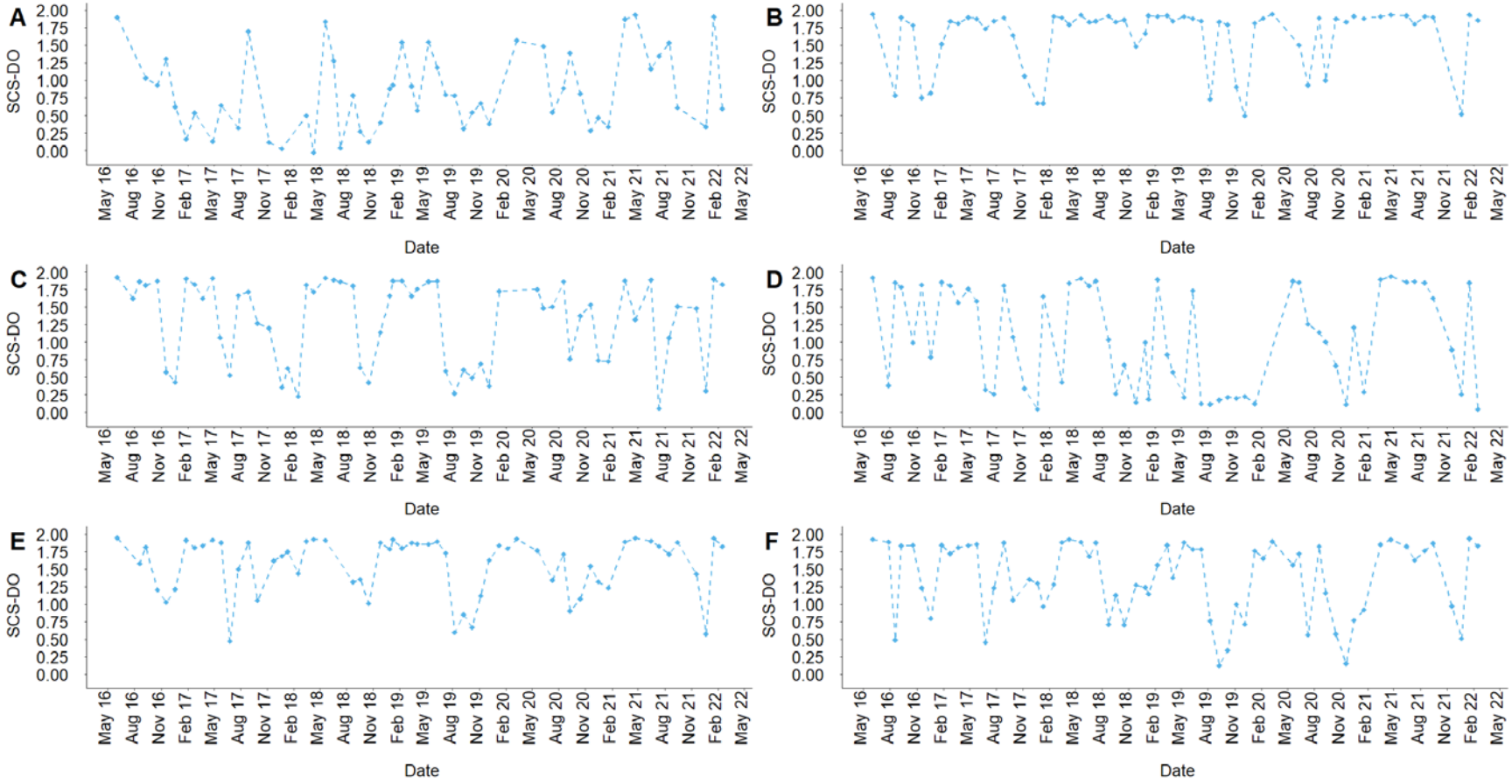

Source: The author.

Figure S 4 – Thermocline strength index (TSI). A TSI of value zero indicates no stratification. A) Is sampling point P1, B) P2, C) P3, D) P4, E) P5, F) P6.

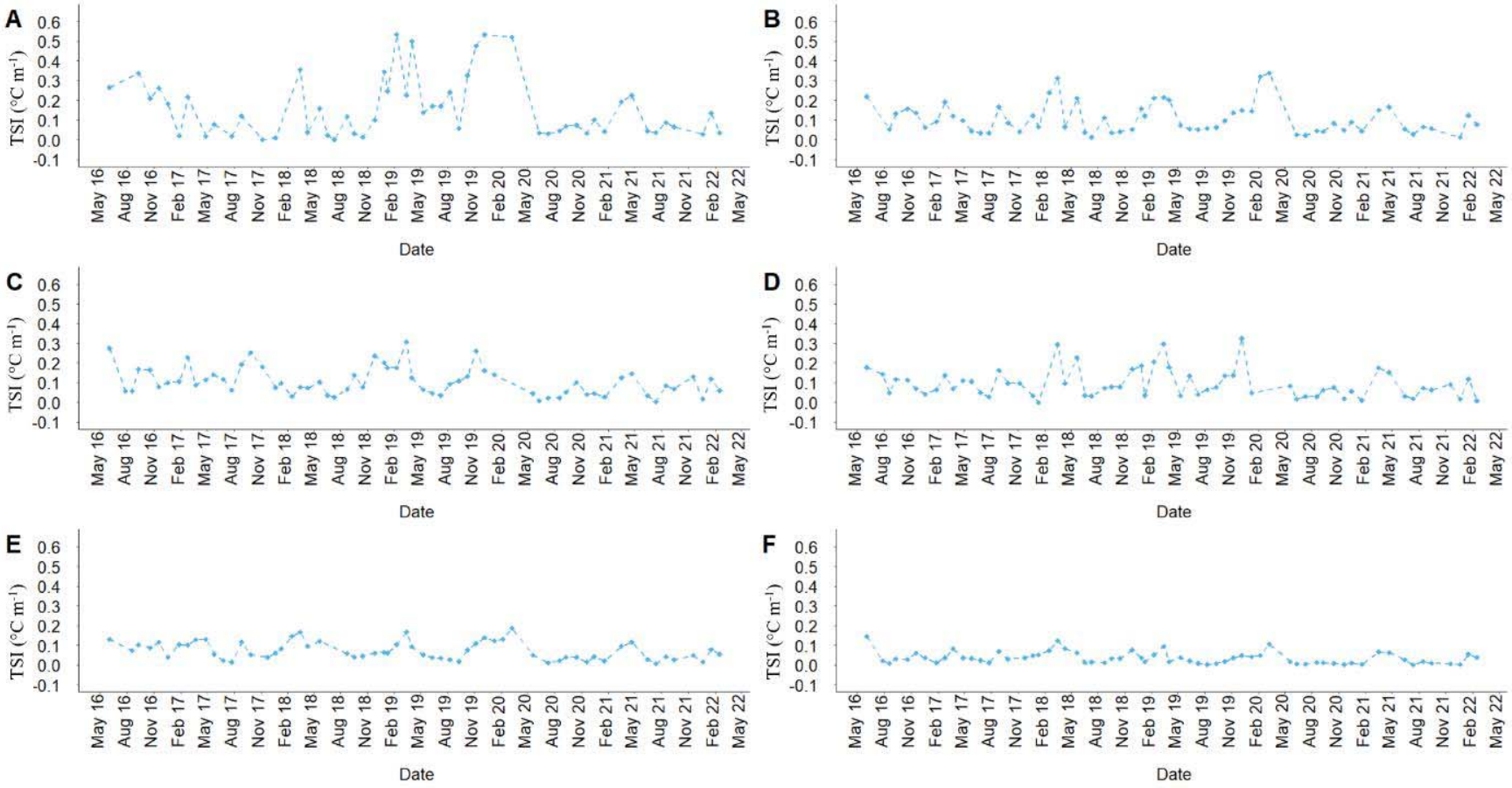

Source: The author.

Figure S 5 – Time series of the Relative Water Column Stability (RWCS). The red line represents the the limiting condition of RWCS ≥50 considered as a reference to characterize the thermal stratification in the water column. A) Is sampling point P1, B) P2, C) P3, D) P4, E) P5, F) P6.

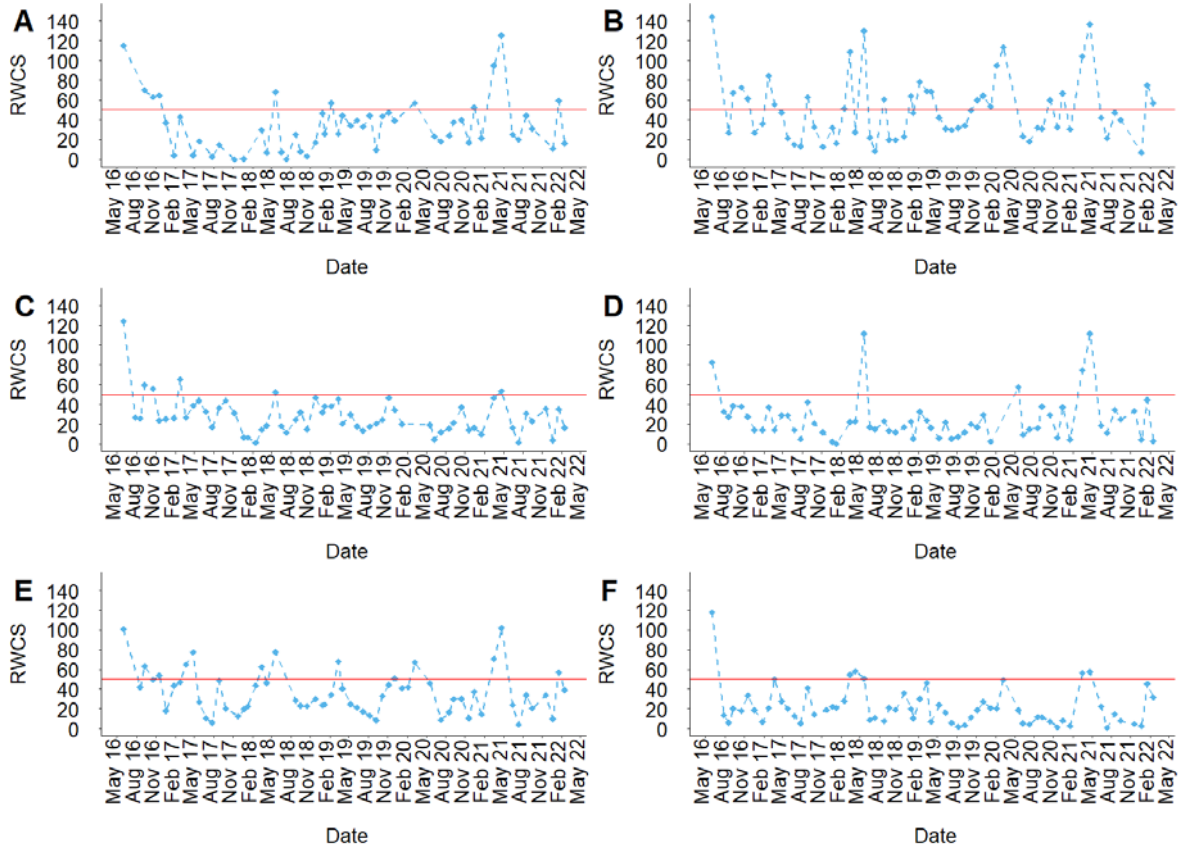

Source: The author.

PEARSON'S CORRELATION ANALYSIS

Figure S 6 – Pearson's correlation of water quality values between the surface samples (0.3 m depth) of points 3, 4 and 6. A) Represents the correlation values for total phosphorus, B) for total nitrogen, C) for chlorophyll a concentration, and D) for cyanobacteria cell density.

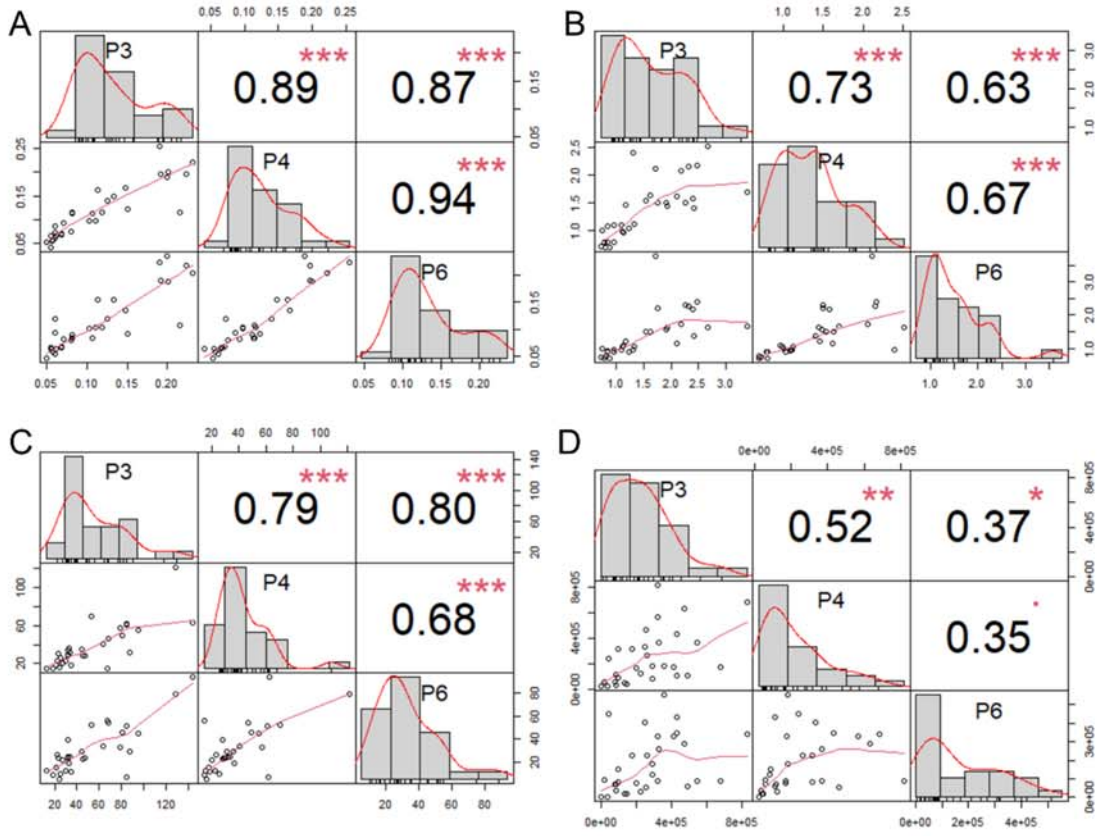

Source: The author.

Figure S7 – Pearson's correlation analysis of profiling variables in point P1 (0.3 m depth). The distribution of each variable is shown on the diagonal. On the bottom of the diagonal the bivariate scatter plots with a fitted line are displayed. On the top of the diagonal, the value of the correlation plus the significance level as stars. Each significance level is associated to a symbol: the p-values 0, 0.001, 0.01, 0.05, 0.1, 1 correspond to the symbols “***”, “**”, “*”, “.”, “ ”, respectively.

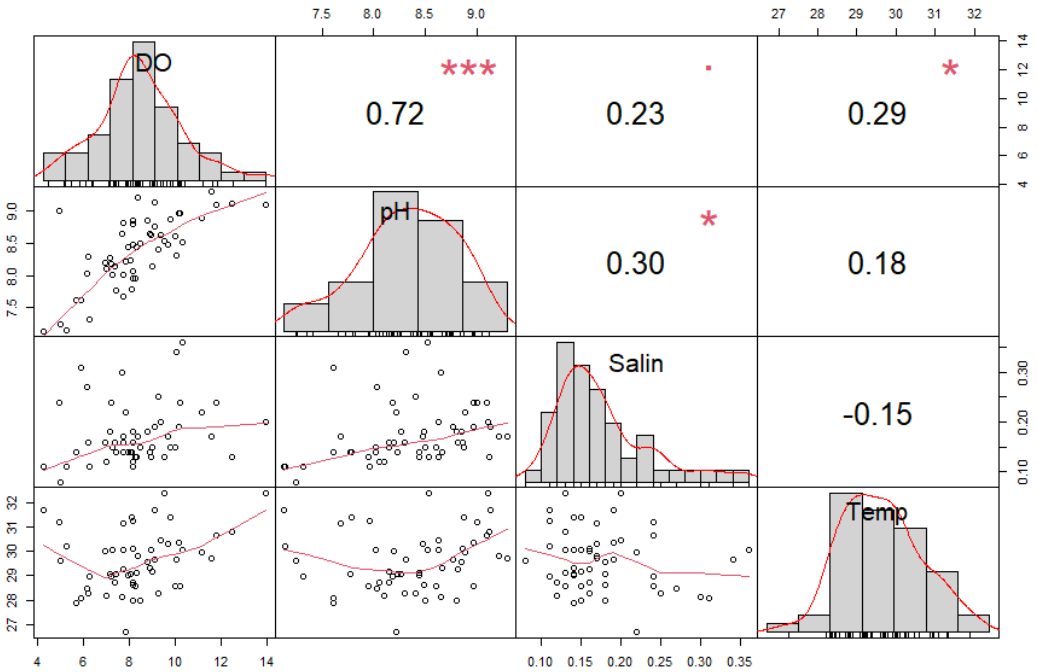

Source: The author.

Figure S8 – Pearson's correlation analysis of profiling variables in point P1 (0.5 m above sediment layer). The distribution of each variable is shown on the diagonal. On the bottom of the diagonal the bivariate scatter plots with a fitted line are displayed. On the top of the diagonal, the value of the correlation plus the significance level as stars. Each significance level is associated to a symbol: the p-values 0, 0.001, 0.01, 0.05, 0.1, 1 correspond to the symbols “***”, “**”, “*”, “.”, “ ”, respectively.

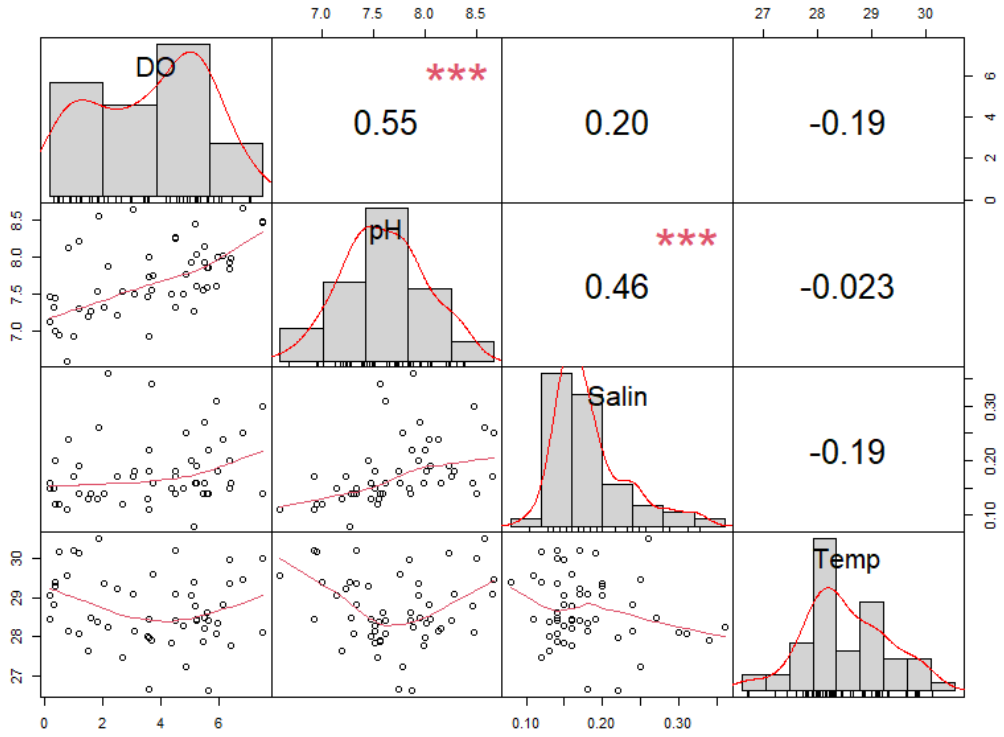

Source: The author.

Figure S9 – Pearson's correlation analysis of profiling variables in point P2 (0.3 m depth). The distribution of each variable is shown on the diagonal. On the bottom of the diagonal the bivariate scatter plots with a fitted line are displayed. On the top of the diagonal, the value of the correlation plus the significance level as stars. Each significance level is associated to a symbol: the p-values 0, 0.001, 0.01, 0.05, 0.1, 1 correspond to the symbols “***”, “**”, “*”, “.”, “ ”, respectively.

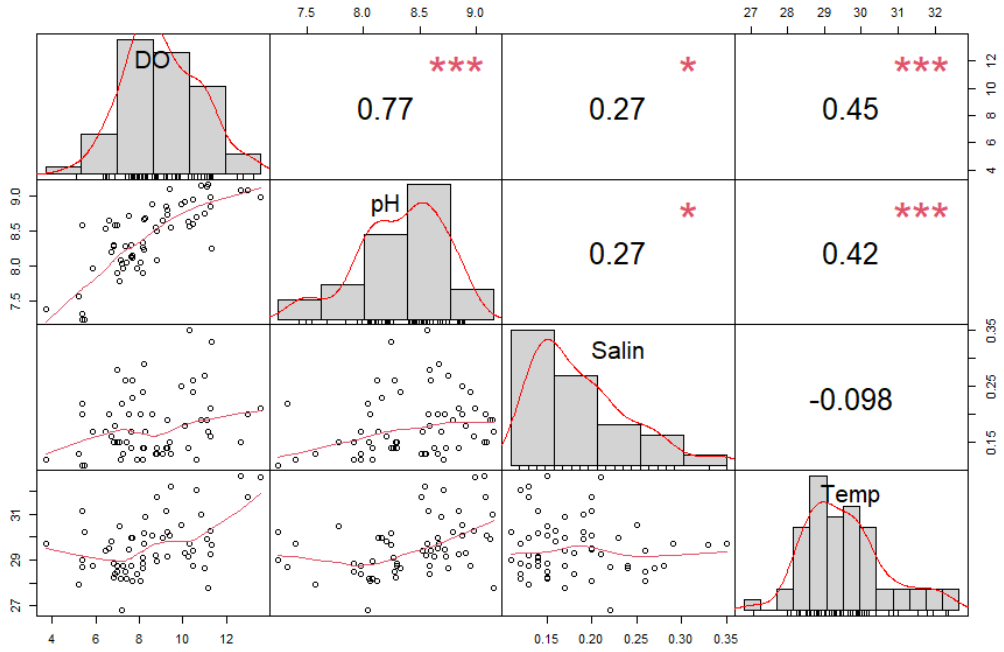

Source: The author.

Figure S10 – Pearson's correlation analysis of profiling variables in point P2(0.5 m above sediment layer). The distribution of each variable is shown on the diagonal. On the bottom of the diagonal the bivariate scatter plots with a fitted line are displayed. On the top of the diagonal, the value of the correlation plus the significance level as stars. Each significance level is associated to a symbol: the p-values 0, 0.001, 0.01, 0.05, 0.1, 1 correspond to the symbols “***”, “**”, “*”, “.”, “ ”, respectively.

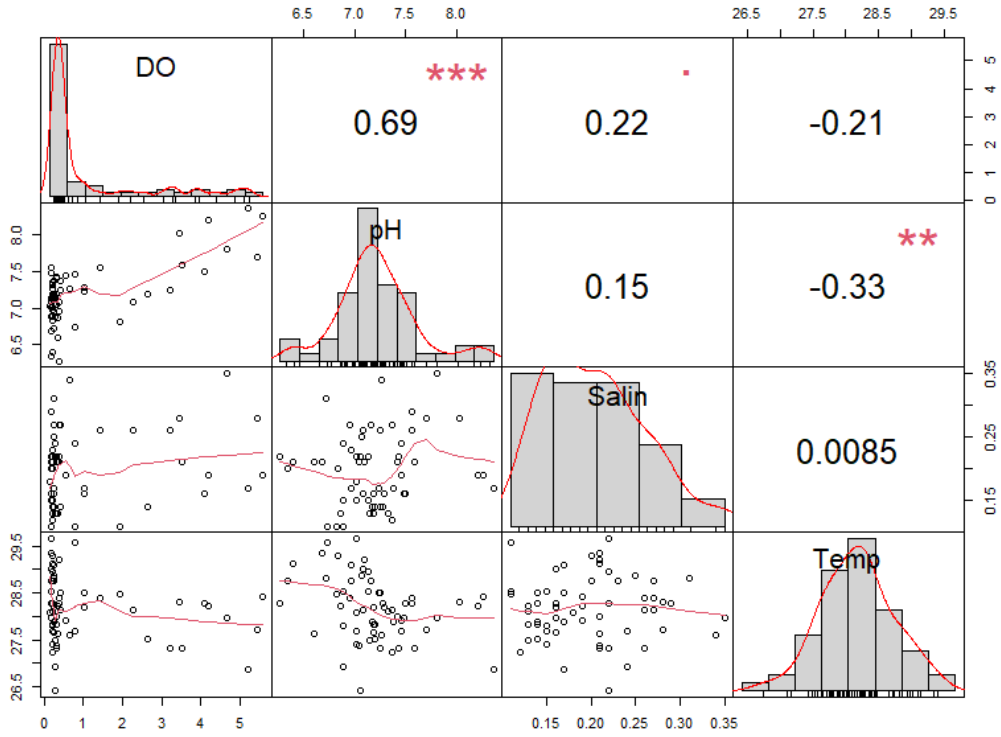

Source: The author.

Figure S11 – Pearson's correlation analysis of profiling variables in point P3 (0.3 m depth). The distribution of each variable is shown on the diagonal. On the bottom of the diagonal the bivariate scatter plots with a fitted line are displayed. On the top of the diagonal, the value of the correlation plus the significance level as stars. Each significance level is associated to a symbol: the p-values 0, 0.001, 0.01, 0.05, 0.1, 1 correspond to the symbols “***”, “**”, “*”, “.”, “ ”, respectively.

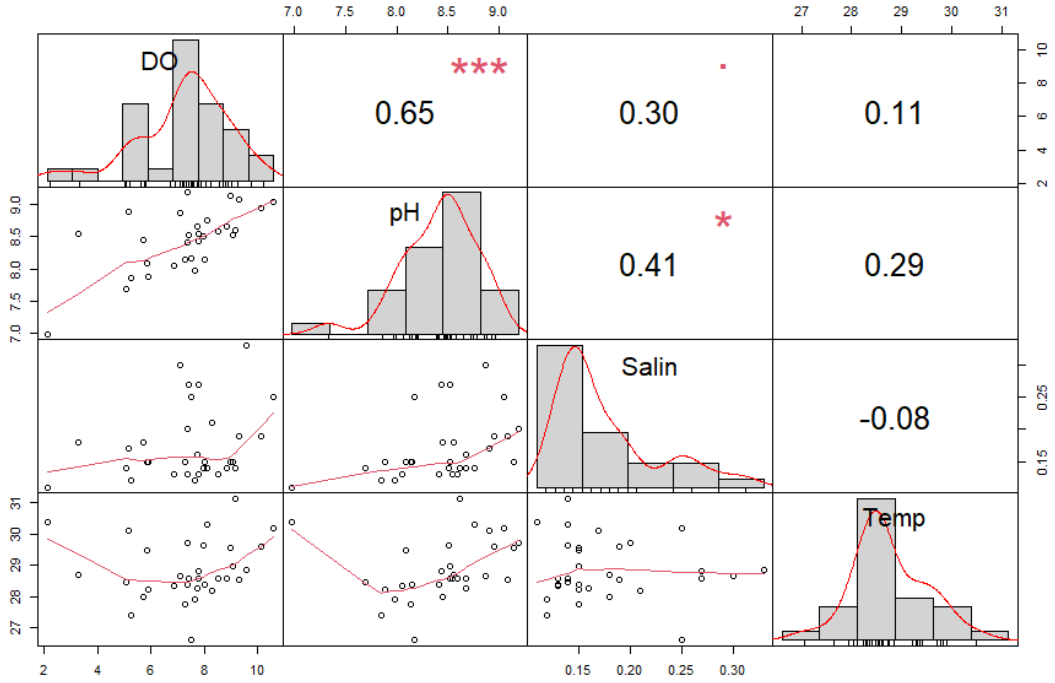

Source: The author.

Figure S12 – Pearson's correlation analysis of profiling variables in point P3(0.5 m above sediment layer). The distribution of each variable is shown on the diagonal. On the bottom of the diagonal the bivariate scatter plots with a fitted line are displayed. On the top of the diagonal, the value of the correlation plus the significance level as stars. Each significance level is associated to a symbol: the p-values 0, 0.001, 0.01, 0.05, 0.1, 1 correspond to the symbols “***”, “**”, “*”, “.”, “ ”, respectively.

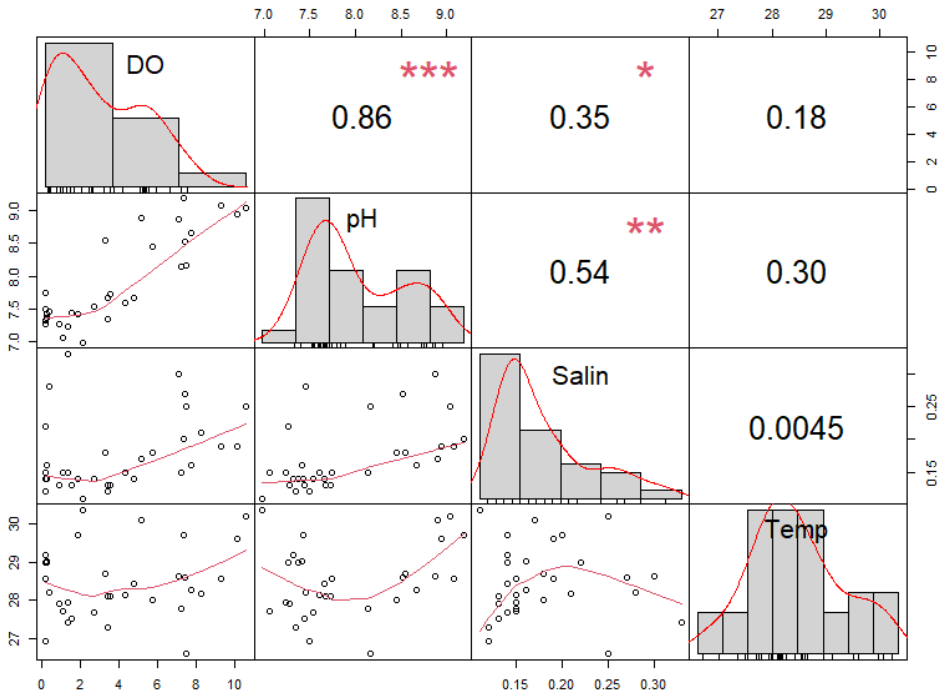

Source: The author.

Figure S13 – Pearson's correlation analysis of profiling variables in point P4 (0.3 m depth). The distribution of each variable is shown on the diagonal. On the bottom of the diagonal the bivariate scatter plots with a fitted line are displayed. On the top of the diagonal, the value of the correlation plus the significance level as stars. Each significance level is associated to a symbol: the p-values 0, 0.001, 0.01, 0.05, 0.1, 1 correspond to the symbols “***”, “**”, “*”, “.”, “ ”, respectively.

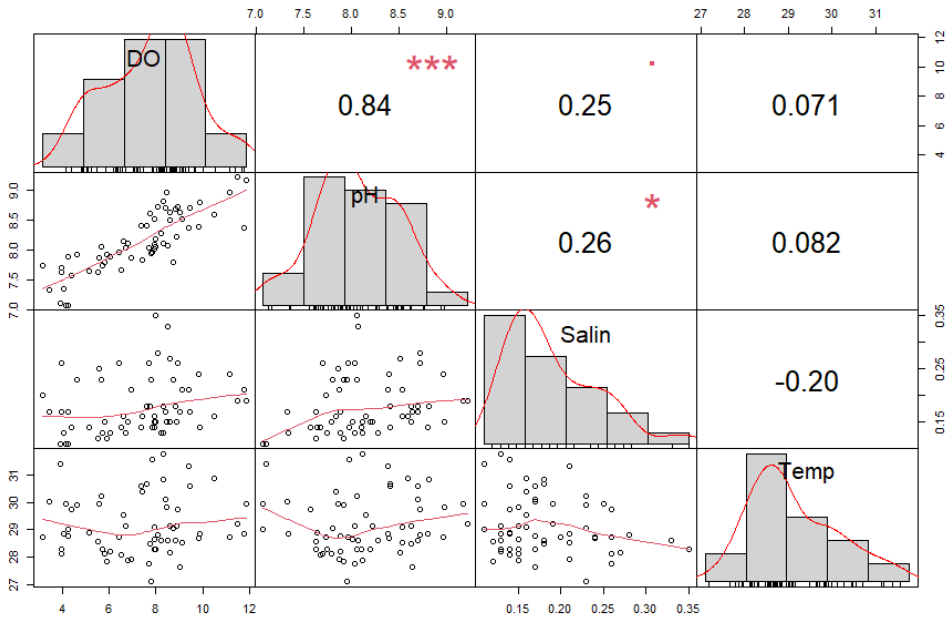

Source: The author.

Figure S14 – Pearson's correlation analysis of profiling variables in point P4(0.5 m above sediment layer). The distribution of each variable is shown on the diagonal. On the bottom of the diagonal the bivariate scatter plots with a fitted line are displayed. On the top of the diagonal, the value of the correlation plus the significance level as stars. Each significance level is associated to a symbol: the p-values 0, 0.001, 0.01, 0.05, 0.1, 1 correspond to the symbols “***”, “**”, “*”, “.”, “ ”, respectively.

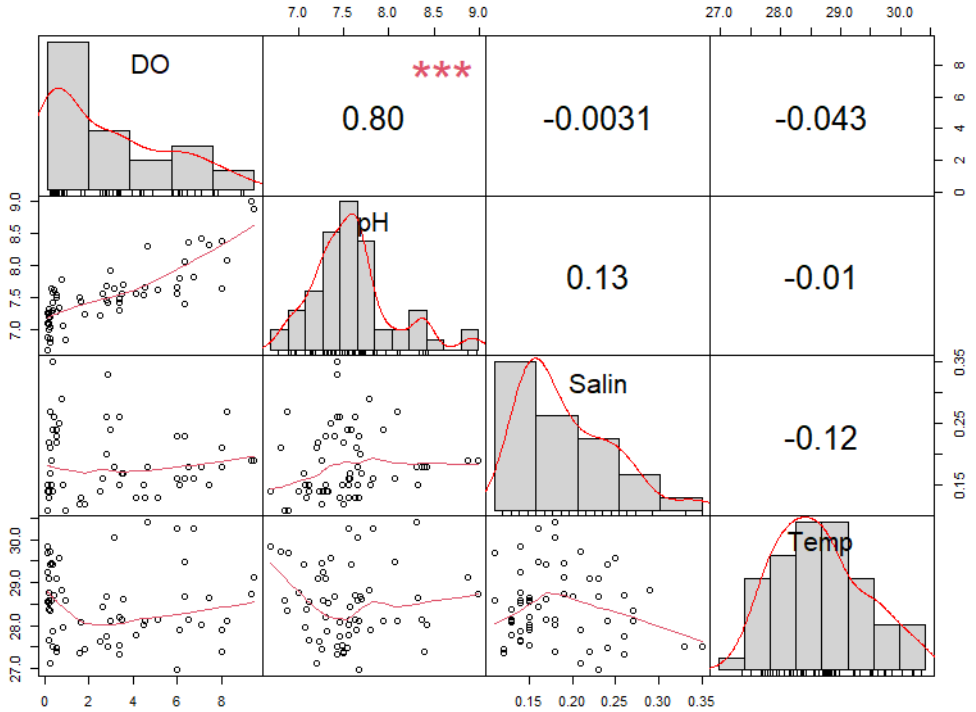

Source: The author.

Figure S15 – Pearson's correlation analysis of profiling variables in point P5 (0.3 m depth). The distribution of each variable is shown on the diagonal. On the bottom of the diagonal the bivariate scatter plots with a fitted line are displayed. On the top of the diagonal, the value of the correlation plus the significance level as stars. Each significance level is associated to a symbol: the p-values 0, 0.001, 0.01, 0.05, 0.1, 1 correspond to the symbols “***”, “**”, “*”, “.”, “ ”, respectively.

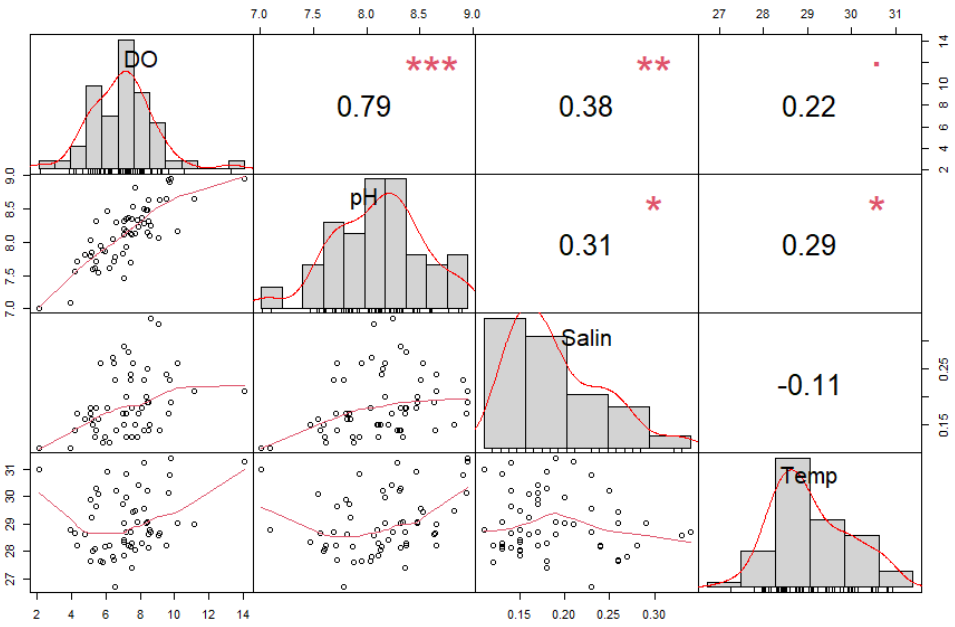

Source: The author.

Figure S16 – Pearson's correlation analysis of profiling variables in point P5 (0.5 m above sediment layer). The distribution of each variable is shown on the diagonal. On the bottom of the diagonal the bivariate scatter plots with a fitted line are displayed. On the top of the diagonal, the value of the correlation plus the significance level as stars. Each significance level is associated to a symbol: the p-values 0, 0.001, 0.01, 0.05, 0.1, 1 correspond to the symbols “***”, “**”, “*”, “.”, “ ”, respectively.

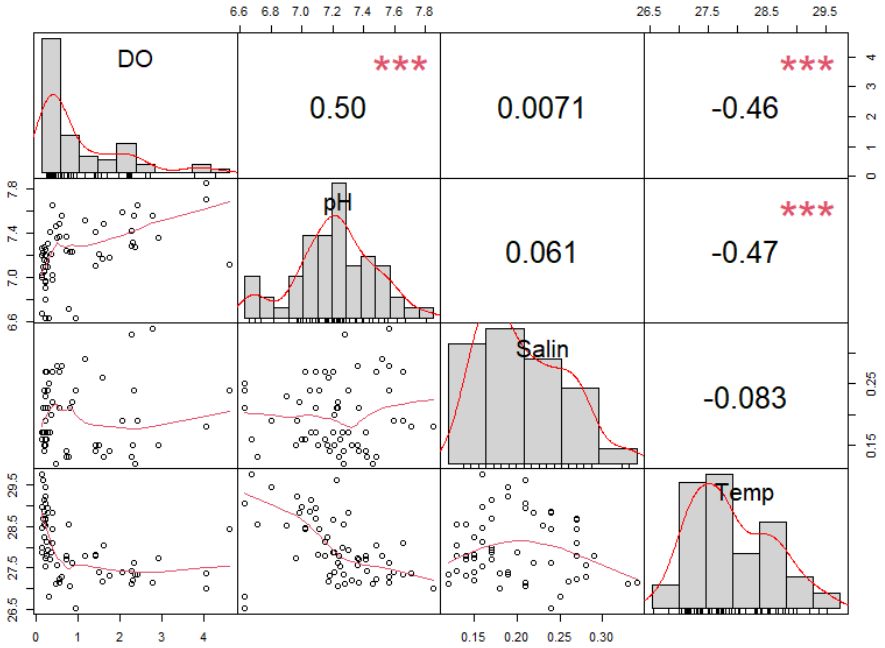

Source: The author.

Figure S17 – Pearson's correlation analysis of profiling variables in point P6 (0.3 m depth). The distribution of each variable is shown on the diagonal. On the bottom of the diagonal the bivariate scatter plots with a fitted line are displayed. On the top of the diagonal, the value of the correlation plus the significance level as stars. Each significance level is associated to a symbol: the p-values 0, 0.001, 0.01, 0.05, 0.1, 1 correspond to the symbols “***”, “**”, “*”, “.”, “ ”, respectively.

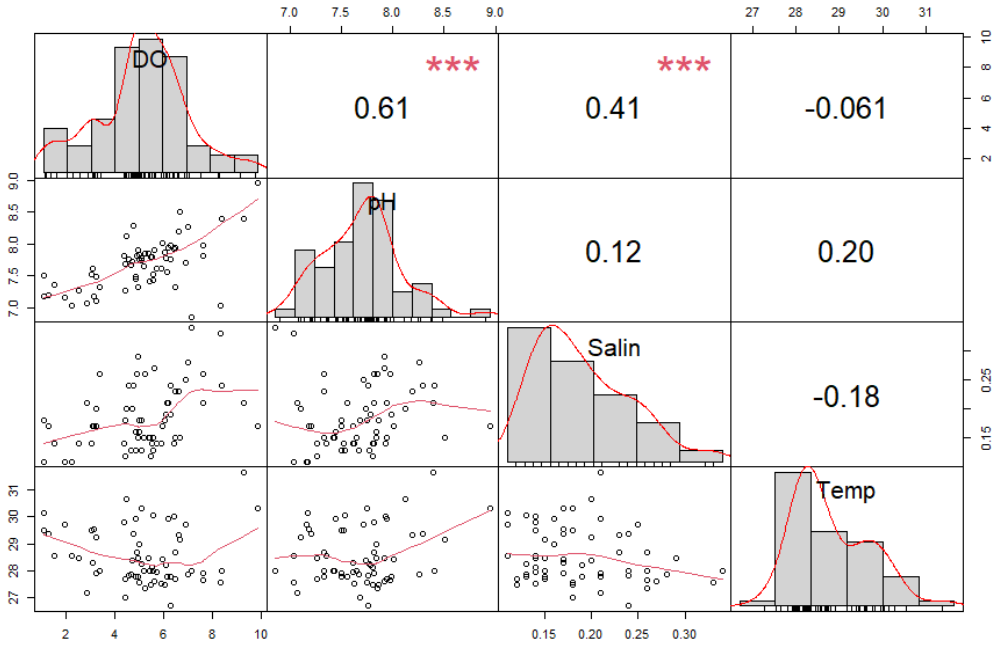

Source: The author.

Figure S18 – Pearson's correlation analysis of profiling variables in point P6(0.5 m above sediment layer). The distribution of each variable is shown on the diagonal. On the bottom of the diagonal the bivariate scatter plots with a fitted line are displayed. On the top of the diagonal, the value of the correlation plus the significance level as stars. Each significance level is associated to a symbol: the p-values 0, 0.001, 0.01, 0.05, 0.1, 1 correspond to the symbols “***”, “**”, “*”, “.”, “ ”, respectively.

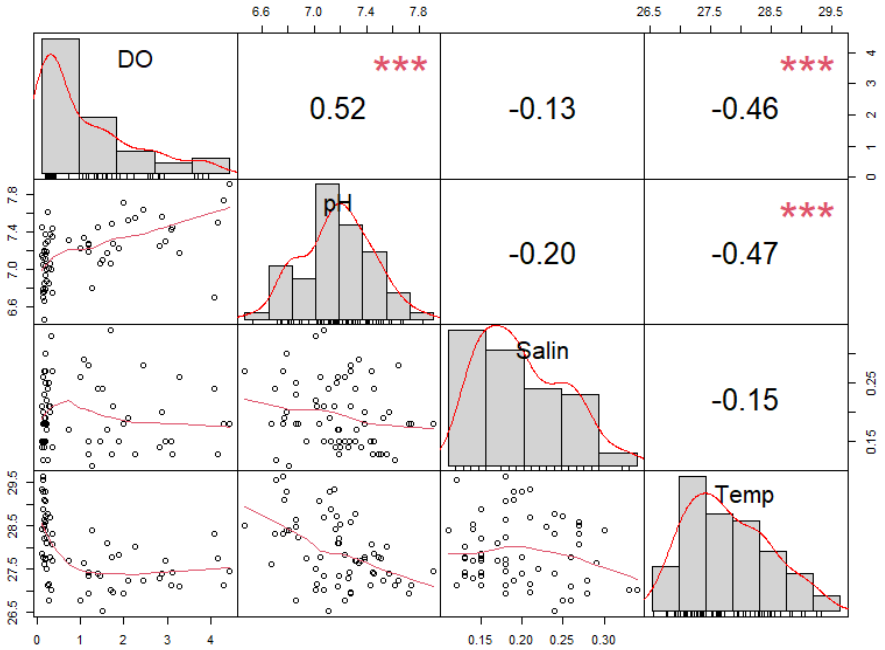

Source: The author.

Figure S19 - Pearson's correlation analysis of water quality variables at the sampling point P3 (0.3 m depth). The distribution of each variable is shown on the diagonal. On the bottom of the diagonal the bivariate scatter plots with a fitted line are displayed. On the top of the diagonal, the value of the correlation plus the significance level as stars. Each significance level is associated to a symbol: the p-values 0, 0.001, 0.01, 0.05, 0.1, 1 correspond to the symbols “***”, “**”, “*”, “.”, “ ”, respectively.

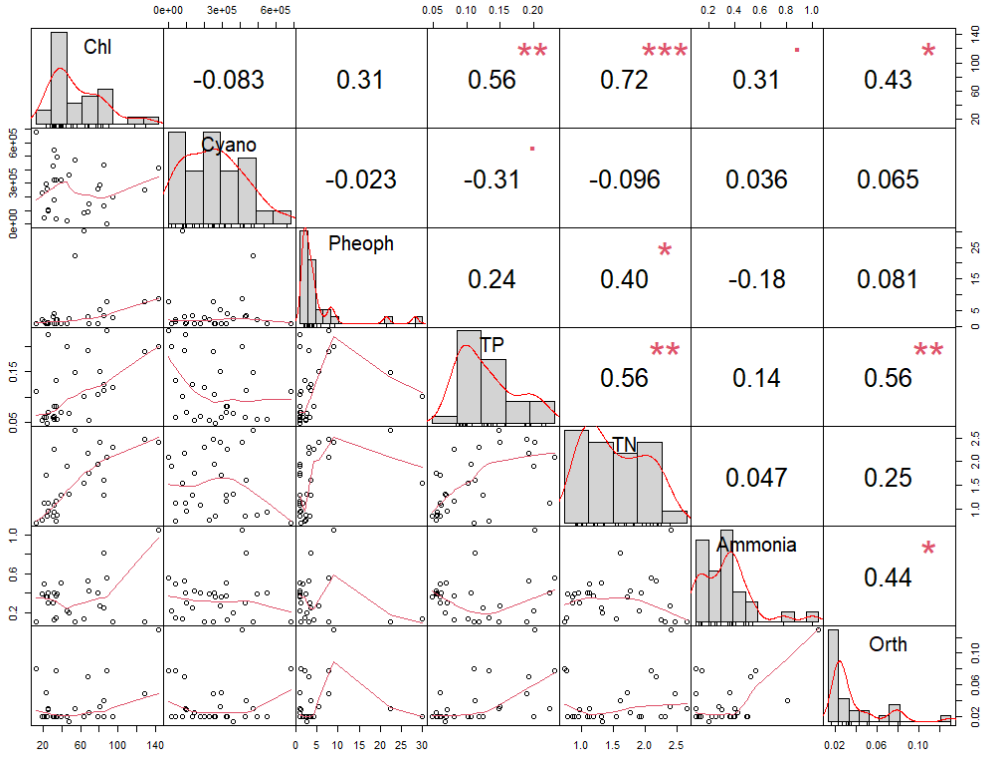

Source: The author.

Figure S20 – Pearson's correlation analysis of water quality variables at the sampling point P4 (0.3 m depth). The distribution of each variable is shown on the diagonal. On the bottom of the diagonal the bivariate scatter plots with a fitted line are displayed. On the top of the diagonal, the value of the correlation plus the significance level as stars. Each significance level is associated to a symbol: the p-values 0, 0.001, 0.01, 0.05, 0.1, 1 correspond to the symbols “***”, “**”, “*”, “.”, “ ”, respectively.

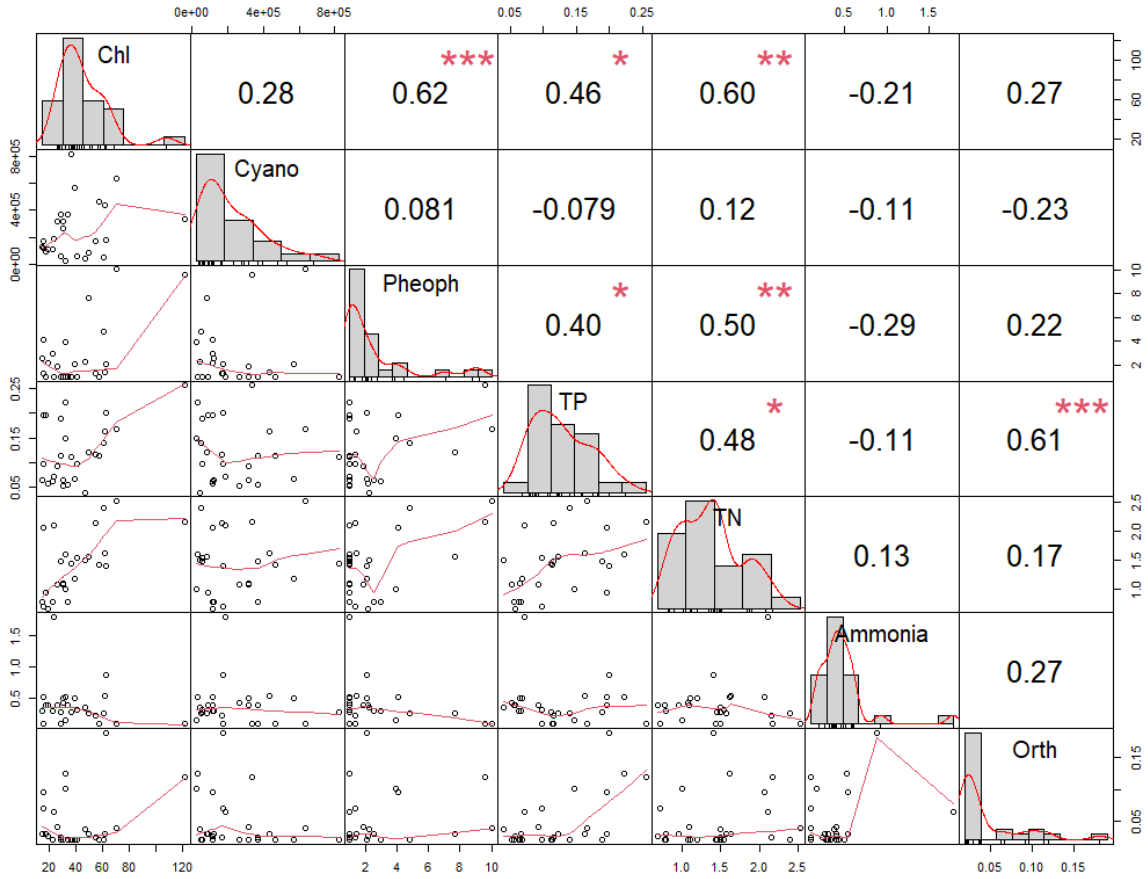

Source: The author.

Figure S21 - Pearson's correlation analysis of water quality variables at the sampling point P6 (0.3 m depth). The distribution of each variable is shown on the diagonal. On the bottom of the diagonal the bivariate scatter plots with a fitted line are displayed. On the top of the diagonal, the value of the correlation plus the significance level as stars. Each significance level is associated to a symbol: the p-values 0, 0.001, 0.01, 0.05, 0.1, 1 correspond to the symbols “***”, “**”, “*”, “.”, “ ”, respectively

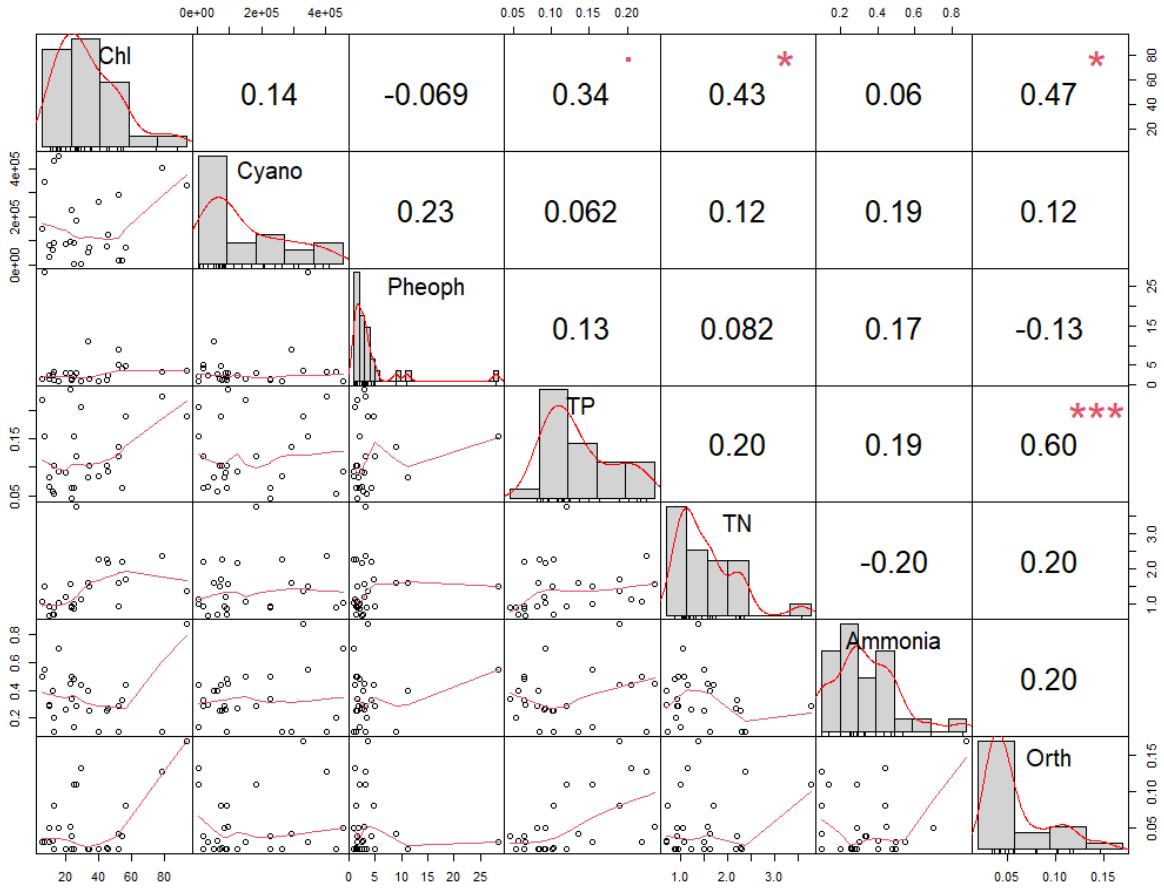

Source: The author.

BOXPLOT ANALYSIS

Figure S22– Boxplots comparing variables of the profiling monitoring differences between the points, with sampling depths ranging from 0.3 m under the water surface to 0.5 m above sediment layer. A) dissolved oxygen concentrations, B) temperatures, C) Total dissolved solids.

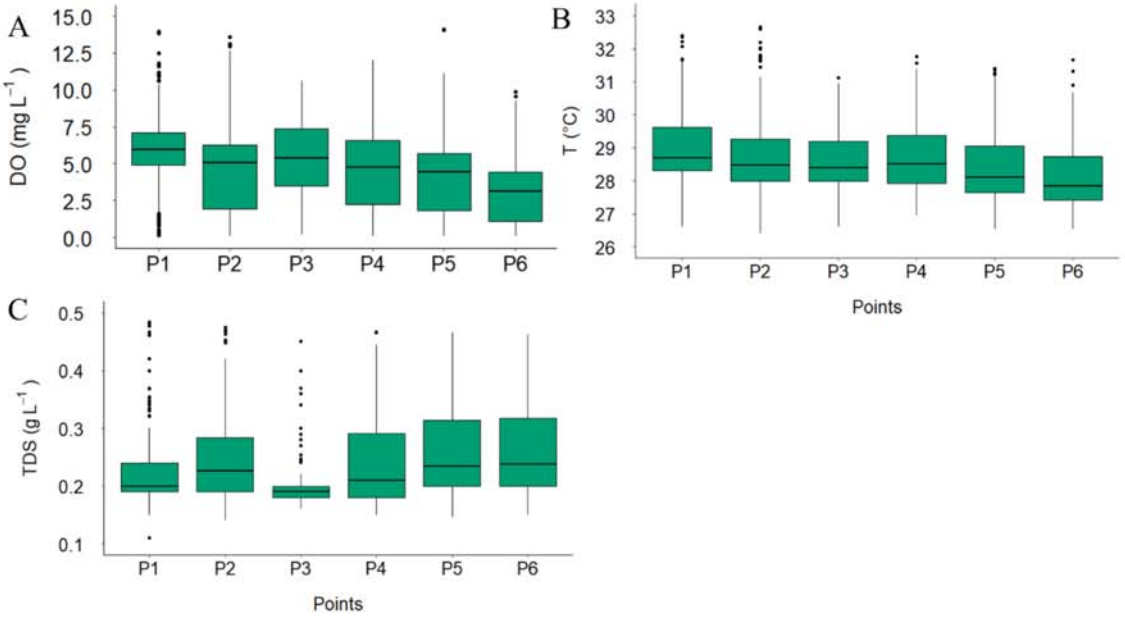

Source: The author.

Figure S23 – Boxplots comparing the interannual changes of water quality parameters, with sampling depths ranging from 0.3 to 24.6 m. A) presents total phosphorus concentrations, B) total nitrogen, C) chlorophyll a and D) cyanobacteria cell density.

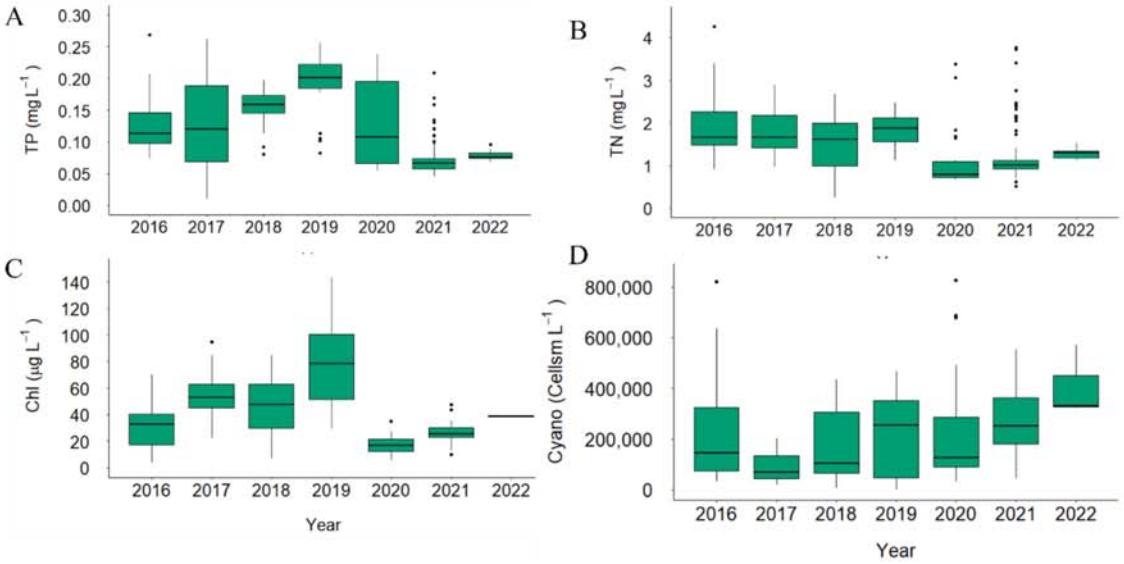

Source: The author.

Figure S24 – Boxplots comparing profiling monitoring variables interannual changes, with sampling depths ranging from 0.3 m under the water surface to 0.5 m above sediment layer. A) presents dissolved oxygen concentrations, B) temperatures, C) Total dissolved solids.

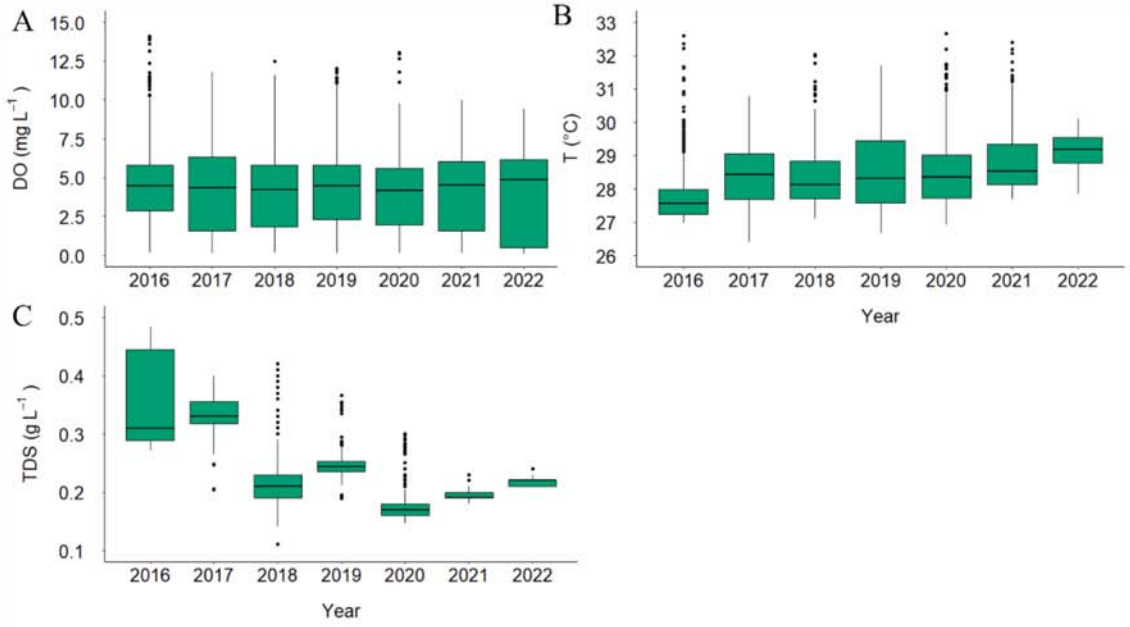

Source: The author.

TIME SERIES WITH BOXPLOTS

Figure S25 –Time series of total phosphorus concentration.

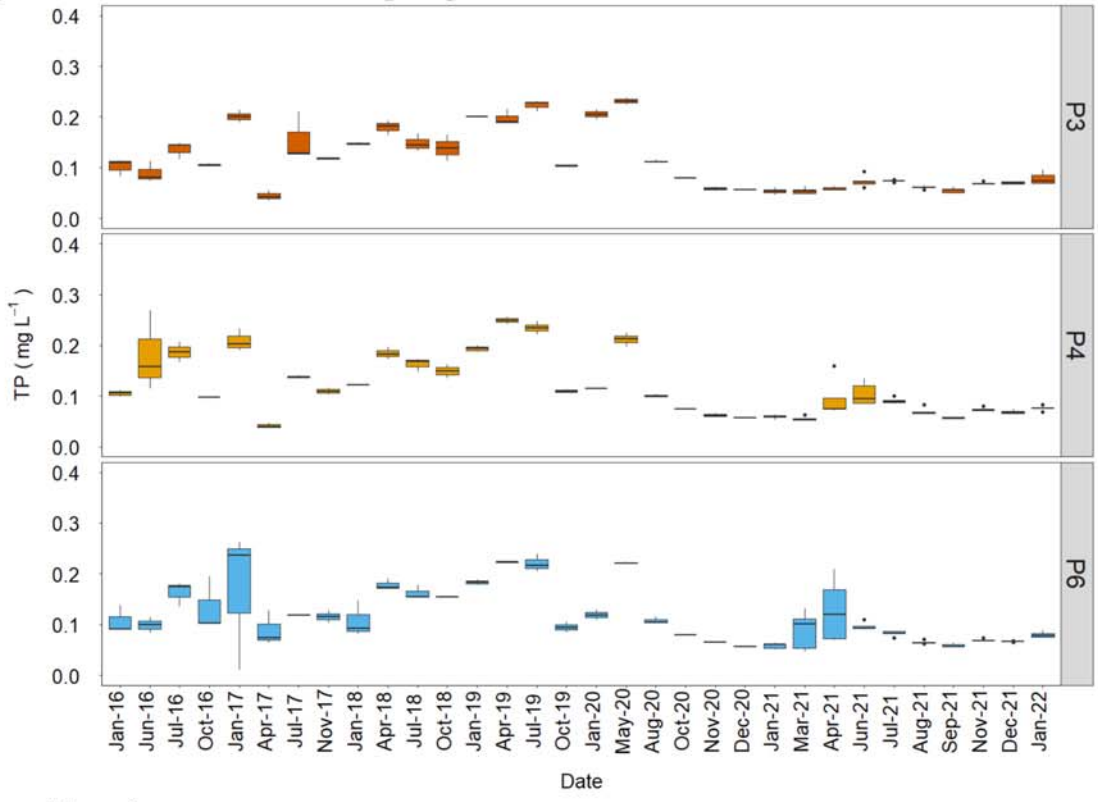

Source: The author.

Figure S26 – Time series of total nitrogen concentration.

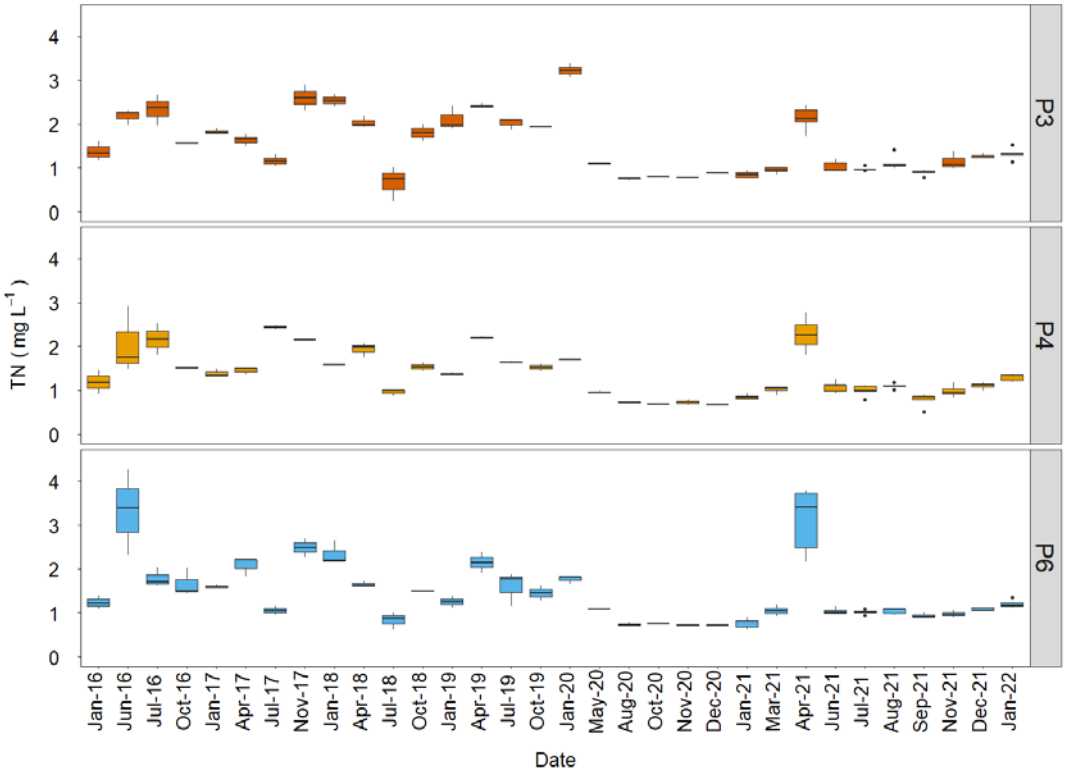

Source: The author.

Figure S27 – Time series of chlorophyll a concentration at 0.3 m depth.

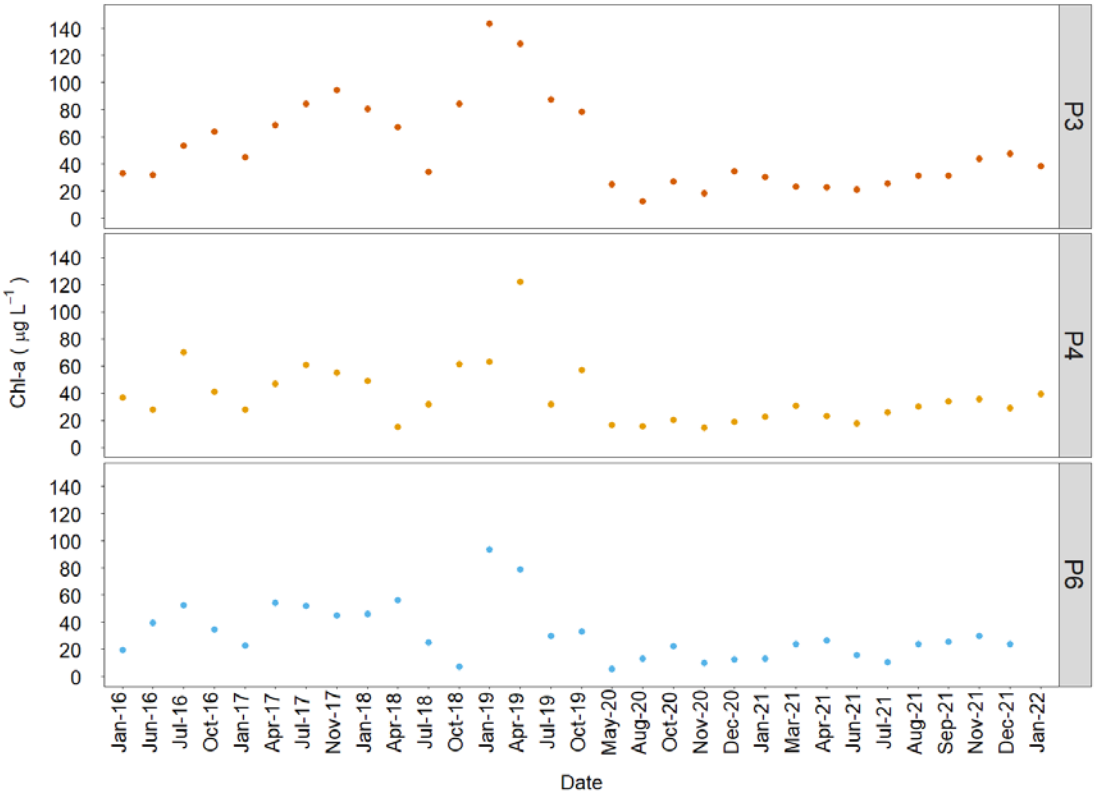

Source: The author.

Figure S28 – Time series of cyanobacteria cell density at 0.3 m depth.

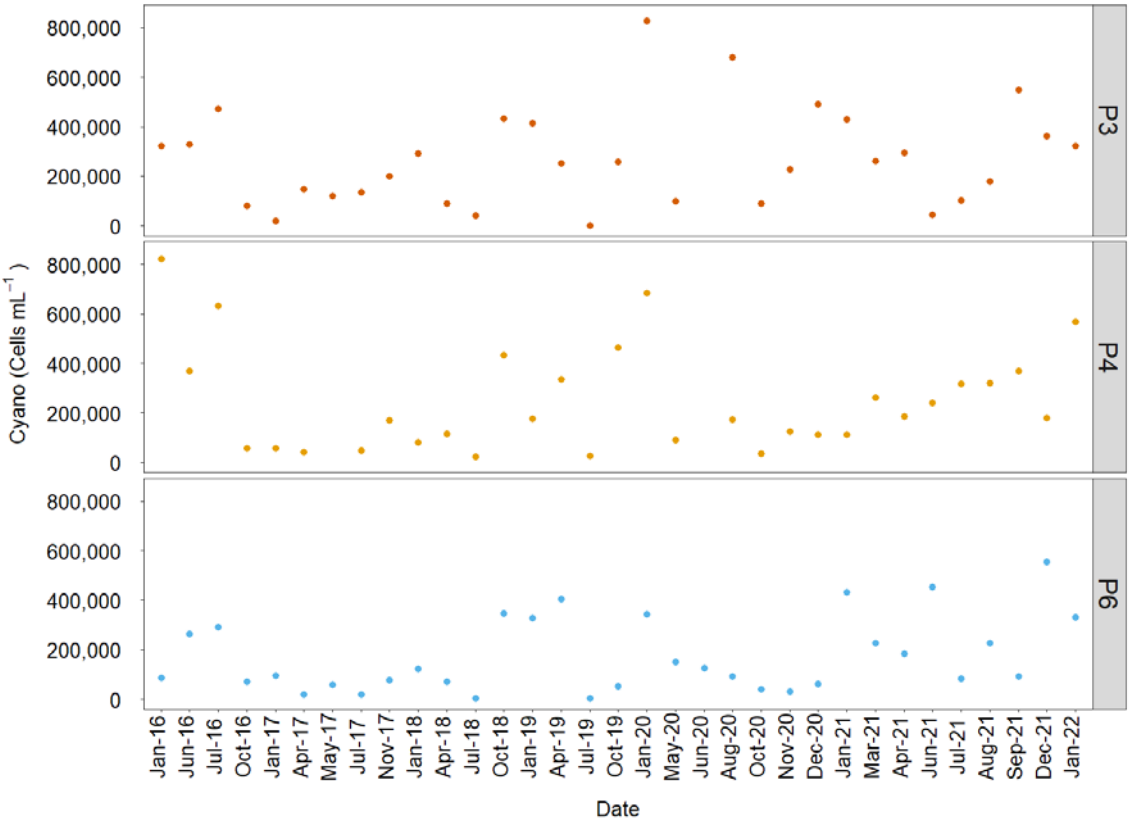

Source: The author.

Figure S 29 – Time series of dissolved oxygen concentration.

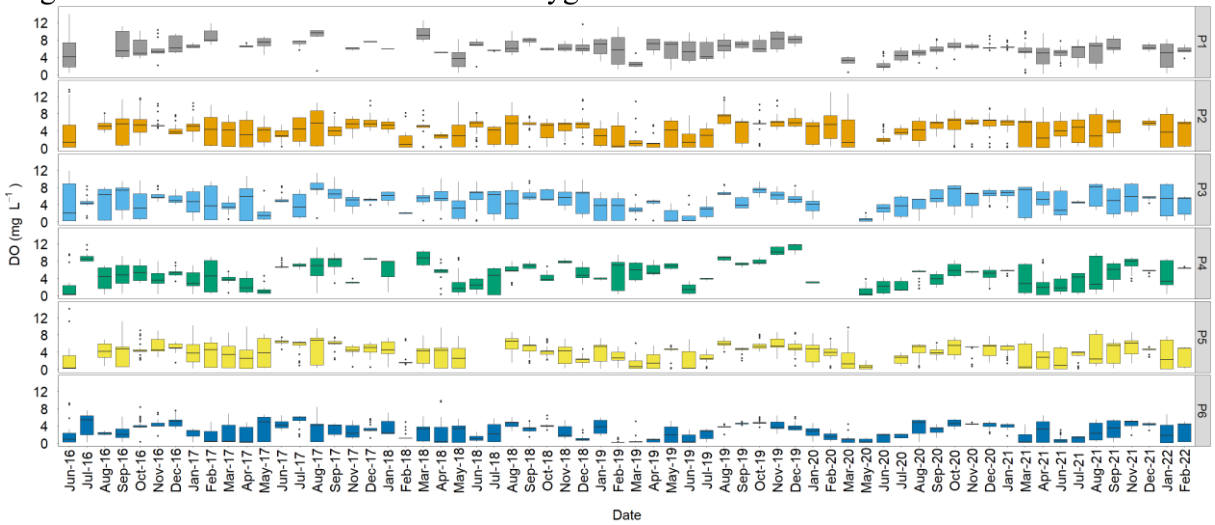

Source: The author.

Figure S 30 – Time series of pH concentration.

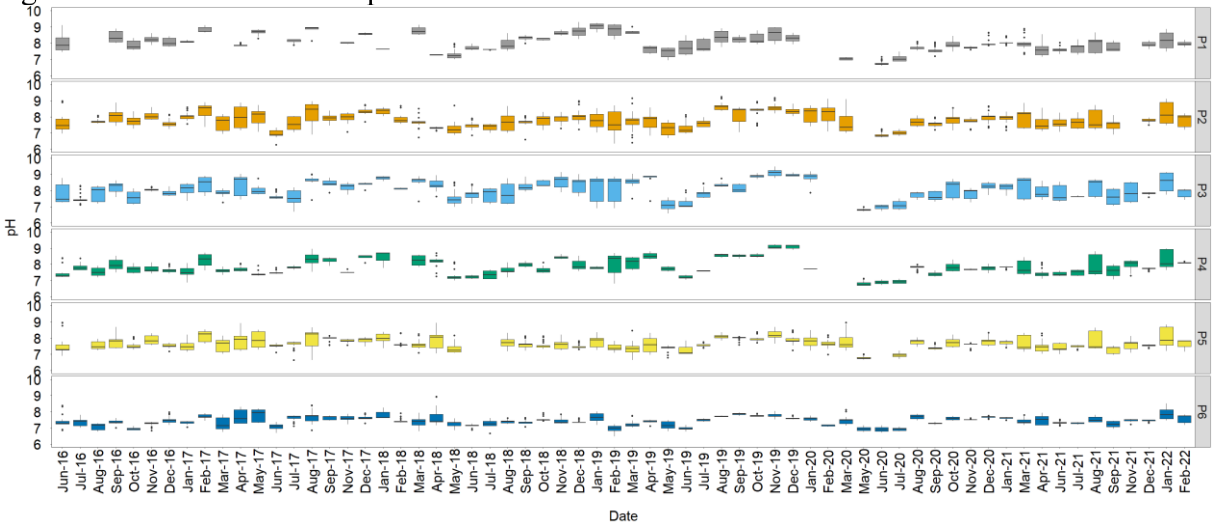

Source: The author

Figure S 31 – Time series of temperature.

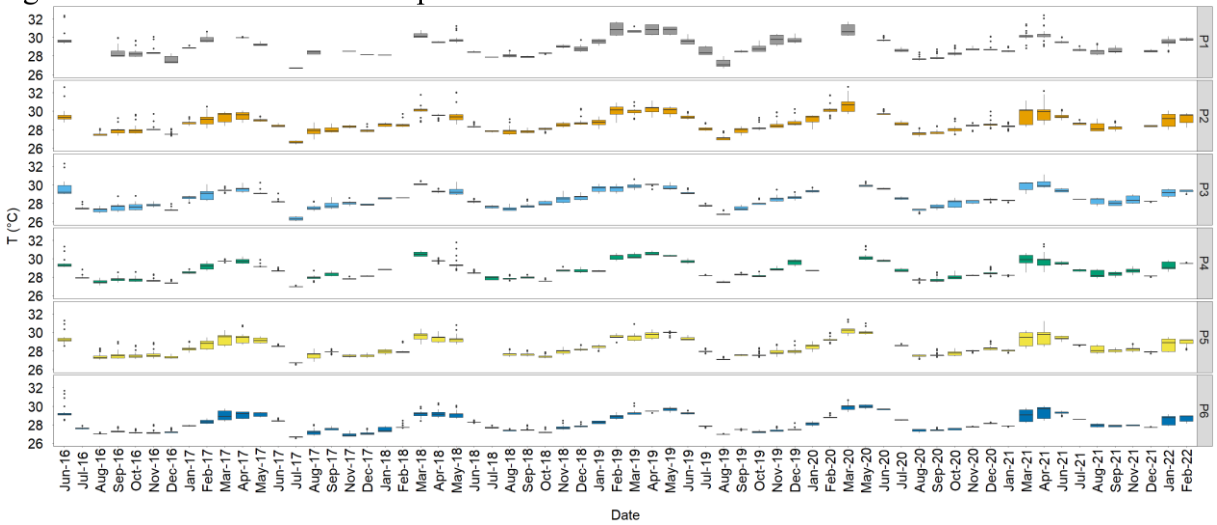

Source: The author

Figure S 32 – Time series of salinity.

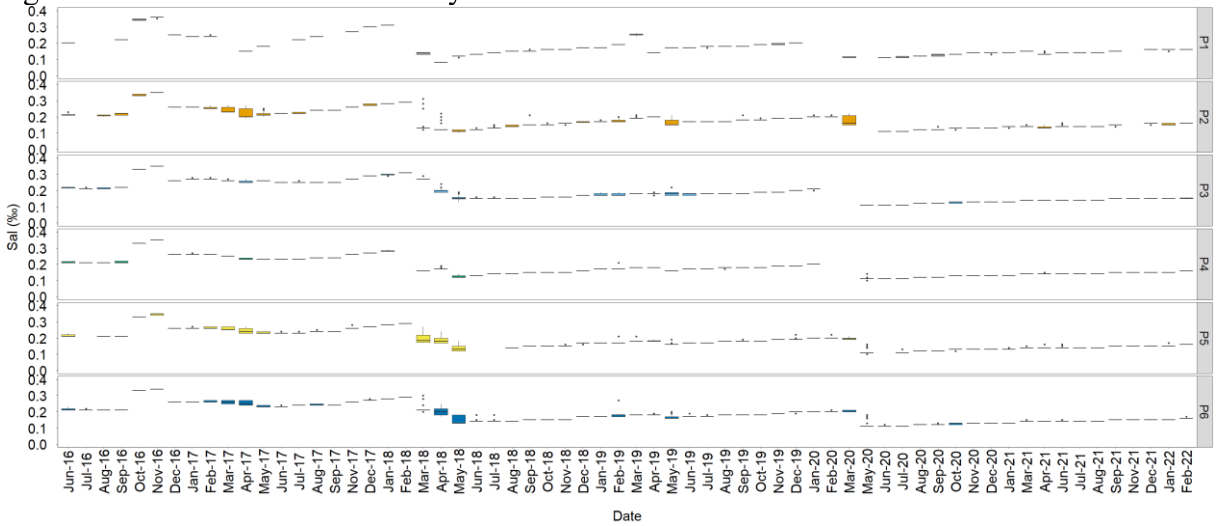

Source: The author.

Figure S 33 – Time series of total dissolved solids concentration.

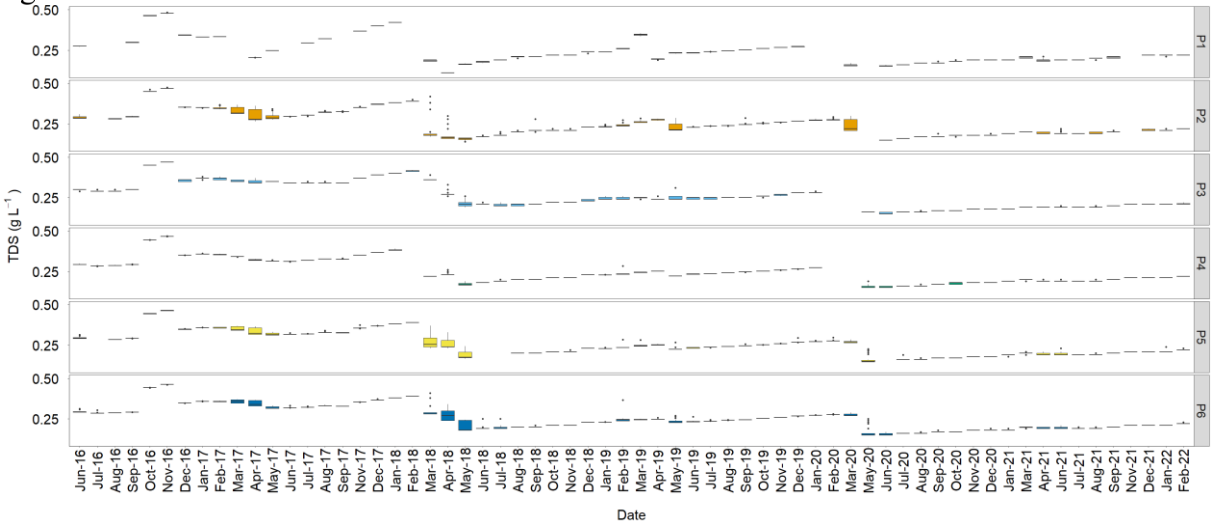

Source: The author.

APPENDIX B – SUPPLEMENTARY RESULTS FROM CHAPTER 3

THERMAL AND CHEMICAL REGIME OF THE CASTANHÃO RESERVOIR

Figure S 34 – Water temperature profiles at P7 with data collected in A) October 2021 (dry season), B) March 2022 (rainy season), C) November 2022 (dry season), and D) May 2023 (rainy season).

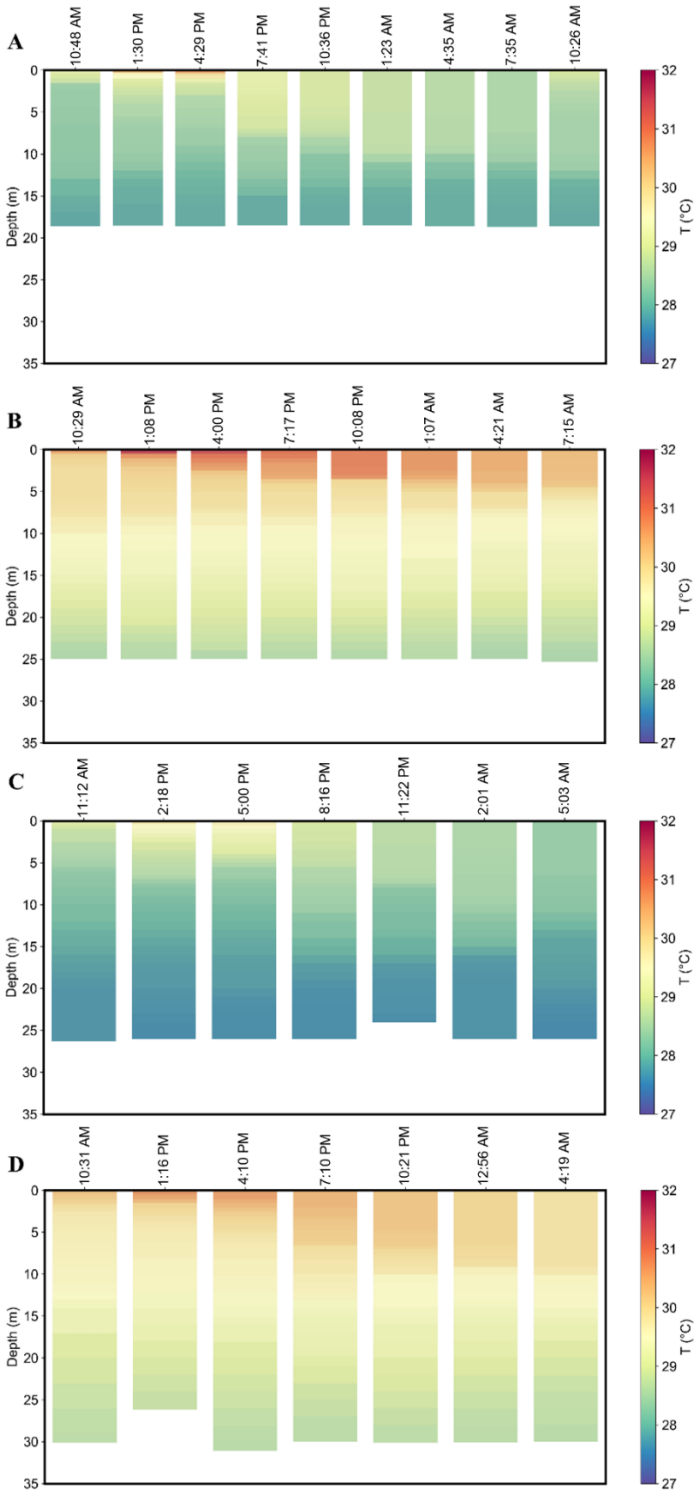

Source: The author.

Figure S 35 – RWCS index at P6 and P7 calculated for A) October 2021 (dry season), B) March 2022 (rainy season), C) November 2022 (dry season), and D) May 2023 (rainy season). The horizontal line represents the limit where above 50 it characterizes thermal stratification in the water column.

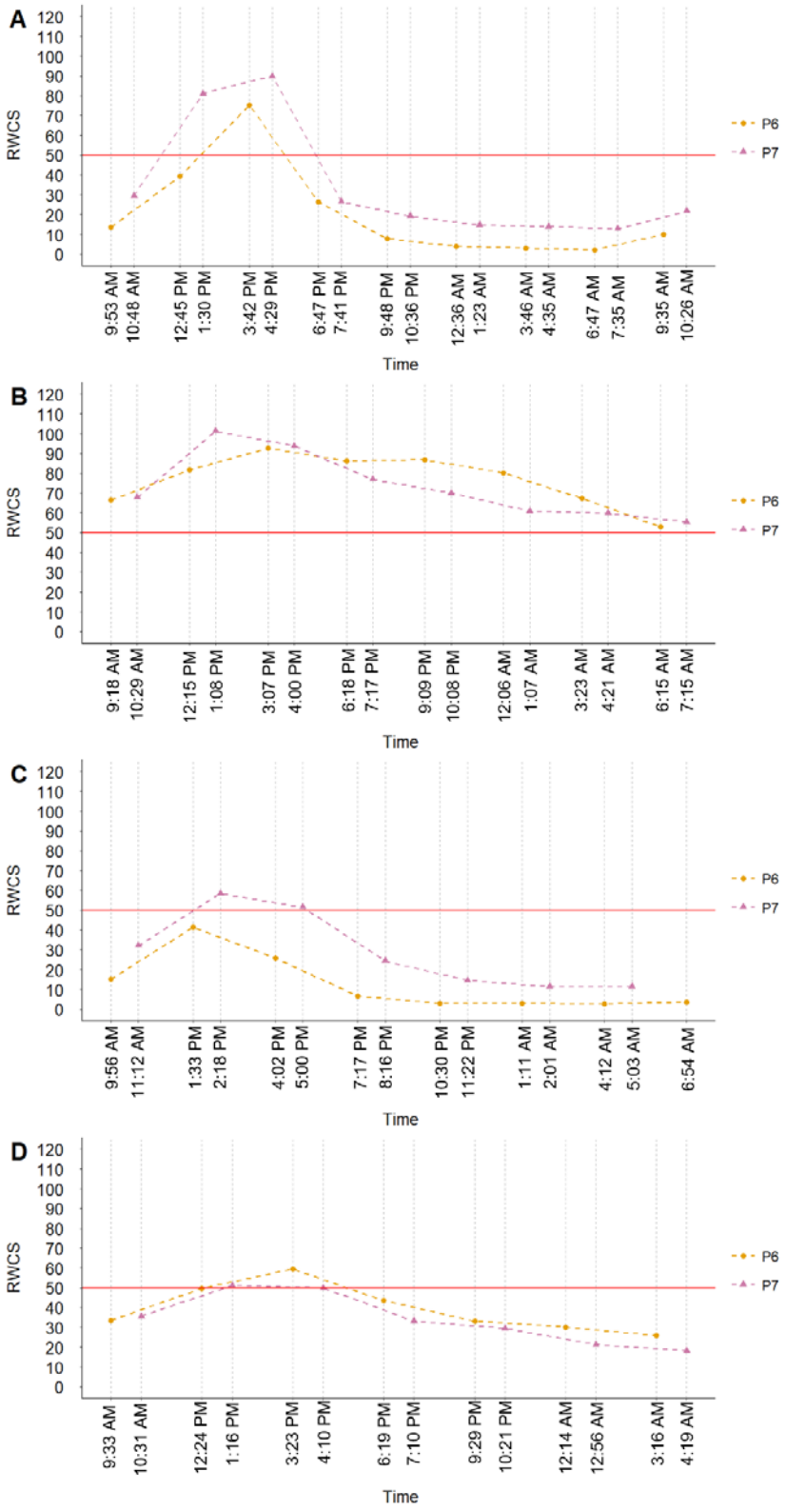

Source: The author.

Figure S 36 – Daily reservoir volume from A) October 2021 (dry season), B) March 2022

(rainy season), C) November 2022 (dry season), and D) May 2023 (rainy season). The dashed red dotted lines represent the dates where the diel analyses were performed.

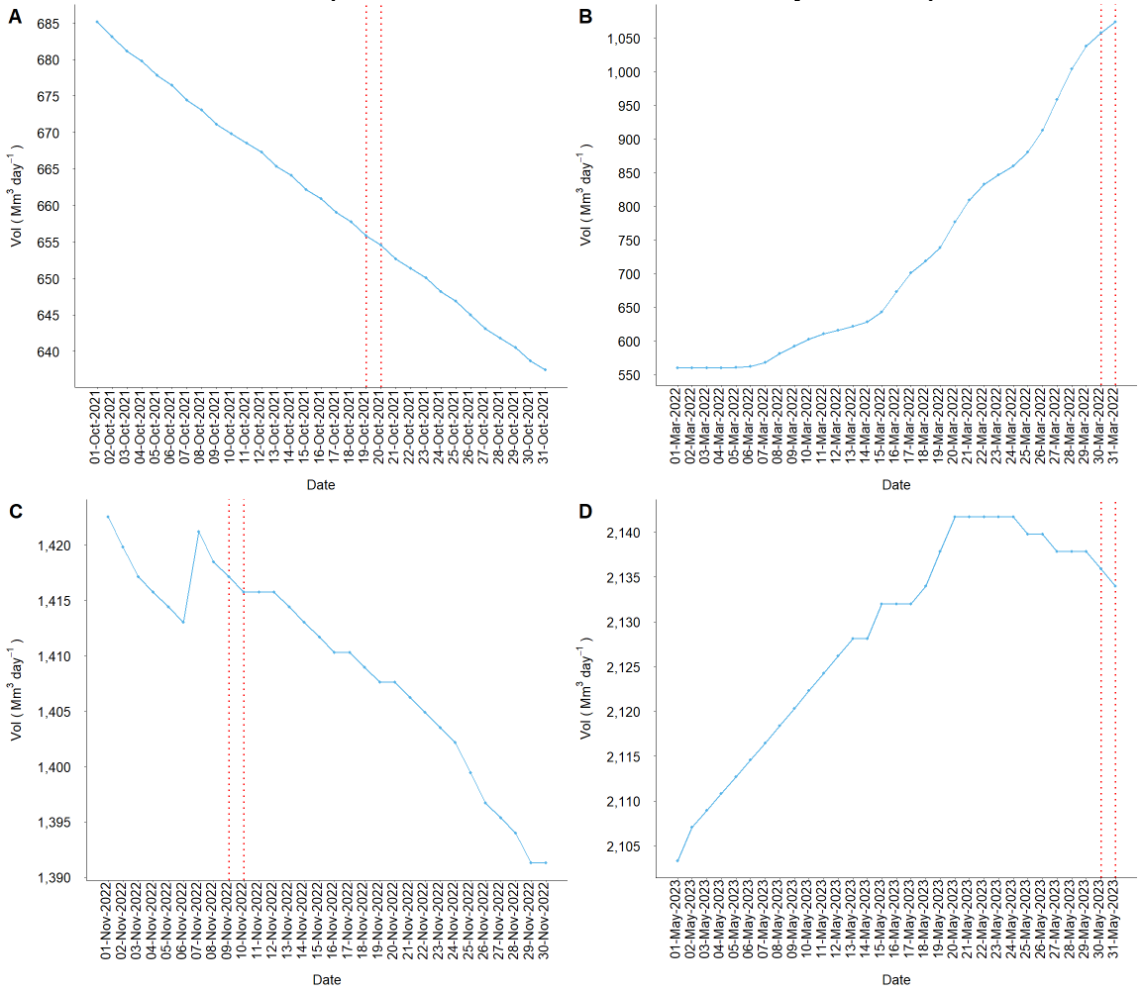

Source: The author.

Figure S 37 – Influence of reservoir inflow on thermal stratification. A) Time series of temperature variation in three different sampling points in Jaguaribe river upstream the reservoir. The boxplots show the temperature variation within six sampling points in the reservoir within different depths. The horizontal line at each boxplot represents the median values within the sampling points and within the water column. B) Time series of relative water column stability index in each date for six sampling points within the reservoir. The horizontal line in B) represents the limit where above 50 it characterizes thermal stratification in the water column.

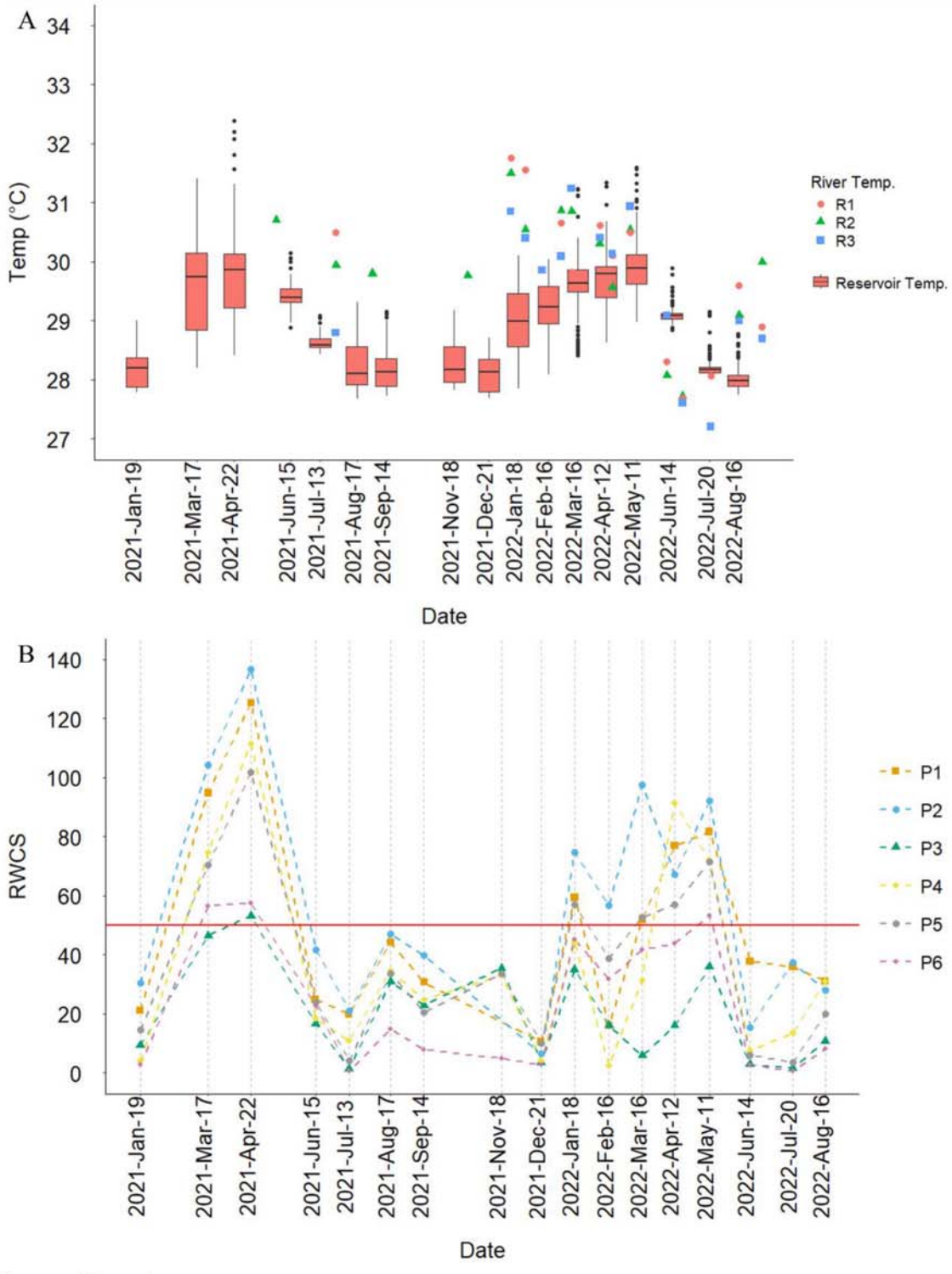

Source: The author.

Figure S 38 – Wind speed at the water dam of Castanhão reservoir in A) March 2022 (rainy season) and B) November 2022 (dry season).

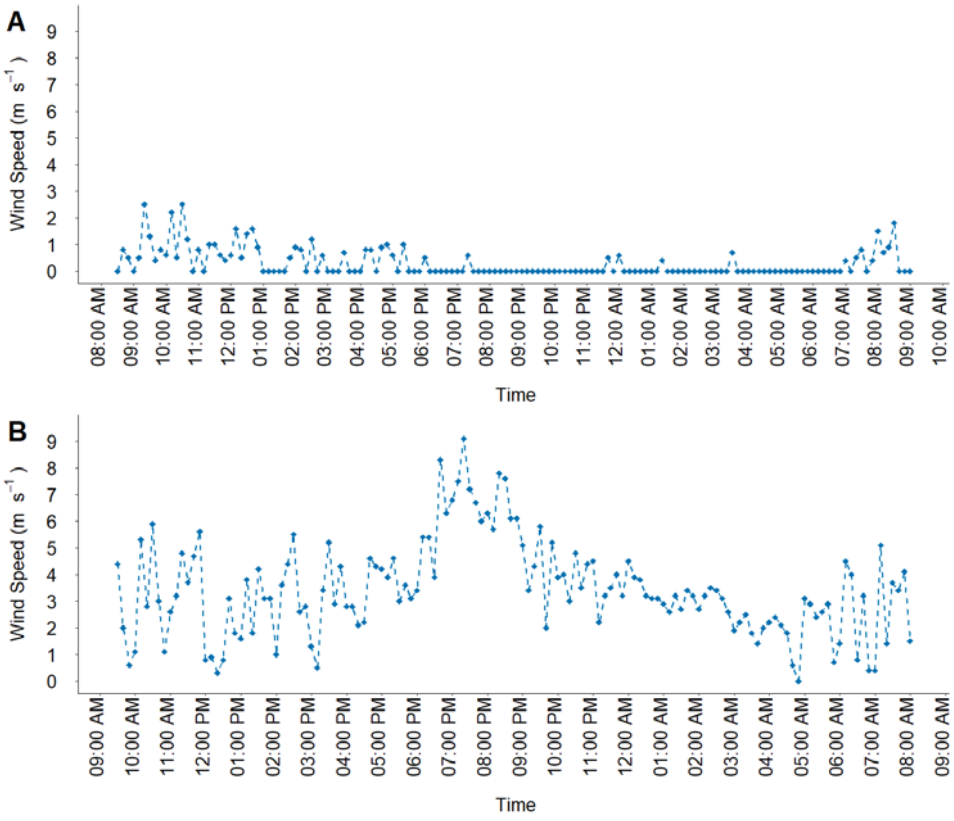

Source: The author.

Figure S 39 – Dissolved oxygen profiles at the P7 in A) October 2021 (dry season), B) March 2022 (rainy season), C) November 2022 (dry season), D) May 2023 (rainy season).

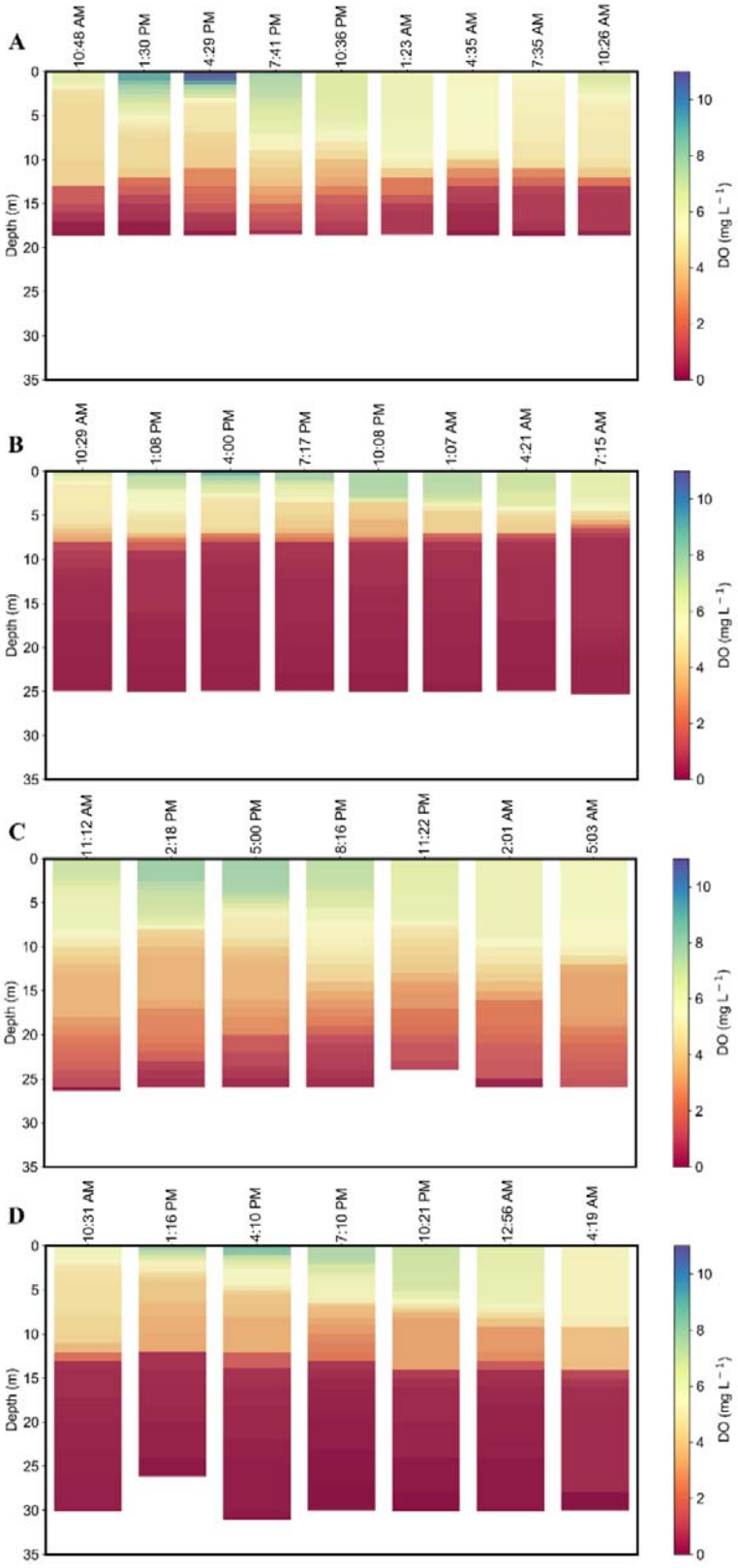

Source: The author.

Figure S 40 – SCS variation through the day in A) October 2021 (dry season), B) March 2022 (rainy season), C) November 2022 (dry season), and D) May 2023 (rainy season).

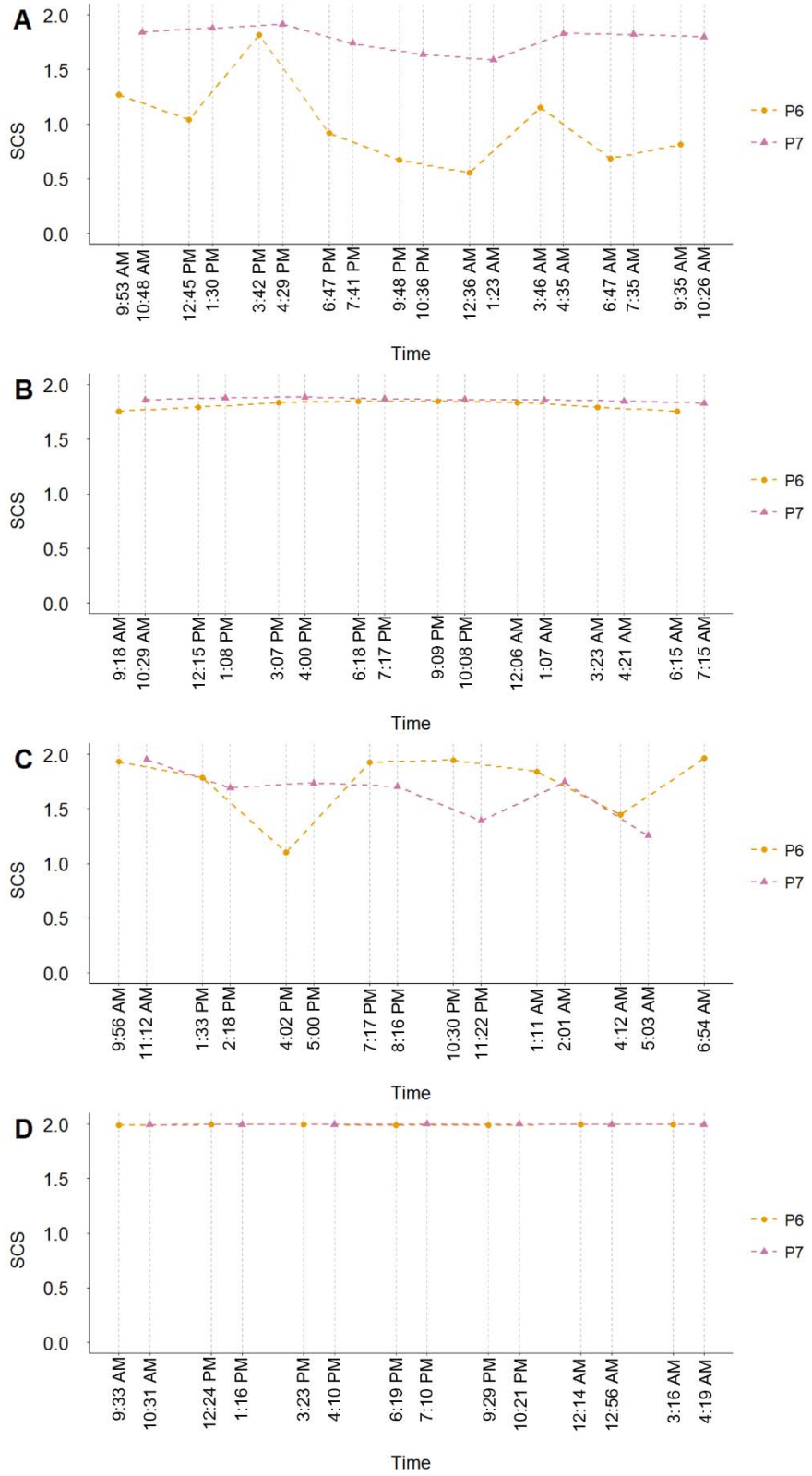

Source: The author.

Figure S 41 – Boxplots presenting the Temperature variations throughout the day at each measurement time at P6 in A) October 2021 (dry season), B) March 2022 (rainy season), C) November 2022 (dry season), D) May 2023 (rainy season). The horizontal line at each boxplot represents the median values within the water column.

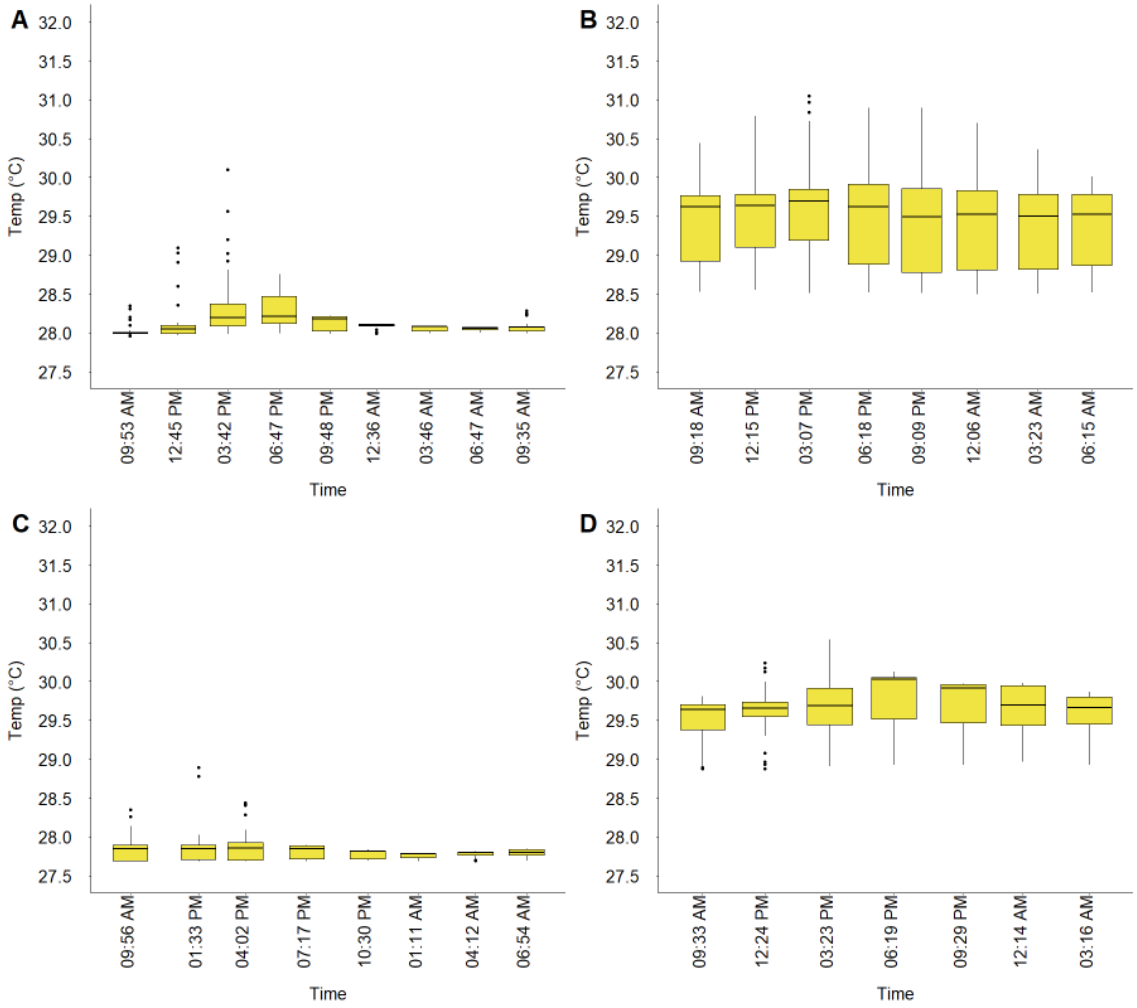

Source: The author.

Figure S 42 – Boxplots presenting the Temperature variations throughout the day at each measurement time in an analysis at P7 in A) October 2021 (dry season), B) March 2022 (rainy season), C) November 2022 (dry season), D) May 2023 (rainy season). The horizontal line at each boxplot represents the median values within the water column.

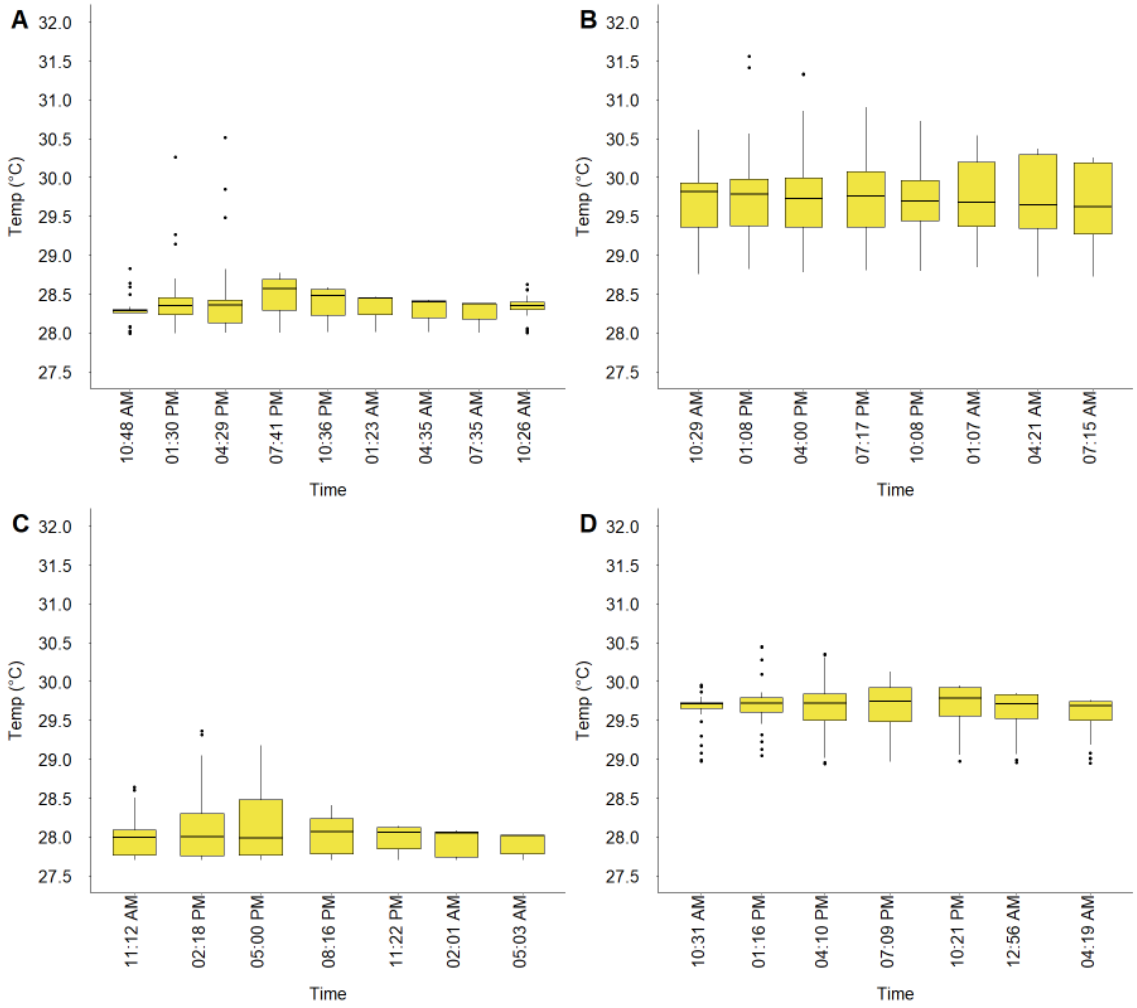

Source: The author.

SEASONAL DIEL NUTRIENT VARIATION

Figure S 43 – Variation of TP concentration in the water through time in A) October 2021 at P6, B) October 2021 at P7, C) March 2022 at P6, D) March 2022 at P7, E) November 2022 at P6 and F) November 2022 at P7. The horizontal line at each boxplot represents the median values within the water column.

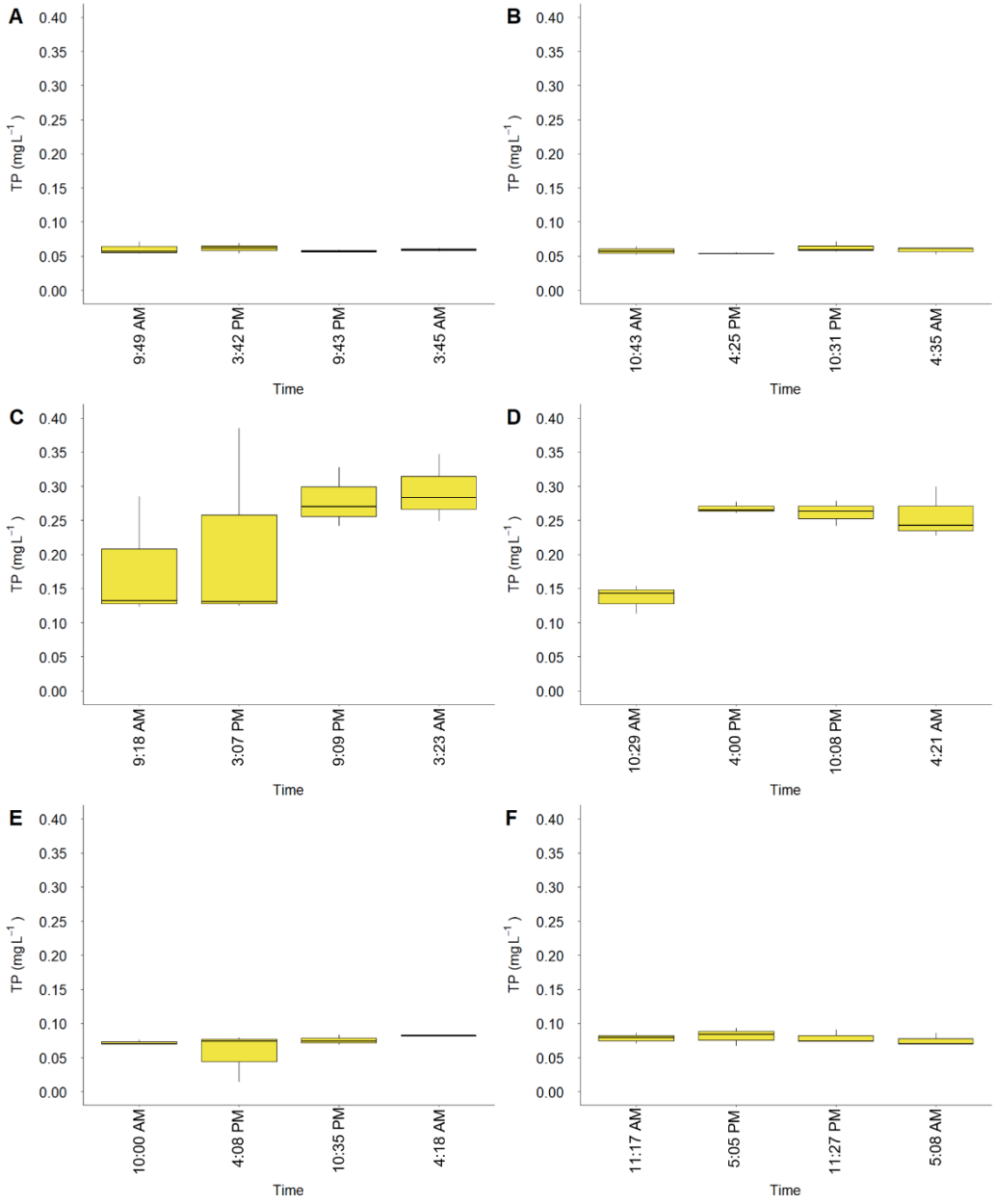

Source: The author.

Figure S 44 – TN concentration variation throughout the day in A) October 2021 (dry season), B) March 2022 (rainy season), C) November 2022 (dry season). The horizontal line at each boxplot represents the median values within the water column.

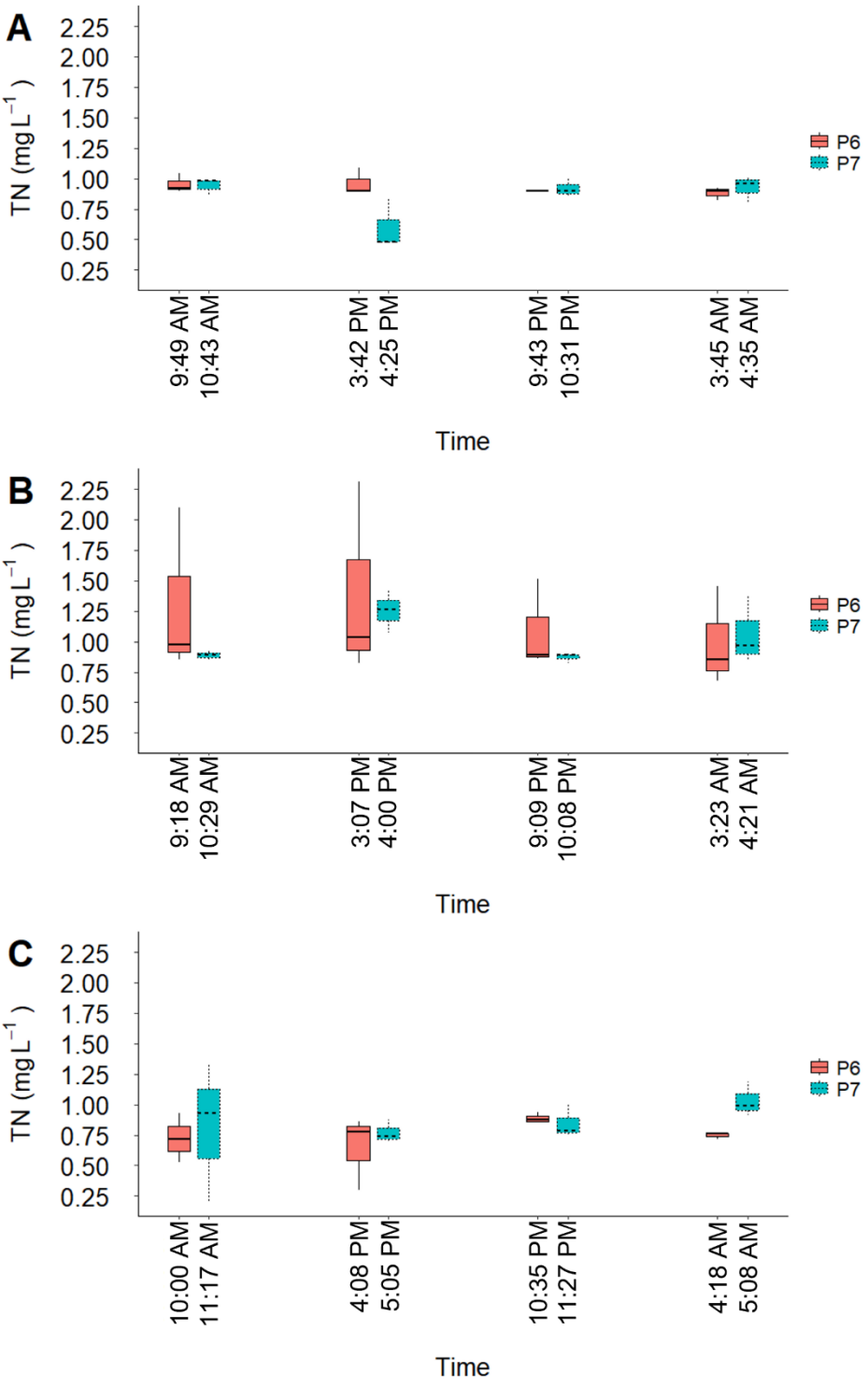

Source: The author.

Figure S 45 – Nitrite concentration variation throughout the day in A) October 2021 (dry season), B) March 2022 (rainy season), C) November 2022 (dry season). The horizontal line at each boxplot represents the median values within the water column.

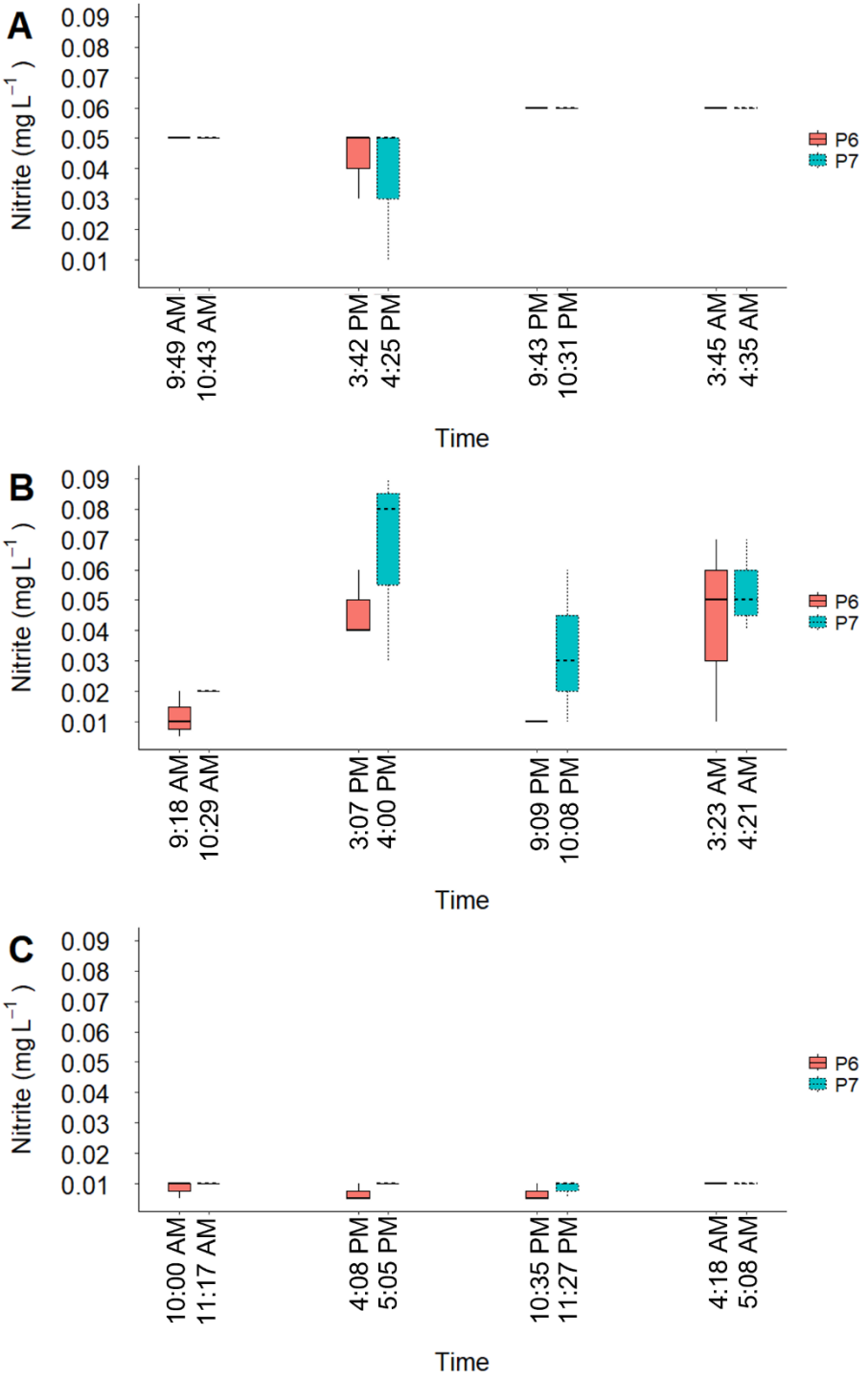

Source: The author

PHYTOPLANKTON DIEL VARIATION

Figure S 46 – Difference in chlorophyll a concentration between the measurements at each month. The horizontal line at each boxplot represents the median values within the water column.

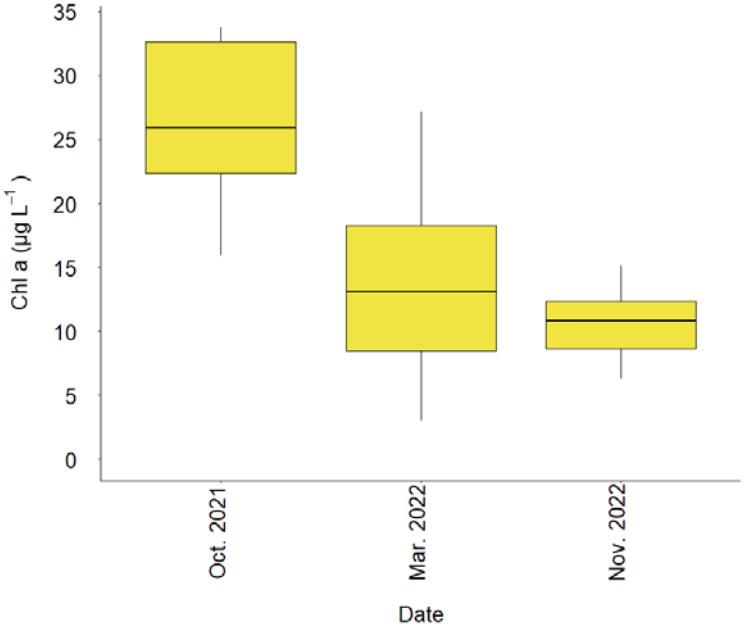

Source: The author.

Figure S 47 – Cyanobacteria abundance in October 2021 at a 0.3 m depth.

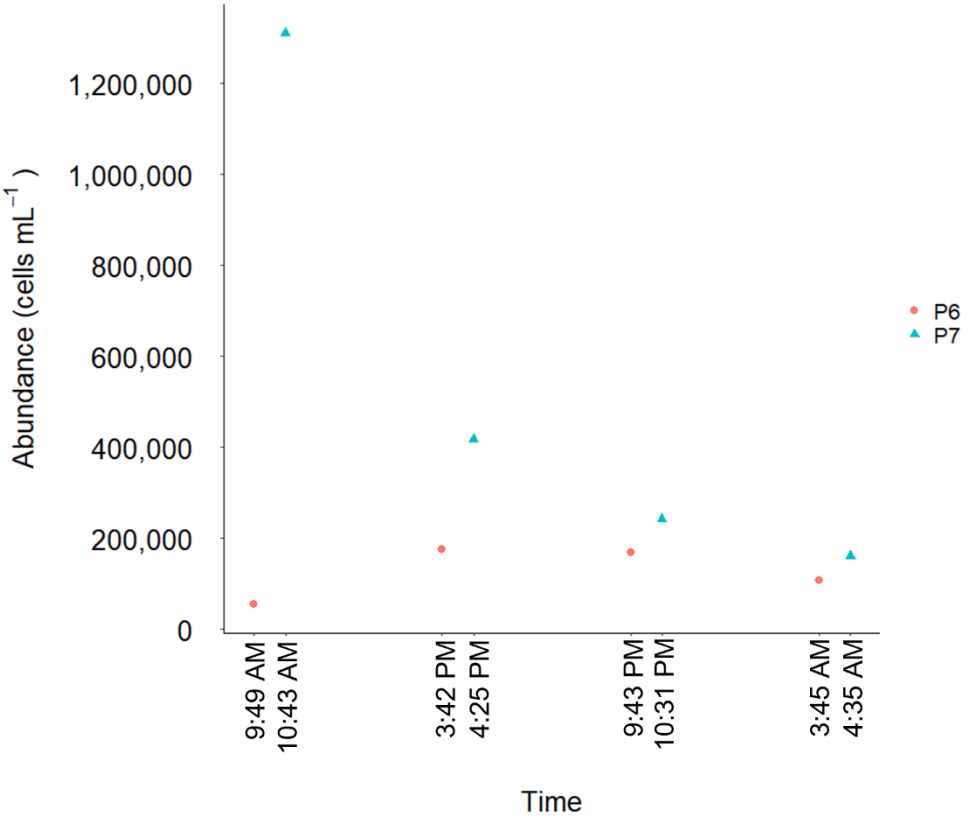

Source: The author.

Figure S 48 – Other organisms of the phytoplankton community in October 2021 at a 0.3 m depth.

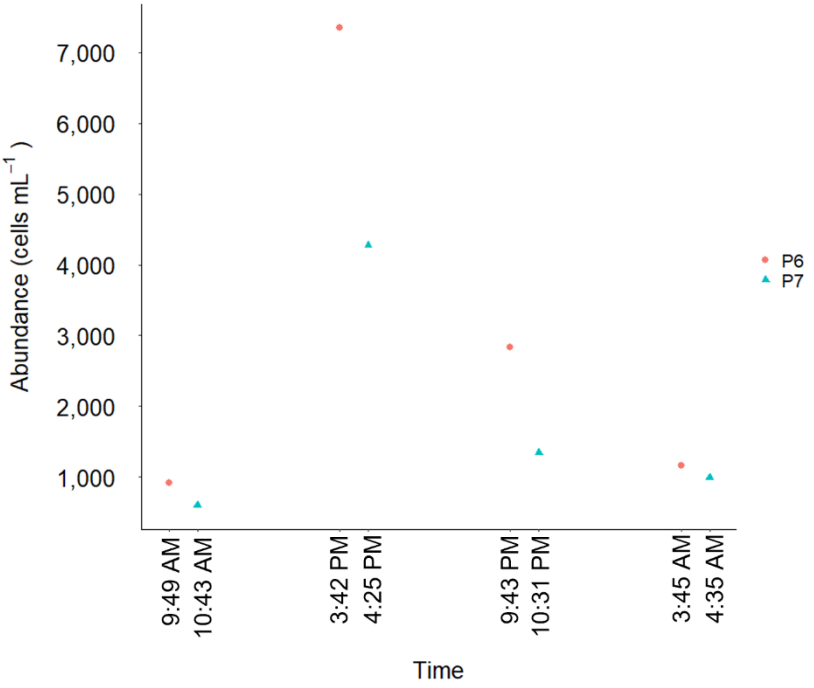

Source: The author.

Figure S 49 – Comparison of cyanobacteria abundance in March 2022 between the sampling points. The horizontal line at each boxplot represents the median values within the water column.

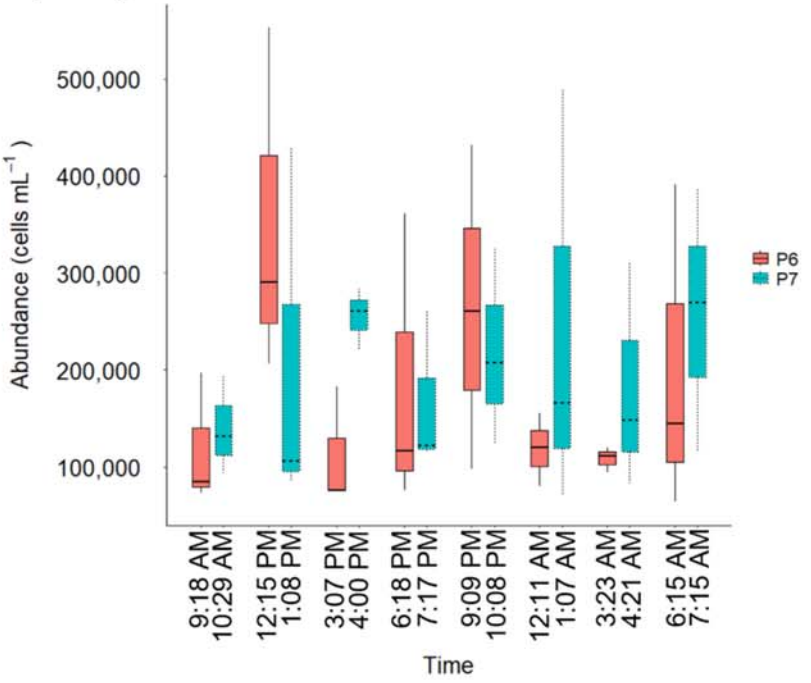

Source: The author.

Figure S 50 – Comparison of the abundance of other organisms of the phytoplankton community in March 2022 between the sampling points. The horizontal line at each boxplot represents the median values within the water column.

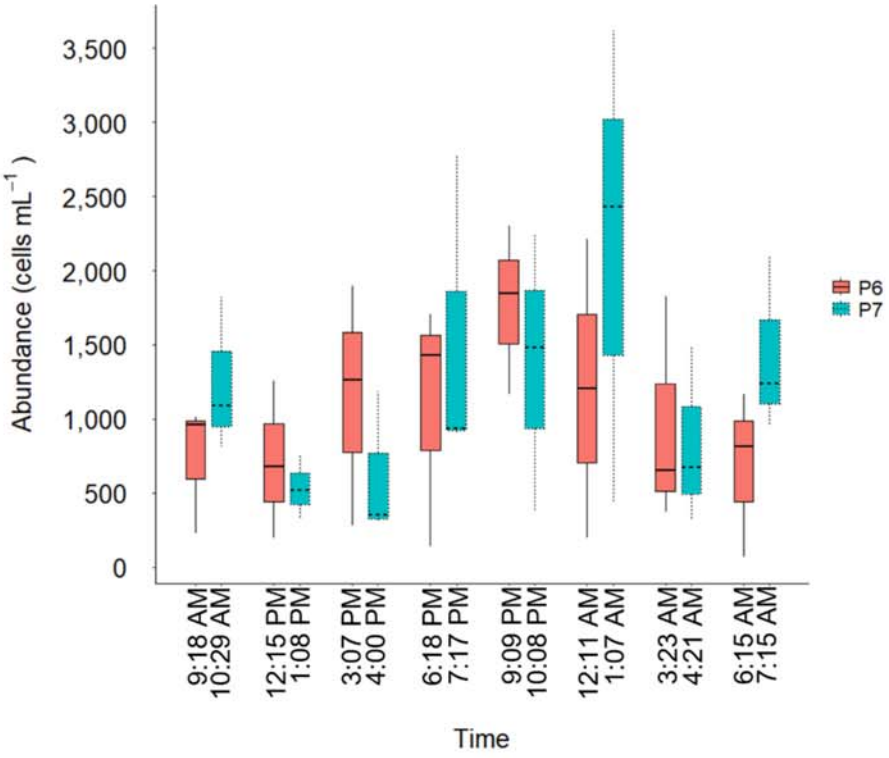

Source: The author.

NUTRIENT VARIATION WITH DEPTH

Figure S 51 – Variation of TP concentration with depth at P6 and P7 in A) October 2021 (dry season), B) March 2022 (rainy season), C) November 2022 (dry season).

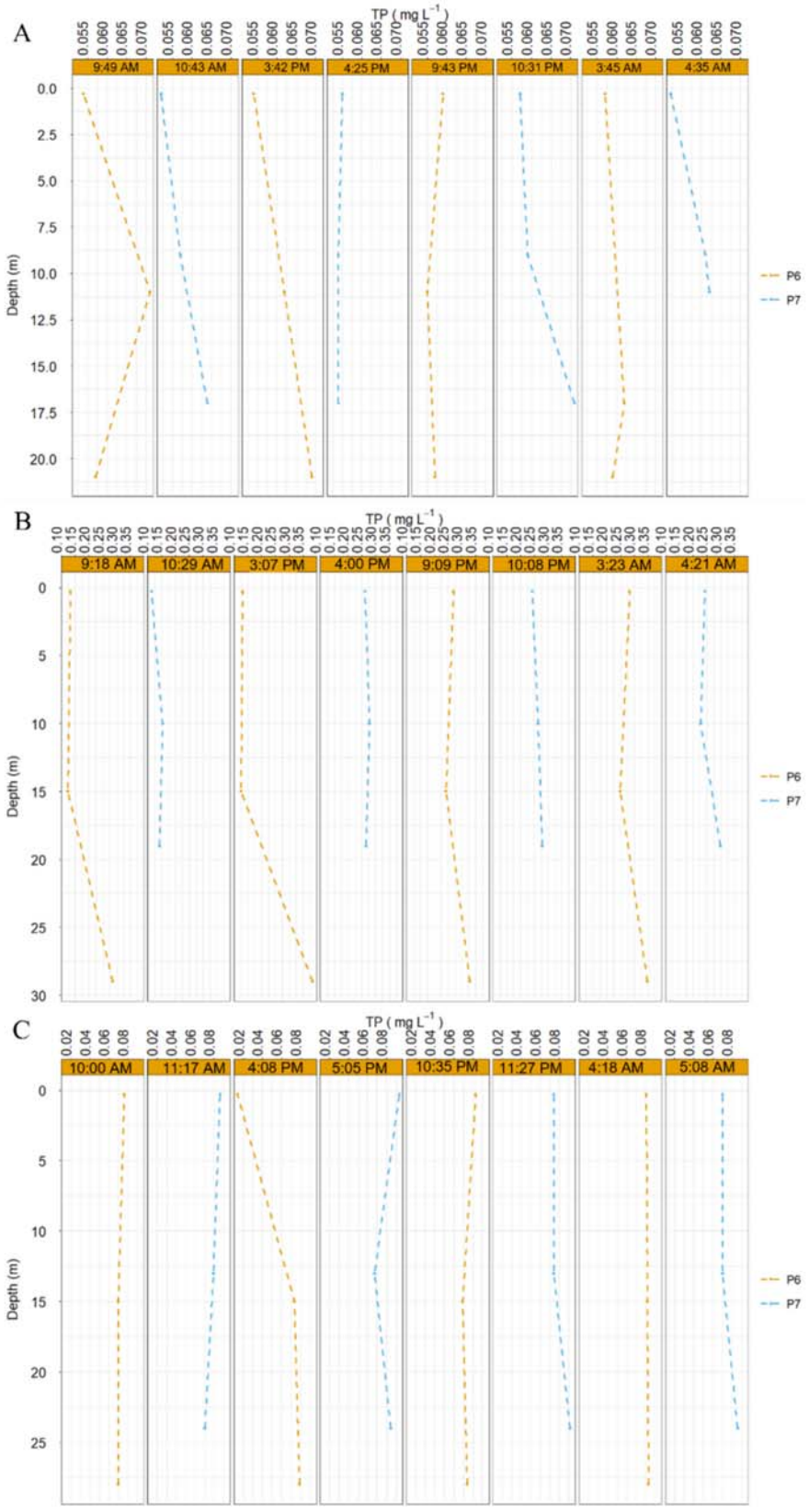

Source: The author.

Figure S 52 – Variation of orthophosphate concentration with depth at P6 and P7 in A) October 2021 (dry season), B) March 2022 (rainy season), C) November 2022 (dry season).

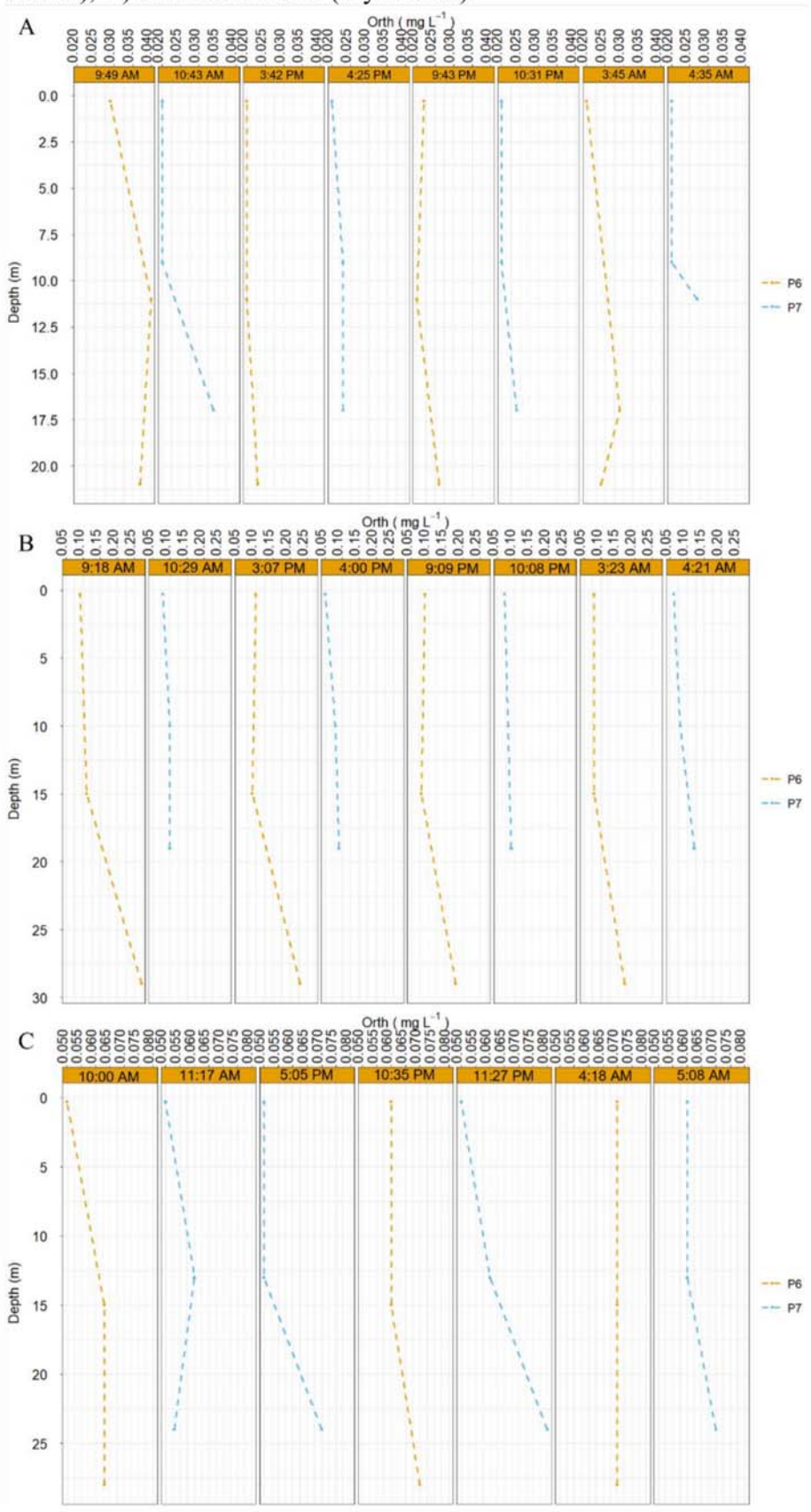

Source: The author.

Figure S 53 – Variation of TN concentration with depth at P6 and P7 in A) October 2021 (dry season), B) March 2022 (rainy season), C) November 2022 (dry season).

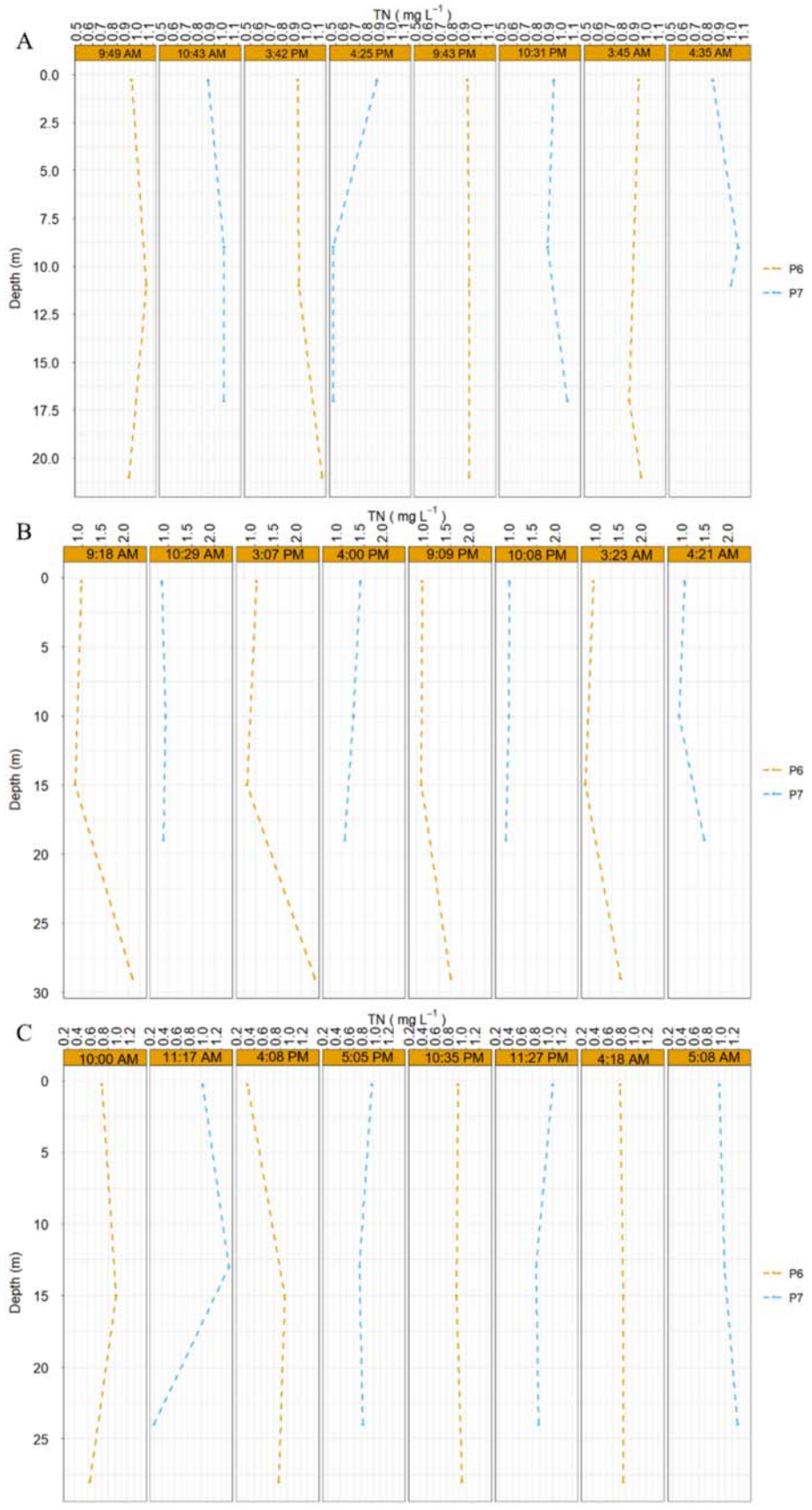

Source: The author.

APPENDIX C – SUPPLEMENTARY RESULTS FROM CHAPTER 5

Figure S 54 – Spatial variation of A) Aluminum B) Iron, and C) Total nitrogen concentration in the reservoir's sediment.

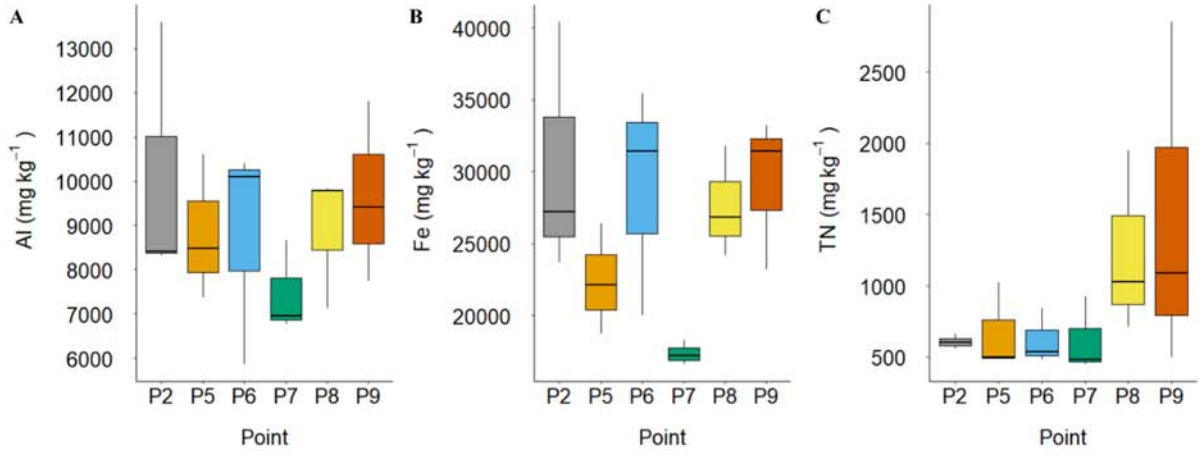

Source: The author.

Figure S 55 - Spatial variation of A) Organic matter and B) Solid percentage in the reservoir's sediment. The % w/w unit stand for the percent of weight.

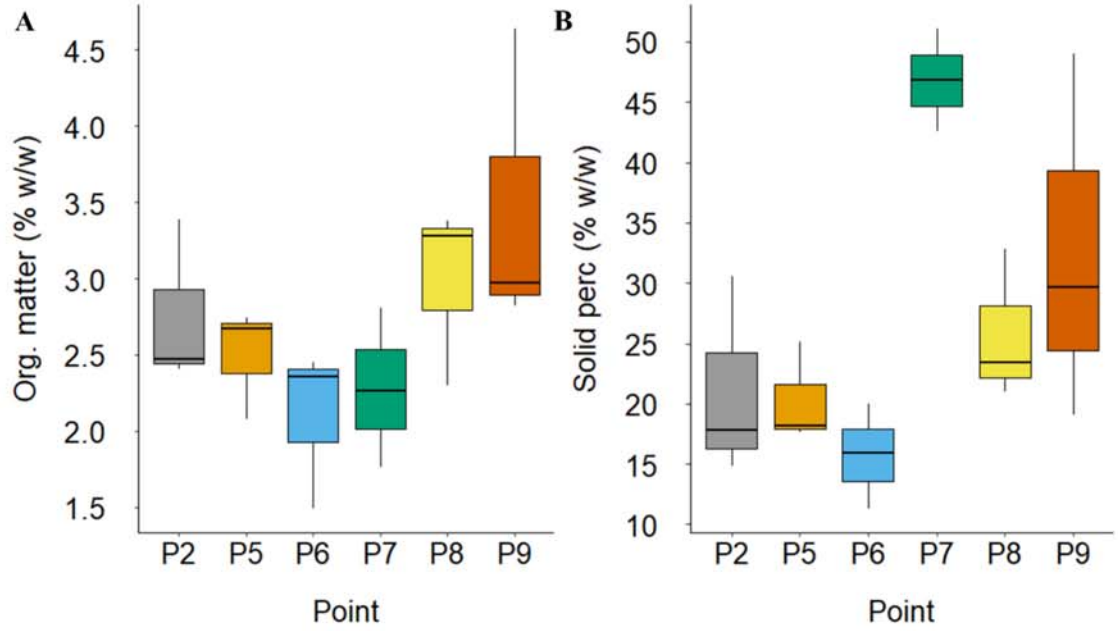

Source: The author.

Figure S 56 – Time series of the concentration of phosphorus fractions in the reservoir's sediment. A) shows the Iron-Aluminum bound Phosphorus, B) the Calcium bound phosphorus, C) Mobile phosphorus, and D) the residual phosphorus.

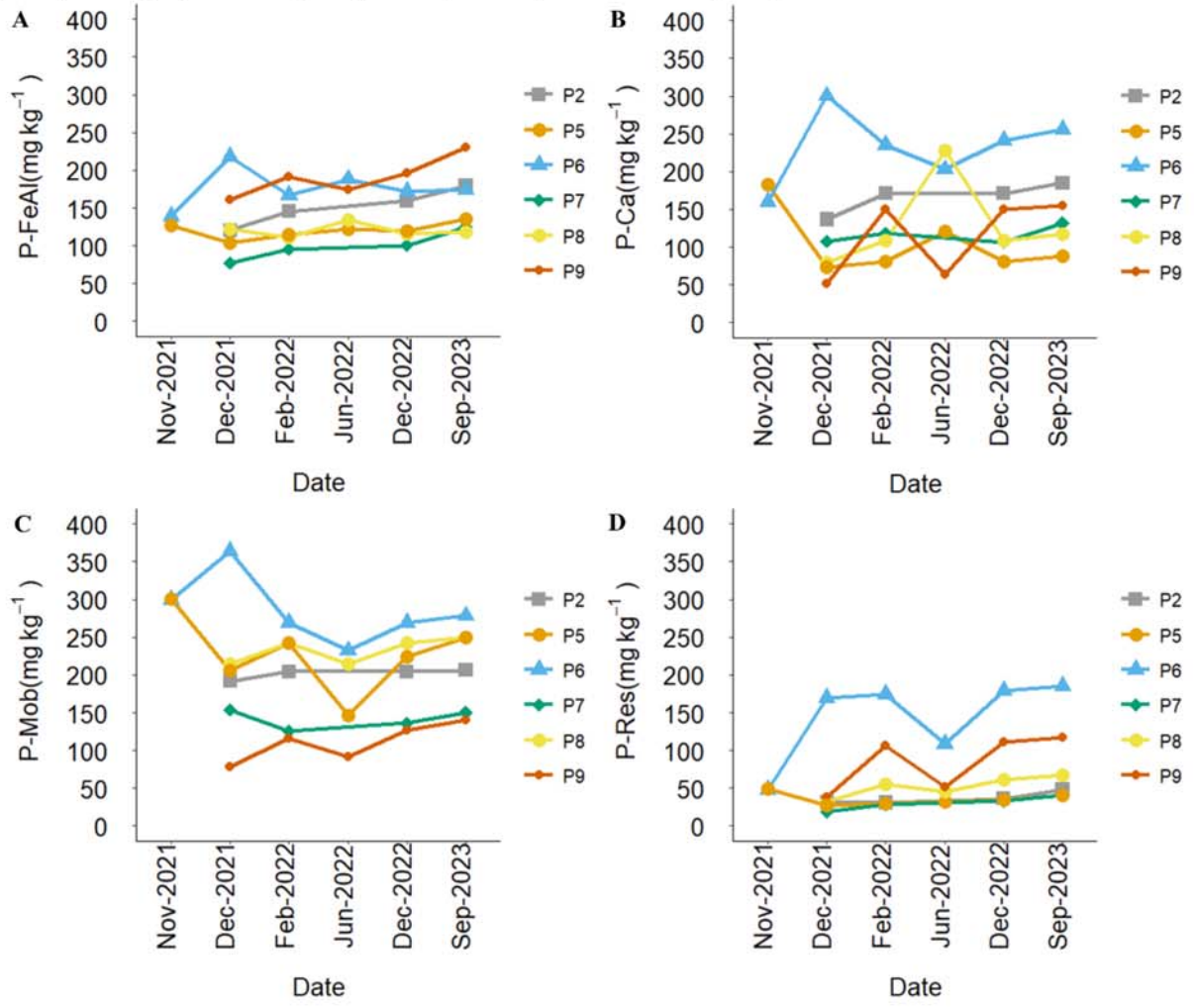

Source: The author.

Figure S 57 – Time series of the concentration of A) Iron, B) Aluminum, and C) Total nitrogen in the reservoir's sediment.

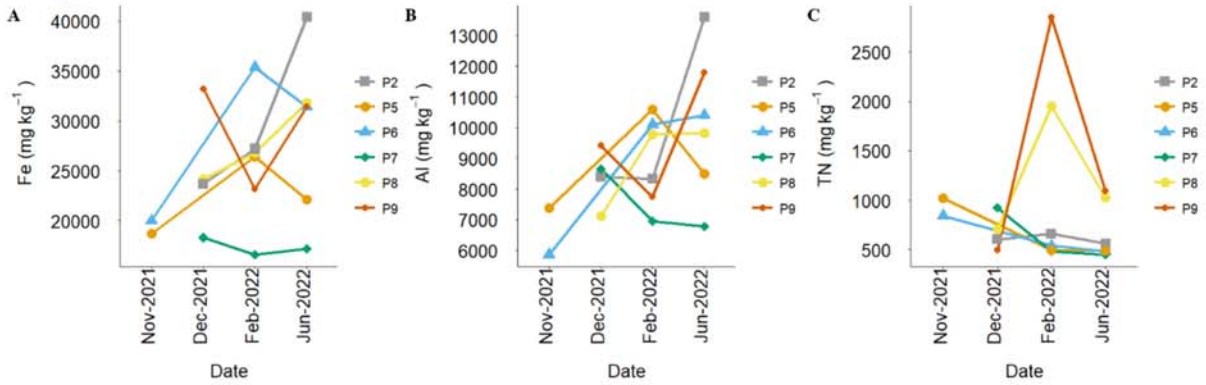

Source: The author.

Figure S 58 – A) Organic matter, and B) Solid percentage variation in the reservoir's sediment grouped by each measurement date. The horizontal line in each boxplot represents the median concentration for the different measurements.

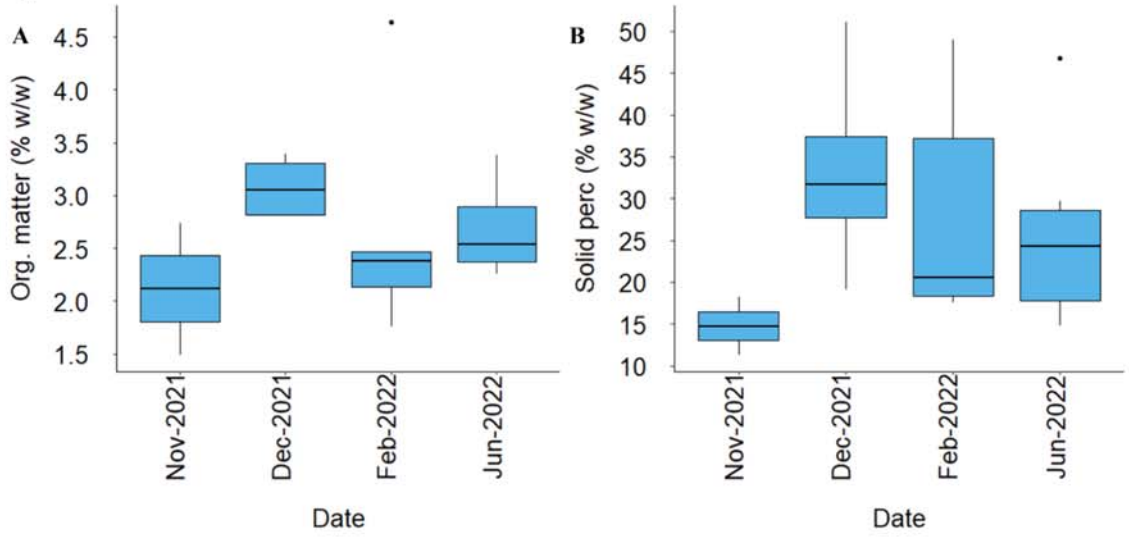

Source: The author.

Figure S 59 – Time series of the concentration of A) Organic matter, and B) Solid percentage in the reservoir's sediment.

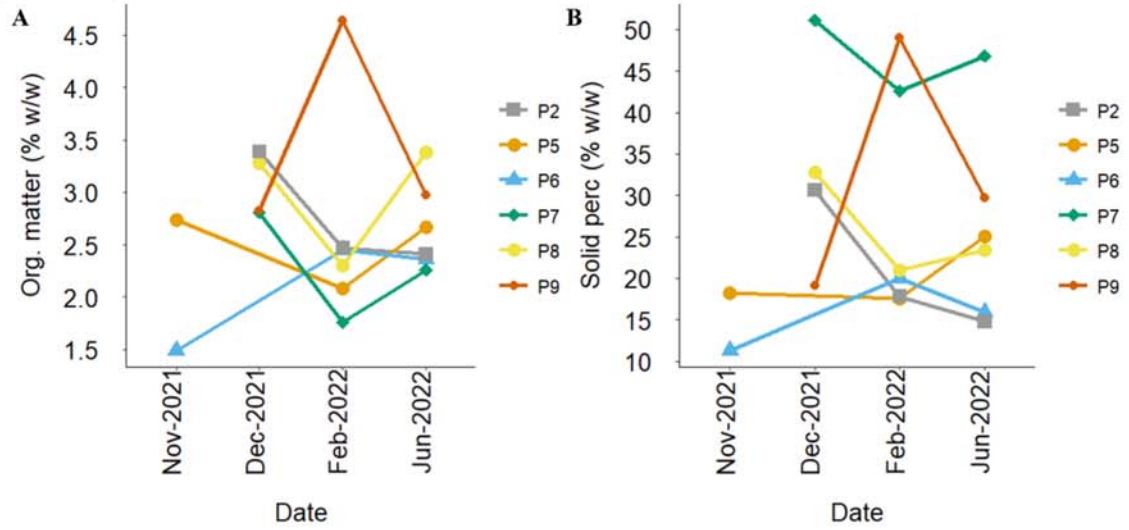

Source: The author.

Figure S 60 - Comparison of measurements performed by the laboratories Merieux and LABOSAN for total phosphorus concentration in the sediment analysis.

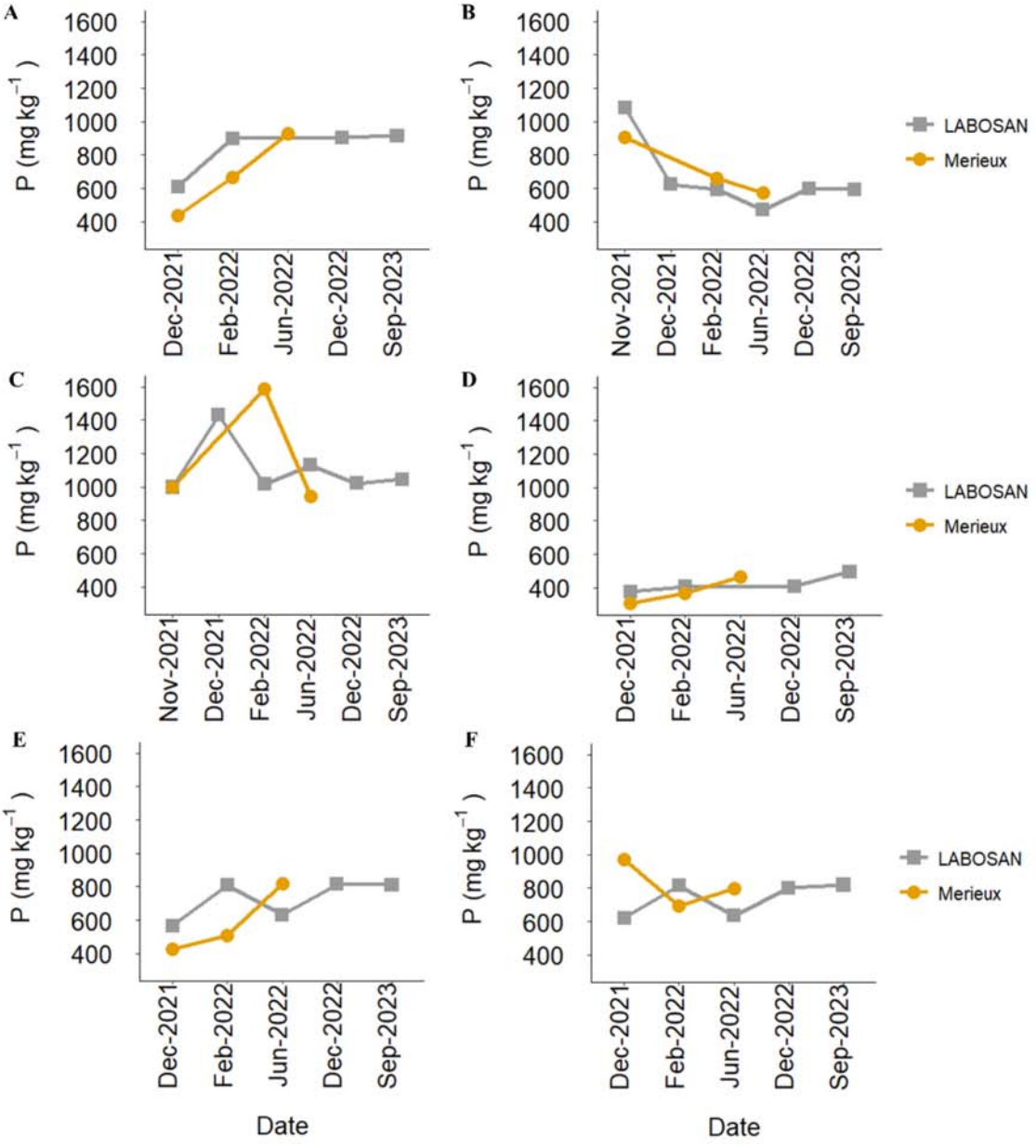

Source: The author.

APPENDIX D –ADDITIONAL ACTIVITIES OF THE PROJECT BEYOND SCIENTIFIC PUBLICATION – THESIS SOCIAL IMPACT AND RELEVANCE

The present thesis was developed by being part of a bigger project called “Carrying capacity of the Castanhão reservoir” with a direct application at the State’s water agency and an indirect impact on society. Therefore, the production of scientific articles was not the only purpose of this thesis. The development of this project also consisted of several meetings with important agencies related to the water management in the State and the country, workshops to share with society both the progress and the results found in the research, and several field visits.

1) Meetings (online and in-person):

Figure S 61 - The research team held weekly online meetings during the pandemic.

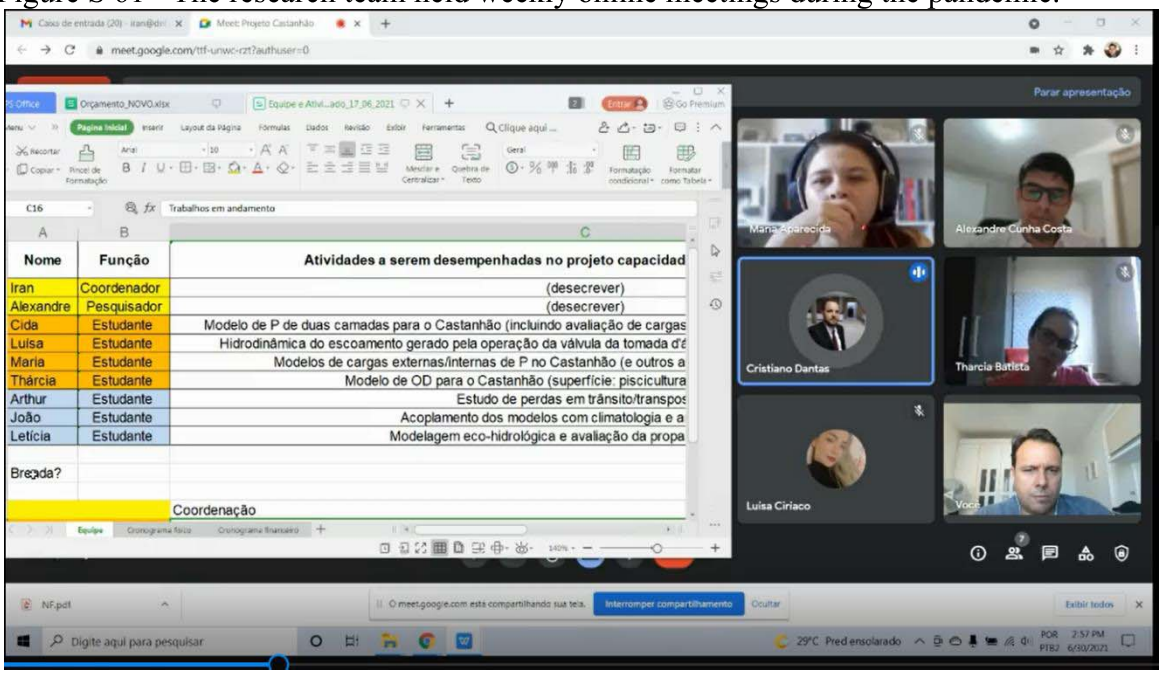

Source: The author.

Due to the high potential positive impact of the present thesis in several areas of water management and society during the project period occurred meetings and presentations with several important agencies. Among them were the national water and sanitation agency (ANA), the water resources management company in the state of Ceará (COGERH), Department of Water Resources of the State of Ceará (SRH), Ceará Foundation for Meteorology and Water Resources (FUNCEME), Water and Sewage Company of the State of Ceará (CAGECE), and Ministry of Fisheries and Aquaculture (MPA).

Figure S 62 – Meeting of the research team with the national water and sanitation agency (ANA) and the water resources management company in the state of Ceará (COGERH).

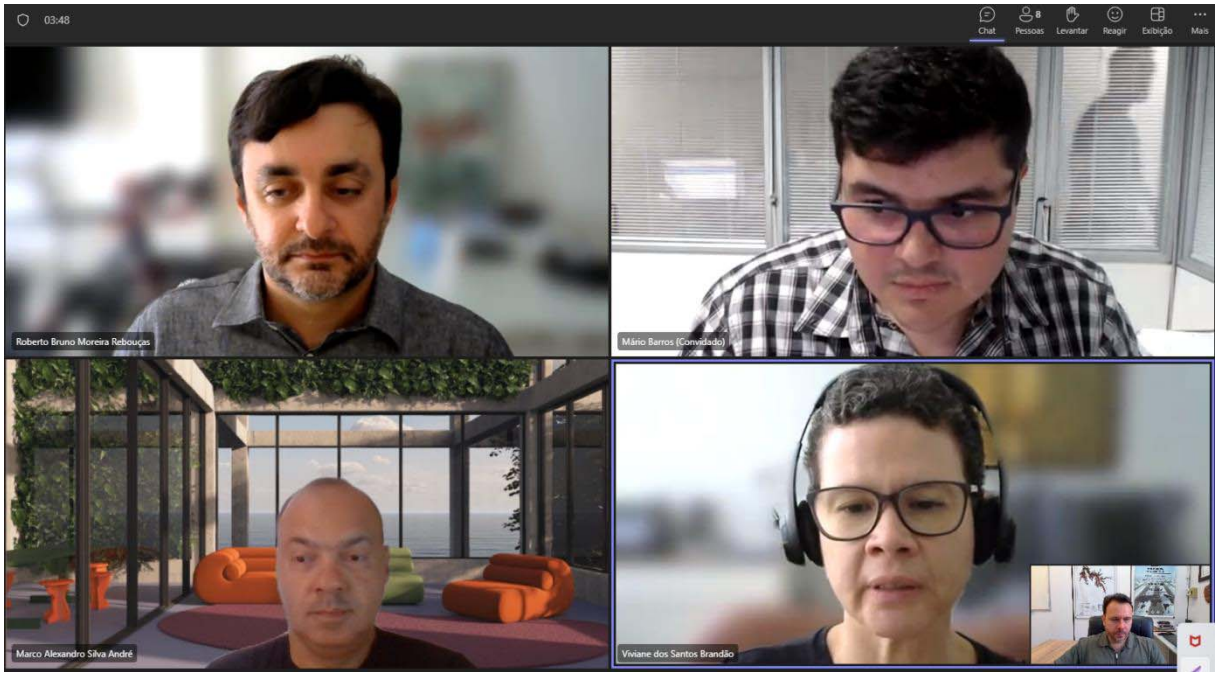

Source: The author.

Figure S 63 – Meeting with the management team of COGERH in the city of Limoeiro do Norte - CE, where part of the field monitoring team is located.

Source: The author.

2) National and International presentations:

Figure S 64 – Visit at the Institute of Freshwater Ecology and Inland Fisheries (IGB) in Berlin, Germany and at the Embassy of Brazil in Berlin.

Source: The author.

Figure S 65 – Participation of the research team on the XXV Brazilian Symposium on Water Resources held in Aracaju-SE.

Source: The author.

3) Water quality monitoring campaigns:

Figure S 66 - Water quality monitoring campaigns with river flowrate measurements, reservoir's bed sediment sampling, and water sampling.

Source: The author.

Figure S 67 - Water quality monitoring campaigns also included the use of weather station, drone images.

Source: The author.

4) Workshops and questionnaire application:

Two workshops were held in the city of Jaguaribara-CE, where the study area is located. The watershed committees, the Water Resources Management Company of the state of Ceará (COGERH), researchers from UFC who are part of the project, fish farmers, and political figures from the city of Jaguaribara participated in the workshop. In addition, a questionnaire was applied to fish farmers in order to improve the assessment of fish farming production in the Castanhão reservoir.

Figure S 68 - First workshop of the project held in Jaguaribara-CE.

Source: The author.

Figure S 69 – COGERH applied a questionnaire to fish farmers to obtain more information on fish farming production for the project.

Source: The author.

Figure S 70 – Promotional banner of the Castanhão Reservoir Capacity Support project on COGERH's social media platform.

Source: The author.

Figure S 71 – Second workshop held in Jaguaribara-CE to present the partial results of the project to the community.

Source: The author.

On April 19th, 2024, COGERH hosted the third and final seminar of the project (Figure S 72 and Figure S 73). It featured two concluding presentations showcasing the project's final results, followed by a discussion on applying these findings to water management and allocation processes, engaging several pivotal institutions. Among the attendees were COGERH, the Secretary of Water Resources of Ceará (SRH), the National Water and Basic Sanitation Agency (ANA), the Ministry of Fisheries and Aquaculture (MPA), the Brazilian Agricultural Research Corporation (EMBRAPA), the Ceará Foundation for Meteorology and Water Resources (FUNCEME), the Water and Sewage Company of the State of Ceará (CAGECE), and the Federal University of Ceará (UFC). Representatives from civil society and fish farmers were also in attendance.

Figure S 72 – Promotional poster for the third and final seminar of the Castanhão Reservoir Carrying Capacity Project

Source: The author.

Figure S 73 – Presentations and discussion of the final results of the Carrying Capacity of Castanhão Reservoir Project.

Source: The author.

On April 26th, 2024, the project's conclusive findings were presented in Brasília, DF to representatives from ANA and MPA (Figure S 74). This was followed by a discussion on how to implement these results and explore potential avenues for further studies aimed at advancing reservoir water quality management.

Figure S 74 – Presentation of the final results of the Castanhão reservoir carrying capacity project in Brasília-DF to ANA and MPA representatives.

Source: The author.